



UNIL | Université de Lausanne

Unicentre
CH-1015 Lausanne
<http://serval.unil.ch>

Year: 2023

Oxygen contribution, production and impact of reactive oxygen species after FLASH irradiation

Kacem Houda

Kacem Houda, 2023, Oxygen contribution, production and impact of reactive oxygen species after FLASH irradiation

Originally published at : Thesis, University of Lausanne

Posted at the University of Lausanne Open Archive <http://serval.unil.ch>

Document URN : [urn:nbn:ch:serval-BIB_9AF231C88CD51](https://nbn-resolving.org/urn:nbn:ch:serval-BIB_9AF231C88CD51)

Droits d'auteur

L'Université de Lausanne attire expressément l'attention des utilisateurs sur le fait que tous les documents publiés dans l'Archive SERVAL sont protégés par le droit d'auteur, conformément à la loi fédérale sur le droit d'auteur et les droits voisins (LDA). A ce titre, il est indispensable d'obtenir le consentement préalable de l'auteur et/ou de l'éditeur avant toute utilisation d'une oeuvre ou d'une partie d'une oeuvre ne relevant pas d'une utilisation à des fins personnelles au sens de la LDA (art. 19, al. 1 lettre a). A défaut, tout contrevenant s'expose aux sanctions prévues par cette loi. Nous déclinons toute responsabilité en la matière.

Copyright

The University of Lausanne expressly draws the attention of users to the fact that all documents published in the SERVAL Archive are protected by copyright in accordance with federal law on copyright and similar rights (LDA). Accordingly it is indispensable to obtain prior consent from the author and/or publisher before any use of a work or part of a work for purposes other than personal use within the meaning of LDA (art. 19, para. 1 letter a). Failure to do so will expose offenders to the sanctions laid down by this law. We accept no liability in this respect.



UNIL | Université de Lausanne

Faculté de biologie
et de médecine

Oxygen contribution, production and impact of reactive oxygen species after FLASH irradiation

Thèse de doctorat ès sciences de la vie (PhD)

Présentée à la

Faculté de biologie et de médecine
de l'Université de Lausanne

Par

Houda KACEM

Diplômée Master Erasmus Serp+
Master en physico-chimie de l'Université Paris-Saclay Paris Sud
Et l'Université de Porto

Jury

Prof. Matthias Stuber, President
Dre Elke Beyreuther, External Expert
Dre Katarzyna Pierzchala, External Expert
Prof Nukhet Aykin, External Expert
Dre Marietta Straub, Internal Expert
Prof. Marie-Catherine Vozenin, Thesis director

Lausanne 2023



UNIL | Université de Lausanne

Faculté de biologie
et de médecine

CHUV – Département d’Oncologie
Laboratoire de Radio-Oncologie

Oxygen contribution, production and impact of reactive oxygen species after FLASH irradiation

Thèse de doctorat ès sciences de la vie (PhD)

Présentée à la

Faculté de biologie et de médecine
de l’Université de Lausanne

Par

Houda KACEM

Diplômée Master Erasmus Serp+
Master en physico-chimie de l’Université Paris-Saclay Paris Sud
Et l’Université de Porto

Jury

Prof. Matthias Stuber, President
Dre Elke Beyreuther, External Expert
Dre Katarzyna Pierzchala, External Expert
Prof Nukhet Aykin, External Expert
Dre Marietta Straub, Internal Expert
Prof. Marie-Catherine Vozenin, Thesis director

Lausanne 2023

Imprimatur

Vu le rapport présenté par le jury d'examen, composé de

Président·e	Monsieur	Prof.	Matthias	Stuber
Directeur·trice de thèse	Madame	Prof.	Marie-Catherine	Vozenin
Expert·e·s	Madame	Dre	Elke	Beyreuther
	Madame	Dre	Katarzyna	Pierzchala
	Madame	Prof.	Nukhet	Aykin
	Madame	Dre	Marietta	Straub

le Conseil de Faculté autorise l'impression de la thèse de

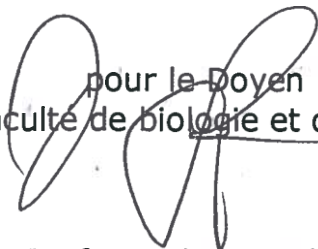
Houda Kacem

Master en Physique Chimie Serp+ Program, Université Paris Sud XI, France

intitulée

**Oxygen contribution, production and impact
of reactive oxygen species after FLASH irradiation**

Lausanne, le 15 février 2024


pour le Doyen
de la Faculté de biologie et de médecine
Prof. Matthias Stuber

List of abbreviations	8
Summary of the thesis	12
Acknowledgments.....	15
Institutions & funding.....	17
Résumé en français	19
Résumé de vulgarisation	22
Description of the manuscript organization.....	24
Chapter I: Introduction	26
1- Radiotherapy: Past, present, and ongoing advancements.....	27
1.1 Radiotherapy, time of discovery	27
1.2 Kilovoltage and Megavoltage era	27
1.3 Computer-assisted: 3D conformal radiotherapy, IMRT & Stereotactic radiotherapy ...	29
1.4 4D radiotherapy	30
1.5 Ion beam radiotherapy	30
1.6 FLASH radiotherapy	32
2- Types of ionizing sources in radiotherapy	33
2.1 X-rays:.....	34
2.2 Energetic electrons:	36
2.3 Protons:.....	37
3- Cascade of events activated after radiotherapy.	38
3.1 Radiation-induced physico-chemical effects: Radiation chemistry	38
3.2 Radiation-induced biological effects.....	42
Objectives of the thesis project.....	63
1- Can we investigate the mechanisms underlying the FLASH effect in chemical solutions?.....	64
2- What are the beam parameters essential to trigger the FLASH effect?	64
3- Are reactive oxygen species involved in the FLASH effect in biological systems?	64
Chapter II: Results	66
1- Publication 1 literature review: Understanding the FLASH effect to unravel the potential of ultra-high dose irradiation.	67
2- Publication 2: Comparing radiolytic production of H ₂ O ₂ and development of Zebrafish embryos after ultra-high dose rate exposure with electron and Transmission proton beams.	86
3- Publication 3: Instantaneous dose rate is a critical parameter linking the FLASH sparing effect across different high dose rate modalities.....	105
Chapter III: Supplementary results.....	161

1- Impact of transmission proton irradiations on physico-chemical events, DNA damage and development of zebrafish embryos	162
2- Investigations of cellular ROS levels after FLASH exposure using 2D cell culture.....	178
3- Investigation of ROS involvement after FLASH vs CONV exposure using a transgenic zebrafish model deficient in Nrf2.....	180
Chapter IV: General Discussion	183
1- Discussion.....	184
2- Conclusion	189
3- Perspectives	190
Curriculum Vitae	193
Bibliography.....	198

List of abbreviations

ACOX: Acyl-CoA oxidases

Akt: Protein kinase B

AMPK: AMP-activate protein kinase

ARE: Antioxidant response elements

Arg: Arginine

ART: Adaptive Radiotherapy

ATM: Ataxia-telangiectasia mutated

ATP: Adenosine triphosphate

CAFs: Cancer-associated fibroblasts

CAMKII: Ca²⁺ kinase II

cAMP: Adenosine monophosphate Cul3: Cullin 3

CAT: Catalase

⁶⁰**Co:** Cobalt 60

CoA: Coenzyme A

CONV-RT: Conventional radiotherapy

CLEAR: Linear Electron Accelerator for Research

CREB: cAMP response element binding protein

CT: Computerized tomography

CTV: Clinical tumor volume

Cu/Zn-SOD: Copper/zinc-dependent superoxide dismutase

Cys: Cysteine

C I-IV: Complex I-IV

DDP: Dose depth profile

DMSO: Dimethyl sulfoxide

DPF: Days post-fertilization

DPP4/CD26 protein: Dipeptidyl peptidase-4/Cluster of differentiation 26 protein

e_(aq)⁻: Aqueous electron

H₂O₂: Hydrogen peroxide

EBRT: External-beam radiotherapy

eCONV: electron CONV

eFLASH: electron FLASH

ER: Endoplasmic Reticulum

ERK: Extracellular signal-regulated kinase

ERO1: Endoplasmic reticulum oxidoreductin 1

ETC: Electron transport chain

Fe²⁺: Ferrous iron

Fe³⁺: Ferric iron

Fe-S cluster: Iron–Sulfur cluster

FLASH-RT: FLASH radiotherapy

GAPDH: Glyceraldehyde 3-phosphate dehydrogenase

GPX: Glutathione-peroxidases

GR: Glutathione reductase

Grx: Glutaredoxin

GSH: Glutathione

GTV: Gross tumor volume

Gy: Gray

G6PD: Glucose-6-phosphate dehydrogenase

H⁺: Hydrogen ion

H₂: Molecular hydrogen

HIF-1 α : Hypoxia-inducible factor 1

NOS: Nitric oxide synthase

HO₂[•]: Hydroperoxyl radical

HO[•]: Hydroxyl radical

Hpf: hours post-fertilization

IEE: Intermediate energy electron

IGRT: Image-Guided Radiotherapy

IMM: Inner mitochondrial membrane

IMRT: Intensity-modulated radiotherapy

IMS: Intermembrane space

IR: Ionizing radiation

Keap1: Kelch-like ECH associated protein 1

KO: Knockout

LD10: Length deficit at 10 Gy

LD100: Lethal dose at 100%

LET: Linear energy transfer

LQ model: Linear quadratic model

Lys: Lysine

MAPK: Mitogen-activated protein kinase

MDA: Malondialdehyde

MDSCs: Myeloid-derived suppressor cells

MnSOD: Manganese-dependent superoxide dismutase

mTOR: mammalian target of rapamycin

MZT: Maternal-to-zygotic transition

NADH: Nicotinamide adenine dinucleotide

NFκB: Nuclear Factor kappa-light-chain-enhancer of activated B cells

NO[•]: Nitric oxide

NOO[•]: Peroxynitrite

NOQ1: NADPH dehydrogenase quinone 1

NOX: NADPH oxidase

Nrf2: Nuclear erythroid-related factor 2

OAR: Organs at risk

ONOO⁻: Peroxynitrite

OXPHOS: Oxidative phosphorylation

PBS: Pencil beam scanning

pCONV: proton CONV

PDI: Protein disulfide isomerase

pFLASH: proton FLASH

PI3K: Phosphatidylinositol 3-kinase

PKM2: Pyruvate kinase M2

PPP: Pentose phosphate pathway

Prdxs: Peroxiredoxins

PTEN: Phosphatase and tensin homolog

PTV: Planning target volume

R[•]: Lipid radical

Rad: radiation absorbed dose

RBE: Relative biological effectiveness

RO[•]: Alkoxy radical

RO[•]₂ or ROO[•]: Peroxyl radical

ROOH: Hydroperoxide or lipid peroxide

ROS: Reactive oxygen species

RNS: Reactive nitrogen species

RT: Radiotherapy

SBRT: Stereotactic body radiotherapy

SOBP: spread-out of the Bragg peak

SOD: Superoxide dismutase

SSD: Source–surface–distance

TAMs: tumor-associated macrophages

TFs: Transcription factors

TI: Transmission

TME: Tumor microenvironment

TPS: Treatment planning systems

Trp: Tryptophan

Trx: Thioredoxin

Tyr: Tyrosine

UHDR: Ultra high dose rate

UPR: Unfolded protein response

VHEE: Very high energy electron

VEGF: Vascular endothelial growth factor

ZFE: Zebrafish embryos

Summary of the thesis

Today, radiotherapy (RT) constitutes one of the pillars of modern cancer therapy, alongside surgery, chemotherapy, targeted drugs and immunotherapy. It contributes to the treatment of over 50% of cancer patients and is combined with other therapies to efficiently eradicate cancer cells. Despite significant technological improvements in beam delivery and image guidance used today, the dose required for tumor control is still limited by normal tissue toxicity. Additionally, some tumors remain highly radio-resistant, relapse and metastasize. Therefore, one ultimate challenge in our field is to develop novel radiotherapy strategies to overcome these limitations. In this context, our team conceptualized and developed FLASH radiotherapy (FLASH-RT). With the potential to change medical paradigms, FLASH-RT has the capacity to increase the therapeutic index for almost all cancers. This innovative approach relies on ultrahigh dose rates (UHDR), which are at least over a thousand times greater than dose rates used in conventional radiation therapy (CONV). FLASH-RT limits normal tissue damages at a given cytotoxic isodose for tumors; this phenomenon is known as **the FLASH effect**. Our group has discovered and confirmed the FLASH effect in several experimental animal models (mice, rats, zebrafish, pigs, cats) and multiple organs (lung, skin, gut, brain). Today, many other groups have reproduced the FLASH effect with different beams. The biological outcomes of FLASH-RT are under investigations and are the consequence of radiation interaction with matter, starting at "t0" with the transfer of radiation energy to the substrate (physical stage, femtosecond scale). Following this, highly reactive chemical species are being produced, leading to chemical reactions occurring at sub-picosecond and millisecond scales.

The chemical changes produced by ionizing radiation (IR) are generally described in liquid water, since it is a major component of living organisms. The interaction of ionizing particles with water is called water radiolysis. As a result, water molecules break and form highly reactive byproducts that can interact with soluble substances (solute). The reactive intermediates react and disappear at different constant rates ending with many repercussions at biological time scale. **This PhD work aimed at investigating the possible continuum existing between early radiation chemistry and radiobiology.** I investigated the FLASH effect from the earliest physico-chemical processes that result in reactive oxygen species (ROS) production in cell-free system (water) to more complex models such as plasmid DNA going to biological systems including cell lines and zebrafish embryos (ZFE). To perform those investigations, I used various beams capable of operating at CONV and UHDR:

- 1) The FLASH-validated experimental linear accelerator of intermediate energy electron (IEE) (5.5 MeV) eRT6 Oriatron,
- 2) The transmission proton beam (235 MeV) at Gantry 1/PSI,
- 3) And the very high energy electron (VHEE) CLEAR beam (190-220 MeV) at the CERN.

With all investigated beams, in water, primary yields of H₂O₂ were similar using CONV and FLASH dose rates which suggested that chemistry at the microsecond time scale (homogenous phase of chemistry) is similar. However, longer-term investigations showed reduced H₂O₂ yield in water irradiated with FLASH as compared to CONV. This was found under various conditions of oxygen tension, scavengers and temperature. This suggest that FLASH reduces ROS yields. DNA damages in a cell-free plasmid system without any repair machinery are globally similar after FLASH and CONV. These results demonstrate that early physico-chemical assessments based on hydrogen peroxide and DNA damage do not recapitulate the biological response *in vivo*. However, experiments in ZFE enable us to identify the instantaneous dose rate as a critical factor to observe the FLASH sparing effect, providing unique information for the development of the next generation of FLASH devices.

Lastly, our preliminary results obtained in cells and with normal cell lines and ZFE deficient in nuclear erythroid-related factor 2 (Nrf2 +/-) support a major role for ROS in the biological response to FLASH, supporting the idea that FLASH irradiation is associated with a reduced ROS production in a biological model.

Our work is the first to correlate the physico-chemical events associated with the FLASH and unveil fundamental parameters to trigger the FLASH sparing effect. Our findings have significant implications at the physics and mechanistic level, indicating that the scanning of high intensity beamlets will be the modality of choice for clinical developments of FLASH. They also suggest that the FLASH effect is a biological effect that defies simple chemical environments.

Acknowledgments

Mon mémoire de thèse a été une aventure stimulante au cours de laquelle j'ai exploré de nouveaux domaines en science radiologique. Ce voyage n'aurait pas été possible sans le soutien précieux de nombreuses personnes. En concluant ma thèse, je réalise que les mots ne sauraient exprimer pleinement ma gratitude envers ceux à qui je dois le plus et envers qui je serai éternellement reconnaissante.

J'exprime ma gratitude envers le professeur Matthias Stuber pour avoir accepté de présider le comité d'évaluation de ma thèse ainsi que la doctoresse Elke Beyreuther, la doctoresse Katarzyna Pierzchala, la professeure Nukhet Aykin-burns et la doctoresse Marietta Straub pour leurs rôles d'experts. Je tiens à vous remercier chaleureusement pour l'opportunité que vous me donnez d'évaluer ce travail.

Je souhaite du fond du cœur remercier la professeure Marie-Catherine Vozenin. Je tiens à exprimer ma gratitude pour ta présence régulière, tant sur le plan professionnel que personnel, au cours de ces quatre années passées sous ta direction. J'ai vécu des moments incroyablement enrichissants grâce à toi. Je te remercie pour tes efforts à comprendre la chimie sous rayonnement, tes réflexions et tes discussions précieuses. Je t'admire beaucoup et je suis honorée de t'avoir ma directrice de la thèse. J'espère sincèrement que nos chemins continueront à se croiser. Tu excelles en tant que femme, mère et scientifique. Un immense merci.

Un grand merci à tous mes collègues du laboratoire de Radio-Oncologie et de l'IRA. Je remercie particulièrement Jonathan, et Adrien. Grâce à vous, j'ai acquis des nouvelles compétences en biologie dont je suis très reconnaissante. Sans doute, je remercie également Louis pour son travail qui a beaucoup apporté pour la finalisation de ma thèse. C'est grâce à votre participation que ce travail de thèse est ce qu'il est aujourd'hui.

Ce travail de thèse est également le fruit de nombreuses collaborations, et c'est pourquoi je souhaite remercier l'équipe de PSI particulièrement Serena Psoroulas et Michele Tognò. L'équipe de CLEAR/CERN, notamment Pierre Korysko, Wilfrid Farabolini, Roberto Corsini et Manjit Dosanjh. J'ai sincèrement beaucoup apprécié le travail avec vous. J'adresse un merci tout particulier à Charlie Limoli, pour ses conseils, son encouragement et sa participation à ce projet.

Merci à Aymeric, Céline, Ron, Benoit, Jackie, Paola, Javier, Jeanette, Antoine, Louis et Kelly. Vous avez enrichi ma vie quotidienne pendant quatre années avec nos moments de joie, nos soirées, nos pauses café, mais aussi grâce à vos précieux conseils et votre soutien.

Il y a également tous ceux qui ont été un soutien précieux grâce à leur amitié : Emma et Daniela, mes amies et mes voisines au travail, les anciens amis de l'Université Paris-Sud et du CEA-Saclay, Mekan et Jean-Daniel, ainsi que les amies tunisiennes, Ameni et Nouha. Je tiens à exprimer ma gratitude envers vous. Vous m'avez apporté un soutien inestimable malgré la distance qui nous séparait.

Enfin, je tiens sincèrement à remercier du fond du cœur ma famille bien aimée, ma mère, mon père, mes frères Salah et Foued, pour leur soutien, leur amour, et leurs motivations qui ont joué un rôle déterminant dans ma réussite. Cette thèse est pour vous. Un grand merci également à la famille Desponds pour tous les précieux moments partagés ensemble. Je remercie aussi mon petit Xo pour son amour et sa douceur.

Ce travail de thèse et ce manuscrit sont dédiés à Kamel Kacem, Radhia Chatti, Salah Kacem et Foued Kacem pour leur amour et leurs encouragements inconditionnels.

Institutions & funding



This PhD work has been realized in the Radiation Oncology laboratory of the Oncology Department at the University Hospital of Lausanne (CHUV) and the University of Lausanne (UNIL), Switzerland. The project has been funded by the Swiss National Science Foundation (FNS CRS II5_186369).

Résumé en français

Aujourd'hui, la radiothérapie constitue, aux côtés de la chirurgie, de la chimiothérapie, des thérapies ciblées et de l'immunothérapie, un pilier de la thérapie moderne contre le cancer. Elle contribue au traitement de plus de 50% des patients atteints de cancer et est associée à d'autres thérapies pour éradiquer efficacement les cellules cancéreuses. Malgré les améliorations technologiques significatives dans l'émission de faisceaux et le guidage d'images qui permettent la radiothérapie conformationnelle, la toxicité au niveau des tissus sains reste un facteur limitant pour optimiser le contrôle tumoral. De plus, certaines tumeurs restent hautement radio-résistantes, échappant aux traitements avancés pour récidiver et métastaser. Par conséquent, l'un des défis ultimes dans notre domaine consiste à développer de nouvelles stratégies de radiothérapie pour surmonter ces limites. Dans ce contexte, notre équipe a conceptualisé et développé la radiothérapie FLASH (FLASH-RT), capable de changer les paradigmes médicaux. La FLASH-RT a le potentiel d'augmenter l'index thérapeutique dans tous les cancers. Cette approche innovante repose sur l'administration de débits de dose ultra-élevés (UHDR), qui sont au moins mille fois supérieurs aux débits de dose utilisés en radiothérapie conventionnelle (CONV). La FLASH-RT limite les dommages tissulaires normaux à une isodose cytotoxique donnée pour les tumeurs ; ce phénomène est connu sous le nom d'**effet FLASH**. Notre groupe a découvert et confirmé l'effet FLASH dans plusieurs modèles animaux expérimentaux (souris, rat, poisson zèbre, cochon, chat) et plusieurs organes (poumon, peau, intestin, cerveau). Aujourd'hui, de nombreux autres groupes ont également reproduit cet effet FLASH avec différents faisceaux. Cependant les mécanismes biologiques de la FLASH-RT restent méconnus et pourrait être la conséquence de l'interaction du rayonnement avec la matière, commençant à "t0" avec le transfert de l'énergie du rayonnement vers le substrat (stade physique, échelle femtoseconde). Des espèces chimiques hautement réactives sont produites et conduisent à des réactions chimiques qui se produisent à des échelles de temps très court allant de la picoseconde et à la milliseconde.

Les modifications chimiques produites par les rayonnements ionisants sont généralement décrites dans l'eau liquide, puisqu'elle constitue un composant majeur des organismes vivants. L'interaction des particules ionisantes avec l'eau est appelée radiolyse de l'eau. En conséquence, les molécules d'eau se brisent et forment des sous-produits hautement réactifs qui peuvent interagir avec des substances solubles (solutés). Les intermédiaires réactifs réagissent et disparaissent à des constantes de vitesse différentes, ce qui entraîne de nombreuses répercussions à l'échelle de temps biologique. **Ce travail de thèse visait à étudier le continuum possible existant entre la chimie sous rayonnement précoce et la radiobiologie.** J'ai étudié l'effet FLASH depuis les processus physico-chimiques initiaux entraînant la production d'espèces réactives de l'oxygène (ROS) dans l'eau, en ajoutant une molécule biologique l'ADN plasmidique pour finalement faire mes investigations sur des lignées cellulaires et des embryons de poisson zèbre (ZFE). J'ai utilisé différents faisceaux capables de fonctionner à des débits de dose CONV et UHDR pour réaliser ces expériences :

- 1) L'accélérateur linéaire expérimental d'électrons d'énergie intermédiaire validé pour l'effet FLASH (5,5 MeV) eRT6 Oriatron,

- 2) Le faisceau de protons en transmission (235 MeV), Gantry 1 au PSI,
- 3) Et le faisceau d'électrons de très haute énergie (VHEE) CLEAR (190-220 MeV) au CERN.

Avec tous les faisceaux étudiés, dans l'eau, les rendements primaires de H₂O₂ étaient similaires avec CONV et FLASH, suggérant qu'à l'échelle de temps de la microseconde (phase homogène de la chimie), les événements précoces sont similaires. Les rendements à long terme en H₂O₂ sont réduits dans l'eau irradiés avec FLASH par rapport à CONV. Ceci a été reproduit dans diverses conditions de tension d'oxygène, de capteurs et de température. Ceci suggère que FLASH modifie la production de ROS. Les dommages à l'ADN dans un système plasmidique non cellulaire sans mécanisme de réparation sont similaires après FLASH et CONV. Ces résultats montrent que les mesures physico-chimiques ne reproduisent pas la réponse biologique *in vivo*. Mais grâce aux ZFE, nous avons identifié le débit de dose instantané comme un facteur critique pour observer l'effet protecteur du FLASH, ce qui constitue une information essentielle pour la construction des futurs irradiateurs FLASH. Enfin, les résultats préliminaires obtenus *in vitro* et avec des lignées cellulaires et des ZFE déficients en facteur nucléaire érythroïde 2 lié (Nrf2 +/-) conforte l'idée selon laquelle l'irradiation FLASH est associée à une production réduite de ROS dans un modèle biologique.

Ce travail est le premier à corréliser les événements physico-chimiques associés au FLASH et à dévoiler les paramètres fondamentaux pour déclencher l'effet d'épargne du FLASH. Nos résultats ont des implications significatives au niveau physique et mécanistique ; ils montrent aussi que l'effet FLASH est un effet biologique qui défie une modélisation simple utilisant des environnements chimiques contrôlés.

Résumé de vulgarisation

Aujourd'hui, plus de 50% des patients atteints du cancer bénéficient un traitement de la radiothérapie. Une technologie qui utilise des rayonnements pour cibler précisément les cellules cancéreuses. Malgré les améliorations technologiques récentes, la radiothérapie traditionnelle peut entraîner des effets secondaires graves et permanents tels que la fibrose pulmonaire, la perte de mémoire etc. Pour surmonter ces défis, notre équipe a développé la radiothérapie FLASH (FLASH-RT), avec laquelle il est possible de détruire la tumeur sans effets secondaires. Cet effet découvert par notre équipe est connu sous le nom d'effet FLASH. Il est rendu possible par la réduction du temps d'irradiation en quelques millisecondes. Il pourrait améliorer l'efficacité du traitement des tumeurs et la qualité de vie des patients à long terme.

Le but de ma thèse était d'explorer la relation possible entre les événements de chimie sous rayonnement et la radiobiologie. J'ai étudié les effets de la technologie FLASH, sur une solution très simple d'eau puis je me suis intéressé à des modèles biologiques plus complexes, tels que des lignées cellulaires et des embryons de poisson zèbre. J'ai utilisé différents faisceaux, dont un accélérateur linéaire expérimental FLASH appelé eRT6 capable de délivrer des doses ultra-élevées au CHUV, un faisceau de protons en transmission au Gantry 1 au PSI, et l'accélérateur à haute énergie électrons CLEAR au CERN. Mes résultats montrent que les approches réductionnistes utilisant des solutions ne sont pas de bons substituts pour étudier l'effet FLASH. Mais notre découverte la plus importante concerne l'identification du débit de dose instantané comme paramètre clé pour déclencher l'effet d'épargne du FLASH, du moins avec les faisceaux d'électrons. Ces conclusions ont des implications importantes pour la conception de nouveaux dispositifs FLASH destinés aux futures applications cliniques.

Description of the manuscript organization

In **Chapter I**, a comprehensive analysis of the literature is provided, including the history, current advancements and the theoretical framework. This synthesis facilitates a better understanding of the physical, chemical, and biological processes that taking place when ionizing radiations interact with matter at Ultra-high dose rate. The general objectives of this doctoral work are then outlined, and the scientific articles produced during this work are presented in **Chapter II** of results to address the specific questions. Publication 1 is a review article that compares physico-chemical and biological mechanisms after FLASH and CONV. Publication 2 presents the first study establishing a correlation between (H₂O₂) production in water and zebrafish embryos' morphogenesis after FLASH and CONV irradiation with electron and proton beams. The impact of various electron beams with different temporal structure is detailed in publication 3 at the chemical, biochemical, and biological level. **Chapter III** provides the supplementary results and **Chapter IV** integrates the principal findings into a general discussion and perspectives.

Chapter I: Introduction

1- Radiotherapy: Past, present, and ongoing advancements

1.1 Radiotherapy, time of discovery

The late 19th century marked a prestigious era for radiotherapy, witnessing the awarding of three Nobel prizes for discoveries related to ionizing radiation (1). In December 1895, Röntgen unveiled X-rays (2) (**Figure 1**), swiftly followed in June 1896, by Becquerel's revelation of natural radioactivity. In 1898, by Marie Skłodowska and Pierre Curie who isolated radium (3) (**Figure 1**). These three groundbreaking discoveries laid the foundation for the two primary techniques of radiotherapy: Teleradiotherapy, utilizing a long source–surface–distance (SSD), later referred to as external-beam radiotherapy (EBRT); and brachytherapy, initially employing radium and later transitioning to Iridium sources, based on a short SSD. This period also witnessed successful transitions from laboratory discoveries to practical applications. In 1896, only six months after Röntgen's discovery, radiation therapy was applied to treat the first cancer patients for gastric cancer and basal-cell carcinoma in France, USA, and Sweden (4–6). The adverse effects of radiation also became apparent very swiftly (7), leading to immediate consideration of the concept of dose-limiting toxicity to optimize the therapeutic ratio and prioritize patient safety and quality of life.

1.2 Kilovoltage and Megavoltage era

By 1913, Coolidge tubes and radium tubes or needles had been developed to facilitate the routine application of radiation in cancer treatment (6) (**Figure 1**). Since then, the goal of radiotherapy has been to administer the lowest possible dose to organs at risk (OAR) while delivering 100% of the dose to the target gross tumor volume (GTV) or subclinical disease. A significant milestone during this period was the ability to measure radiation exposure using ionizing chambers (8) with the introduction of the first precise dose unit (the Röntgen unit) in 1932. However, with energies between 50 kV and 200 kV and the associated dose depth profile (DDP), delivering sufficient doses to deep-seated tumors proved challenging, primarily due to the unavoidable skin toxicity. In the 1920s, radiotherapy represented an oncological revolution, with the ability to cure early-stage laryngeal cancers without the need for the mutilation induced by permanent tracheostomy (9). The fundamental laws discovered at that time continue to underpin today's practices. Firstly, Bergonié and Tribondeau demonstrated in 1906 the different patterns of intrinsic radiosensitivity among cells and tissues (10). Secondly, the role of fractionation in creating a differential effect between cancer and normal cells was discovered (11). The common contemporary fractionation regimen of 2 Gy per fraction originated from Coutard's proposal of 200 Röntgen per fraction was already used. It was administered five times each week and was later aligned with the linear quadratic (LQ) model to characterize its biological effect (12). Thirdly, in 1928, the International Commission on Radiological Protection (ICRP) was established to address all questions related to radioprotection. In 1934, the discovery of artificial radioactivity (13) (**Figure 1**) earned Irène and Frédéric Joliot-Curie the Nobel Prize. This discovery, along with the work of Jones

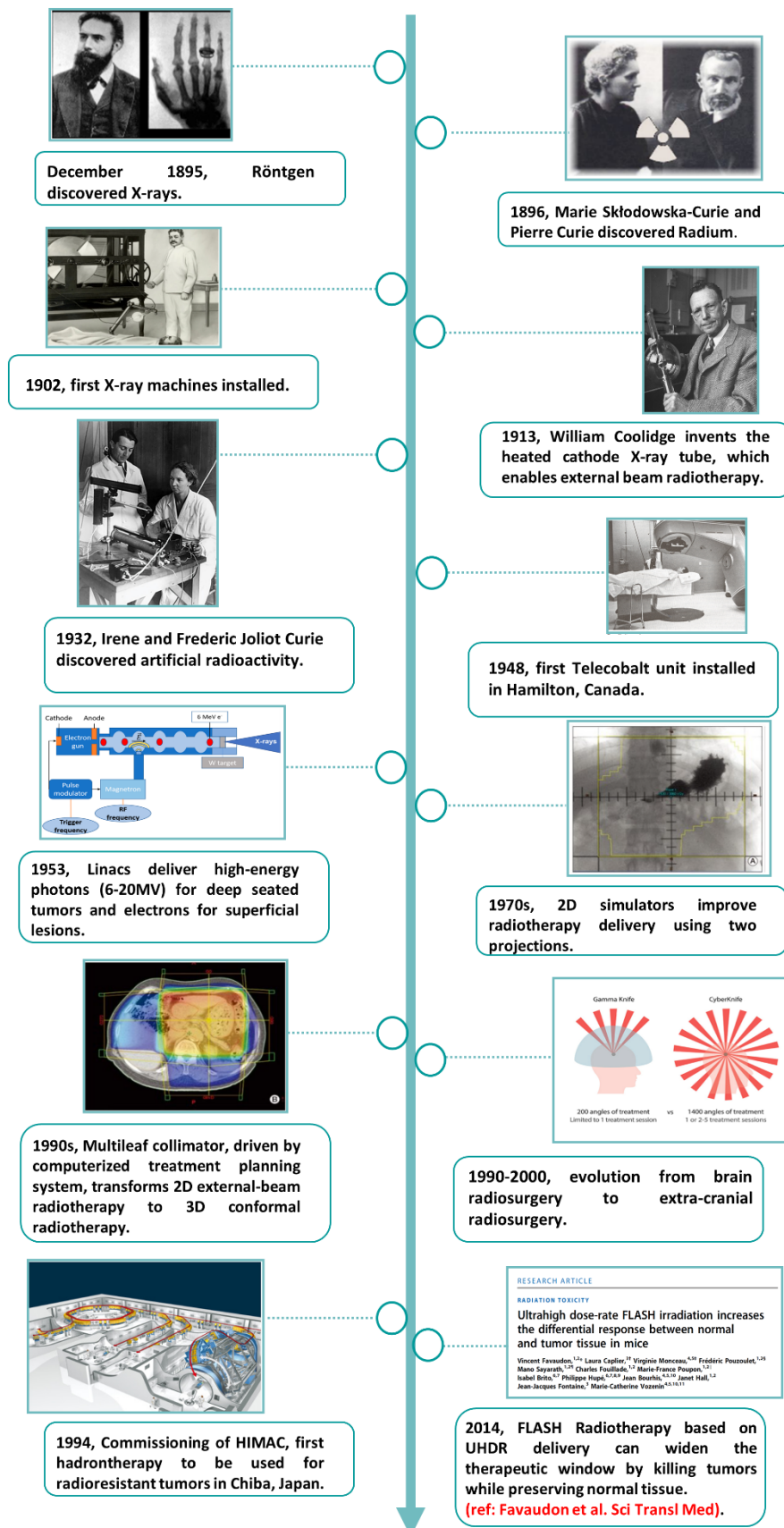


Figure 1 Evolution of landmark discoveries in radiotherapy.

and Cunningham (14), led to the adoption of Cobalt 60 (^{60}Co) as an alternative high-energy ray source for teleradiotherapy, offering a higher dose rate than possible with radium. In 1948, the first Telecobalt unit (**Figure 1**) was installed in Hamilton, Canada. Over the next ten years, more than 1000 devices were purchased by hospitals worldwide, and while they proved effective in curing cancer, delayed toxicity emerged as an evident side effect in the first long-term survivors (14). Subsequently, the introduction of 1.2 MeV photon beam energy allowed the delivery of doses up to 45-60 Gy to deeply seated tumors without exceeding the tolerance dose of OARs and preserving the skin at the entrance point for the first time. Moreover, these devices could also produce electron beams, well-suited for superficial targets (0.5-4.0 cm in depth) (15). During the same period, dosimetry saw dramatic improvement with the use of new detectors, and the unit of the radiation absorbed dose (Rad) was replaced by the Gray (Gy) where $1 \text{ Rad} = 0.01 \text{ Gy} = 0.01 \text{ J/kg}$. The introduction of treatment planning systems (TPS) utilizing the first computerized algorithms (16) further enhanced the accuracy of dose distribution. The International Commission on Radiation Units and Measurements (ICRU) defined the concepts of gross tumor volume (GTV), clinical tumor volume (CTV), planning target volumes (PTV), which remain essential parameters in current treatment planning (17). These concepts developed by ICRU serve as a basic, common language that harmonizes the prescription and the recording of radiotherapy treatment. Since then, radiotherapy has been regarded as a model in risk management and quality assurance programs. It significantly improved local control, enabled conservative treatment, and increased survival rates. Radiation oncologists have become integral members of multidisciplinary oncology teams, and radiotherapy has become a standard curative treatment in the oncologist's toolbox.

1.3 Computer-assisted: 3D conformal radiotherapy, IMRT & Stereotactic radiotherapy

The computerized tomography (CT) scan, developed by Hounsfield in 1971 (18), became clinically available in the 1980s. The evolution of radiation delivery progressed from 2D to 3D planning (**Figure 1**), facilitated by the integration of computers into radiotherapy planning (19). Planning and modeling using CT data, allowed for more precise prediction of radiation dose distributions. A significant shift occurred with the introduction of multileaf collimators, guided by computer algorithms (20), and the advent of new TPS providing beam-eye views (21). By sculpting in 3D, the target and avoiding OAR, radiation treatment could be applied with increased accuracy. Specific tolerance doses for OAR were defined through the use of dose-volume histograms and cumulative data on clinical tolerance and dose-effect correlations. The subsequent technical advancement allowed for further modulation of photon beam intensity during fractions and the utilization of inverse dose planning for treatment optimization through TPS. This advancement was termed intensity-modulated radiotherapy (IMRT). IMRT was particularly effective in treating patients with head and neck cancer by creating concave isodoses around the parotids. This technique enabled parotid preservation, reducing the occurrence of severe xerostomia often associated with traditional

2D radiotherapy, while maintaining a comparable level of local control. In the 1990s, Leksell designed the first stereotactic devices for treating intracranial benign or malignant lesions (22). These devices, initially called Gamma Units and later known as the gamma knife (**Figure 1**), utilized multiple ^{60}Co sources and non-coplanar small beams to deliver high doses into small target volumes with exceptional precision, using a stereotactic frame. This approach allowed for hypofractionation in a single fraction (23). Although the primary indications for these systems are intracranial lesions, including brain metastases, technological advancements in stereotactic body radiotherapy (SBRT) planning have extended its use to extracranial lesions, including those in the spine and mobile tumors. Clinical studies currently randomize patients to SBRT or surgery in operable cases, with SBRT demonstrating excellent outcomes compared to surgery, especially in patients with early-stage lung tumors (24).

1.4 4D radiotherapy

Another challenge in advancing radiotherapy technology is associated with the patient's specific shape, organ characteristics, and tumor movements. While highly conformal EBRT is increasingly utilized, efforts are being made to reduce the PTV by minimizing geometric uncertainty throughout the radiation course. Tumor and patient contours undergo changes in shape and volume over the 5-7 weeks of radiotherapy, necessitating an Image-Guided Radiotherapy (IGRT) approach. IGRT, utilizing kV control or cone-beam CT offline or online, can adapt to variations in the patient's position, tumor location, or organ movement (25,26). The clinical benefits of IGRT are currently under formal evaluation. Adaptive Radiotherapy (ART), a form of IGRT, involves "replanning" and occasionally optimizing the treatment method during radiotherapy, aiming to optimize the dose distribution based on changes in the patient's anatomy and the morphology of their organs and tumors. Addressing the challenge of moving targets, sophisticated equipment like the CyberKnife[®] was designed in the early 2000s (**Figure 1**), equipped with dedicated software for real-time tracking of moving targets.

1.5 Ion beam radiotherapy

In 1929, Lawrence and Livingstone, at the University of California in Berkeley, invented the cyclotron, a particle accelerator that is the forerunner of the machines used today in proton treatment facilities (27). Physicist Robert R. Wilson designed the Harvard cyclotron, initiating proton therapy in 1946 (28). The beam was first tested by the Lawrence Berkeley National Laboratory (LBNL) in 1954, and more than 2500 patients were treated with proton, helium, carbon, and neon ions. Despite encouraging results, the LBNL's clinical treatment program was interrupted in 1993 (29). Accelerated to high energies (70 to 400 MeV/u), proton therapy or hadrontherapy, a modality of radiation therapy based on the use of charged atoms accelerated to high energies (70 to 400 MeV/u), is proposed as a superior technique to eradicate radioresistant tumors as well as those located in critical organs. In 1994 the Heavy Ion Medical Accelerator (HIMAC) was constructed in Japan (**Figure 1**). The main advantage of

ions is their physical properties when interacting with matter and the resulting energy deposition. Ions exhibit a characteristic differential energy deposition, which is low at the beginning of the track and reaches a peak at the end of their trajectory, named the Bragg peak. By correctly choosing the energy of the ions correctly, they can be stopped in the tumor, unlike X-rays, which penetrate the entire body. The depth and magnitude of the Bragg peak are determined by the mass and energy of the particle. Ions are biologically more efficient than X-rays (relative biological effectiveness, RBE), theoretically allowing an increase in the therapeutic index of radiotherapies for the treatment of radioresistant tumors (e.g., glioblastoma and chordoma). These properties make hadron therapy a more powerful oncological technique. During treatment, ions may be delivered by i) passive spreading or ii) active spreading or scanning (30). Passive spreading is achieved by using scattering materials to sufficiently broaden and creating larger Bragg Peak over the total tumor volume. This technique is known as spread-out of the Bragg peak (SOBP). While passive scanning has been an effective and widely used technique in ion therapy, it has some limitations. The fixed nature of the devices means that adjustments cannot be made during treatment, making it less adaptable to changes in the tumor or patient anatomy. Nowadays, an alternative approach is the active spreading. It involves dynamical control of the position and intensity of the ion beam using magnetic or electrostatic fields. For example, pencil beam scanning (PBS), a technique used in proton therapy, implies delivering a narrow proton beam, referred to as a “pencil beam,” that allows for a more precise and targeted delivery of radiation. The narrow proton beam is controlled to move across the tumor volume with high accuracy. The use of SOPB in particle therapy can result in an increase in the entrance dose in front of the tumor, although it is lower when compared to X-rays. This residual effect on patients makes it a key limitation, in addition to the substantial machine cost.

Despite introduction of combined techniques and advancements in ballistic and imaging technology, the quality of life for cancer patients is still adversely affected by the toxicities induced by radiation therapy. Even though several preclinical studies have been conducted with the goal of reducing radiation-induced normal tissue injury, toxicity is still an issue. Furthermore, certain cancers remain highly radioresistant, eluding current treatment regimens and leading to recurrence and metastasis. To overcome these limitations and enhance treatment outcomes, it is imperative to propose innovative solutions in the field of radiation oncology. With this objective, our team in Paris and later in Lausanne has been at the forefront of developing FLASH radiation.

1.6 FLASH radiotherapy

A novel form of radiation therapy, known as FLASH-RT utilizes ultra-high dose rates, that are thousands of times higher, or more than the typical dose rates used in clinical practice. Our team discovered and documented the fact that FLASH-RT was well tolerated by normal tissues but was able to successfully eliminate tumors, an effect we named the FLASH effect. To date, the FLASH effect has been demonstrated using a prototype linear accelerator that delivers ultra-high dose rate electrons, as well with photon, proton, and carbon ion beams as well Reviewed in (31,32). The journey began in the 2010s, a paradigm-shifting set of experiments was conducted collaboration between V. Favaudon at Institute Curie (Orsay) and M.C. Vozenin at Institut Gustave Roussy (Villejuif) (33). The research was later transported to the University Hospital of Lausanne (CHUV) when M.C. Vozenin established her group in Lausanne in 2013. This study reevaluated the role of ultra-high dose rates in radiotherapy, assessing the effects of FLASH irradiation on both non-malignant and tumor tissue. It demonstrated that ultra-high dose rate irradiation can widen the therapeutic window by killing tumors while sparing non-malignant tissues (34,35) (**Figure 1**). The study utilized the Kinetron LINAC at Institute Curie (Orsay), a linear accelerator (Linac) originally built for studying pulsed radiolysis, capable of reaching extremely high dose intensities. Standard dose rates of electrons or γ -rays (0.03 Gy/s) and high dose rate electrons (> 40 Gy/s) were used to deliver a single dose of 15–17 Gy to the entire thorax region. Mice with orthotopic syngeneic lung tumors and human xenografted tumors showed equal levels of lung fibrosis and growth control with both dose rate modalities. Notably, no pulmonary fibrosis was observed when electrons were delivered with ultra-high dose rates, while tumor control remained unaltered. The FLASH unexpected impact has since been replicated in many other preclinical models, utilizing radiation of various qualities and in numerous laboratories worldwide, Reviewed in (31,32). Understanding how FLASH-RT works and the processes underlying the difference between normal and malignant tissue responses to FLASH-RT is currently one of the intense subjects of research in the field. One hypothesis is that ultra-high dose rates alter the initial physico-chemical processes, leading to changes in subsequent biochemical and biological cascades involved in tissue response; exploring this hypothesis is the focus of my thesis.

2- Types of ionizing sources in radiotherapy

Ionizing radiation (IR) is a form of energy produced by atoms, either in the form of electromagnetic waves for γ and X-ray radiation or in the form of particles for alpha, beta, and neutron radiation. This radiation possesses enough energy to detach electrons from their atoms, leading to the formation of ions, hence the term “ionizing radiation” (36). The action of ionizing radiations spans a broad timescale, from early physical processes to chemical effects and, finally, late biological effects. The following paragraphs will concentrate on radiation sources used in the project, specifically conventional X-rays, electrons, and protons. Before delving into the various radiation types, let’s review some essential definitions.

Dose: At the macroscopic level, the quantity of the energy absorbed in the medium due to a particle-matter interaction is measured by the dose (D), where the dose corresponds to the incident energy (dE, Joule) absorbed per unit mass of the target (dm, kg). The SI unit is expressed in $\text{J} \times \text{kg}^{-1}$ or given the special name “Gray” (symbol Gy).

Notion of LET effect: The absorbed energy emitted by IR in the medium is not uniformly distributed, as it results from events like excitations and ionizations of molecules along the particle track. To describe this non-uniform energy distribution, the concept of linear energy transfer (LET) was introduced (37). LET is the energy loss, dE, of a fast-charged particle per unit length, dx, traveled in the medium. $\text{LET} = -dE/dx$. The units used to express this linear energy transfer are: $\text{keV} \times \mu\text{m}^{-1}$ or $\text{eV} \times \text{nm}^{-1}$. The density of ionization events, or LET, is higher for radiation with heavy ions than for photons and protons. In the case of electromagnetic radiation, the defined LET comes from the secondary electrons ejected (Compton electrons). The LET depends on the nature of the radiation as well as the material traversed. As LET increases, the spatial distribution of free radicals in the tracks changes due to increased radical-radical recombination.

Notion of dose rate: The dose rate of an ionizing source is defined as the radiation dose absorbed (Gy) per unit of time (s^{-1}). Clinical dose rates or conventional (CONV) dose rates are relatively low in the range of 0.01 to 1 Gy/s. This means the overall irradiation time lasts for a couple of minutes depending on the delivered dose and the dose rate. Ultrahigh dose rates (UHDR) are above a prescribed threshold ≥ 100 Gy/s. In this case, the total irradiation time becomes relatively short, ranging from few microseconds to milliseconds. UHDR interactions with the matter and its biological impact are the focus of this study and are further described in the manuscript.

2.1 X-rays:

Conventional radiotherapy, relying on the utilization of high-energy photons (X-rays), is the prevailing approach in clinical settings. X-rays, a form of electromagnetic radiation, akin to visible, possesses higher energy light (**Figure 2**).

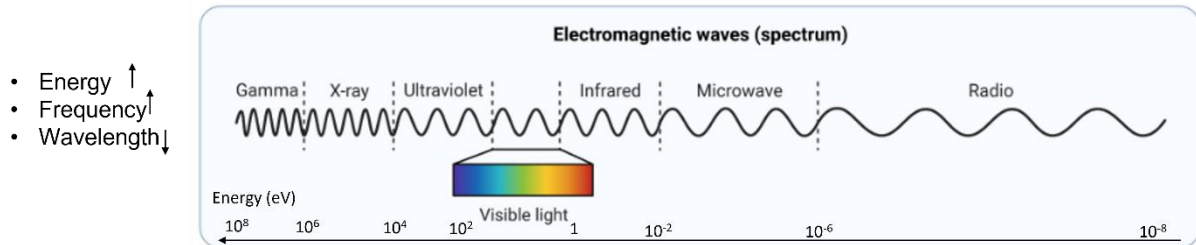


Figure 2 The electromagnetic spectrum. X-rays have higher energy than visible light. (Adapted with BioRender.com).

As they enter the body, X-rays experience gradual attenuation. Nevertheless, a substantial dose is delivered deep inside the body because, having zero mass and zero charge, they penetrate tissues and deeply, depositing energy along the entire length of their path. Typically, medical linear accelerators generate X-rays with energies ranging from few MeV (between 1 and 25 MeV) and with low dose rates in the range of 0.01 to 0.05 Gy/s. Their interaction with matter is driven by three physical processes: Photoelectric absorption, Compton effect and hole-electron pairs production (38), as illustrated in **Figure 3**.

The photoelectric process occurs in the range of $10^2 < E_0 < 10^6$ eV. The photon interacts with an inner shell electron of an atom in the absorbing medium, transferring its entire energy, and ejecting an energetic photoelectron (**Figure 3a**). Depending on the target atom's mass (Z , the atomic number) and the incident photon's energy ($h\nu$ incoming), the interaction probability varies. The photo absorption cross-section can be calculated by: $\sigma_{\text{photoelectric}} = Z^5 / (h\nu)$. In **Compton scattering**, the interaction process is inelastic, where incoming radiation loses energy upon being scattered to an angle θ from its initial direction (**Figure 3b**). The photons transfer part from their energy to an outer shell electron (the recoiled electron), emitted from the target atom. The energy range of this process is $0.1 < E_0 < 10$ MeV. In principle, Compton effect is a dominant effect in Curie therapy and conventional radiotherapy. When photon energy exceeds 1.02 MeV, **electron-positron pair production** may occur, where the incident photon, passing near the nucleus, converts into an electron and a positron due to strong field effects. Later the reaction of the e^+ and the e^- produces two γ -rays (**Figure 3c**). **Auger effects** can be observed in the case of the photoelectric effect where the innermost shell (K) of the target atom is ionized. The filling of the inner shell vacancy is readjusted by the emission of a secondary electron from the same atom (**Figure 3d**). The interactions of the latter with the target may also ionize inner-shell electrons, accompanied by the emission of the Auger electron; the residual atom then has two electron vacancies.

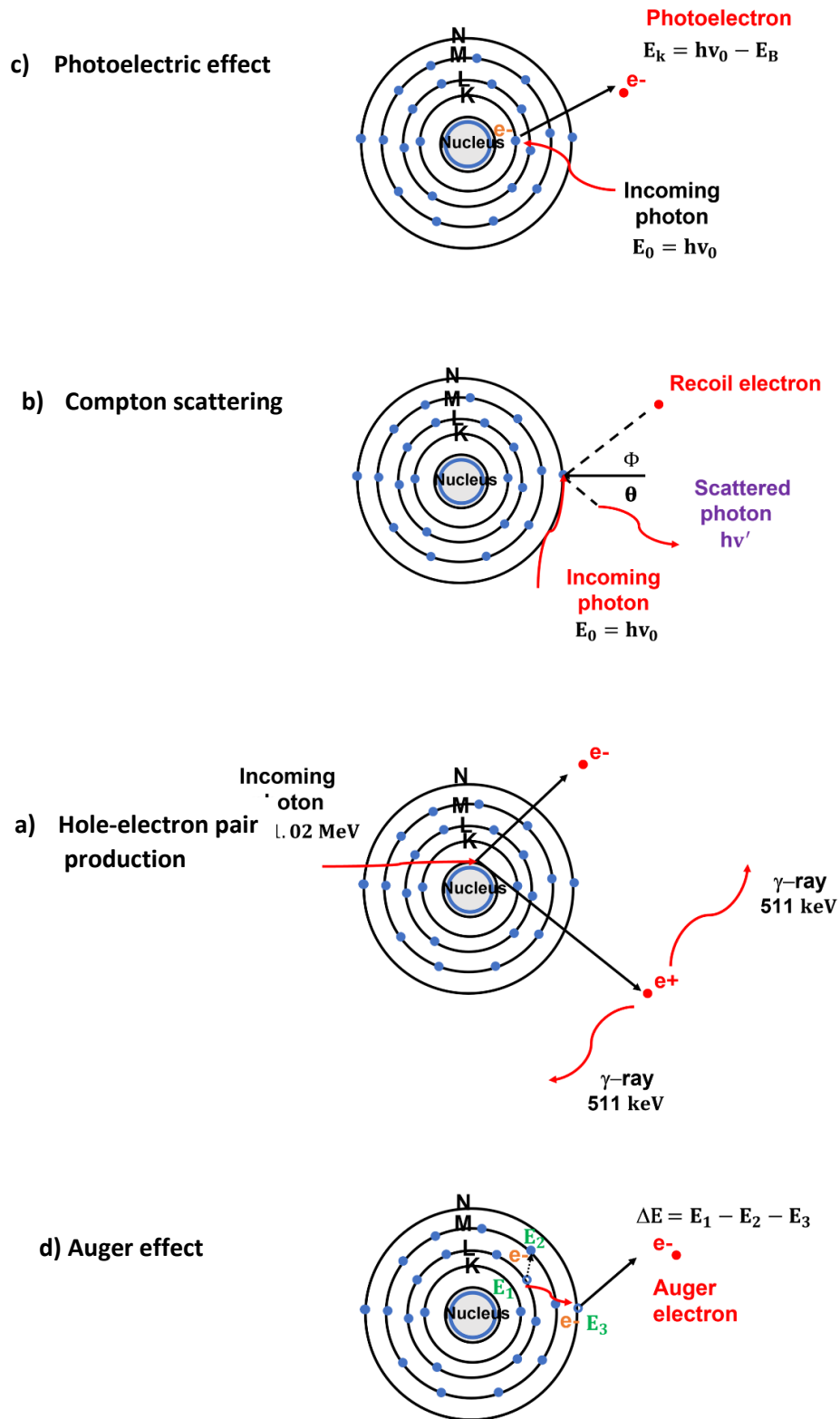


Figure 3 The major forms of interaction between photons and matter (Created with Biorender.com).

High-energy conventional photons penetrate tissue, facilitating non-invasive tumors treatment. Unfortunately, they lack selectivity and cause damage not only in abnormal cells but also in healthy tissues, inducing side effects in patients. This effect is explained by the physical properties of photons and their interaction with biological matter at the treatment's energy.

The photons used in this project are conventional X-rays of energies between 160-225 kVp from Pxi Precision X-ray at 0.037 Gy/s and RS200 at 0.07 Gy/s.

2.2 Energetic electrons:

The physics of charged particles is different than that of photons. Electrons create excitations and ionizations while traversing the matter, losing energy due to Coulomb interactions over a large width. Electrons, being negatively charged particles, penetrate matter more than protons. They lose some of their energy through various modes of interactions along their route: inelastic or elastic collisions with the nucleus or with bound atomic electrons (39).

In **inelastic collisions**, electrons lose a part of their kinetic energy (energy transfer) through Coulombic interactions with electrons in the traversed medium, leading to electronic excitations and ionizations of molecules and a slight deviation of the incident electron (momentum transfer). Although the energy transfer during each collision is low, the number of collisions is crucial for inducing biological damage. In **elastic interactions**, electrons do not lose energy but are highly deflected. This process is dominant for electrons of few hundred of eV, with its probability increasing with the atomic number (Z) of the medium and decreasing with the energy of the incident electrons (E_0).

When electrons with high kinetic energy (MeV) are decelerated by positively charged nucleus, they emit bremsstrahlung, a German term meaning named "breaking radiation," resulting in electromagnetic radiation (i.e., X-rays). The cross-section of this energy loss increases with the energy of the electrons and the atomic number of the absorbing medium. The interactions of these charged particles with condensed matter (excitations and ionizations) lead to the production of the primary track with emitted electrons from the target. The elastic and inelastic interaction collisions cause the electrons to travel nonlinearly, resulting in the corresponding track (spurs formation) shown in **Figure 4**.

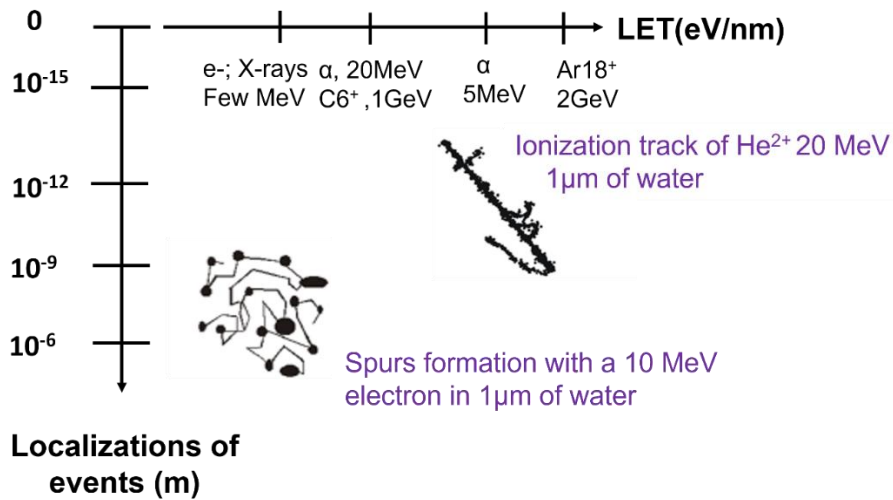


Figure 4 Comparison of track structure resulted from 10MeV electrons and 20MeV of He²⁺. Adapted from (36).

The electrons used in this project had intermediate energies of 5.5MeV from an experimental linear accelerator (linac) eRT6/Oriatron (PMB-Alcen) at CHUV operating at CONV and UHDR (0.1 Gy/s to 10⁷ Gy/s). Additionally, a linac of very high energy electrons (VHEE) of 190-220 MeV at CLEAR/CERN was used, delivered in CONV and UHDR modes (0.125 Gy/s to 10¹¹ Gy/s).

2.3 Protons:

Protons, being positively charged particles, have three main interactions with matter: inelastic Coulomb interaction with atomic electrons, elastic Coulomb scattering with atomic nuclei, and non-elastic nuclear interaction. The dominant interaction is **inelastic Coulomb interaction** with atomic electrons, which is crucial in detaching atomic electrons, a process significant in killing cells. Protons deposit energy along their path in matter, exhibiting a unique depth-dose distribution. A proton deposits energy along the transmission path and most of the energy is deposited in a steep and localized peak dose called the Bragg peak (**Figure 5**) (30). This unique energy profile of protons makes them suitable for treating tumors located in sensitive organs (head, neck, eyes) and childhood cancers (central nervous system tumors).

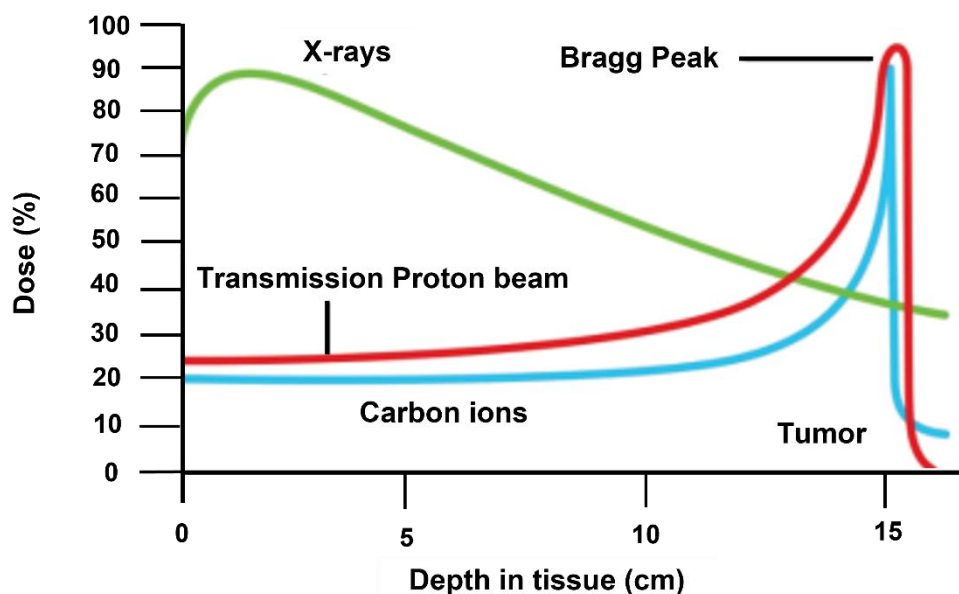


Figure 5 Comparison the dose deposition profile of X-rays and ions (protons and carbons) at the rising Bragg peak. Adapted from (40).

Energetic transmission protons of 235 MeV from the Paul Scherrer Institute (PSI) were used during this project, with LET = 0.2 keV/ μm at the transmission phase (TI) and 5.5 keV/ μm at the Bragg peak. PSI protons operated at CONV and UHDR dose rates (0.1-1 Gy/s and 1260-1400 Gy/s).

3- Cascade of events activated after radiotherapy.

3.1 Radiation-induced physico-chemical effects: Radiation chemistry

Radiation chemistry, a branch of chemistry, explores the chemical reactions in materials when they are exposed to ionizing energy. Its history dates back to before 1942 when it was coined by Burton (41). Pioneers like Skłodowska-Curie and Debierne observed gas bubbling from radium salt solutions in 1901, a phenomenon replicated by Giesel in 1902 (42) and Ramsay in 1903. The allure of radiation chemistry lies in its diverse applications and its ability to generate and explore nearly any reactive atomic species pivotal in chemical reactions, syntheses, industrial processes, or biological systems. This field's techniques apply to gaseous, liquid, solid, and heterogeneous systems. The early 20th century witnessed sustained progress and enthusiasm (43), aligning with simultaneous evolution of radiobiology and radiotherapy propelled by Despeignes and Grubbe—the pioneering physicians who first utilized X-rays for therapy in 1896 (44). In the 1920s, Fricke emphasized the need to establish a connection between radiation chemistry and radiobiology. Consequently, he founded a laboratory to investigate the early chemical steps preceding observable outcome in humans (45). Within this framework, the radiation chemistry of water and aqueous solutions took center stage due to water's unique importance, especially in biological systems. Furthermore, water serves as

the standard reference material in clinical radiation therapy, boasting absorption properties akin to biological tissues.

3.1.1 Notion of direct and indirect damage:

Radiation can damage cellular macromolecules either directly or indirectly. Direct radiation damage occurs when incoming radiation is absorbed by an atom, releasing an electron (i.e., secondary electron), which in turn causes damage to biomolecules. Indirect action takes place when the secondary electron interacts with a water molecule, a phenomenon known as water radiolysis, leading to the creation of reactive oxygen species (ROS). These ROS can migrate and damage biomolecules (46), as illustrated in **Figure 6**. Through both mechanisms, radiation has the potential to induce various types of damage, including DNA damage, lipid peroxidation, and protein oxidation.

The extent and severity of the radiation-induced lesions depend on the type of radiation, particularly the LET, with higher LET radiation causing a larger production of direct damage (47). In contrast, Low LET radiation (**Figure 6**), such as photons or energetic electrons, are admitted to have significantly lower probability of causing direct damage and their impact largely relies on indirect ROS-induced damage (48).

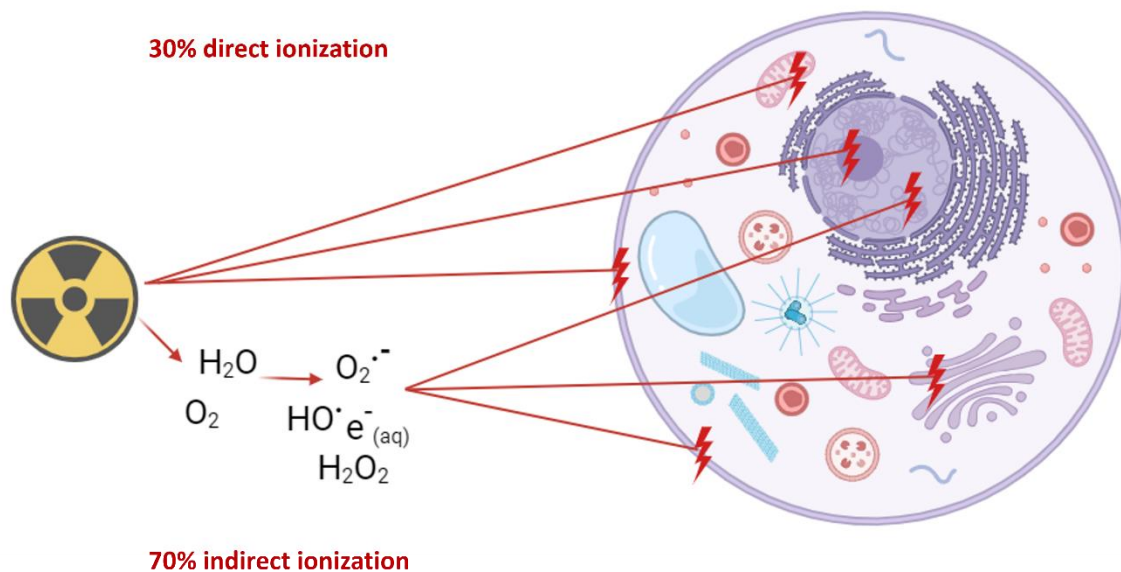
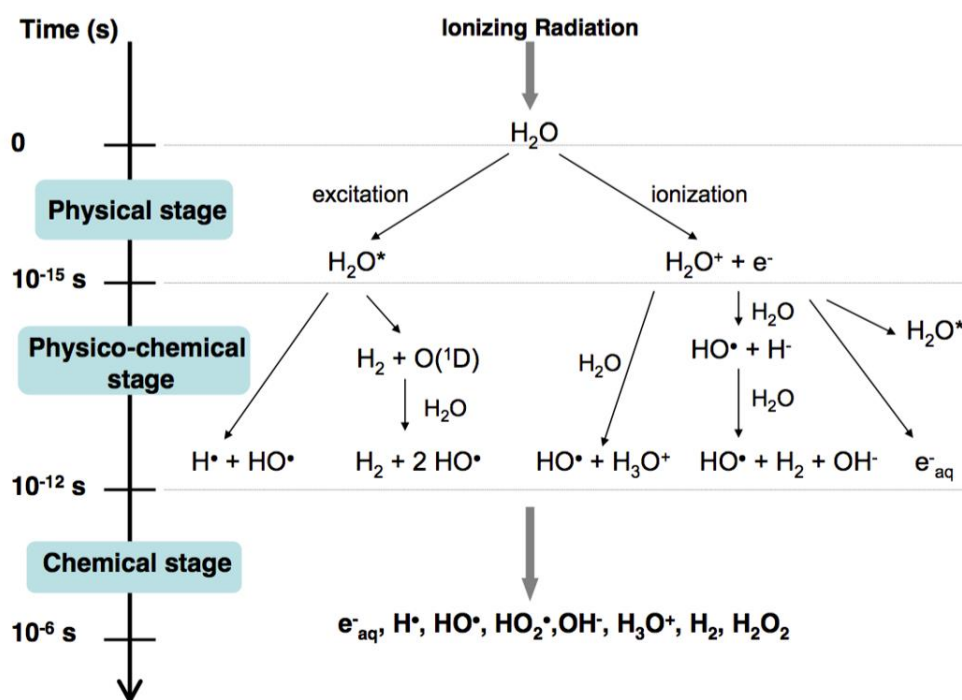


Figure 6 Direct and indirect actions of the ionizing radiations (low LET) with the biological macromolecules. Direct action is due to the direct ionization on the macromolecules whereas indirect action is mediated by free radicals produced by water and dioxygen radiolysis. (Created with Biorender.com).

3.1.2 Water radiolysis

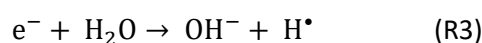
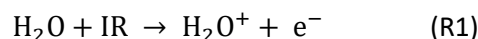
As mentioned earlier, radiation interacts with atoms or molecules in the cell, most likely water, to produce oxygen-derived free radicals that can either travel short distances and damage critical cellular targets such as DNA, lipids or proteins or continue to react with hydrogen and oxygen. These radiolytic events, however, occur on a very short timescale. These timescales can be classified as follows: **(i)** the physical stage, lasting approximately 1 fs (femto-second), **(ii)** the physico-chemical stage of non-homogenous chemistry lasting about 10^{-15} s - 10^{-12} s, and **(iii)** the chemical stage or homogenous chemical phase, which has the longest, albeit still short, lifetime of 10^{-12} s - 10^{-6} s. The different radiolysis stages and the corresponding reactions are illustrated in **Figure 7**, adapted from (49).



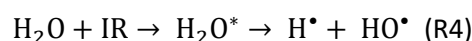
[Figure 7](#) Principal physico chemical reactions produced during water radiolysis (49).

The potential reactions involved in the radiolysis of water (50) are as follows:

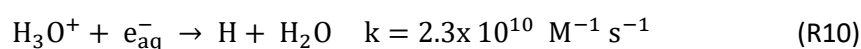
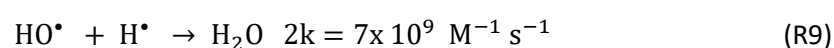
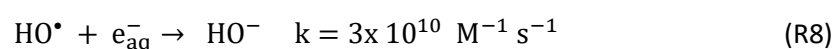
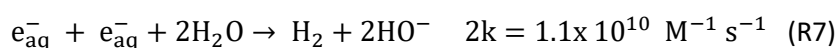
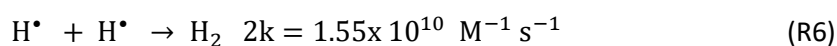
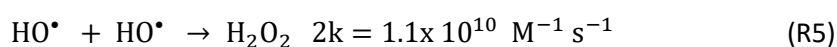
Ionization of water:



Excitation of water:



Following ionization and excitation of water molecules, the free radicals undergo a series of chemical reactions at different rates in a very short time scale. This stage is known by heterogenous phase of chemistry or physico chemical stage (**Figure 7**). Products of these radical reactions are either recombination of similar free radicals or new radical species. The free electron produced in reaction (R1) become stabilized after polarization of a water molecule and is referred to as an aqueous electron (e_{aq}^-) (R3). Hydrogen radical (H^\bullet) and hydroxyl radical (HO^\bullet) are also produced. All three free radicals are essential radiolytic products in biological systems (50). This stage results in the production of molecular reactive oxygen species, including H_2 and H_2O_2 resulting from recombination reactions (R5 to R7), and remaining free radicals will escape recombination reactions (R8 to R10) and continue to

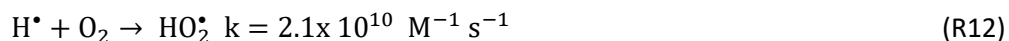
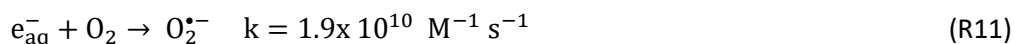


diffuse until reaching the homogenous phase of chemistry or the chemical stage, where at this stage, radical yields are called primary radiolytic yields, G° -values. These values have been computed for conventional photons, energetic electrons, and ions with significant LET (51–53). G° -values have been measured through pulse radiolysis or scavenging methods (51). They are expressed in $\text{mol} \times \text{J}^{-1}$ or in molecule/100 eV in the original literature. In **Table 1**, a summary table is provided of primary radiolytic yields under γ -rays in deoxygenated conditions.

[Table 1](#) Primary yields for water radiolysis under gamma rays (LET=0.23keV/ μm) in deoxygenated conditions (51).

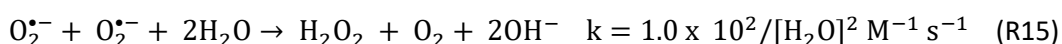
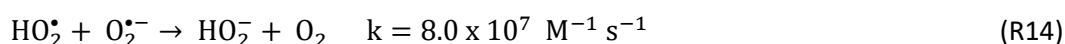
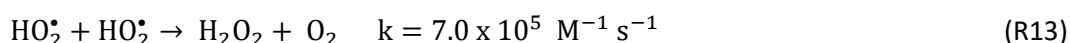
G-values [molecules/100eV]	H_2	$e_{(aq)}^-$	H^\bullet	H_2O	HO^\bullet	HO^-	H_2O_2	H_3O^+	$O_2^{\bullet -}/HO_2^\bullet$
γ -rays ^{60}Co	0.47	2.7	0.6	-6.9	2.8	0.1	0.72	2.85	0

After the homogenous stage of chemistry, at time scales greater than microseconds, radicals react further with oxygen (R11&R12).

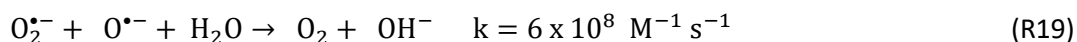
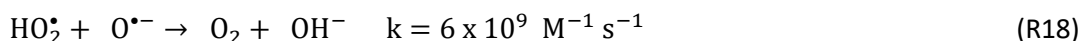
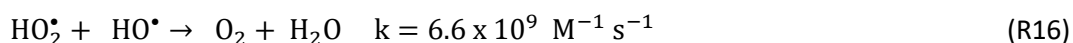


Reactions with oxygen will have important impact on radical-radical recombination and more protracted time points. Products of these reactions ($\text{HO}_2^{\bullet -}/\text{O}_2^{\bullet -}$) either recombine to form H_2O_2 according to reactions R13 to R15 or scavenge HO^\bullet radicals according to reactions R16 to R19.

Long rate reactions producing hydrogen peroxide:



Short rate reactions scavenging hydroxyl radicals:



At these late time points, the yields can be computed and are called long-term radiolytic yields, G-values. The chemical changes produced in water by ionizing radiation will have important biological repercussions when they occur within complex biological systems like cells and tissues. That is why it is important to study the impact of reactive species at the cell and tissue level.

3.2 Radiation-induced biological effects

Biological matter is composed of a variety of cellular “bricks,” including nucleic acids (DNA and RNA), proteins, and lipids (in cytosol and membranes) interacting with each other in a dynamic manner. They are all targets of ionizing radiation (IR), either directly or indirectly driven by ROS produced through water radiolysis. While ROS are also produced endogenously, they play essential roles in physiology and pathology (54). Radiation-induced exogenous ROS production alters the cell’s redox state, causing an imbalance between ROS and the cellular defense system known as the antioxidant response. This section highlights the role of cellular ROS during physiological and pathological conditions, as well as the role of ROS produced after radiotherapy.

3.1.1 Redox Properties of ROS in cells

Cellular ROS are produced by reactions involving up to 5% of cellular oxygen, while the remaining 95% is consumed in energy production and ultimately becomes water (55). ROS have similar electron configurations, but exhibit significant differences in structure, stability, solubility, chemical reactivity, and other physicochemical properties (**Figure 8**). They include superoxide anion ($O_2^{\bullet-}$), hydroxyl radicals (HO^\bullet), hydrogen peroxide (H_2O_2), alkoxy and peroxy radicals (RO^\bullet and RO_2^\bullet).

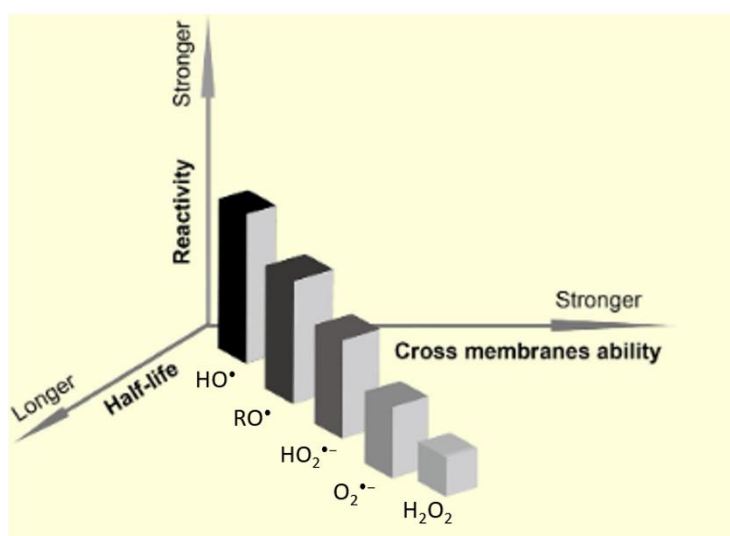


[Figure 8](#): Physicochemical properties of some reactive oxygen species (ROS). The gradual increasing trend of ROS in their ability to cross membranes is as follows: HO^\bullet , RO^\bullet , $HO_2^{\bullet-}$, $O_2^{\bullet-}$ and H_2O_2 . As the reactivity of the ROS weakens, the half-life of the ROS increases (56).

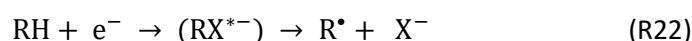
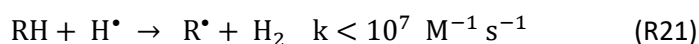
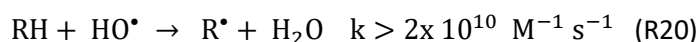
HO^\bullet possesses highly positive reactivity; it has been recognized as the most active ROS (**Table 2**) (57). HO^\bullet can oxidize almost all biological molecules through three main reaction types: hydrogen abstraction, addition, and electron transfer (57). HO^\bullet can abstract hydrogen atoms from some compounds, including H_2O and ethyl alcohol, and add to guanine and unsaturated fatty acids, forming other radicals (58–61). HO^\bullet can also react with chemical groups (nitrite, bicarbonate ion) or ions (halide ions) (62,63). HO^\bullet is very short-lived, with a half-life of 10^{-9} s; it can only react with biological molecules located in its vicinity. This prevents oxidative injury (64,65). Moreover, owing to the high reactivity of HO^\bullet , it also acts as a messenger by quickly reacting with other molecules under physiological conditions (64,66). On the contrary, elevated levels of HO^\bullet found in pathology or occurring after radiotherapy result in unavoidable cellular damage because of its high reactivity towards organic molecules, including lipids, proteins, and DNA. Hydroxyl radicals induce lipid peroxidation, protein misfolding, chromosome breaks, and formation of numerous micronuclei in dividing cells (67–69)

[Table 2](#) The standard reduction potential of main ROS forms (70).

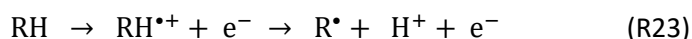
Couple	Standard reduction potential [V]
O ₂ /O ₂ ^{•-}	-0.35
O ₂ ^{•-} , 2H ⁺ /H ₂ O ₂	0.32
HO ₂ ^{•-} , H ⁺ /H ₂ O ₂	1.06
RO [•] , H ⁺ /H ₂ O ₂	1.60
HO [•] , 2H ⁺ /H ₂ O	2.31

The high redox potentials (E°) of alkoxy (RO[•]) radicals and peroxy (RO₂[•]) make them easily able to react with other biomolecules (**Table 2**) (71,72). The general pathway of formation of these radicals is the following: First, R[•] is produced from interaction of organic molecules with free radicals (HO[•], H[•] and e⁻_{aq}) in indirect action (R20-22) or by a direct action (R23).

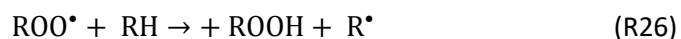
Indirect action:



Direct action:



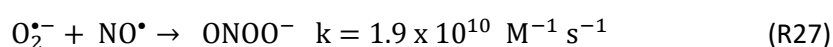
In a nearly diffusion-controlled manner, oxygen reacts with the organic radical R[•] to form the more stable peroxy radicals ROO[•] (R24), fixing the state of the radical in the biomolecule and presumably leading to chemically irreparable damage (73,74). ROO[•] can recombine with another ROO[•] radical to give alkoxy radical and oxygen. Finally, RO₂[•] can abstract H[•] from other molecules (R26), including membrane lipids, ascorbate, and nicotinamide adenine dinucleotide (NADH) (72,75,76), and initiates a new chain reaction.



The reactive activities of RO[•] and ROO[•] depend in part on their physicochemical properties. The reactive activity of aliphatic alkoxy radicals is higher than that of aromatic alkoxy and peroxy radicals because the electron donating group of aliphatic alkoxy radicals enhances the reactivity of alkoxy radicals (72). RO[•] and ROO[•] are transformed easily because of their high reactivity. Therefore, there are only minute quantities of RO[•] and ROO[•] in living systems, but they are essential to sustain normal physiological processes (77–79). RO[•] and ROO[•] can induce the formation of numerous other ROS that are essential to sustain physiological functions. The tyrosyl radical, derived from RO[•] and ROO[•], is implicated in a wide variety of biological

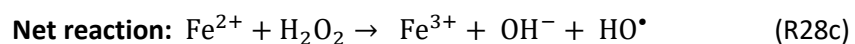
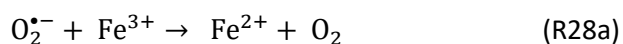
reactions, including photosynthesis and prostaglandin biosynthesis, under physiological conditions (80). In contrast, as sensitive sensor molecules, RO• and ROO• can exacerbate oxidative stress through secondary reactions, especially lipid peroxidation, under pathologic conditions or after exposure to ionizing radiation (81).

Superoxide (O₂^{•-}), with a single unpaired electron, is an unstable chemical entity and is easily converted into other ROS forms in the presence of specific enzymes like superoxide dismutase (SOD) and substrate such as ascorbate and hydroquinone (82,83). Under physiological conditions, O₂^{•-} detoxification is catalyzed by SOD, forming hydrogen peroxide (H₂O₂) and O₂^{•-} can react with nitric oxide (NO•) to form peroxynitrite (ONOO⁻) by endothelial nitric oxide synthase uncoupling (84) as shown in reaction 27.

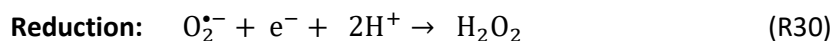


Superoxide anion radical toxicity also arises from its capacity to react through iron-catalyzed Haber–Weiss reaction vicious circle/Fenton chemistry (R28a, b, and c) leading to the formation of OH•.

Haber – Weiss reaction – vicious circle:



The reactivity of O₂^{•-} is dependent on the chemical environment (85). The disproportionation reaction of O₂^{•-} has been demonstrated to occur fastest at pH 4.7, and the oxidizing capability of O₂^{•-} is highly proton-dependent (83,85,86). It is also worth noting that O₂^{•-} is not only an oxidant (R29) but also a reductant (R30).



O₂^{•-} can reduce organic redox species, such as quinines (87). Although O₂^{•-} can oxidize or reduce substrates, it does not react with most biomacromolecules in organisms (70), as O₂^{•-} lacks the capability to cross biological membranes. Membranes crossing of O₂^{•-} can only occur through anion exchange proteins that are present only in specialized cytomembranes and subcellular compartments, such as mitochondrial inner membranes (88) and endosomes (89). This property also accounts for the specificity of redox signal transduction mediated by O₂^{•-} (70,90). Under physiological conditions, the O₂^{•-} concentration is approx. 10⁻¹¹ M (91), which is necessary for certain types of physiological signal transduction. Excessive O₂^{•-} production upon IR exposure can alter the intracellular redox balance and promote reactions with other radicals to form more reactive species and leading to oxidative damage.

H₂O₂ is a small, hydrosoluble, and diffusible molecule. It has a longer half-life than other ROS, such as O₂^{•-} and HO[•], but is poorly reactive with most biomolecules even at millimolar concentrations (92,93). H₂O₂ is best characterized as a 2-electron oxidant that is subject to reaction with proteins with thiol groups, (94) but not all thiol proteins can rapidly react with H₂O₂ at physiological pH in the absence of catalytic assistance. For example, cysteine and glutathione possess very low-rate constants (< 5 M⁻¹·s⁻¹) for their reaction with H₂O₂ under physiological conditions (pH 7.4, 37°C) (92,95). There are a few thiol-containing proteins, such as the various peroxidases and catalases, with significant rate constants for reaction with H₂O₂ in biological systems (92,95,96). Moreover, it has been demonstrated that H₂O₂ can cross biological membranes through aquaporins (97,98). Based on the physicochemical properties of H₂O₂, many reports have suggested that H₂O₂ play a role as a molecular messenger (92,95,96). On the opposite side, in case of oxidative stress like the one induced by ionizing radiation, accumulated hydrogen peroxide is converted into hydroxyl radicals by a Fenton-type reaction (R27b) and results in multiple cellular lesions. For example, H₂O₂ oxidizes protein cysteinyl residues, creating sulfenic acid adduct that can form disulfide cross-links with other cysteines (99). It is also a potent mediator of inflammation and immune response released by neutrophils and macrophages.

3.1.2 Sites of ROS production in cells

Reactive oxygen species are produced under normal physiological conditions in cells through four main pathways: (i) the electron transport chain in the mitochondria, (ii) enzymatic processes involving the nicotinamide adenine dinucleotide phosphate (NADPH) oxidase (NOXs) family of enzymes in the cytosol, and (iii) reactions occurring in the peroxisomes or in the (iv) endoplasmic reticulum where H₂O₂ is produced during protein folding (100).

ROS production in mitochondria

Mitochondria serve as the central regulators of aerobic energy production. The process involved in this energy production is known as oxidative phosphorylation (OXPHOS), where cells generate energy (phosphate bonds) in the form of adenosine triphosphate (ATP) through the reduction of oxygen. This process takes place in the electron transport chain (ETC) located within the inner membranes of the mitochondria, known as cristae (**Figure 9**) (101). The ETC comprises transmembrane protein complexes (I-IV) and the freely mobile electron transfer

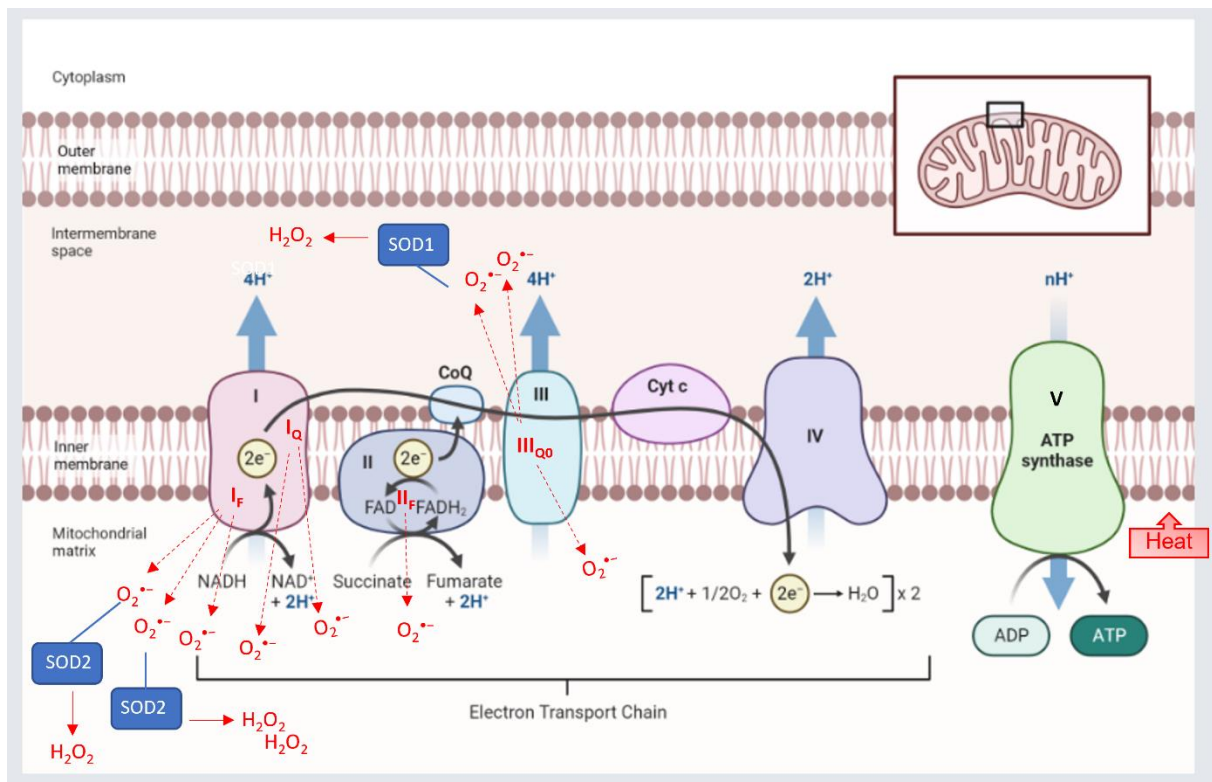


Figure 9 Generation of electron leaks and proton leaks in the electron transport chain. Electrons derived from oxidizable substrates are passed through CI/III/IV or CII/III/IV in an exergonic process that drives the proton into the IMS of CI, CIII and CIV. The energy of the proton gradient drives the ATP synthesis by CV. The sites of superoxide production in each complex are also indicated in red, including sites IF and IQ in CI, sites IIF in CII and site IIIQ0 in CIII. The $O_2^{\bullet-}$ released into the mitochondria matrix or the intermembrane space (IMS) can be catalyzed by superoxide dismutase 1 or 2 into H_2O_2 that may diffuse into the cytoplasm. The long black arrow indicates electrons pathways. The black arrows indicate substrate reactions. The red dotted arrows indicate the electron leak or superoxide production. The blue arrows show the protons movement via proton pump across the inner mitochondrial membrane (IMM). Q ubiquinone; C, cytochrome C. Adapted from (102) (Created with BioRender.com).

carrier's ubiquinone and cytochrome c. Electrons traverse this chain of complex proteins with increasing reduction potential (CI, CII, coenzyme Q, CIII, cytochrome C, and CIV), leading to the release of energy. While a portion of this energy is dissipated as heat, the rest is utilized to pump hydrogen ions (H^+) from the mitochondrial matrix to the intermembrane space (IMS), establishing a proton gradient. This gradient enhances the acidity in the IMS, resulting in an electrical difference with a positive charge outside and a negative charge inside. Crucially, for cellular energy production, the energy of the proton gradient powers ATP synthesis in F_1F_0 ATP synthase, also known as complex V (101).

Mitochondria are significant source of cellular ROS. Under physiological normal conditions, 0.2-2% of the electrons in the ETC diverge from their regular transfer path. Instead, they directly leak out of the ETC and react with oxygen, producing superoxide anion ($O_2^{\bullet-}$) or hydrogen peroxide (H_2O_2) (103,104) (**Figure 9**). There are 11 sites of production of $O_2^{\bullet-}$ and/or H_2O_2 associated with substrate oxidation in the ETC (105). ROS are primarily generated in

complex I (CI) during the electrons transfer from NADH to CoQ. In this location, inhibitors of electron transfer, such as rotenone and piericidin, can increase ROS production. Complex II (CII) typically production exhibits negligible ROS production under normal conditions, but increased ROS production is observed in diseases related to CII mutations. Complex III (CIII) produces small amounts of ROS, which are relatively minor compared to the ROS production in CI (106). In CIII, electrons are transferred through the Q-cycle. During this process, (QH₂) is oxidized to ubisemiquinone (QH⁻). Before this oxidation occurs, an electron can directly leak to O₂, forming a superoxide anion that can be released into both the matrix and intermembrane space (IMS) (107,108). The O₂^{•-} released in the IMS can permeate through the mitochondrial membrane into the cytosol via anions channels (109). Alternatively, O₂^{•-} can be converted to H₂O₂ by superoxide dismutase (SOD). H₂O₂ freely disperses through the outer mitochondrial membrane, acting as an intracellular signaling molecule and affecting physiologically function through the direct modification of amino acids (110). Complex IV (CIV) is less likely to produce ROS because in this complex, O₂ is bound to redox-active metal centers such as heme (Fe_{a3}²⁺) or is negatively polarized to O₂⁻. This arrangement allows O₂ to receive three electron equivalents, providing complete reduction of O₂ and minimizing ROS production (111). Besides the ROS-producing pathways, mitochondria also possess ROS buffering systems, including the glutaredoxin (Grx), glutathione (GSH) and thioredoxin (Trx) systems (112). The dismutation of O₂^{•-} into H₂O₂ is facilitated through superoxide dismutase (SOD) family proteins (113). In the matrix, this primarily occurs through SOD2 (MnSOD: manganese-dependent superoxide dismutase), while in the intermembrane space, it is performed by SOD1 (Cu/Zn-SOD: copper/zinc-dependent superoxide dismutase) (**Figure 9**). Then, H₂O₂ is decomposed into O₂ via the GSH redox system, which includes glutathione reductase (GR), glutathione-peroxidases (GPX), and peroxiredoxins (PRDXS) (114).

Cytosolic ROS production by NADPH oxidase enzymes

The NADPH oxidase (NOX) family, comprising seven isoforms (Nox1-5 and Duox1-2), is acknowledged as a primary source of cytosolic ROS (115). This family consists of membrane-bound proteins that facilitate the electron transfer across membranes. They generate superoxide by transferring electrons from the intracellular electron donor NADPH across the membrane, coupling a single electron with molecular oxygen to produce O₂^{•-}. This O₂^{•-} can subsequently be converted into other ROS forms (116,117) (**Figure 10**).

ROS produced by the NOX enzymes are involved in a variety of physiological and pathological states, including development, infection, immunity, metabolic processes, and cell death (117,118). NOX acts as a regulator of cell responses carried out in lymphocytes, fibroblasts, endothelial cells, myocytes, and chondrocytes, moderating ROS levels (119). O₂^{•-} produced by NOX in different subcellular locations occurs through distinct processes and serves varying functions, underpinning the concept of ROS compartmentalization (120). Vascular NOX can generate superoxide species within minutes to hours (121), whereas neutrophilic NOX releases dioxygen radical almost instantaneously (122). O₂^{•-} produced by NOX predominantly

transfers electrons from NADPH to extracellular oxygen in lymphocytes, forming $O_2^{\bullet-}$, while in vascular cells, it appears to be mainly released intracellularly (123).

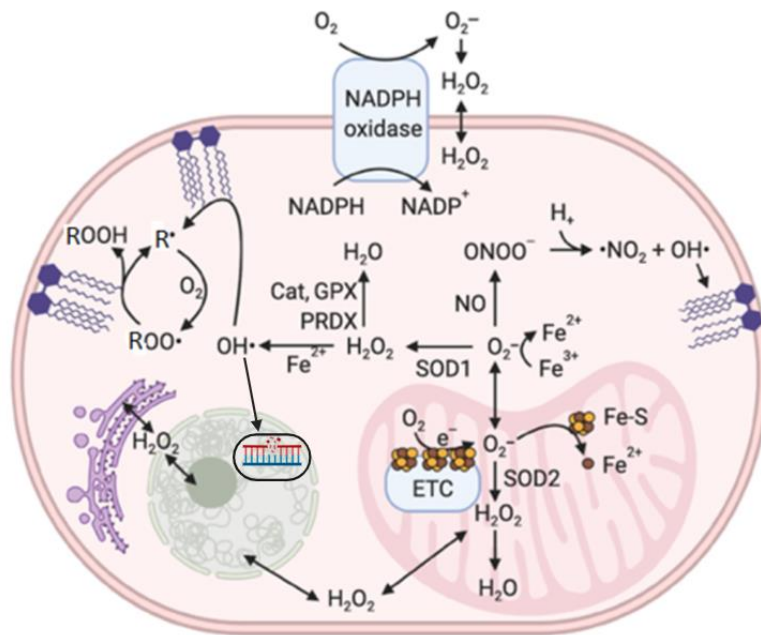


Figure 10 Sites and targets of ROS in the cell: Superoxide $O_2^{\bullet-}$ is produced extracellularly by NADPH oxidase or intracellularly by the mitochondrial electron transport chain (ETC). In the mitochondria, it targets iron–sulfur (Fe-S) clusters to release iron (Fe^{2+}) and reduces ferric iron (Fe^{3+}) to ferrous iron (Fe^{2+}). $O_2^{\bullet-}$ is dismutated to hydrogen peroxide (H_2O_2) by superoxide dismutases (SOD1, SOD2). H_2O_2 diffuses through membranes to react with proteins and DNA and is detoxified to water by cellular peroxidases [catalase (Cat), glutathione peroxidase (GPX), peroxiredoxins (PRDX)]. $O_2^{\bullet-}$ produces peroxynitrite ($ONOO^-$) through a reaction with nitric oxide (NO). The hydroxyl radical (HO^\bullet) is formed from the reaction of H_2O_2 with Fe^{2+} and the decomposition of $ONOO^-$. It initiates the lipid peroxidation cascade. First, HO^\bullet reacts with lipids to form lipid radicals (R^\bullet), which react with oxygen to form lipid peroxide radicals (ROO^\bullet). ROO^\bullet reacts with lipids to reform R^\bullet plus lipid peroxides (ROOH) and the cycle continues. Excessive lipid peroxidation leads to ferroptosis. HO^\bullet radical reacts also with nucleus components (DNA and RNA) to cause strand breaks. Adapted from (124).

In lymphocytes, superoxide can be rapidly generated via NADPH oxidase catalysis and is primarily expelled from the cell, aiding in the swift eradication of invading pathogens. NOX also plays a role in inducing apoptosis, acting as a crucial regulator of lipid raft–derived signals (125). ROS produced by NOX1, NOX2, and NOX4 are also involved in ferroptosis—an iron-dependent, regulated form of cell death caused by excessive lipid peroxidation—in cancer cells, highlighting NOX’s extensive role in programmed cell death (126,127). Oncogenes and tumor suppressor genes can affect NOX activity in ferroptosis. For example, inactivation of the tumor suppressor genes can influence NOX activity in ferroptosis. For instance, inactivation of the tumor suppressor gene p53 inhibits the nuclear accumulation of dipeptidyl peptidase-4/Cluster of differentiation 26 (DPP4/CD26). thereby stimulating plasma membrane–associated DPP4-dependent lipid peroxidation. The formation of the DPP4-NOX1 complex leads to cell death (126). During Rat Sarcoma protein (Ras) activation, NOX1-induced ROS promote ferroptosis by activating the Extracellular Signal-Regulated Kinase (ERK) signaling

pathway (128,129). Currently, further research is required to elucidate the potential signaling pathways which NOX is involved in ferroptosis in cancer cells.

Peroxisome

Peroxisome, similar to mitochondria, are essential organelles in aerobic metabolism and play a crucial role in regulating key processes such as α - and β -oxidation, glyoxylate metabolism, amino acid catabolism, the pentose phosphate pathway (PPP), ketogenesis, polyamine oxidation and isoprenoid and cholesterol metabolism (130). They also serve as significant source of ROS. Peroxisomes produce H_2O_2 through an array of oxygen-consuming oxidases (**Figure 11**), including ACOX (acyl-CoA oxidases), D-amino acid oxidase, D-aspartate oxidase, polyamine oxidase, xanthine oxidase (which also produces $O_2^{\cdot-}$), L- α -hydroxy acid oxidase, and L-pipecolic oxidase (131,132). However, unlike mitochondria, peroxisomal electron transfer does not result in ATP generation. Instead, free electrons are transferred to H_2O , forming H_2O_2 (131). Additionally, peroxisomes can produce nitric oxide (NO^*) through the catalysis of L-arginine to nitric oxide by nitric oxide synthase (NOS). NO^* can react with $O_2^{\cdot-}$ radicals to form peroxynitrite ($ONOO^-$), a potent oxidant. H_2O_2 and NO^* can cross the peroxisomal membrane and participate in cellular signaling (133). Similarly to mitochondria, peroxisomes house numerous scavenging enzymes, including GPX, CAT, Prdx1 and 5, peroxisomal membrane-associated protein 20, SOD1, and SOD2 (131,134).

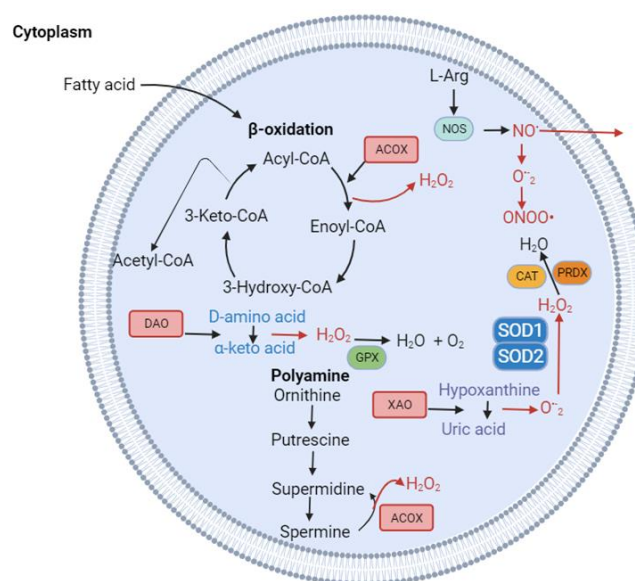


Figure 11 Peroxisomal reactive oxygen species (ROS) and metabolism. Peroxisomal ROS are produced as byproducts of enzymatic reactions within β -oxidation, polyamine synthesis, d-amino acid deamination, and hypoxanthine oxidation and have been found to be key regulators of pexophagy. ACOX indicates acyl-coenzyme A (CoA) oxidases; ATM, ataxia-telangiectasia mutated; CAT, catalase; CoA, coenzyme A; DAO, d-amino acid oxidase; GPX, glutathione peroxidase; LC3, light chain 3; mTOR, mammalian target of rapamycin; PAO, polyamine oxidase; PEX, peroxin; PRDX, peroxiredoxin; SOD, superoxide dismutase; TSC1, tuberous sclerosis protein 1; ULK1, uncoordinated 51-like kinase 1; XAO,

xanthine oxidase; NOS, Nitricoxide synthase and L-Arg, L-Arginine. Adapted from (102) (Created with BioRender.com).

ROS and the Endoplasmic Reticulum (ER)

Protein folding is highly sensitive to ER redox status, and the dysregulation of disulfide bond formation in response to ER stress increases luminal oxidative stress, leading to a decline in ER function (135). One of the best-understood routes for disulfide bond introduction into folded proteins is the protein disulfide isomerase (PDI) and endoplasmic reticulum oxidoreductin 1 (ERO1) pathway (**Figure 12**).

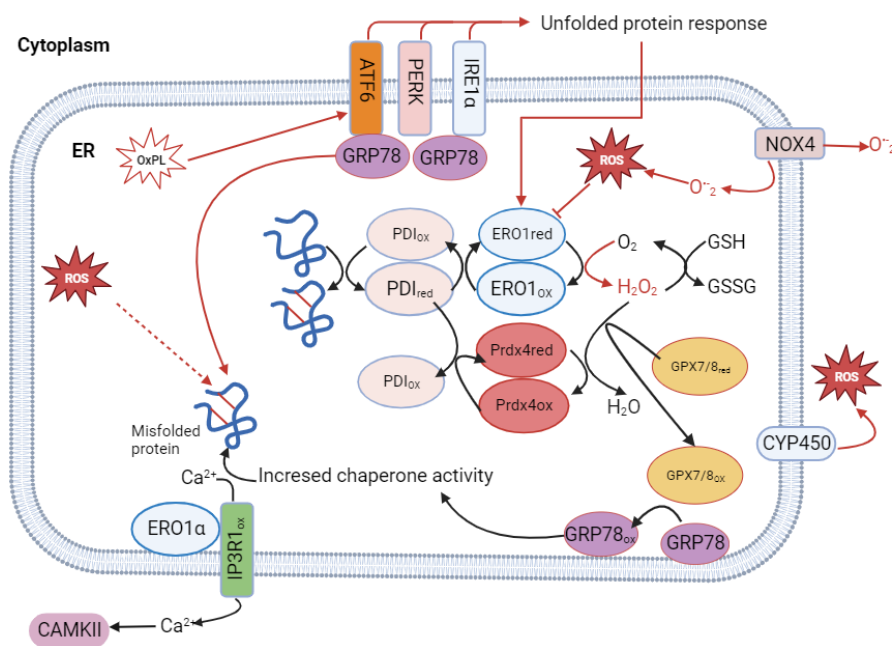


Figure 12 Endoplasmic reticulum and reactive oxygen species (ROS). The endoplasmic reticulum (ER) is highly sensitive to redox status, and altered ROS signaling can influence protein folding, Ca²⁺ release, and mitochondrial respiration. ATF6 indicates activating transcription factor 6; CAMKII, Ca²⁺/calmodulin-dependent protein kinase II; ER, endoplasmic reticulum; ERO1, ER oxidoreductin 1; GPX, glutathione peroxidase; GRP78, glucose-regulated protein, 78 kDa; GSH, glutathione; GSSG, glutathione disulfide; IMS, intermembrane space; IP3R, inositol 1,4,5-trisphosphate receptor; IRE1α, inositol-requiring enzyme 1α; MCU, mitochondrial calcium uniporter; NOX, nicotinamide adenine dinucleotide phosphate (NADPH) oxidase; OxPL, oxidized phospholipid; p66shc, SHC-transforming protein 1 isoform p66; PDI, protein disulfide isomerase; PERK, protein kinase R (PKR)-like endoplasmic reticulum kinase; and Prdx, peroxiredoxin. Adapted from (102) (Created with BioRender.com).

PDI introduces disulfide bonds through thiol oxidation in folding substrates, leaving PDI in a reduced state. Reduced PDI is reoxidized through ERO1, which transfers acquired electrons through a flavin adenine dinucleotide cofactor to molecular oxygen, forming H₂O₂. ER H₂O₂ can further be used by Prdx4 to reoxidize PDI, thereby increasing the efficiency of ERO1-mediated disulfide bond transfer (136,137). Overexpression of a human hyperactive mutant of ERO1 induces severe oxidative stress and the induction of the unfolded protein response

(UPR), an ER stress response involved in the pathogenesis of metabolic and cardiovascular diseases, highlighting the sensitivity of the ER to changes in redox balance (138). Furthermore, UPR activation can induce ERO1 activation, leading to increased oxidative stress and sustained UPR signaling, while administration of antioxidants can attenuate the UPR and improve downstream protein secretion (139). In addition to the PDI/ERO1 pathway, ROS are produced through the membrane-associated monooxygenase system via cytochrome P450, cytochrome b5 reductase, and through ER-localized NOX4 (140–142).

3.1.3 ROS detoxification in cells

Under physiological conditions, cells generate ROS and reactive nitrogen species (RNS) as an unavoidable consequence of the mitochondrial respiratory chain and cellular metabolism. These species are potentially harmful but are used as intracellular signaling molecules. To ensure ROS/RNS signaling is maintained and oxidative damage avoided, cells possess an array of antioxidant systems (124). The acute response is carried out by glutathione peroxidase (GPX), catalase (CAT), and superoxide dismutase (SOD) to maintain redox homeostasis. For example, catalase dismutates H_2O_2 to H_2O and O_2 or reduces H_2O_2 to H_2O by oxidizing hydrogen-donating compounds (143). Furthermore, there is a non-enzymatic antioxidant contribution by glutathione (GSH) and thioredoxin (TRX). The availability of GSH and TRX is made possible by NADPH, which maintains both in a reduced state. The longer-term response to oxidative stress involves metabolic reprogramming driven by genetic factors (54).

Acute exposure to ROS activates NADPH production by glucose-6-phosphate dehydrogenase (G6PD). For instance, non-toxic levels of H_2O_2 (1–100 nM) (54), leads to the activation of G6PD and reroute glucose metabolism from glycolysis through the oxidative arm of the pentose phosphate pathway (PPP) toward nucleotide synthesis, thereby allowing increased reduction of NADP^+ to NADPH (144) (**Figure 13A**). This rapid metabolic rerouting is due to a decrease of the negative feedback regulation of G6PD activity exerted by NADPH, which occurs constitutively under non-stressed conditions (145). ROS drive the acute depletion of NADPH and, therefore, the rapid metabolic switch. Consequently, the increase in NADPH enables GSR1 and TXNRD1/2 to augment the GSH and TXN1/2-based antioxidant systems, subduing ROS to homeostatic levels.

If cells are exposed to non-toxic doses of H_2O_2 for a short period (e.g., 15 min), they utilize redox switches in glyceraldehyde 3-phosphate dehydrogenase (GAPDH) and pyruvate kinase M2 (PKM2) to inhibit glycolysis and enhance glucose catabolism via the PPP (**Figure 13B**). This induces an accumulation of upper glycolysis intermediates and a spill-over of glucose-6-phosphate into the oxidative arm of the PPP. The redox switch in GAPDH is controlled by the amino acid residue Cys-152, and for PKM2, it is Cys-358. Under these conditions, GAPDH activity can be further increased by phosphorylation performed by ataxia telangiectasia mutated (ATM), as a consequence of formation of an intermolecular disulfide bridge in ATM at Cys-2991, which also increases flux through the PPP. The effects of ROS on GAPDH, PKM2,

and G6PD activities are likely coordinated by the oxidation of Cys residues in at least six protein subunits within complexes I, III, and IV of the mitochondrial electron transport chain that

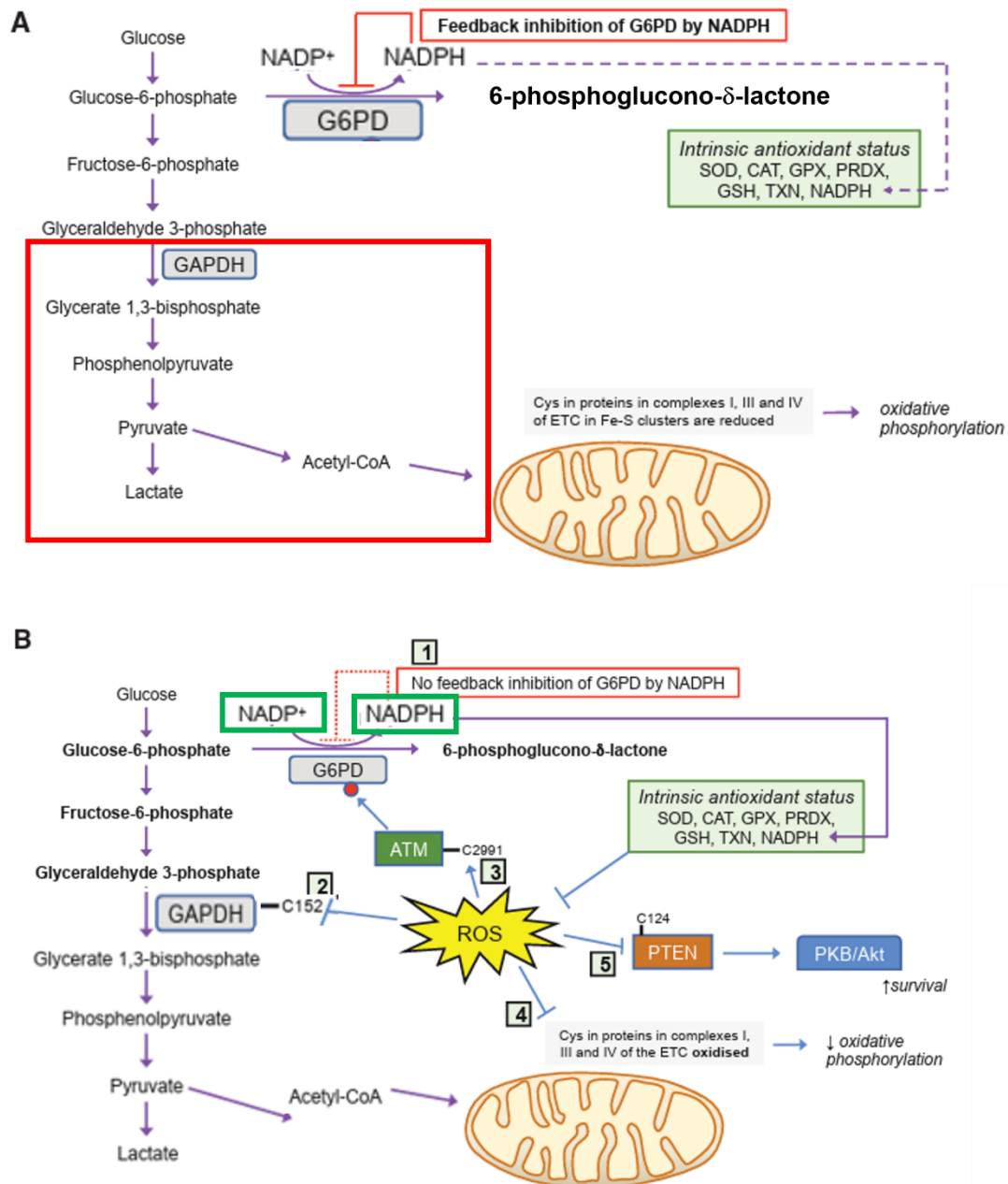


Figure 13 Metabolic Responses to Acute Oxidative Stress. In cells under normal redox homeostatic conditions (**A**), glucose is principally oxidized by glycolysis to pyruvate and, via acetyl-CoA, through the tricarboxylic acid cycle, with G6PD inhibited by NADPH and minimal flux through the pentose phosphate pathway (PPP). However, upon acute oxidative stress (**B**), feedback inhibition of G6PD by NADPH is greatly diminished (1) and Cys residues in GAPDH (2), ATM (3), and complexes I, III, and IV of the electron transport chain (4) are oxidized, a combination of circumstances that result in inhibition of glycolysis, phosphorylation of G6PD, and increased metabolism through the PPP. Moreover, oxidation of Cys residues in PTEN (5) causes activation of PKB/Akt, resulting in increased cell survival. Adapted from (54).

contain Fe-S clusters, resulting in decreased O₂ consumption and a reduction in ROS production (146). Acute oxidative stress may also inhibit phosphatase and tensin homolog (PTEN) by oxidizing Cys-124, thereby activating PKB/Akt through phosphatidylinositol 3-kinase (PI3K), upregulating antioxidant gene expression, and increasing cell survival (147).

In contrast, chronic oxidative stress involves activation of genetic programs. In the short-to-medium timeframe, oxidative stress can alter the abundance and/or subcellular distribution of hypoxia-inducible factor 1 (HIF-1 α) (148), leading to metabolic reprogramming. Traditionally, this involves hypoxia and oxidation of Cys 326 in PHD2 that stabilizes HIF-1 α and results in transcriptional changes that shift from glucose oxidation to glycolysis (148). Importantly, in chronic oxidative stress models involving the accumulation of endogenous electrophiles or depletion of GSH/TXN, adaptation includes upregulation of antioxidant genes (149).

The expression of many antioxidant factors involves the nuclear erythroid-related factor2 (Nrf2) and kelch-like ECH associated protein 1 (Keap1) pathway (150), the Nuclear Factor kappa-light-chain-enhancer of activated B cells (NF κ B) pathway (151), and the PI3K/Akt pathway (152). The Nrf2/Keap1 pathway is also known to be involved in cellular responses to irradiation (150). Nrf2 is a transcription factor that coordinates the activation of a large number of cytoprotective genes, encoding ROS detoxification enzymes such as catalase, components of the glutathione and thioredoxin antioxidant systems, and enzymes involved in the regeneration of NADPH (153). Studies have highlighted the role of Nrf2 in the response to ionizing radiation, many studies have highlighted a role of Nrf2 in the response of most cells to ionizing radiation (150), showing its activation post-irradiation. Additionally, cells deficient in Nrf2 exhibit enhanced radiosensitivity (150), while those cells overexpressing it are radio-resistant (154). This also applies to transgenic (Nrf2 +/-) and knockout (KO) mice as well (155). Nrf2 is highly regulated (i) transcriptionally via many other signaling pathways, of such as PI3K/Akt or NF κ B, (ii) post-transcriptionally via splicing phenomena or microRNAs, and (iii) at the protein stability level, mainly through its binding with the Keap1 protein (153) (**Figure 14**). Under homeostasis conditions, the Nrf2 protein is bound to the protein Keap1 which sequesters Nrf2 in the cytoplasm and binds Nrf2 to E3-Cullin 3 (Cul3) ubiquitin ligase. Cul3 will continuously ubiquitinyrate Nrf2, facilitating its degradation by the proteasome (156) (**Figure 14**). Oxidative stress leads to the modification of certain cysteine residues of Keap1, resulting in a change in its conformation. This alteration allows thereby the release of Nrf2, which is then translocate into the cell nucleus (157). Inside the nucleus, Nrf2 heterodimerizes with small musculoaponeurotic fibrosarcoma (Maf) proteins.

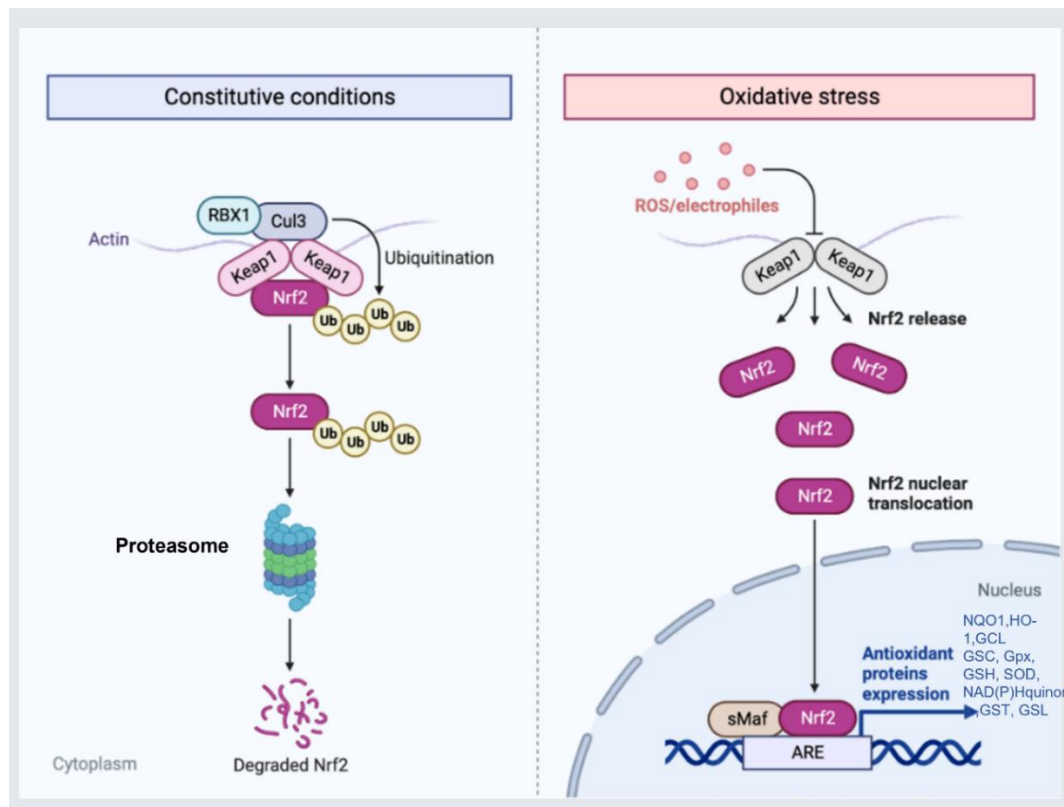


Figure 14 Regulation of the transcription factor Nrf2. At equilibrium (constitutive conditions), the Nrf2 protein is bound to Keap1 and is continuously ubiquitinated by Cul3, which induces its degradation by the proteasome. During oxidative stress, such as that caused by irradiation, destabilization of the Nrf2-Keap1 complex is induced. Nrf2 then translocates to the nucleus where it binds to small Maf proteins and binds to antioxidant response elements (AREs) of DNA, which induces transcription of its target genes. Adapted from (153) (Created with BioRender.com).

This heterodimer binds to antioxidant response elements (AREs), facilitating the expression of Nrf2 target genes such as for example Nqo1 (158) and HMOX1(159) (**Figure 15**). Besides oxidative stress, certain proteins like p21Cip1/Waf1 or p62, which increase during irradiation, can competitively bind to Keap1. This prevents Keap1 from binding to Nrf2 (153), thus promoting Nrf2's entry into the nucleus. It is noteworthy that Nrf2 not only induces the expression of anti-inflammatory proteins but also acts as a suppressor of certain pro-inflammatory gene expressions (160). Nrf2 is also crucial for iron metabolism; it controls the intracellular level of free iron by regulating storage proteins and SLC40A1, which is responsible for transporting free iron out of the cell, thereby regulating ferroptosis (161). Furthermore, Nrf2 can regulate multiple glutathione synthetases and enzymes involved in glutathione metabolism (162,163). GPX4 is also a transcriptional target of Nrf2 (164,165). Therefore, Nrf2 is considered a key regulator of lipid peroxidation and ferroptosis (166).

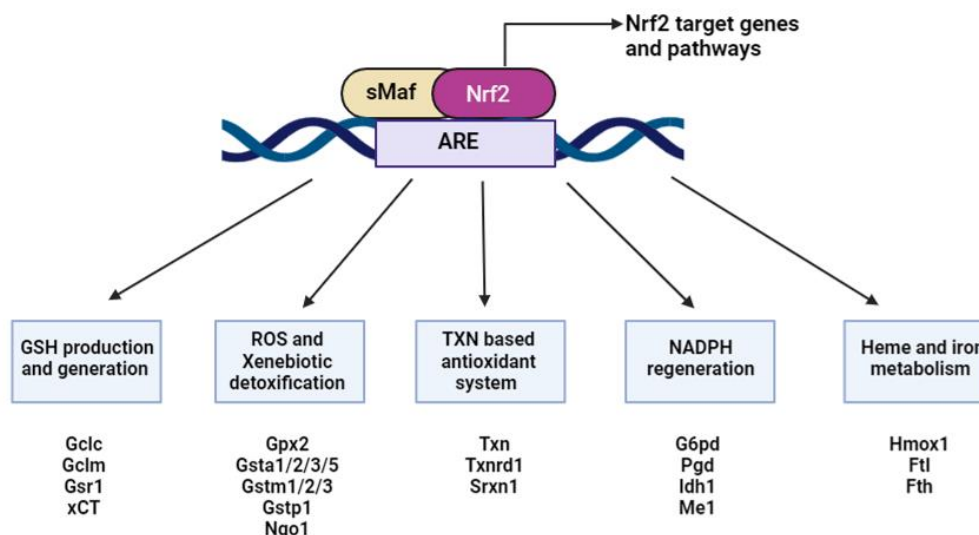


Figure 15 Nrf2 cytoprotective defense system. Through the coordinated regulation of GSH and TXN production, utilization and regeneration, NADPH regeneration, heme and iron metabolism, ROS and xenobiotic detoxification, Nrf2 provides the main cytoprotective defense system in the cell. GSH, glutathione; HMOX1, heme oxygenase 1; Idh1, isocitrate dehydrogenase 1; NADPH, nicotinamide adenine dinucleotide phosphate; Nqo1, NADPH quinone dehydrogenase 1; Pgd, 6-phosphogluconate dehydrogenase; ROS, reactive oxygen species; TXN, thioredoxin. Adapted from (153) (Created with BioRender.com).

3.1.4 Role of ROS in physio-pathological conditions

ROS act as signaling molecules in physiological conditions

Under normal physiological conditions, ROS are important signaling molecules and second messengers, initiating and coordinating intracellular signaling pathways (105,110). ROS mediate oxidative modifications in various types of proteins, including receptor kinases, phosphatases, caspases, ion channels and transcription factors (167–169). The ROS produced from the mitochondrial electron transport complex III (CIII) are crucial for stabilizing HIF-1 α , contributing to cell survival. ROS also play a role in protein kinase signaling cascades, such as the protein kinase B (AKT), AMP-activate protein kinase (AMPK), and mitogen-activated protein kinase (MAPK), influencing cell fate decisions like apoptosis or autophagy (170). In physiological hypoxia, ROS activate AMPK, which, in turn, upregulates cytoprotective autophagy (a survival response) by inhibiting downstream mammalian target of rapamycin (mTOR) activity (171).

In the brain where the response to FLASH-RT has been investigated extensively in our laboratory, ROS are known to regulate signaling molecules related to synaptic plasticity (172), receptors, and channels, including N-methyl-d-aspartate receptors (173), Ca²⁺ channels, Ca²⁺ kinase II (CAMKII) (174), extracellular signal-regulated kinases, cyclic adenosine monophosphate (cAMP), cAMP response element binding protein (CREB) (172,175). ROS are also essential for long-term potentiation, a phenomenon of synaptic plasticity widely

considered one of the main molecular mechanisms underlying learning and memory (172,176), and protected upon FLASH exposure (177,178). Physiological levels of ROS can promote the establishment of neuronal polarity and regulate neuronal cytoskeletal organization and dynamics by modulating intracellular Ca^{2+} release (179,180).

ROS production in pathological conditions

In pathological conditions, such as in cancer cells, the steady-state levels of both intracellular and extracellular ROS are generally elevated compared to normal cells. Several endogenous mechanisms are proposed to explain this increase. These include heightened metabolic rates, mutations in mitochondrial DNA, oncogenic lesions, and the hypoxic tumor microenvironment (TME) (181,182). Firstly, the high energy and nutrient demands of a rapidly proliferating cells lead to hypermetabolism, resulting in increased production of intracellular and extracellular ROS in cancer cell mitochondria, ER, and membranes (167,181). Secondly, mutations in mitochondrial DNA mutations can cause defects in respiratory complexes along the electron transport chain, leading to an overproduction of ROS (182,183). Thirdly, oncogenic mutations alter key intracellular signaling pathways that affect metabolism and protein translation, leading to ROS accumulation (184). For instance, oncogenic K-Ras-transformed pancreatic cancer cells have been shown to stimulate ROS generation through a signaling cascade activating NADPH oxidase 1 (NOX1) (185).

On the other side of the redox balance equation, certain tumor suppressors such as BRCA1, p53, and SIRT3 promote antioxidant function in the cell; consequently, their loss associated with cancer enhances ROS accumulation (186,187). Additionally, the hypoxia/reperfusion processes associated with the TME of solid tumors trigger local ROS generation, possibly through effects on cytochrome oxidase (188). The oxidative stress associated with cancer extends beyond the tumor cells to the TME and adjacent non-cancerous cells and tissues (189). NOX enzymes on the cancer cell promote extracellular ROS production, creating an oncogenic TME (189). Moreover, several tumor-associated cells in the TME, like cancer-associated fibroblasts (CAFs), myeloid-derived suppressor cells (MDSCs), and tumor-associated macrophages (TAMs), generate ROS, contributing to immunosuppression and/or extra-tumoral mutagenic oxidative stress (189,190).

The elevated ROS levels in cancer cells act as a double-edged sword with either pro-tumorigenic or cytotoxic effects, depending on concentration. At levels above a cytotoxic threshold, ROS cause cancer cell death via DNA, lipid, and protein damage (167,184). Below this cytotoxic threshold, yet above the levels found in non-cancerous cells, ROS stimulate tumor growth and progression (167,184). To maintain ROS accumulation below the cytotoxic threshold, cancer cells enhance their antioxidant defense mechanisms. The most crucial of these is the upregulation of Nrf2, a master transcription factor and key regulator of redox balance that controls the expression of antioxidant enzymes such as NADPH dehydrogenase quinone 1 (NQO1) (167,184). Nrf2 upregulation and activation have been observed in several solid tumor types, along with overexpression of its target antioxidant enzymes, including NQO1 (191,192).

Another mechanism employed by cancer cells to limit oxidative stress is the metabolic reprogramming from OXPHOS and to aerobic glycolysis known as the Warburg effect, regardless of the presence of oxygen (193). Blockade of the glycolytic metabolism pathway increase oxidative stress and cell death (194). Other metabolic alterations, such as a switch from the PPP pathway to AMPK and one-carbon metabolism pathways. occur in hypoxic and low-glucose TMEs, boosting NADPH production, a ROS scavenger (195). These antioxidant and metabolic defense mechanisms allow cancer cells to maintain ROS levels below the cytotoxic threshold but significantly above the level in healthy tissues, playing vital roles in tumor initiation, growth, progression, and metastasis (189). The presence of mutagenic ROS in the TME can create a conducive environment for premalignant transformation via oxidative stress and immunosuppression (189). For instance, chronic elevation of hydrogen peroxide levels was found to drive premalignant transformation in non-cancerous epithelial cells and stromal fibroblasts (196). ROS can oxidize and inactivate phosphatases, leading to upregulation of tumorigenic signaling pathways like the PI3K/Akt/mTOR and MAPK/ERK cascades (167,184). Furthermore, endogenous ROS induce angiogenesis through mechanisms mediated by vascular endothelial growth factor (VEGF). (197).

3.1.5 Role of ROS in response to Radiotherapy

Radiotherapy is source of exogenous ROS in biological systems. The ROS levels induced by radiotherapy disrupt redox homeostasis and lead to oxidative stress, potentially resulting in cell death (198,199). The cytotoxic properties of ROS are exploited in cancer therapies to destroy cancer cells; however, ROS can also damage nearby normal cells. Additionally, radiation can increase endogenous ROS production in the mitochondria and alter mitochondrial membrane permeability, which in turn stimulates further ROS production (198). ROS can disrupt the levels of ETC components in mitochondria, induce intracellular redox imbalances, and cause oxidative stress by reacting with biological molecules such as lipids, DNA, and proteins to cause lipid peroxidation, DNA damage and protein oxidation (200). The extent of damage to these different biomolecules can be dependent on the qualities of the radiation beam.

It is important to discuss impact of oxygen on radiation. For instance, tumor cells, which are usually hypoxic (low levels of O₂), tend to be more radioresistant than normal cells (which have physioxic levels of O₂). This is because radiation-induced ROS will react with O₂ to form additional reactive species.

Role of oxygen in radiotherapy

Oxygen is a key parameter that significantly influences the effectiveness of radiation. Nearly a century ago, it was demonstrated that molecular oxygen was a crucial factor for cellular responses to irradiation (182,183). As early as 1955, Thomlinson and Gray published a paper suggesting that hypoxia could be a cause for radio resistance (203). The "Oxygen fixation hypothesis" postulates that radicals biomolecule radicals may react either with radical-

reducing species, resulting in "chemical repair," or with radical oxidizing species, resulting in "fixation" of radical damage is a form lethal to the cell (204). Under atmospheric pressure in pure water at room temperature, O₂ concentration is about 2.5×10^{-4} M. In contrast, the average O₂ in tissues under physiological conditions is estimated to 30 μM (205).

The impact of oxygen also varies depending on the irradiation modality. For high LET irradiation, which primarily causes direct damage, the oxygen tension in normal and tumor tissues has less impact. In the case of FLASH irradiation, oxygen consumption and depletion have been suggested as the main hypothesis to explain the differential response between FLASH-RT and CONV-RT. The radiochemical depletion of oxygen by UHDR was proposed to confer radio-resistance to normal tissues while not affecting tumor response, as they are already poorly oxygenated (206). Furthermore, the concept of physiologically relevant oxygen concentrations, or "physioxia," should be considered. Depending on the tissue type, physioxia typically ranges between 3.4% and 6.8% oxygen (205) whereas *in vitro* studies are mostly conducted under atmospheric conditions (21% O₂), creating an artificially hyperoxic situation. For example, skin oxygenation increases with depth, from around 1.1% in the epidermis to 4.6% in the dermis (207). The high variability of physiological oxygen levels among different tissues suggests that the sensitivity to oxygen depletion might vary accordingly.

The role of oxygen depletion in mediating the sparing effect of UHDR was first proposed in the 1970s when Hendry (in 1974) and Weiss (in 1982) showed that doses of pulsed electrons at UHDR were protective under hypoxic conditions in bacteria, and a break in the survival curve was observed (208,209). In mouse-tail, irradiation at UHDR did not induce necrosis as observed after exposure to conventional irradiation. These results supported the idea that UHDR irradiation could induce radiolytic oxygen depletion. This concept was reinforced more recently by experiments in our laboratory, which showed that hyperoxygenation with carbogen was able to reverse normal tissue protection in the brains of mice exposed to FLASH-RT (210). Since then, numerous theoretical models have been published, all based on calculations focused on FLASH-induced oxygen depletion (211–213). However, interestingly, recent experimental work involving direct oxygen measurements after CONV vs. UHDR irradiation refuted the depletion theory (214–216). These studies indicated that UHDR is unlikely to deplete sufficient oxygen in tissues to elicit radioprotection. Nonetheless, UHDR may alter the yields of other free radicals and downstream processes, affecting later biological responses, as also proposed by Montay-Gruel et al. in the same paper (210).

Role of ROS in radiotherapy

Classic target theory posits DNA damage to be the major cell-death-inducing factor following exposure to ionizing radiation. However, damage to the biomolecules is also involved, and its relevance may depend on beam qualities and irradiation modalities.

A summary of the effects of radiations in the different cellular macromolecules is presented, with specific emphasis on FLASH.

DNA damage: Irradiation induces several types of DNA damage, such as base modifications, micronuclei, single-strand breaks (SSB), or double-strand breaks (DSB). Among these lesions, DSBs are the most damaging to cells because they can induce chromosomal breaks or translocations, which can lead if they are not or are badly repaired, to cell death (217). DSBs also initiates the DNA damage response (DDR) which facilitates the detection and rapid repair of breaks or triggers apoptosis to eliminate excessively damaged cells (217).

Past literature has extensively investigated radiation-induced DNA damage using several models, including plasmids (218,219). These models allow for quick, qualitative evaluations of DNA damage, such as investigations into FLASH parameters and conditions (220–223). Plasmid DNA damage has been shown to be dose-dependent but dose rate-independent at atmospheric conditions (222). At 21% oxygen, Milligan et al. found no dose rate dependency within the range of 0.1 Gy/s to 1 Gy/s (224,225). This absence of sparing was also observed in the presence of scavengers like dimethyl sulfoxide (DMSO), aligning with Milligan et al.'s results (226,227). In contrast, more recently, Perstin et al. reported reduced plasmid DNA damage when irradiating at 21% oxygen with a 16 MeV electron beam at 46.6 Gy/s (221). These discrepancies could be due to differences in beam energy and structure or dose rate. Other technological limitations can be found in Perstin et al.'s study, such as insufficient purification of the plasmids and limited number of measurements, suggesting that these data might be interpreted with caution (221). Cooper et al. used comet assays to study DNA damage in an *ex-vivo* model of human peripheral blood lymphocytes (WB-PBL) irradiated with 6 MeV electrons at FLASH (2000 Gy/s) or CONV (0.1 Gy/s) dose rates under varying oxygen tensions (228). They observed reduced DNA damage after FLASH at doses higher than 20 Gy, modulated by oxygen concentration, with a peak difference of 30–40% at 0.25–0.5% oxygen tension (228). Fouillade et al. examined γ H2AX levels and the recruitment of p53-binding protein 1 (53BP1) *in vitro* and *in vivo* lung model. They used two nontransformed human lung fibroblasts cell lines, MRC5 and IMR-90, and the human lung epithelial carcinoma A-549 irradiated with 5 Gy after FLASH and CONV electrons. The number of γ H2AX foci was slightly reduced in FLASH (2×10^2 to 4×10^7 Gy/s) relative to CONV conditions in the two fibroblast cell lines, but this tiny difference was not statistically significant. In contrast, the response of A549 tumor cells in terms of 53BP1 foci was indifferent to the modality of radiation (229). In normal mouse lung, they reported less γ H2AX foci after FLASH electrons (229). Levy et al. showed similar levels of γ H2AX foci in ID8 tumors after FLASH (216 Gy/s) and CONV electrons (0.079 Gy/s), and a slight decrease in repair foci after UHDR in the normal gut at early time-points, that normalized by 24h post-irradiation (230). However, a recent *in vitro* study by Barghouth et al. who used a functional and quantitative DNA damage repair (DDR) assay, showed that FLASH electrons (1×10^2 to 5×10^6 Gy/s) do not affect chromosome translocations and junction structures in HEK293T cells more than CONV electrons (0.08 Gy/s to 0.13 Gy/s) (231). In addition to that, there was no apparent increase in chromosome translocations under hypoxia-induced apoptosis (231).

Protein oxidation: Proteins, constituting about 20% of cellular biomass, are crucial functional units in cells (232). Although the study of protein oxidation by radiation is minimal, it is a significant aspect of radiation effects. Radiation-induced protein oxidation, mediated by ROS, leads to oxidative and nitrosative stress in cells. The specific molecular degradation mechanisms of amino acids and peptides, the building blocks of proteins, are not fully understood, particularly in the context of accelerated particle exposure (233). Oxidation can result in irreversible changes like carbonylation of lysine (Lys) and arginine (Arg), formation of di-tyrosine bonds, protein-protein crosslinking, and nitration of tyrosine (Tyr) and tryptophan (Trp) (99), often leading to permanent functional loss. In enzymes, interaction with free radicals can damage the prosthetic group, causing functional inactivation. Recent studies by Gupta et al. and Arnone et al. have begun to explore protein oxidation post FLASH and CONV irradiations (234,235). Gupta's study quantified radiation-induced oxidative damage in peptides using X-ray footprinting mass spectrometry (XFMS), comparing low dose rate X-rays and electrons with FLASH X-rays and electrons. The study found more peptide damage at lower dose rates (234). Arnone's research also showed reduced protein oxidation in irradiated mouse brain tissue under FLASH compared to conventional doses (235). These findings are encouraging, indicating potential cellular protection against protein oxidation under FLASH conditions. However, the exact mechanisms behind these differences remain to be explored.

Lipid peroxidation: Lipid peroxidation by ROS occurs in cell membranes through three phases: initiation, propagation, and termination. The initiation phase, as illustrated in **Figure 16**, involves the reaction of free radicals with cellular lipids, leading to the formation of peroxy radicals (ROO^\bullet). During the propagation phase, these newly formed peroxy radicals with intact lipids, setting off a chain reaction. This can be halted by antioxidants, marking the termination phase. Lipid peroxidation is toxic to cells as it alters membrane fluidity and can compromise cell integrity. It may also inactivate transporters and transmembrane enzymes. A hypothesis has been proposed to explain the FLASH effect, which involves peroxidative chain reactions initiated by organic peroxy radicals (ROO^\bullet). This hypothesis suggests a differential accumulation of ROO^\bullet and hydroperoxides (ROOH) in normal tissue vs tumors (236). The reasoning is that normal cells more efficiently regulate endogenous levels of labile iron (Fe^{II}) and have a greater reserve capacity for enzymatic reduction of hydroperoxides. Consequently, FLASH-induced hydroperoxides could be more efficiently removed by antioxidant pathways in normal tissues than in tumors, preventing the induction of Fenton chemistry or further peroxidation chain reactions. Additionally, a theoretical study by Labarbe et al. (212) supports the concept of reduced peroxy radicals following UHDR irradiation. This model suggests that a reduction in the lifespan of ROO^\bullet is a key mechanism underlying the FLASH effect, aligning well with published experimental results (212).

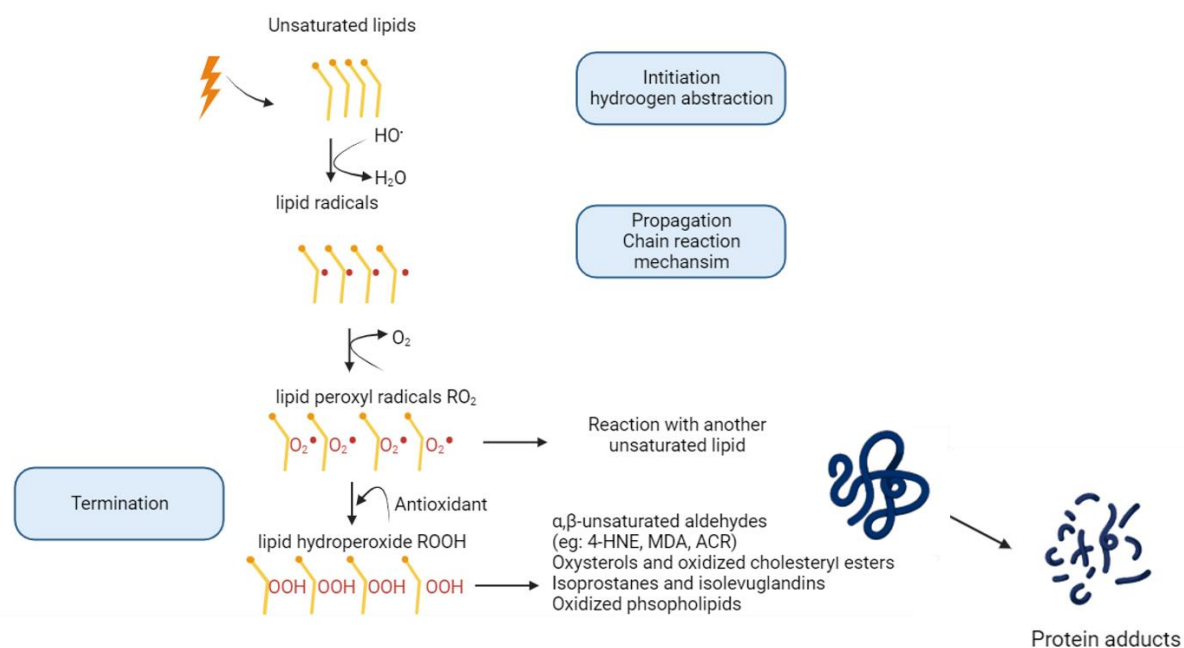


Figure 16 Scheme of the lipid peroxidation reaction and its toxic products following irradiation that can interact with proteins generating adducts. 4-HNE, 4-Hydroxynonenal; MDA, Malondialdehyde and ACR, Acrolein (Created by Biorender.com).

Radical recombination could shorten the lifespan or limits the radiolytic yield of ROO^{\bullet} , thus protecting normoxic tissues from the harmful effects of radiation. However, experimental validation is needed for this hypothesis (212,236). Recent work performed in simple micelles and liposomes by our team support this hypothesis and showed that FLASH-RT does not induce lipid peroxidation, as evidenced by a lack of Malondialdehyde (MDA) production. In contrast, a dose-dependent MDA production was observed following CONV-RT (237). Further research is necessary to fully understand the functional significance of these findings as these measurements cannot explain why tumor cells are not protected.

Impact of radiotherapy on cellular redox system

Radiation-induced ROS have long been known to disrupt OXPHOS, enhance mitochondrial-derived ROS, and elevate oxidative stress lasting for a long time after irradiation (238–241). Exposure to radiation results in induction and persistence of genomic instability and an oxidative phenotype (242,243). At the mechanistic level, cancer cells exhibit an increased level of oxidative damage compared to normal cells, where increased H_2O_2 levels in cancer cells were caused by dissociation of the subunits comprising electron transport chain (ETC) complex II (see page 38-40) (238,239,244). Other routes can elevate oxidative stress following radiation exposure as well (245,246); however, based on significant past work (247–250), the possibility that mitochondrial metabolism is differentially disrupted by dose rate modulation deserves further consideration. So far, FLASH induces less free radicals yields when compared to CONV-RT in cell free systems (251,252) and could constitute the primary mediator of the FLASH effect if validated in tissues.

Objectives of the thesis project

My thesis project stands at the interface of physics, chemistry, and biology. The aim was to unravel the potential continuum between the physico-chemical and radiobiological mechanisms underlying the FLASH effect. This exploration utilized cell-free systems, *in vitro* models including both tumoral and normal cell lines, and *in vivo* studies on normal tissue using zebrafish embryos (ZFE) and was structured in three main scientific questions:

1- Can we investigate the mechanisms underlying the FLASH effect in chemical solutions?

During the first phase of my thesis, a primary focus of my work was to investigate water radiolysis following FLASH and CONV-RT. The goal was to explore the potential use of this process as a simple and high-throughput surrogate of the FLASH effect. We examined possible differences in radical reactions that might occur during the early chemical steps post-exposure to FLASH and CONV dose rates, using a simple solution and eRT6 as the reference beam for FLASH. Hydrogen peroxide, a stable end-product of water radiolysis, was measured using the fluorometric Amplex Red Assay (Thermo Fisher). We calculated the primary radiolytic yields of H₂O₂ utilizing the scavenging method. Additionally, long-term hydrogen peroxide yields were evaluated under varying dose rates and different chemical environments, including oxygen level and temperature. Furthermore, I explored the formation of DNA damage under a variety of beam structures and chemical environments. These environments encompassed different oxygen levels, pH values, scavengers (DMSO), and the impact of labile iron.

2- What are the beam parameters essential to trigger the FLASH effect?

To identify the essential beam parameters necessary to induce the FLASH effect, we carried out a comprehensive analysis across a variety of distinct beamlines. These included intermediate electron beams from eRT6-CHUV, Very High-Energy Electron beams (VHEE) at CLEAR-CERN, transmission proton beams at Gantry1-PSI, and conventional photon beams from PXI sources. Our rigorous investigation involved assessing the impact of these diverse beams, each with its unique temporal structure, on both physico-chemical and biological responses. This extensive research enabled us to pinpoint the crucial FLASH parameters necessary for achieving the sparing effect.

3- Are reactive oxygen species involved in the FLASH effect in biological systems?

The second axis of my project involved translating these measurements to biological samples, using 2D tissue culture (normal and tumor cell lines) as well as zebrafish embryos (ZFE). Given the potential for redox imbalance in normal vs tumor cells to explain the FLASH effect, this possibility was thoroughly investigated. At the cellular level, we monitored the kinetics of ROS production following FLASH vs CONV irradiation under physiological oxygen conditions. This was done in tumor cell line (U87) and the outcomes were compared with those in normal cell line (Jurkat). For detecting intracellular ROS levels, we used ROS-Glo™ H₂O₂ luminescent assay.

Acknowledging that the observation of normal tissue sparing by FLASH-RT necessitates *in vivo* studies, we utilized ZFE to investigate functional and redox responses to FLASH *versus* CONV-RT. We examined survival and growth, as well as cell death and proliferation, in AB Wild Type ZFE. To explore the role of ROS, we used Nrf2 deficient ZFE (+/- and -/-) in which the antioxidant cascade is impaired and found that Nrf2-induced antioxidant pathway is required for ZFE survival after CONV but dispensable after FLASH.

Chapter II: Results

1- Publication 1 literature review: Understanding the FLASH effect to unravel the potential of ultra-high dose irradiation.

Published in International Journal of Radiation Biology, 2021.

DOI: [10.1080/09553002.2021.2004328](https://doi.org/10.1080/09553002.2021.2004328)

The resurgence of research on ultra-high dose rate (UHDR) irradiation has sparked considerable interest in the field of radiation science, opening new avenues in radiobiology. The promise of UHDR irradiation largely hinges on the FLASH effect, a biological response observed *in vivo* when tissues are exposed to UHDR and that maintains anti-tumor efficacy while reducing the complications in normal tissue typically associated with conventional dose rates (CONV). FLASH radiotherapy (FLASH-RT) holds the potential for improving the therapeutic index and offers new opportunities for non-toxic eradication of radioresistant tumors. Our group has formed an interdisciplinary team of biologists, chemists, and physicists dedicated to exploring the mechanisms and clinical applications of the FLASH effect. This review, supervised of MC Vozenin and collaboratively written by myself focusing on the chemistry aspects, Aymeric Almeida investigating FLASH mechanisms in biological systems for his PhD thesis, and Nicolas Cherbuin studying the impact of FLASH on plasmids, provides a mechanistic perspective.

Our review starts with the initial physicochemical events in simplified chemical systems (such as water, plasmid DNA) and progresses to more complex biological systems using mice models and zebrafish embryos. It includes a bibliographical summary of studies describing the *in vivo* FLASH effect, as well as some negative results. We also propose an integrated experimental approach to studying the FLASH effect.

A few years ago, we performed a dose rate escalation study to define a dose rate threshold using normal brain toxicity in mice (253) as a model. 10 Gy was delivered in a single pulse of 1.8 μ s (5.6×10^6 Gy/s) and progressively the dose rate was decreased down to 0.1 Gy/s. Full preservation of neurocognitive function was achieved above 100 Gy/s, but it diminished at 33 Gy/s and was absent at 0.1 Gy/s. Interestingly, this study was reproduced in ZFE. Our experiments with pBR322 plasmid DNA irradiated in aqueous solutions equilibrated at physiological oxygen conditions (4%) revealed no difference in DNA damages after FLASH vs CONV irradiation, although, the G(H₂O₂) (μ M/10 Gy) was lower at the highest dose rates of 5.6×10^6 Gy/s and 100 Gy/s.

Understanding the FLASH effect to unravel the potential of ultra-high dose irradiation.

Houda Kacem^a, Aymeric Almeida^a, Nicolas Cherbuin^b & Marie-Catherine Vozenin^a

^a Department of Oncology, Laboratory of Radiation Oncology, Radiation Oncology Service, CHUV, Lausanne University Hospital and University of Lausanne, Lausanne, Switzerland.

^b Department of Medical Radiology, Institute of Radiation Physics, CHUV, Lausanne University Hospital and University of Lausanne, Lausanne, Switzerland



Understanding the FLASH effect to unravel the potential of ultra-high dose rate irradiation

Houda Kacem, Aymeric Almeida, Nicolas Cherbuin & Marie-Catherine Vozenin

To cite this article: Houda Kacem, Aymeric Almeida, Nicolas Cherbuin & Marie-Catherine Vozenin (2022) Understanding the FLASH effect to unravel the potential of ultra-high dose rate irradiation, *International Journal of Radiation Biology*, 98:3, 506-516, DOI: [10.1080/09553002.2021.2004328](https://doi.org/10.1080/09553002.2021.2004328)

To link to this article: <https://doi.org/10.1080/09553002.2021.2004328>



This material is published by permission of the laboratory of radiation oncology of the CHUV, operated by MC Vozenin for the Department of Oncology, Radiotherapy service under contract number PO1CA244091. The US Government retains for itself, and others acting on its behalf, a paid-up, non-exclusive, and irrevocable worldwide license in said article to reproduce, prepare derivative works, distribute copies to the public, and perform publicly and display publicly, by or on behalf of the Government.



View supplementary material [↗](#)



Published online: 02 Dec 2021.



Submit your article to this journal [↗](#)



Article views: 6014



View related articles [↗](#)



View Crossmark data [↗](#)

Understanding the FLASH effect to unravel the potential of ultra-high dose rate irradiation

Houda Kacem^{a*}, Aymeric Almeida^{a*}, Nicolas Cherbuin^{b*}, and Marie-Catherine Vozenin^a 

^aDepartment of Oncology, Laboratory of Radiation Oncology, Radiation Oncology Service, CHUV, Lausanne University Hospital and University of Lausanne, Lausanne, Switzerland; ^bDepartment of Medical Radiology, Institute of Radiation Physics, CHUV, Lausanne University Hospital and University of Lausanne, Lausanne, Switzerland

ABSTRACT

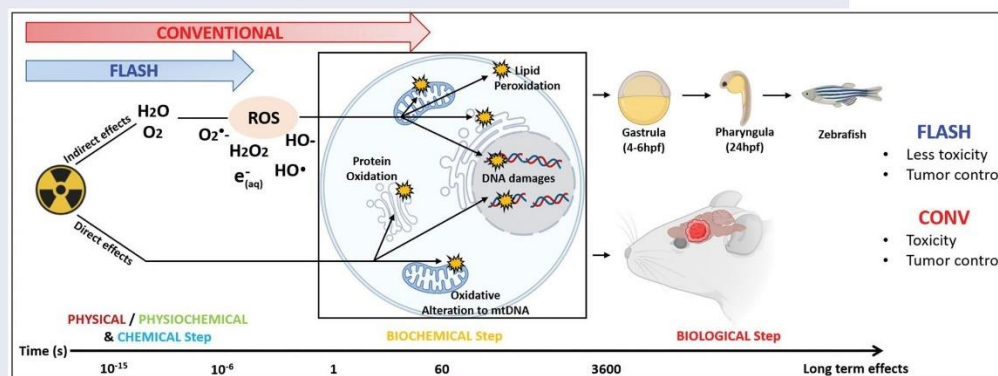
A reemergence of research implementing radiation delivery at ultra-high dose rates (UHDRs) has triggered intense interest in the radiation sciences and has opened a new field of investigation in radiobiology. Much of the promise of UHDR irradiation involves the FLASH effect, an in vivo biological response observed to maintain anti-tumor efficacy without the normal tissue complications associated with standard dose rates. The FLASH effect has been validated primarily, using intermediate energy electron beams able to deliver high doses (>7 Gy) in a very short period of time (<200 ms), but has also been found with photon and proton beams. The clinical implications of this new area of research are highly significant, as FLASH radiotherapy (FLASH-RT) has the potential to enhance the therapeutic index, opening new possibilities for eradicating radio-resistant tumors without toxicity. As pioneers in this field, our group has developed a multidisciplinary research team focused on investigating the mechanisms and clinical translation of the FLASH effect. Here, we review the field of UHDR, from the physico-chemical to the biological mechanisms.

ARTICLE HISTORY

Received 8 May 2021
Revised 20 October 2021
Accepted 25 October 2021

KEYWORDS

Ultra-high dose rate;
FLASH-RT; ROS; plasmid;
pre-clinical models




Introduction

Today, radiation therapy is used in combination with other therapies to treat over 50% of cancer patients. Radiotherapy remains highly efficient at eradicate cancer cells and despite significant technological improvements related to tumor targeting by image-guidance, the dose required for tumor control is still limited by normal tissue toxicity. In addition,

some tumors remain highly radio resistant, escaping modern treatment plans to recur and metastasize. Therefore, one major challenge in our field is to develop novel radiotherapy strategies to overcome these limitations.

CONTACT Marie-Catherine Vozenin  marie-catherine.vozenin@chuv.ch  Department of Oncology, Laboratory of Radiation Oncology, Radiation Oncology Service, CHUV, Lausanne University Hospital and University of Lausanne, Lausanne, Switzerland

*These authors contributed equally to this work.

 Supplemental data for this article can be accessed [here](#).

This material is published by permission of the laboratory of radiation oncology of the CHUV, operated by MC Vozenin for the Department of Oncology, Radiotherapy service under contract number P01CA244091. The US Government retains for itself, and others acting on its behalf, a paid-up, non-exclusive, and irrevocable worldwide license in said article to reproduce, prepare derivative works, distribute copies to the public, and perform publicly and display publicly, by or on behalf of the Government. This is an Open Access article distributed under the terms of the Creative Commons Attribution-NonCommercial-NoDerivatives License (<http://creativecommons.org/licenses/by-nc-nd/4.0/>), which permits non-commercial re-use, distribution, and reproduction in any medium, provided the original work is properly cited, and is not altered, transformed, or built upon in any way.

Ionization (H_2O^+), where one electron (e^-) is removed from the water molecule (Nikjoo et al. 1998). In water, a strong polar solvent, the geminate recombination of electrons with their positive parent cation is less favored; they become separated within 10^{-15} s. The resultant ionized and excited molecules are highly unstable and dissipate excess energy in the form of energy transfer to neighboring molecules. This physicochemical stage occurs between 10^{-15} and 10^{-12} s and surprisingly, is not well characterized experimentally in liquid phase. However, by analogy with the behavior of water molecules in gas phase under photolysis, three steps of de-excitation events were proposed: proton transfer to a neighboring molecule, dissociation of excited water molecule and electron thermalization and solvation. Proton transfer from the positive radical water ion H_2O^+ to neighboring water molecule is an important event since it leads to the production of the hydroxyl (HO^*) radical. The electronically excited molecules, H_2O^* can return to their fundamental state without dissociation by heat loss. Alternatively, higher excitation states can dissipate energy by emitting an electron, thus becoming an ion and dissociate into hydrogen and hydroxyl radicals. Another dissociation pathways can lead to formation of dihydrogen and oxygen in a singlet state $\text{O}^*(1\text{D})$. Singlet oxygen is not stable, and reacts in a third step with water to form molecular hydrogen (H_2) and two hydroxyl radicals (2HO^*) or hydrogen peroxide (H_2O_2). The formation of oxygen in a triplet state (O^3P) was also observed but in very low yield (Auclair 2001). The dissociation reactions take place in $\sim 10^{-13}$ s, which is on the same scale as the vibrational state of a water molecule (10^{-13} to 10^{-14} s).

The electrons emitted in the medium, depending on their kinetic energy, migrate either further and form secondary ionizations themselves or lose energy in multiple steps (Spotheim-Maurizot 2008). First, by vibrational and rotational relaxation then becoming thermalized in 10^{-12} s. Thermalized electrons orient the dipole moments of neighboring water molecules, forming a 'cage', and are referred to as aqueous electrons $e^-(\text{aq})$.

For low LET radiations, such as accelerated electrons, end products of the physico-chemical stage (H^* , $e^-(\text{aq})$, HO^* , H_2 , H_2O_2) are clustered together in small widely separated spurs. On average, one spur can contain two or three ion pairs (Baldacchino et al. 2019). Next, the non-homogeneous chemical stage starts between 10^{-12} and 10^{-6} s. Radical species diffuse and react with each other at different rates. Eventually, certain radical products encounter others from different spurs and form new radical species. While, some escape the spur to the bulk liquid and become homogeneously distributed with the rest of the radical species. Over 10^{-7} to 10^{-6} s, molecular yields are computed for photons, energetic electrons and ions, and are termed G -values, classically referred to as 'primary yields'. G -values have been measured by pulse radiolysis or through scavenging methods (Hiroki et al. 2002; Wasselin-Trupin et al. 2002) and correspond to the yields of formation at the start of the homogeneous stage (i.e. not at time '0'). They are expressed in mol J^{-1} or in molecule/100 eV in the original literature.

In summary, a G -value of a given species is given by the relationship between the dose D and the concentration C in units of mol dm^{-3} with a density correction ρ : $C = \rho \times D \times G$. Noteworthy too is that G -values are usually measured in deaerated samples to remove any oxygen contribution, known to have a significant impact on free radicals reactions due to its ultra-high reactivity for unpaired electrons.

In the case of CONV-RT, the result of the competition between recombination and diffusion strongly depends on how the energy deposition is done. It means that the initial distribution of ionizations in space, which is reflected by the LET, will dictate whether more or less radicals will escape the spurs, and alter the yields of molecular products on the scale of 10^{-7} s. The question is what will happen in the case of exposure to UHDR? Under this scenario, a recombination event can be expected to transpire within a time scale that is short enough to interfere with early chemical reactions, when radicals form and disappear. For example, with the eRT6/Oriatron (PMB, Peynier, France), energetic electrons with an $\text{LET} = 0.2 \text{ keV } \mu\text{m}^{-1}$ are deposited within a $1.8 \mu\text{s}$ pulse (Jaccard et al. 2018) (when the dose is applied in a single pulse) or in milliseconds (if multiple pulses are required). This time frame is relatively long for early chemical reactions and does not support the occurrence of radical-radical recombination, as pulse delivery extends to the end of the homogenous phase of chemistry between $100 \text{ ns}^{-1} \mu\text{s}$. At this stage, radical-radical interactions have taken place and free radicals begin to diffuse. Thus, recombination reactions are unlikely to explain a potential radiochemical basis of the FLASH effect.

In summary, the physicochemical cascade activated after UHDR and CONV dose rate needs to be carefully studied in order to determine whether initial radiolytic yield could be or not involved in the subsequent biological FLASH effect. It is important to explore furthermore other sources like protons where radiochemical processes can differ regarding the particle type, energy and LET. A radiation chemistry study describing the effect or not of dose rate in other sources is relevant especially that in literature such studies have not been done before. This would provide a guide/link to explain or not downstream biological effects observed after UHDR. Although, one should note that such studies require rigorous experimental conditions in order to have solid results and would be able then to compare with literature. Among the relevant parameters, the role of oxygen tension in mediating a certain fraction of the FLASH effect has come under intense scrutiny. The impact of oxygen in mediating the FLASH effect was first proposed based on the observation that hyperoxygenation was able to reverse normal tissue protection in the brain (Montay-Gruel 2019). Since then, numerous theoretical models were published, all based on calculations focused on FLASH-induced oxygen depletion (Pratx and Kapp 2019; Hu et al. 2020; Labarbe et al. 2020; Petersson et al. 2020; Zhou et al. 2020). Interestingly, recent experimental work done by direct oxygen measurements after CONV vs. UHDR irradiation refutes this depletion theory (Cao et al. 2021; Jansen et al. 2021) and shows that UHDR is not likely to deplete

sufficient oxygen in tissues to elicit a transient state of hypoxic radioprotection. Nonetheless, FLASH may alter the yields of other free radicals and downstream processes to impact later biological responses (Montay-Gruel et al. 2019). Clearly, a major limitation in the field, is the lack of direct control of tissue oxygenation status, a complex biological process that is difficult to model *ex vivo*. The physicochemical cascade summarized in Figure 1 needs to be carefully studied in order to determine whether initial radiolytic yield could be or not involved in the subsequent biological FLASH effect.

DNA damage after irradiation at conventional and ultra-high dose rate

In living organisms, irradiation triggers the direct ionization of biomolecule (nucleic acids, lipids, proteins) and the production of reactive oxygen species (ROS) and reactive nitrogen species (RNS) that can alter molecules essential for life. Oxidative reactions in the presence of oxygen predominate in the irradiated cell and are driven by the most reactive radical, the hydroxyl radical (von Sonntag 1991). Interactions of HO^\bullet with proteins can change signaling, gene expression, and protein half-lives. The action of hydroxyl radicals on lipids results in peroxidation chain reactions. Although these damages have the potential to disrupt cell metabolism and proliferation, irreparable damage to DNA in the form of DSB is seen as the primary determinant of cell survival.

The action of HO^\bullet on DNA is primarily mediated through the abstraction of a hydrogen atom from a 2-deoxyribose moiety exposed to solvent (more often at C4' position), resulting in a frank single strand break (SSB) or the

formation of an abasic site (Pogozelski and Tullius 1998). The hydroxyl radical can also oxidize a nucleoside, with no preference for purines or pyrimidines, forming a variety of products that are generally stable but also able, in some cases, to induce the loss of the base or an SSB. Hydrogen radicals and aqueous electrons also react with nucleobases in reductive reactions, mostly in anaerobic conditions and especially with pyrimidines, but their actions on the sugar-phosphate backbone are less important. Direct effects act most likely by ionization of the phosphate group (von Sonntag 1991). Double-strand breaks (DSBs) are then the consequence of either a radical transfer from a cleaved strand to the complementary strand or the action of multiple hydroxyl radicals in spatially defined regions (spurs, blobs) at track ends that result in locally multiply damaged sites or 'clustered' damage (Ward 1985, 1981; Siddiqi and Bothe 1987; Krisch et al. 1991). Non-DSB clusters, defined by the presence of multiple damages (SSB, abasic sites, or nucleoside lesions) concentrated within a turn of the DNA helix, can be lethal as well (Ward 1985; Shikazono et al. 2009).

The appearance and type of DNA damage are related to the concentration and diffusion velocity of selective reactive species, i.e. the competition between reactions with DNA, with oxygen and recombination at track ends. DNA damage varies with the LET of the incident radiation. Increasing the LET leads to clusters with higher levels of damage multiplicity or complexity (Georgakilas et al. 2013). The modification of reaction equilibrium in the presence of specific scavengers also influences the rate and type of strand breaks. In that respect, the recombination of HO^\bullet with the aqueous electron is an important reaction. Interestingly, in the presence of oxygen, its combination with the products of water radiolysis causes its depletion. More specifically, oxygen acts

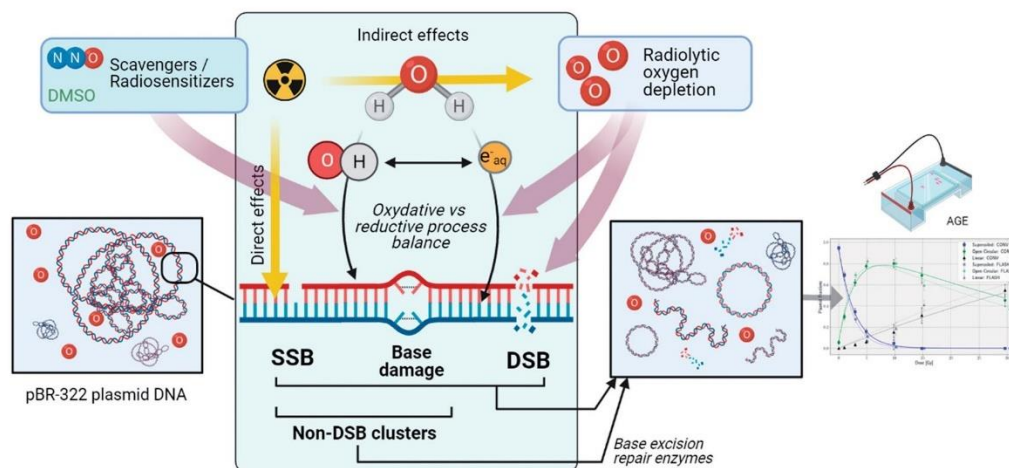


Figure 2. Plasmid DNA as a tool to study DNA damage after CONV vs. UHDR irradiation. The induction of SSB and DSB after irradiation of a supercoiled plasmid releases mechanical constraints in the molecule and causes its spatial conformation to change. These isomers (circular (relaxed) or linear form after SSB or DSB, respectively) have different migration speeds in a gel matrix and are therefore easily separated and quantified by a simple agarose gel electrophoresis (AGE). To investigate the mechanisms underlying the FLASH effect, plasmids can be irradiated dry, or in atmospheric, physiologic or hypoxic aqueous solutions, in presence of various radiosensitizers or scavengers. In addition, several beam parameters such as instantaneous dose, dose per pulse, frequency, and total irradiation time can be investigated.

as a potent scavenger of aqueous electrons to yield superoxide radicals. A model defining the distribution of DNA damage attributable to different reactive species with respect to the partial pressure of oxygen in water has been proposed (Barilla and Lokajíček 2000). Oxygen is also a potent radiosensitizer, able to fix radiolytic lesions that inhibits their efficient repair (so called oxygen fixation hypothesis).

DNA damage study with plasmids

Ongoing experiments aim to assess the direct and indirect effects of UHDR vs. conventional dose rate on DNA damage by systematically varying parameters such as beam structure or the biochemical environment. Between oligonucleotides and cellular DNA, a widespread model for the study of DNA damage in the absence of DNA repair involves isolated plasmid DNA. From bacterial preparations, the supercoiled plasmid conformation changes after the induction of an SSB or DSB to an open circular or linear form, respectively. Quantification of the conversion of supercoiled DNA to these topologically distinct conformations after irradiation can be accomplished by standard agarose gel electrophoresis (Figure 2). However, at higher doses the fragmentation of the plasmid by damage multiplicity requires more sensitive methodologies, such as atomic force microscopy (Pachnerová Brabcová et al. 2019). Plasmid irradiations have been widely used to understand the effects of different parameters on DNA damage, such as the type of radiation, the ratio of direct to indirect effects, the effect of supercoiling density, or the physicochemical mechanisms delineated by the presence of radiosensitizers or radioprotectors. However, regarding the dose rate dependence of strand break yields, only one recent study aimed to assess the relative biological effect using very high energy electron and UHDR (Small et al. 2021). Under atmospheric conditions, no significant dependence of DSB on dose rate was observed. The addition of base excision repair enzymes increases the sensitivity of such approaches (Sutherland et al. 2001). Mathematical models also provide for the capability to compute strand break yields of selective plasmid conformations as a function of dose (Cowan et al. 1987; McMahon and Currell 2011). However, these models are insensitive to the time signatures used in UHDR, and results obtained should be interpreted with these caveats in mind (Moeckli et al. 2020).

Biological steps after irradiation at conventional and ultra-high dose rate

The beneficial effect of FLASH-RT irradiation, named the 'FLASH effect' involves normal tissue sparing at doses known to provide tumor control. The benefits of FLASH-RT have now been described in many organs, in various animal models and from various groups over the world. Despite differences in nature and structure of the radiation beams, the FLASH effect has been validated in preclinical experiments with electron, proton and photon beams operating at dose rate above 40 Gy/s (Montay-Gruel et al. 2017, 2018;

Diffenderfer et al. 2020; Cunningham et al. 2021). The field is advancing rapidly, with clinical trials in domestic animals (Vozenin et al. 2019; Konradsson et al. 2021). A feasibility study in a human patient (Bourhis et al. 2019b) and a FAST01-trial, concurrent with a wealth of mechanistic studies in multiple model systems.

The FLASH effect in experimental mouse models

Normal lung and tumors

Our group was the first to demonstrate the FLASH effect in the lung (Favaudon et al. 2014). Delayed pulmonary fibrosis after exposure to 17 Gy electron at UHDR irradiation was reduced whereas conventionally irradiated C57Bl6 mice developed massive fibrotic lesions. This sparing effect was associated with a reduction of apoptosis in blood vessels and bronchi. At the tumor level, 15 Gy UHDR irradiation was as efficient as CONV-RT in controlling the growth of orthotopic TC-1 tumor cells implanted in the lung. Dose escalation up to 28 Gy was made feasible and resulted in tumor control. Cell repopulation following radiation exposure was then studied in the normal lung (Fouillade et al. 2020). As a surrogate for DNA damage and senescence, DNA repair foci (53BP1) were used. Findings revealed that both processes were minimized after 17 Gy electron at UHDR in normal cells in situ. Interestingly, the number of 53BP1 foci was also reduced in vitro in human fibroblast cell lines after 5.2 Gy at UHDR vs. CONV-RT whereas no difference between the two modalities was reported in human lung adenocarcinoma cells, A549. Subsequent RNA sequencing analysis revealed that fibrogenic and proinflammatory gene expression (TGF- β 1, Cebpb) was attenuated after UHDR vs. CONV-RT, an effect attributed to the preservation of stem/progenitor cells in the lung. These studies suggest a differential impact of UHDR irradiation at the genomic level which might impact the response in normal and tumor cells.

Normal brain and GBM

The biological FLASH effect has been investigated extensively in the brain, another late responding organ (Figure 3), using 10 Gy whole brain irradiation. Systematic investigations using behavioral testing as a functional outcome enabled the determination of a dose rate threshold necessary to trigger the FLASH effect at 100 Gy/s when a small volume (1.7 cm diameter) was irradiated (Montay-Gruel et al. 2017). Subsequent analyses were performed at higher dose rates (10^7 Gy/s) which is the maximum achievable dose rate of the eRT6/Oriatron (PMB, Peynier, France) electron beam. Using these UHDRs, neuroinflammation was minimized, neurogenesis and neuronal morphology were preserved after exposure to UHDR while conventional dose rate (0.01 Gy/s) induced persistent structural degradation and apoptosis of hippocampal cells and memory loss (Montay-Gruel et al. 2019). Interestingly, carbogen-breathing during UHDR irradiation reversed the neuroprotection. Neuroprotection was further validated at lower dose rates ranging between 200 and 300 Gy/s and with a single fraction of 30 Gy

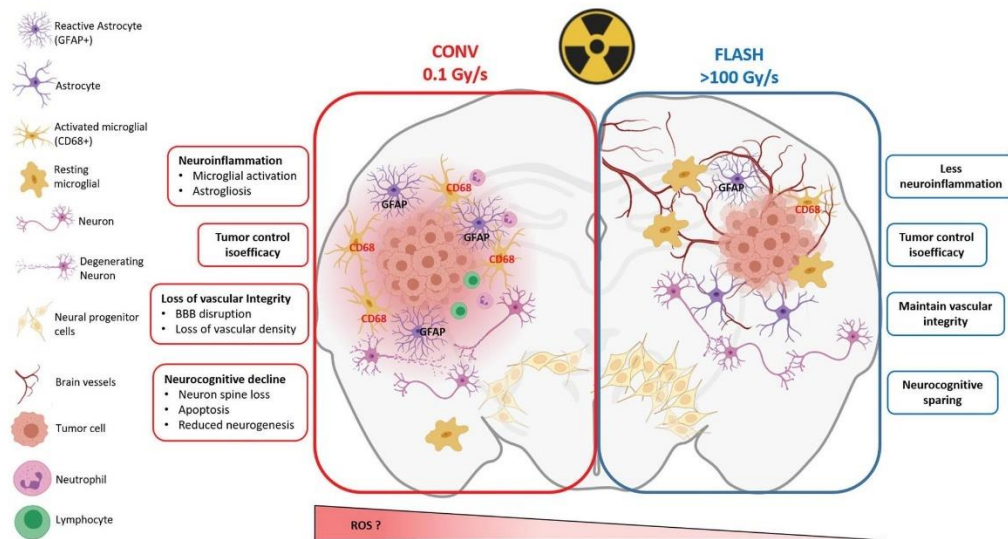


Figure 3. The FLASH effect in normal brain and GBM. Taking the brain as organ-model, this figure shows the cascade of biological events that occur after tissue exposure to conventional dose rate and UHDR. Exposure of the brain to conventional dose rate irradiation (0.1 Gy/s) (left side of the scheme) is associated with early loss of vascular integrity due to endothelial cell damages as well as neuroinflammatory processes involving at longer terms astrogliosis, microglial activation and local immune cell infiltration. This pathogenic process perpetuates in time and ultimately results in neurocognitive disorders associated with loss of neurons and decreased neurogenesis. Interestingly, the delivery of radiation at UHDR (>100 Gy/s) (right side of the scheme) does not activate any of these pathogenic pathways. It spares the vascular network, does not induce neuroinflammation and preserves the neurogenic niche. One possible mechanism to explain the sparing effect of UHDR on normal tissue is the decreased formation of free radicals including reactive oxygen species (ROS) that occurs via early chemical reactions following irradiation (see Figures 1 and 2) but other mechanisms can occur and are under investigations. Interestingly, while the normal brain is not damaged by UHDR irradiation, GBM tumor cells are equally sensitive to UHDR and irradiation at conventional dose rate, suggesting that tumor sensitivity is independent on the dose rate. Many factors might be involved in tumor sensitivity to UHDR, including gene expression. A putative susceptibility profile in T-acute lymphoblastic leukemia tumors was related to the expression of GADD45 and FAT1. In contrast, AGAP9 and PDLIM1 expressions seem to be associated to a resistant profile to UHDR (Chabi et al. 2020). Furthermore, Spitz et al. proposed another hypothesis explaining the differential impact of UHDR vs. conventional dose rate irradiation on cancer and normal tissue responses (as described in the summary at the end of the biological section).

(Simmons et al. 2019). Reactive astrogliosis, microglial and C3 complement activation were also found to be reduced following UHDR irradiation (Montay-Gruel et al. 2020), along with a preservation of vascular integrity and the blood-brain barrier (Allen et al. 2020) (Figure 3), data that provided new physiopathological insights. More recently, with the goal to overcome radiation-induced toxicities of pediatric patient stricken with medulloblastoma and to improve their long-term quality of life, the effect of UHDR has been evaluated using juvenile mice. Memory loss, anxiety-like behaviors and the neurogenic niche were spared after whole brain irradiation at 8 Gy using electron at UHDR (Alaghband et al. 2020). In parallel, while UHDR spared normal brain tissue toxicity and reduced neuro-inflammation, its efficacy on glioblastoma (GBM) was found to be similar to irradiation at conventional dose rate, suggesting that the anti-tumor efficacy of radiotherapy was independent of dose rate (Montay-Gruel et al. 2021). As fractionated regimens are the standard of care for GBM treatment in current clinical practice, 4×3.5 Gy, 2×7 Gy, and 3×10 Gy regimens were investigated. UHDR reduced neurocognitive decline in GBM tumor bearing mice while tumor control was comparable to CONV-RT (Montay-Gruel et al. 2021).

Normal skin and subcutaneous tumors

In a subcutaneous mouse model of Lewis lung carcinoma (LLC), the normal vasculature was also shown to be preserved after exposure to 15 Gy electron at UHDR (352 Gy/s) whereas critical vascular collapse was observed after exposure to CONV dose rate (0.06 Gy/s) (Kim et al. 2020). The preservation of the vasculature after UHDR exposure was associated with reduced phosphorylation of the myosin light chain (p-MLC) known to be involved in the contraction of endothelial cells and reduction of immune cell infiltration. Interestingly, combination of CONV-RT with an MLC kinase inhibitor (ML-7) replicated UHDR results identifying the MLC pathway as one potential molecular target of irradiation at UHDR. In another study, a dose escalation study was performed and showed that 30 and 40 Gy irradiation at UHDR (electron, 180 Gy/s) resulted in reduced skin ulceration in contrast to CONV-RT (0.07 Gy/s) (Soto et al. 2020). Recent studies performed with proton beams, reported similar results with 35 Gy delivered with a FLASH scanning proton pencil beam (FLASH-Proton-PBS) (Cunningham et al. 2021) and a FLASH transmission proton beam (Velalopoulou et al. 2021). In Cunningham et al. study, skin toxicity and leg contraction were decreased significantly after exposure to UHDR (115 Gy/s) (Cunningham et al. 2021). Furthermore, this study showed similar tumor

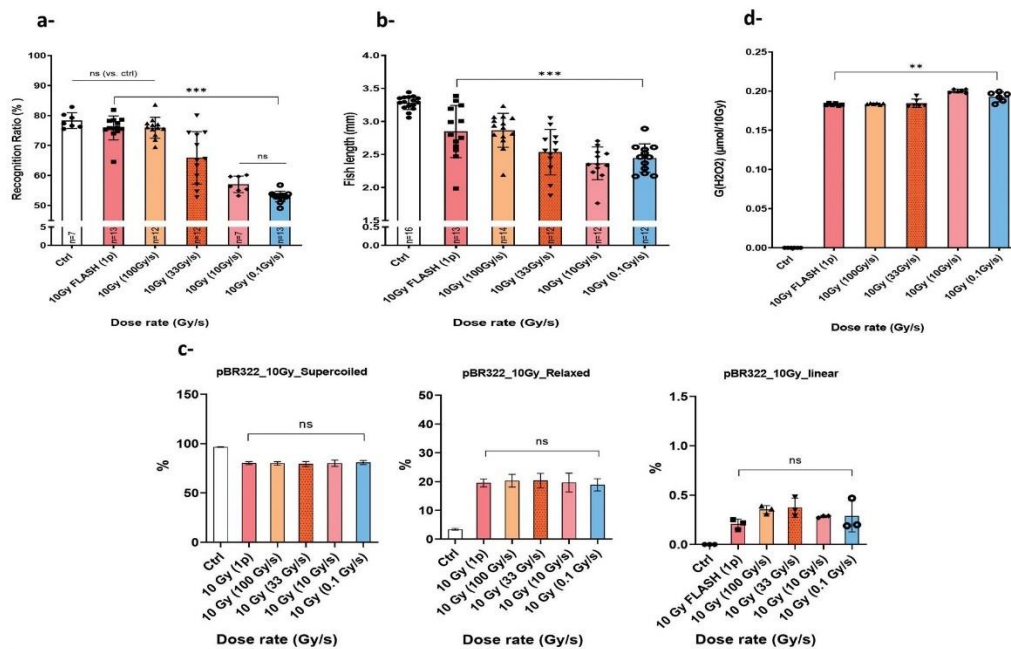


Figure 4. Dose rate de-escalation was performed in mice, zebrafish embryos, plasmid and water using 10 Gy. (a) Recognition ratio (RR) evaluation two months post irradiation for control mice group and groups that received 10 Gy WBI delivery with a dose rate delivered in a single 1.8 μ s electron pulse and ranging from (0.1, 10, or 100, 33, 10, 0.1 Gy/s). No memory alteration was observed in the groups irradiated with 100 Gy/s or higher, RR was comparable to the control group. Whereas a significant drop in the RR was observed for the group irradiated at 33 Gy/s. The drop became even slightly larger as the dose rate was further lowered (adapted from Montay-Gruel 2017). (b) Wild-type zebrafish embryos were irradiated four hours post fertilization and body length measurement five days post fertilization was used to assess radiation-induced injury. Similarly, with the murine recognition ratio results, both highest dose rates (5.6×10^5 Gy/s and 100 Gy/s) showed less alteration in body length as compared to non-irradiated embryos. Whereas, less protection was observed at lower dose rates and no protection at CONV-RT dose rate. Mean \pm SD. *p* Values derived from Mann–Whitney’s test: **p* < .05; ***p* < .01; ****p* < .001 (*N* = 12–16 embryos/group). (c) Dose rate de-escalation involved irradiation at 10 Gy of pBR322 plasmids in aqueous solutions equilibrated at physiological oxygen conditions (4%). Notably, no difference in DNA damage was measured after UHDR compared to CONV-RT. Mean \pm SD. *p* Values were derived from one-way ANOVA and Tukey’s multiple comparisons test. (d) H₂O₂ was quantified with the fluorogenic assay AmplexRed after 10 Gy irradiation of water samples equilibrated at 4% O₂ following dose rate de-escalation similarly like described in the previous models. The radiolytic yield of H₂O₂ was significantly lower for the highest dose rates. Whereas, an increase in G(H₂O₂) was observed when the dose rate is lowered. This differential production reveals a decrease in ROS production following UHDR. Mean \pm SD. *p* Values were derived from Mann–Whitney’s *U* test: **p* < .01.

control of subcutaneous MOC1 and MOC2 head and neck cancer cells after UHDR protons and CONV protons (CONV-PRT) in immunocompetent mice. In Velapoulou et al. study, 30 Gy using UHDR proton radiotherapy (UHDR-PRT, 69–124 Gy/s) spared the skin leg and mesenchymal tissues of muscles and bones from severe toxicities. In contrast, CONV-PRT (0.39–0.65 Gy/s) increased TGF- β 1 both in murine and canine skin. UHDR-PRT and CONV-PRT equally controlled subcutaneous and intramuscular sarcoma tumors (Velapoulou et al. 2021).

Gastrointestinal track and abdominal tumors

In addition to the benefits reported in late responding organs, UHDR irradiation was also beneficial in acute responding organs such as the gastrointestinal track and the hematopoietic system (see section ‘The FLASH effect validated in patient and human samples’, and Chabi et al. 2020). Intestinal function, epithelial integrity and regenerating crypts were preserved while DNA damage and apoptosis

in the columnar cells of the crypt were reduced after exposure to 14 Gy at UHDR (216 Gy/s, electron). Again, anti-tumor efficacy in a preclinical mouse model of ovarian cancer (ID8) was comparable to that obtained with CONV-RT (0.08 Gy/s) (Levy et al. 2020). The beneficial effects of UHDR were again validated with proton and photon beams using pancreatic tumor models. The radiation-induced gastrointestinal syndrome did not occur upon UHDR irradiation using 18 Gy proton radiotherapy (UHDR-PRT) (Diffenderfer et al. 2020) and with 15 Gy X-rays (Gao et al. 2020) suggesting that the FLASH effect is relatively independent of the ionizing radiation modality. Recently, using GI as model, the FLASH effect was confirmed with spread-out Bragg peak irradiation. Using a pulsed synchrocyclotron, Evan et al. showed that mice irradiated at 10–16 Gy UHDR (96 Gy/s) exhibited enhanced survival with LD50 reaching 14.1 Gy with UHDR vs. 13.5 Gy with conventional dose rate (Evans et al. 2021). Consistently, Kim et al. study compares the outcome of the proton transmission at UHDR (UHDR-PRT transmission) vs. the spread-out Bragg peak (UHDR-

PRT SOBP) in mouse intestine and pancreatic tumor control. Toxicity was significantly decreased in both configurations, i.e. 15 Gy UHDR-PRT SOBP (108.2 ± 8.3 Gy/s) vs. UHDR-PRT transmission (107.1 ± 15.2 Gy/s). In contrast, conventional dose rate proton transmission (CONV-PRT transmission, 0.83 ± 0.19 Gy/s) and SOBP (CONV-PRT SOBP, 0.82 ± 0.14 Gy/s) both generated important damages with reduced regenerating and proliferating crypts. Importantly, 18 Gy at UHDR and conventional dose rate irradiation were equipotent to control subcutaneous MH641905 mouse pancreatic tumors in both transmission and spread-out Bragg peak dose regions. All mice treated with CONV-PRT and UHDR-PRT transmission survived the treatment. In SOBP, 70% of the mice treated at conventional dose rate died 20 days after irradiation whereas UHDR induced only 15% of lethality (Kim et al. 2021). Ultimately, Ruan et al. also reported a decreased gastrointestinal toxicity and better crypt survival at UHDR (electron, 7.5–12.5 Gy, $2-6 \times 10^6$ Gy/s) with a relatively low dose-modifying factor of 1.1, in comparison to conventional dose rate (CONV, 0.25 Gy/s). The FLASH effect was lost when delivery time between two pulses and pulse repetition number were increased, highlighting the relevance of parameterization studies to define the FLASH effect (Ruan et al. 2021).

Negative studies

While studies on the FLASH effect have now been extended and validated across multiple animal models, other studies investigating UHDR irradiation have not reported beneficial effects. Exposure of 24 hour post-fertilization (hpf) zebrafish embryos with a proton beam at 100 Gy/s and 0.08 Gy/s showed no difference in survival and morphology (Beyreuther et al. 2019). With synchrotron X-ray at 37–41 Gy/s and 0.06 Gy/s, no difference was reported after total body, thoracic and abdominal irradiation (Smyth et al. 2018). Similarly, cardiac and splenic irradiation of mice with electron beams, 35 Gy/s and 0.1 Gy/s caused lymphopenia (Venkatesulu et al. 2020). While the basis of these negative results have to be carefully explored, certain caveats may well be related to the low dose rates and experimental setup used in these studies.

The FLASH effect validated in patient and human samples

With the principal aim to transfer FLASH-RT into early clinical trials, our group investigated the FLASH effect on the skin of a mini-pig. A dose escalation study in cat-cancer patients with squamous cell carcinoma of the nasal planum identified 34 Gy as a tolerated and efficacious dose (Vozenin et al. 2019) and a phase III validation trial is currently ongoing. A dose escalation trials in dog patients with various superficial solid tumors has been published with only three/six month follow up (Konradsson et al. 2021). In addition, a feasibility study on dog-patients with osteosarcoma evaluated acute production of TGF- β and found minimal production following 12 Gy UHDR protons irradiation (Velalopoulou et al. 2021). Similarly, one feasibility study in one human patient is available (Bourhis et al. 2019a, 2019b)

and one with UHDR protons is ongoing (FATS01); however, only few results are available with human cells and samples. Recently, we evaluated the effect of FLASH-RT on three patient-derived xenograft (PDX) of human T-acute lymphoblastic leukemia (T-ALL). We found that two out of three were sensitive to UHDR irradiation. Their genomic imprint revealed a putative susceptibility profile in T-ALL tumors and suggests that T-ALL sensitivity to UHDR could be related to the expression of certain genes including GADD45, involved in the control of the cell cycle G2/M checkpoint and FAT1 that regulates wnt pathway and cell division. In contrast, AGAP9 and PDLIM1 expressions seem to be associated to a resistant profile to UHDR (Chabi et al. 2020). Further studies are ongoing to elucidate this question.

Table 1 and Table 2 (Supplementary material) summarize positive and negative studies investigating the FLASH effect.

Interestingly, UHDR and conventional dose rate irradiation are equipotent to control tumors, suggesting that tumor but not normal tissue sensitivity is dose rate independent. The mechanistic basis of this differential effect triggered by UHDR on tumors vs. normal tissue is under scrutiny. One interesting hypothesis has been proposed by Spitz et al. and is based on differential distribution of organic hydroperoxides after UHDR vs. conventional dose rate irradiation. Hydroperoxides, derived from Fenton and peroxidation chain reactions are produced immediately at equal levels in normal and tumor tissue following UHDR. In normal tissues, antioxidants pathways remove more effectively than the organic hydroperoxides as compared to the tumor (higher levels of redox-active iron). Thus, explaining the beneficial therapeutic index of the FLASH effect in normal tissue compared to tumor. Whereas, at conventional dose rates, levels of hydroperoxides seem too low to uncover the differences in the tumor vs. normal tissue in oxidative metabolism (Spitz et al. 2019).

Example of experiments integrating biology and chemistry to investigate dose rate effect: from murine cognition and zebrafish embryo development to plasmid damage and H₂O₂ Yield

In this paper, we reviewed the current knowledge and approaches available to investigate the impact of dose rate from chemical systems to complex biological models. In this paragraph, we will give an example of integrated experiments performed to investigate the FLASH effect. We started from the first systematic investigation of the FLASH effect, that we performed several years ago using normal brain toxicity as the main outcome for the FLASH sparing effect (Montay-Gruel et al. 2017). The dose rate de-escalation study started with 10 Gy delivered in one pulse of 1.8 micros (5.6×10^6 Gy/s) until 0.1 Gy/s, the latter of which corresponds to conventional dose rates used in the clinic. Full preservation of neurocognitive function was obtained above 100 Gy/s, whereas it dropped at 30 Gy/s and was abolished at 0.1 Gy/s (Figure 4(a)). Then to derive different dose rate threshold data for a separate endpoint, dose rate escalation was performed at a fixed 10 Gy total dose in zebrafish

embryos with body length measurement as an outcome (Figure 4). Interestingly, zebrafish embryos corroborated data derived from mice (Figure 4(b)) with a remarkable consistency (correlation coefficient >0.94). Next, experiments were pursued with pBR322 plasmids irradiated in aqueous solutions equilibrated at physiological oxygen conditions (4%). Notably, no difference in SSB yields (open circular DNA) was measured after UHDR compared to CONV-RT, whereas DSB yields (linear DNA) after 10 Gy were close to the detection limit of AGE (Figure 4(c)). Importantly, assuming that 4% oxygen mimics normal tissue oxygenation, these results suggest that UHDR irradiation does not modify DNA damage under physiological conditions. Finally, H_2O_2 production in terms of $G(H_2O_2)$ ($\mu M/10$ Gy) was measured in cell-free systems and at physiological oxygen levels. Interestingly, the radiolytic production of H_2O_2 was reduced at the highest dose rates 5.6×10^6 Gy/s and 100 Gy/s, whereas an increase in $G(H_2O_2)$ was observed with lower dose rates (Figure 4(d)) as previously described (Montay-Gruel et al. 2019). The beam parameters required to perform these studies are summarized in Figure 4(e).

The reduced production of H_2O_2 was consistent with the lower toxicities observed in normal tissues. In this context, the role for oxygen, reduced ROS production, altered redox biology and modifications of the biological cascade downstream remain relevant and constitute a key focus of our ongoing research efforts. However, other important physiological factors such as temperature, proliferation status, and metabolism (among others) are likely to play a certain role in mediating the FLASH effect, and will require further experimental validation.

Acknowledgements

The authors thank Charles Limoli for discussions in the preparation of this MS as well as help with English edition. We would like to thank Jonathan Ollivier for the help doing zebrafish experiments as well as Benoit Petit for the animal handling. We would like to thank the team of Institute of Radiation Physics (IRA, CHUV) especially François Bochud, Claude Bailat, Pascal Froidevaux, Jerome Damet, Raphael Moeckli, Veljko Grilj, Patrik Jorge Gonçalves and Jean-François Germond for the development of the physics part of the FLASH-RT program at CHUV as well as Jean Bourhis for his support. We would like to thank the Epalinges Animal Facility for the animal care-taking as well as Francesca Amati at the zebrafish facility. Figures were created with BioRender.com.

Disclosure statement

No potential conflict of interest was reported by the author(s).

Funding

The FLASH studies are supported by a grant from the Fond National Suisse Synergia Grant [FNS CRS I15_186369], ISREC Foundation thanks to Bilema Donation and NIH Program Project Grant PO1CA244091. HK salary is supported by FNS Synergia Grant [FNS CRS I15_186369], AA by NIH Program Project Grant PO1CA244091. This work is also supported by the Fondation ISREC and Schweizerischer Nationalfonds zur Förderung der Wissenschaftlichen Forschung.

Notes on contributors

Houda Kacem, PhD Student Research interest I am investigating the oxygen contribution and production of reactive oxygen species after FLASH irradiation in cell free systems and biological systems such as normal/tumor cells and zebrafish model. Background I'm a chemist by training. I have graduated from the international Erasmus Master's program SERP+, at the University of Paris-Saclay (France) and the University of Porto (Portugal).

Aymeric Almeida, PhD Student Research interest I'm investigating the anti tumor immune response and downstream immune cascade, activated or not, in lung tumor, glioblastoma and normal tissue after irradiation at ultra high dose rate (FLASH). Background I studied at l'Université Claude Bernard Lyon where I obtained my bachelor in physiology and subsequently did a Masters in Immunology & Cancer at the University of Lausanne.

Nicolas Cherbuin, Technician RTT Research interest I have an interest in research for the benefit of radiation protection of patients, workers and the public, and therefore involved in projects ranging from radiobiology to occupational dosimetry monitoring. Background with a Bachelor's in Medical Radiology Technics study (HES-SO, HESAV) gained in 2008, I worked in the Service of nuclear medicine of the Lausanne University Hospital, particularly working on radiation therapies. In 2014, I moved to the hospital's Institute of radiation physics, as a scientific collaborator and radiation protection expert. I completed the joint HES-SO/UNIL Master's in Health Sciences in 2021, in the course of which I had the chance to begin an ongoing collaboration with the Vozenin Lab.

Marie-Catherine Vozenin, PhD Associate professor in the service of Radio-oncology, CHUV/UNIL Head of the radio-Oncology Laboratory, CHUV Adjunct Professor, University of California Irvine Research interest: The research project that I develop with my team aim at finding innovative tools able to protect normal tissue and enhance tumor control. In this context, we have developed a novel of modality of radiation therapy called FLASH radiotherapy that minimizes normal tissue toxicity and eradicates tumors in various organs including the brain, lung and skin, and in various species including mice, zebrafish, pigs and cats. Much of our recent work has focused on investigating the entirely different biological response induced after FLASH exposure. Importantly, we have worked to secure the translation of FLASH-RT into clinical trials for human patient with cancer.

ORCID

Marie-Catherine Vozenin  <http://orcid.org/0000-0002-2109-8073>

References

- Alagbhand Y, Cheeks SN, Allen BD, Montay-Gruel P, Doan N-L, Petit B, Jorge PG, Giedzinski E, Acharya MM, Vozenin M-C, et al. 2020. Neuroprotection of radiosensitive juvenile mice by ultra-high dose rate FLASH irradiation. *Cancers*. 12(6):1671.
- Allen BD, Acharya MM, Montay-Gruel P, Jorge PG, Bailat C, Petit B, Vozenin M-C, Limoli C. 2020. Maintenance of tight junction integrity in the absence of vascular dilation in the brain of mice exposed to ultra-high-dose-rate FLASH irradiation. *Radiat Res*. 194(6): 625–635.
- Auclair G. 2001. Determination of primary yields in the alpha radiolysis of alkaline water [Determination des rendements radiolytiques primaires alpha en milieu alcalin]. Paris, France: University Pierre et Marie Curie. Available from INIS: http://inis.iaea.org/search/search.aspx?orig_q=RN:46133716
- Baldacchino G, Brun E, Denden I, Bouhadoun S, Roux R, Khodja H, Sicard-Roselli C. 2019. Importance of radiolytic reactions during high-LET irradiation modalities: LET effect, role of O_2 and radiosensitization by nanoparticles. *Cancer Nano*. 10(1):3.

- Barilla J, Lokajčec M. 2000. The role of oxygen in DNA damage by ionizing particles. *J Theor Biol.* 207(3):405–414.
- Beyreuther E, Brand M, Hans S, Hideghéty K, Karsch L, Leßmann E, Schürer M, Szabó ER, Pawelke J. 2019. Feasibility of proton FLASH effect tested by zebrafish embryo irradiation. *Radiother Oncol.* 139: 46–50.
- Bourhis J, Montay-Gruel P, Gonçalves Jorge P, Bailat C, Petit B, Ollivier J, Jeanneret-Sozzi W, Ozsahin M, Bochud F, Moeckli R, et al. 2019a. Clinical translation of FLASH radiotherapy: why and how? *Radiother Oncol.* 139:11–17.
- Bourhis J, Sozzi WJ, Jorge PG, Gaide O, Bailat C, Duclos F, Patin D, Ozsahin M, Bochud F, Germond J-F, et al. 2019b. Treatment of a first patient with FLASH-radiotherapy. *Radiother Oncol.* 139:18–22.
- Cao X, Zhang R, Espipova TV, Allu SR, Ashraf R, Rahman M, Gunn JR, Bruza P, Gladstone DJ, Williams BB, et al. 2021. Quantification of oxygen depletion during FLASH irradiation in vitro and in vivo. *Int J Radiat Oncol Biol Phys.* 111(1):240–248.
- Chabi S, Van To TH, Leavitt R, Poglio S, Jorge PG, Jaccard M, Petersson K, Petit B, Roméo P-H, Pflumio F, et al. 2020. Ultra-high-dose-rate FLASH and conventional-dose-rate irradiation differentially affect human acute lymphoblastic leukemia and normal hematopoiesis. *Int J Radiat Oncol.* 109(3):819–829.
- Cowan R, Collis CM, Grigg GW. 1987. Breakage of double-stranded DNA due to single-stranded nicking. *J Theor Biol.* 127(2):229–245.
- Cunningham S, McCauley S, Vairamani K, Speth J, Girdhani S, Abel E, Sharma RA, Perentesis JP, Wells SI, Mascia A, et al. 2021. FLASH proton pencil beam scanning irradiation minimizes radiation-induced leg contracture and skin toxicity in mice. *Cancers.* 13(5): 1012.
- Diffenderfer ES, Verginadis II, Kim MM, Shoniyozov K, Velopoulou A, Goia D, Putt M, Hagan S, Avery S, Teo K, et al. 2020. Design, implementation, and in vivo validation of a novel proton FLASH radiation therapy system. *Int J Radiat Oncol Biol Phys.* 106(2): 440–448.
- Evans T, Cooley J, Wagner M, Yu T, Zwart T. 2021. Demonstration of the FLASH effect within the spread-out Bragg peak after abdominal irradiation of mice. *Int J Part Ther.*
- Favaudon V, Caplier L, Monceau V, Pouzoulet F, Sayarath M, Fouillade C, Poupon M-F, Brito I, Hupé P, Bourhis J, et al. 2014. Ultrahigh dose-rate FLASH irradiation increases the differential response between normal and tumor tissue in mice. *Sci Transl Med.* 6(245):245ra93.
- Field SB, Bewley DK. 1974. Effects of dose-rate on the radiation response of rat skin. *Int J Radiat Biol Relat Stud Phys Chem Med.* 26(3):259–267.
- Fouillade C, Curras-Alonso S, Giuranno L, Queleñec E, Heinrich S, Bonnet-Boissinot S, Beddok A, Leboucher S, Karakurt HU, Bohec M, et al. 2020. FLASH irradiation spares lung progenitor cells and limits the incidence of radio-induced senescence. *Clin Cancer Res.* 26(6):1497–1506.
- Gao F, Yang Y, Zhu H, Wang J, Xiao D, Zhou Z, Dai T, Zhang Y, Feng G, Li J, et al. 2020. First demonstration of the FLASH effect with ultrahigh dose-rate high energy X-rays. *bioRxiv.*
- Georgakilas AG, O'Neill P, Stewart RD. 2013. Induction and repair of clustered DNA lesions: what do we know so far? *Radiat Res.* 180(1): 100–109.
- Hendry JH, Moore JV, Hodgson BW, Keene JP. 1982. The constant low oxygen concentration in all the target cells for mouse tail radionecrosis. *Radiat Res.* 92(1):172–181.
- Hiroki A, Pimblott SM, LaVerne JA. 2002. Hydrogen peroxide production in the radiolysis of water with high radical scavenger concentrations. *J Phys Chem A.* 106(40):9352–9358.
- Hornsey S, Bewley DK. 1971. Hypoxia in mouse intestine induced by electron irradiation at high dose-rates. *Int J Radiat Biol Relat Stud Phys Chem Med.* 19(5):479–483.
- Hu A, Qiu R, Wu Z, Li C, Zhang H, Li J. 2020. Oxygen depletion hypothesis remains controversial: a mathematical model of oxygen depletion during FLASH radiation. *ArXiv200110788 Phys. Q-Bio.*
- Jaccard M, Durán MT, Petersson K, Germond J-F, Liger P, Vozenin M-C, Bourhis J, Bochud F, Bailat C. 2018. High dose-per-pulse electron beam dosimetry: commissioning of the Oriatron eRT6 prototype linear accelerator for preclinical use. *Med Phys.* 45(2): 863–874.
- Jansen J, Knoll J, Beyreuther E, Pawelke J, Skuza R, Hanley R, Brons S, Pagliari F, Seco J. 2021. Does FLASH deplete oxygen? Experimental evaluation for photons, protons and carbon ions. *ArXiv210212762 Phys.*
- Kim MM, Verginadis II, Goia D, Haertter A, Shoniyozov K, Zou W, Maity A, Busch TM, Metz JM, Cengel KA, et al. 2021. Comparison of FLASH proton entrance and the spread-out Bragg peak dose regions in the sparing of mouse intestinal crypts and in a pancreatic tumor model. *Cancers.* 13(16):4244.
- Kim Y-E, Gwak S-H, Hong B-J, Oh J-M, Choi H-S, Kim MS, Oh D, Lartey F, Rafat M, Schüler E, et al. 2020. Effects of ultra-high dose-rate FLASH irradiation on the tumor microenvironment in Lewis lung carcinoma: role of myosin light chain. *Int J Radiat Oncol Biol Phys.* 109(5):1440–1453.
- Konradsson E, Arendt ML, Bastholm Jensen K, Børresen B, Hansen AE, Bäck S, Kristensen AT, Munck af Rosenschöld P, Ceberg C, Petersson K. 2021. Establishment and initial experience of clinical FLASH radiotherapy in canine cancer patients. *Front Oncol.* 11: 658004.
- Krisch RE, Flick MB, Trumbore CN. 1991. Radiation chemical mechanisms of single- and double-strand break formation in irradiated SV40 DNA. *Radiat Res.* 126(2):251–259.
- Labarbe R, Hotoiu L, Barbier J, Favaudon V. 2020. A physicochemical model of reaction kinetics supports peroxy radical recombination as the main determinant of the FLASH effect. *Radiother Oncol.* 153: 303–310.
- Levy K, Natarajan S, Wang J, Chow S, Eggold JT, Loo PE, Manjappa R, Melemenidis S, Lartey FM, Schüler E, et al. 2020. Abdominal FLASH irradiation reduces radiation-induced gastrointestinal toxicity for the treatment of ovarian cancer in mice. *Sci Rep.* 10(1): 21600.
- Mazal A, Vera Sanchez JA, Sanchez-Parcerisa D, Udias JM, España S, Sanchez-Tembleque V, Fraile LM, Bragado P, Gutierrez-Uzquiza A, Gordillo N, et al. 2020. Biological and mechanical synergies to deal with proton therapy pitfalls: minibeam, FLASH, arcs, and gantryless rooms. *Front Oncol.* 10:613669.
- McMahon SJ, Currell FJ. 2011. A robust curve-fitting procedure for the analysis of plasmid DNA strand break data from gel electrophoresis. *Radiat Res.* 175(6):797–805.
- Moeckli R, Germond J-F, Bailat C, Bochud F, Vozenin M-C, Bourhis J. 2020. In regard to van Marlen et al. *Int J Radiat Oncol Biol Phys.* 107(5):1012–1013.
- Montay-Gruel P, Acharya MM, Gonçalves Jorge P, Petit B, Petridis IG, Fuchs P, Leavitt R, Petersson K, Gondré M, Ollivier J, et al. 2021. Hypofractionated FLASH-RT as an effective treatment against glioblastoma that reduces neurocognitive side effects in mice. *Clin Cancer Res.* 27(3):775–784.
- Montay-Gruel P, Acharya MM, Petersson K, Alikhani L, Yakkala C, Allen BD, Ollivier J, Petit B, Jorge PG, Syage AR, et al. 2019. Long-term neurocognitive benefits of FLASH radiotherapy driven by reduced reactive oxygen species. *Proc Natl Acad Sci U S A.* 116(22): 10943–10951.
- Montay-Gruel P, Bouchet A, Jaccard M, Patin D, Serduc R, Aim W, Petersson K, Petit B, Bailat C, Bourhis J, et al. 2018. X-rays can trigger the FLASH effect: ultra-high dose-rate synchrotron light source prevents normal brain injury after whole brain irradiation in mice. *Radiother Oncol.* 129(3):582–588.
- Montay-Gruel P, Markarian M, Allen BD, Baddour JD, Giedzinski E, Jorge PG, Petit B, Bailat C, Vozenin M-C, Limoli C, et al. 2020. Ultra-high-dose-rate FLASH irradiation limits reactive gliosis in the brain. *Radiat Res.* 194(6):636–645.
- Montay-Gruel P, Petersson K, Jaccard M, Boivin G, Germond J-F, Petit B, Doenlen R, Favaudon V, Bochud F, Bailat C, et al. 2017. Irradiation in a flash: unique sparing of memory in mice after whole brain irradiation with dose rates above 100 Gy/s. *Radiother Oncol.* 124(3):365–369.

- Nikjoo H, Uehara S, Wilson WE, Hoshi M, Goodhead DT. 1998. Track structure in radiation biology: theory and applications. *Int J Radiat Biol.* 73:355–364.
- Pachnerová Brabcová K, Sihver L, Ukraintsev E, Štěpán V, Davidková M. 2019. How detection of plasmid DNA fragmentation affects radiation strand break yields. *Radiat Prot Dosimetry.* 183(1–2):89–92.
- Petersson K, Adrian G, Butterworth K, McMahon SJ. 2020. A quantitative analysis of the role of oxygen tension in FLASH radiation therapy. *Int J Radiat Oncol Biol Phys.* 107(3):539–547.
- Pogozelski WK, Tullius TD. 1998. Oxidative strand scission of nucleic acids: routes initiated by hydrogen abstraction from the sugar moiety. *Chem Rev.* 98(3):1089–1108.
- Pratx G, Kapp DS. 2019. A computational model of radiolytic oxygen depletion during FLASH irradiation and its effect on the oxygen enhancement ratio. *Phys Med Biol.* 64(18):185005.
- Ruan J-L, Lee C, Wouters S, Tullis ID, Verslegers M, Mysara M, Then CK, Smart SC, Hill MA, Muschel RJ, et al. 2021. Irradiation at ultra-high (FLASH) dose rates reduces acute normal tissue toxicity in the mouse gastrointestinal system. *Int J Radiat Oncol Biol Phys.*
- Schüller A, Heinrich S, Fouillade C, Subiel A, De Marzi L, Romano F, Peier P, Trachsel M, Fleta C, Kranzer R, et al. 2020. The European Joint Research Project UHDPulse – metrology for advanced radiotherapy using particle beams with ultra-high pulse dose rates. *Phys Med.* 80:134–150.
- Shikazono N, Noguchi M, Fujii K, Urushibara A, Yokoya A. 2009. The yield, processing, and biological consequences of clustered DNA damage induced by ionizing radiation. *J Radiat Res.* 50(1):27–36.
- Siddiqi MA, Bothe E. 1987. Single- and double-strand break formation in DNA irradiated in aqueous solution: dependence on dose and OH radical scavenger concentration. *Radiat Res.* 112(3):449–463.
- Simmons DA, Lartey FM, Schüller E, Rafat M, King G, Kim A, Ko R, Semaan S, Gonzalez S, Jenkins M, et al. 2019. Reduced cognitive deficits after FLASH irradiation of whole mouse brain are associated with less hippocampal dendritic spine loss and neuroinflammation. *Radiother Oncol.* 139:4–10.
- Small KL, Henthorn NT, Angal-Kalinin D, Chadwick AL, Santana E, Aitkenhead A, Kirkby KJ, Smith RJ, Surman M, Jones J, et al. 2021. Evaluating very high energy electron RBE from nanodosimetric pBR322 plasmid DNA damage. *Sci Rep.* 11(1):3341.
- Smyth LML, Donoghue JF, Ventura JA, Livingstone J, Bailey T, Day LRJ, Crosbie JC, Rogers PAW. 2018. Comparative toxicity of synchrotron and conventional radiation therapy based on total and partial body irradiation in a murine model. *Sci. Rep.* 8:12044.
- Soto LA, Casey KM, Wang J, Blaney A, Manjappa R, Breitkreutz D, Skinner L, Dutt S, Ko RB, Bush K, et al. 2020. FLASH irradiation results in reduced severe skin toxicity compared to conventional-dose-rate irradiation. *Radiat Res.* 194(6):618–624.
- Spitz DR, Buettner GR, Petronek MS, St-Aubin JJ, Flynn RT, Waldron TJ, Limoli CL. 2019. An integrated physico-chemical approach for explaining the differential impact of FLASH versus conventional dose rate irradiation on cancer and normal tissue responses. *Radiother Oncol.* 139:23–27.
- Spotheim-Maurizot M, editor. 2008. *Radiation chemistry: from basics to applications in material and life sciences, L'actualité chimique livres.* Les Ulis, France: EDP Sciences.
- Sutherland JC, Monteleone DC, Trunk JG, Bennett PV, Sutherland BM. 2001. Quantifying DNA damage by gel electrophoresis, electronic imaging and number-average length analysis. *Electrophoresis.* 22(5):843–854.
- Velalopoulou A, Karagounis IV, Cramer GM, Kim MM, Skoufos G, Goia D, Hagan S, Verginadis II, Shoniyozov K, Chiango J, et al. 2021. FLASH proton radiotherapy spares normal epithelial and mesenchymal tissues while preserving sarcoma response. *Cancer Res.* 81(18):4808–4821.
- Venkatesulu BP, Sharma A, Pollard-Larkin JM, Sadagopan R, Symons J, Neri S, Singh PK, Tailor R, Lin SH, Krishnan S. 2020. Author correction: ultra high dose rate (35 Gy/sec) radiation does not spare the normal tissue in cardiac and splenic models of lymphopenia and gastrointestinal syndrome. *Sci Rep.* 10:11018.
- von Sonntag C. 1991. The chemistry of free-radical-mediated DNA damage. *Basic Life Sci.* 58:287–317, discussion 317–321.
- Vozenin M-C, De Fornel P, Petersson K, Favaudon V, Jaccard M, Germond J-F, Petit B, Burki M, Ferrand G, Patin D, et al. 2019. The advantage of FLASH radiotherapy confirmed in mini-pig and cat-cancer patients. *Clin Cancer Res.* 25(1):35–42.
- Vozenin M-C, Hendry JH, Limoli CL. 2019. Biological benefits of ultra-high dose rate FLASH radiotherapy: sleeping beauty awoken. *Clin Oncol (R Coll Radiol).* 31(7):407–415.
- Ward JF. 1981. Some biochemical consequences of the spatial distribution of ionizing radiation-produced free radicals. *Radiat Res.* 86(2):185–195.
- Ward JF. 1985. Biochemistry of DNA lesions. *Radiat Res Suppl.* 8: S103–S111.
- Wasselin-Trupin V, Baldacchino G, Bouffard S, Hickel B. 2002. Hydrogen peroxide yields in water radiolysis by high-energy ion beams at constant LET. *Radiat Phys Chem.* 65(1):53–61.
- Wilson JD, Hammond EM, Higgins GS, Petersson K. 2020. Ultra-high dose rate (FLASH) radiotherapy: silver bullet or fool's gold? *Front Oncol.* 9:9.
- Zhou S, Zheng D, Fan Q, Yan Y, Wang S, Lei Y, Besemer A, Zhou C, Enke C. 2020. Minimum dose rate estimation for pulsed FLASH radiotherapy: a dimensional analysis. *Med Phys.* 47(7):3243–3249.

Supplementary Tables

Supp Table 1: Radiobiological investigations of the differential FLASH effect of UHDR-RT in normal tissue toxicity and tumor control.

Ref.	Model/mouse	Beams, particles and parameters	Major outcomes	
			Tumor	Normal tissue
Normal lung and tumors				
Favaudon et al., 2014	Thorax irradiation of mice. Female C57BL/6J TC1 lung tumors & human HBCx-12A / HEP-2 tumor in Swiss Nude mice.	FLASH-RT: Kinetron (4.5 MeV), 15-30 Gy, single dose, 60 Gy/s CONV-RT: kinetron or Cs-137/X-rays, 17 Gy, single dose, 0.03 Gy/s	Isoefficacy to control lung tumors upon 17 Gy FLASH and CONV-RT.	20 Gy FLASH-RT: No fibrosis, no TGF- β signalling, 30 Gy FLASH-RT: apoptosis in blood vessels and bronchi. 17 Gy CONV-RT: Fibrosis, TGF- β signalling. 7.5 Gy CONV-RT: Apoptosis in the blood vessels and bronchi.
Fouillade et al., 2020	Thorax irradiation of mice.	FLASH-RT: Kinetron (4.5 MeV), 17 Gy, single dose, 60 Gy/s CONV-RT: kinetron or Cs-137/X-rays, 17 Gy, single dose, 0.03 Gy/s	Similar γ H2AX and 53BP1 in both modalities.	17 Gy FLASH-RT: no TGF- β 1 and Cebpb (sc-RNA seq), less DNA damages and repair mechanisms (similar γ H2AX, decreased 53BP1), decreased senescent cells (SA- β -gal clusters) and spares lung progenitor. 17 Gy CONV-RT: TGF- β 1 and Cebpb, persistent DNA damages, increased senescent cells.
Gao et al., 2020	Thorax and abdominal irradiation, C57BL6 mice (normal tissue). ETM6 breast tumor homografts in Balb/c mice.	High energy X-rays, Linac 8 MeV. FLASH-RT: 18 Gy (tumor), 30 Gy (thorax), 15 Gy (abdominal), 900-1200 Gy/s CONV-RT: 15 Gy (tumor), 24 Gy (thorax), 12 Gy (abdominal), 0.1 Gy/s	18 Gy FLASH-RT better controlled the tumor than 15Gy CONV-RT.	FLASH-RT: 90% of thorax irradiated mice survived the treatment. Preservation of alveolar structures. CONV-RT: 50% of thorax irradiated mice survived the treatment. Increased inflammation in the lung and loss of alveolar structures.
Normal brain and GBM				
Montay-Gruel et al., 2017	Whole Brain irradiation (WBI), Female C57BL6 mice.	Pulsed electron eRT6 6 MeV. CONV-RT: 10 Gy, single dose, 0.1 Gy/s. FLASH-RT: 10 Gy, single dose, up to 10 ⁷ Gy/s, 1 pulse.	No data	<u>Dose escalation:</u> From 100 Gy/s to 5.6x10 ⁶ Gy/s: spares memory and preservation of neurogenesis, FLASH effect. From 0.1 Gy/s to 30 Gy/s: memory decrement, loss of the FLASH effect.
Montay-Gruel et al., 2019	WBI, Female C57BL6 mice, normoxic and hyperoxic condition. Zebrafish (embryonic development).	Pulsed electron eRT6 6 MeV. CONV-RT: 10Gy, single dose, 0.1G y/s. FLASH-RT: 10 Gy – 14 Gy (mice), 8 Gy-10 Gy(zebrafish), single dose, up to 10 ⁷ Gy/s, 1 pulse.	No data	FLASH-RT: spares memory in normoxic condition (oxygen level 4-6%), decreased neuroinflammation, preservation of neural structures. loss FLASH effect during carbogen breathing (95% O ₂ , 5% CO ₂) in mice. Minimizes embryonic development alteration of zebrafish. CONV-RT: neurocognitive decline, loss of neural structures, neuroinflammation (mice). Alteration of zebrafish development.

Simmons et al., 2019	WBI, Male C57BL6 mice.	Linac 16/20 MeV Electron. CONV-RT: 30 Gy, single dose, 0.13 Gy/s FLASH-RT: 30Gy, single dose, 200-300 Gy/s	No data	FLASH-RT: spares loss of cognitive performance, reduced inflammatory response. Decreased microglial activation and secreted cytokines (IL6, TNFa, IL1b). CONV-RT: neural degradation (hippocampal dendritic spines), memory loss, neuroinflammation.
Montay-Gruel, Markarian, et al., 2020	WBI, Female C57BL6 mice.	Pulsed electron eRT6 6 MeV. FLASH-RT: 10 Gy, single dose, 5.6×10^6 Gy/s CONV-RT: 10 Gy, single dose, 0.1 Gy/s.	No data	FLASH-RT: no astrocyte hypertrophy, decreased astrogliosis, no microglial C1q expression, induced C3 and no TLR4 expression in astrocytes. CONV-RT: astrocyte hypertrophy, astrogliosis, increased TLR4, C3 and microglial C1q protein complement.
Allen et al., 2020	WBI, Female C57BL6 mice.	Pulsed electron eRT6 6 MeV. FLASH-RT: 10 Gy, 25 Gy, single dose, $>10^3$ and 10^6 Gy/s. CONV-RT: 10 Gy, 25 Gy, single dose, 0.09 Gy/s	No data	FLASH-RT: preservation of vasculature, tight junction proteins and blood brain barrier (BBB). Decreased vascular dilation and apoptosis in neurogenic regions. CONV-RT: loss of vascular and BBB integrity, vascular dilation, apoptosis un neurogenic regions (DG, SVZ).
Alaghand et al., 2020	WBI, juvenile mice.	Pulsed electron eRT6 6MeV. FLASH-RT: 8Gy, single dose, 4.4×10^6 Gy/s CONV-RT: 8 Gy, single dose, 0.1 Gy/s	No data	FLASH-RT: preserved cognitive performance, immature neurons, neurogenesis and circulating growth hormone levels, decrease neuroinflammation (microglial activation). CONV-RT: memory loss, loss of neurons, neurogenesis and decreased circulating growth hormones, increased neuroinflammation.
Montay-Gruel et al., 2021	WBI, GBM H454 tumors, Female Nude mice.	Pulsed electron eRT6 6 MeV. 10 Gy, 14 Gy, 25 Gy (hemibrain), 4x3.5 Gy, 2x7 Gy, and 3x10 Gy CONV-RT (0.1 Gy/s) vs. FLASH-RT (up to 7.8×10^6 Gy/s)	Isoefficacy of tumor control by both modalities.	FLASH-RT: Preserved cognitive performance at 10 Gy, 2x7 Gy, 4x3.5 Gy, 3x10 Gy. Neurocognitive decline at 14 Gy. CONV-RT: Preserved cognitive performance at 4x3.5 Gy. Neurocognitive decline at 10 Gy, 2x7 Gy, 3x10 Gy.

Normal skin and subcutaneous tumors

Kim et al., 2020	Subcutaneous tumors of Lewis lung carcinoma, male C57BL6 mice.	Pulsed Electron, clinical Linac 16 MeV. FLASH-RT: 15Gy, single dose, 352 Gy/s CONV-RT: 15Gy, single dose, 0.06Gy/s	FLASH-RT: No vascular collapse and p-MLC, increased immune cells infiltration (myeloid, CD4 and CD8 T cells), decreased DNA damage (gH2AX). CONV-RT: constricted vessels, increased p-MLC and gH2AX.	No data
Soto et al., 2020	Dose escalation study of mouse skin toxicity, Female C57BL6 mice.	Electron, 16 MeV. FLASH-RT: 10, 16, 20, 30 and 40 Gy, 2Gy/pulse, 90 Hz pulse repetition, 180 Gy/s. CONV-RT: 10, 16, 20, 30 and 40 Gy, 0.001Gy/pulse, 72 Hz pulse repetition, 00.07 Gy/s.	No data	FLASH-RT: 0-30 Gy, mice survived the treatment. 40 Gy resulted in 50% of lethality (n=5) and 2 mouse were still alive after 180 days post RT. Reduced radiation-induced skin ulceration. CONV-RT: 0-20 Gy, 30 Gy and 40 Gy were highly toxic for mice, increased skin ulceration and resulted in decreased survival after the treatment.

Cunningham et al., 2021	Skin toxicity, C57BL6 mice. Subcutaneous inj. MOC1 and MOC2 murine oral carcinoma in C57BL6 mice.	Proton Pencil Beam Scanning (PBS), 250 MeV. 35 Gy (toxicity) and 15Gy (tumor) FLASH-RT: 57 Gy/s or 115 Gy/s CONV-RT: 1 Gy/s	Isoefficacy of tumor control by both modalities.	FLASH-RT: decreased skin toxicity and leg contraction. Decreased plasma and skin TGF- β 1 levels (acute time point). Limited changes of cytokine level in the blood of mice, similar GM-CSF/G-CSF ratio to control. CONV-RT: increased skin toxicity and leg contraction. Increased TGF- β 1 level. Decreased GM-CSF/G-CSF ratio.
Velalopoulou et al., 2021	Skin toxicity, C57BL6 mice, subcutaneous and intramuscular sarcoma tumors LSL-KrasG12D/wt.; p53FL/FL GEMM model (C57BL6 mice), RIF mouse sarcoma cell line (C3H background).	Proton C230 Cyclotron 230 MeV FLASH-RT: 30Gy-45Gy (toxicity), 12Gy (tumor), 69-124 Gy/sec CONV-RT: 30 Gy-45 Gy (toxicity), 12Gy (tumor), 0.39–0.65 Gy/sec.	Isoefficacy of tumor control by both modalities.	FLASH-RT: decreased TGF-b1 (acute quantification) in canine and mouse skin, decreased myeloid cells number, reduced toxicities of skin leg and mesenchymal tissues, Lgr6+ stem cell depletion, limited lymphedema. CONV-RT: increased TGF-b1 in canine and mouse skin, increased and constant myeloid cells number, skin and mesenchymal tissues toxicity, increased lymphedema, greater Lgr6+ stem cell depletion.
Gastrointestinal track and abdominal tumors				
Levy et al., 2020	Total abdominal irradiation, C57BL6 mice, ID8 ovarian cancer peritoneal metastasis model.	Pulsed electron, LINAC 16 MeV. 14 Gy FLASH-RT: 14-16Gy (toxicity), 14Gy (tumor), 100-200Hz, 216Gy/s CONV-RT: 14-16Gy (toxicity), 14Gy(tumor), 0.08Gy/s.	Isoefficacy of tumor control by both modalities.	FLASH-RT: mice survived lethal treatment of 16Gy, recover after induced-toxicity, increased regenerating crypts, preservation of intestinal functions, reduced DNA damage (gH2AX) and apoptosis of crypt cells. CONV-RT: All mice died 10 days post 16Gy RT. Increased gastrointestinal toxicity, Decreased regenerating and proliferating crypts, increased gH2AX and apoptosis of crypt cells.
Diffenderder et al., 2020	Abdominal irradiation, female C57BL6 mice, Subcutaneous pancreatic tumors (MH641905).	Proton, IBA proteus plus 250 MeV. FLASH-RT: 15 Gy (normal tissue), 12 and 18 Gy (tumor), 78 ± 9 Gy/s CONV-RT: 15 Gy (normal tissue), 12 and 18 Gy (tumor), 0.9 ± 0.08 Gy/s.	Isoefficacy of tumor control by both modalities.	FLASH-RT: Preservation of proliferating intestinal cells, no increased muscle layer thickness (fibrosis) 8 weeks post-RT. CONV-RT: decreased proliferating cells, increased muscle layer thickness (fibrosis).
Gao et al., 2020	Thorax and abdominal irradiation, C57BL6 mice (normal tissue). ETM6 breast tumor homografts in Balb/c mice.	High energy X-rays, Linac 8 MeV. FLASH-RT: 18Gy (tumor), 30Gy (thorax), 15Gy (abdominal), 900-1200Gy/s CONV-RT: 15Gy (tumor), 24Gy (thorax), 12Gy (abdominal), 0.1Gy/s	18Gy FLASH-RT better controled the tumor than 15Gy CONV-RT.	FLASH-RT: All mice died from abdominal irradiation. Decreased toxicity in the intestine. CONV-RT: All mice died from abdominal irradiation. Increased toxicity in the intestine.
Evans et al., 2021	Evaluation of spread-out Bragg peak, female C57BL6 mouse.	Pulsed syncrotron, Bragg-peak. FLASH-RT: 10-19Gy, 100Gy/s CONV-RT: 10 - 16 Gy, 0.1 Gy/s.	No data	FLASH-RT: LD50 14.1Gy CONV-RT: LD50 13.5Gy
Kim et al., 2021	Gastrointestinal toxicities, C57BL6 mice, subcutaneous MH641905 mouse pancreatic tumor.	<u>Comparison Spread-out Bragg Peak Proton RT (SOBP) vs. PRT entrance</u> FLASH-RT: 15 Gy, SOBP F-PRT 108.2 ± 8.3 Gy/s ; F-PRT entrance 107.1 ± 15.2 Gy/s CONV-RT: 15 Gy, SOBP S-PRT 0.82 ± 0.14 Gy/s ; S-PRT entrance 0.83 ± 0.19 Gy/s. Comparison SOBP PRT vs. PRT entrance	Isoefficacy of tumor control by both modalities.	FLASH-RT: similar toxicity between SOBP PRT vs. PRT entrance: decreased proliferating and regenerating cells in crypts. Higher proliferation and regeneration (relative to CONV-RT). Mice treated with PRT entrance survived the treatment. SOBP induced only 15% of lethality. CONV-RT: similar toxicity between SOBP PRT vs. PRT entrance: decreased proliferating and regenerating cells in crypts. Less proliferation, regeneration, increased damages (vs. FLASH). Mice treated with PRT entrance survived the treatment. 70% of the SOBP-treated mice died 20 days after RT.

Ruan et al., 2021	Abdominal irradiation, C3H mice.	Investigation of temporal pulse structure and average dose rate. Electron LINAC 6MeV FLASH-RT: 7.5 - 12.5 Gy, 2-6 x 10 ⁶ Gy/s CONV-RT: 7.5 - 12.5 Gy, 0.25 Gy/s.	No data	FLASH-RT: 30% reduction of gastrointestinal toxicity using a 3.8 ms single pulse, with a dose modifying factor of 1.1 for FLASH. Decreased alteration of the gut microbiota. Sparing effect lost when delivery time and pulse number were modified. CONV-RT: higher toxicity, increased alteration of gut microbiota associated with intestinal injury.
-------------------	----------------------------------	--	---------	--

The FLASH effect validated in domestic animal and human patients

Vozenin et al., 2019	Skin of a mini-pig and cat-cancer patients with advanced squamous cell carcinoma of the nasal planum.	Pulsed electron, eRT6 (6 MeV) and Kinetron (4.5 MeV). Mini-pig: FLASH-RT: 22 to 34 Gy, 300 Gy/s CONV-RT: 222 to 34 Gy, 5 Gy/min. Cats, dose escalation: 25 – 41 Gy FLASH, single dose.	All cats had complete tumor response.	Mini-Pig: After FLASH-RT, limited skin toxicity. CONV-RT induced fibronecrosis. Cats: after FLASH-RT, 3/6 had no acute toxicity and 3/6 had mild or moderate transient mucositis.
Bourhis et al., 2019	75-year-old patient, multiresistant CD30+ T-cell cutaneous lymphoma.	5.6-MeV linac, FLASH-RT: 15 Gy, 90 ms, 167 Gy/s.	Complete and durable tumor response.	Transient epithelitis and oedema.
Chabi et al., 2020	Total body irradiation, NSG immunodeficient mice. Xenograft transplantation of human acute lymphoblastic leukemia (T-ALL) and normal human hematopoiesis.	Pulsed electron, eRT6 (6 MeV). FLASH-RT: 4Gy, 200 Gy/s CONV-RT: 4 Gy, 0.07 Gy/s	2/3 T-ALL were sensitive to FLASH-RT while 1/3 was more sensitive to CONV-RT.	FLASH-RT: preserved some HSPC/CD34+ cell potential, hematopoietic reconstitution and functionality. CONV-RT: did not preserved HSPC/CD34+ cell potential.
Konradsson et al., 2021	Ten canine cancer patients, follow-up 7 days, 1 to 6 months post FLASH-RT.	Clinical Elekta Precise linear accelerator, electron. Dose escalation trial 15 to 35 Gy (470 Gy/s to 500 Gy/s)	Partial response, complete response or stable disease recorded in 11/13 irradiated tumors.	FLASH-RT: mild toxicity, alopecia, leukotricia, dry desquamation, mild erythema, swelling. One patient had 3 grade skin toxicity (moist desquamation).
Velalopoulou et al., 2021	Skin toxicity of dog-cancer patients with osteosarcoma.	Proton RT FLASH-RT: 8/12 Gy, 61-128 Gy/sec CONV-RT: 8/12 Gy, 0.1–0.5 Gy/sec	No data	FLASH-RT: limites radiation-induced skin toxicities of skin leg with a limited production of TGF- β (acute quantification). CONV-RT: higher levels of TGF- β production.

Supp Table 2: Biological studies using UHDR that did not demonstrate the FLASH effect.

Ref.	Model/mouse	Beams, particles and parameters	Major outcomes	
			Tumor	Normal tissue
Beyreuther et al., 2019	24 hpf zebrafish embryos.	Protons, (224 MeV). FLASH-RT: 10 - 42.5Gy, 100Gy/s CONV-RT: 10 - 42.5Gy, 0.08Gy/s	No data	FLASH-RT: Reduced pericardial edema at 3rd and 4th day after 23 Gy vs. CONV-RT Overall no protective effect of FLASH on survival and morphological integrity of the zebrafish embryos.
Symth et al., 2018	Total body, thoracic and abdominal C56BLJ/6 mice.	X-rays, Synchrotron, dose escalation. CONV-RT : 93 keV,	No data	Similar toxicities were found following irradiation regardless of the modality used or irradiation site.

		0.06 Gy/s FLASH-RT: 124 keV, 37-41 Gy/s		
Venkatesulu et al.,2020	Thorax irradiation, C56BLJ/6 mice.	Electron beam, (20 MeV Varian 2100 IX linac). CONV-RT: 5 Gy, 10 Gy, 16 Gy, 0.1 Gy/s FLASH-RT: 5 Gy, 10 Gy, 16 Gy, 35 Gy/s	No data	FLASH-RT: radiation-induced gastrointestinal toxicity, decreased mouse survival (vs. CONV-RT). Mice experienced severe lymphopenia irrespective of dose rate. No immune compartment sparing in cardiac and splenic models of lymphopenia.

Supp Table 3: eRT6 beam parameters.

Model: Mice									
Nb of pulses	Mean dose rate (Gy/s)	Instantaneous dose rate (Gy/s)	Mode	Prescribed dose (Gy)	Frequency (Hz)	SSD (mm)	Pulse width (μ s)	Grid tension (V)	Treatment time (ms)
1	5.6×10^6	5.6×10^6	UHDR	10	100	340	1.8	300	1.8×10^{-3}
10	111	5.6×10^5	UHDR		100	920	1.8	300	90
30	35	1.9×10^5	UHDR		100	1450	1.8	300	290
100	10	5.6×10^4	UHDR		100	800	1.8	117	990
1000	0.1	1.0×10^4	CONV		10	830	1	100	99900

Model: Zebrafish embryos at 4hpf									
Nb of pulses	Mean dose rate (Gy/s)	Instantaneous dose rate (Gy/s)	Mode	Prescribed dose (Gy)	Frequency (Hz)	SSD (mm)	Pulse width (μ s)	Grid tension (V)	Treatment time (ms)
1	5.6×10^6	5.6×10^6	UHDR	10	100	330	1.78	300	1.8×10^{-3}
10	111	5.6×10^5	UHDR		100	930	1.78	300	90
30	35	1.9×10^5	UHDR		100	1470	1.85	300	290
100	10	5.6×10^4	UHDR		100	1400	1.8	147	990
1000	0.1	1.4×10^4	CONV		10	600	1	100	99900

Model: Plasmids and H ₂ O									
Nb of pulses	Mean dose rate (Gy/s)	Instantaneous dose rate (Gy/s)	Mode	Prescribed dose (Gy)	Frequency (Hz)	SSD (mm)	Pulse width (μ s)	Grid tension (V)	Treatment time (ms)
1	5.6×10^6	5.6×10^6	UHDR	10	100	330	1.78	300	1.8×10^{-3}
10	111	5.6×10^5	UHDR		100	930	1.78	300	90
30	35	1.9×10^5	UHDR		100	1470	1.85	300	290
100	10	5.6×10^4	UHDR		100	1400	1.8	147	990
1000	0.1	1.4×10^4	CONV		10	600	1	100	99900

2- Publication 2: Comparing radiolytic production of H₂O₂ and development of Zebrafish embryos after ultra-high dose rate exposure with electron and Transmission proton beams.

Published in Radiotherapy and Oncology, 2022.

DOI: [10.1016/j.radonc.2022.07.011](https://doi.org/10.1016/j.radonc.2022.07.011)

The study is a collaborative effort involving the group of MC Vozenin, the company Varian, Inc., and D Weber's team at PSI. I have been responsible for conducting water radiolysis experiments, analysis all the experimental data and redaction of the article. The objective was to evaluate and correlate the long-term radiolytic yield of H₂O₂ with the development of ZFE using electron and proton beams operating in FLASH and CONV modes as illustrated in **Figure 1**.

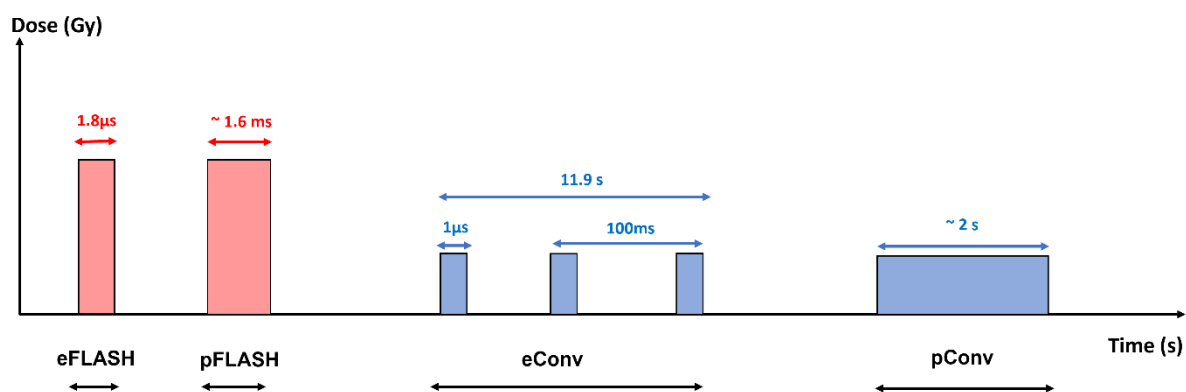


Figure 1: Temporal structure of eRT6 intermediate energy electron (IEE) beam and Gantry1 transmission (TI) proton beam at CONV and FLASH dose rate. eFLASH and eCONV stand for electron FLASH and electron CONV dose rate. pFLASH and pCONV stand for proton FLASH and proton CONV dose rate.

Irradiations were performed using a FLASH-validated pulsed electron beam (5.5 MeV eRT6) at CONV (0.1 Gy/s) and UHDR (100 Gy/s and ≥ 1400 Gy/s). Proton irradiations were delivered with the 235 MeV Gantry1 in transmission mode, with a quasi-continuous beam from PSI Comet Cyclotron at 0.1 and 0.9 Gy/s for CONV dose rate and 90 Gy/s and 1260 Gy/s for UHDR. Conventional 225 keV X-rays irradiations were also conducted at 0.037 Gy/s using the Xrad tube from Pxi Precision and included as a reference.

H₂O₂ production was measured in water samples equilibrated in physiological oxygen conditions (4% O₂) and irradiated with doses ranging from 10-30 Gy. Using the same beams, ZFE were irradiated at 4h-4h30 post-fertilization to 7-12 Gy. A total number of N = 15 to 39

embryos were utilized to investigate survival and radiation-induced developmental alterations, measured by body length 5 days post-fertilization in accordance with ethics regulations. N = 5 embryos were employed to quantify radiation-induced cell death and proliferation at 24h to 72h post RT on the whole body of ZFE using immunofluorescence and confocal microscopy analysis.

The fact that electron beam was pulsed, and proton beam was semi-continuous did not affect H_2O_2 production. However, higher average dose rate produced less H_2O_2 . A $G(\text{H}_2\text{O}_2) = 2.33$ molecules/100 eV was correlated with the maintenance of ZFE development. Conserved developmental features were also associated with the onset of proliferation, presumably to compensate for apoptosis. Surprisingly, ZFE appear to be resistant to proton beam irradiation, and in this model, this irradiation modality and/or beam configuration were inherently less toxic than low-energy photon and electron beams. These results indicated the need for further systematic investigation, which was the goal of my subsequent study.

Comparing radiolytic production of H₂O₂ and development of Zebrafish embryos after ultra-high dose rate exposure with electron and transmission proton beams.

Houda Kacem^a, Serena Psoroulas^b, Gael Boivin^c, Michael Folkerts^c, Veljko Grilj^d, Tony Lomax^{b,d}, Adrien Martinotti^a, David Meer^b, Jonathan Ollivier^a, Benoit Petit^a, Sairos Safai^b, Ricky A. Sharma^c, Michele Togno^b, Marta Vilalta^c, Damien C. Weber^b, Marie-Catherine Vozenin^a

^a Department of Oncology, Laboratory of Radiation Oncology, Radiation Oncology Service, CHUV, Lausanne University Hospital and University of Lausanne, Lausanne, Switzerland.

^b Paul Scherrer Institut-Centre for Proton Therapy, Villigen, Switzerland.

^c Varian, a Siemens Healthineers Company, 3120 Hansen Way, Palo Alto, CA 94304, United States.

^d Institute of Radiation Physics, University Hospital and University of Lausanne, Switzerland.



Short Communication

Comparing radiolytic production of H₂O₂ and development of Zebrafish embryos after ultra high dose rate exposure with electron and transmission proton beams



Houda Kacem^a, Serena Psoroulas^b, Gael Boivin^c, Michael Folkerts^c, Veljko Grilj^d, Tony Lomax^{b,d}, Adrien Martinotti^a, David Meer^b, Jonathan Ollivier^a, Benoit Petit^a, Sairos Safai^b, Ricky A. Sharma^c, Michele Togno^b, Marta Vilalta^c, Damien C. Weber^b, Marie-Catherine Vozenin^{a,*}

^a Radiation Oncology Laboratory, Service of Radiation Oncology, Department of Oncology, Lausanne, University Hospital and University of Lausanne; ^b Paul Scherrer Institut-Centre for Proton Therapy, Villigen, Switzerland; ^c Varian, a Siemens Healthineers Company, 3120 Hansen Way, Palo Alto, CA 94304, United States; ^d Institute of Radiation Physics, University Hospital and University of Lausanne, Switzerland

ARTICLE INFO

Article history:

Received 25 April 2022

Received in revised form 30 June 2022

Accepted 13 July 2022

Available online 19 July 2022

Keywords:

Electron FLASH

Proton FLASH

Hydrogen peroxyde

Zebrafish embryos

ABSTRACT

The physico-chemical and biological response to conventional and UHDR electron and proton beams was investigated, along with conventional photons. The temporal structure and nature of the beam affected both, with electron beam at ≥ 1400 Gy/s and proton beam at 0.1 and 1260 Gy/s found to be isoefficient at sparing zebrafish embryos.

© 2022 The Authors. Published by Elsevier B.V. Radiotherapy and Oncology 175 (2022) 197–202 This is an open access article under the CC BY license (<http://creativecommons.org/licenses/by/4.0/>).

Radiation therapy is a pillar of anti-cancer treatments. However and despite technological improvement of radiation delivery, the dose required to cure tumors remains close to normal tissue tolerance. To enhance the therapeutic window and overcome radiation-induced normal tissue toxicity, we proposed to irradiate at ultra high dose rate, FLASH-RT. At the preclinical level, FLASH-RT is known to increase normal tissue tolerance while maintaining tumor killing [1]; a biological outcome that was named the FLASH effect, now investigated worldwide with various type of beams.

The FLASH effect has been primarily studied in vivo models with electron beams of intermediate energy [2] and reproduced with other beams including proton beams at 60–160 Gy/s [3–7]. Electron beams are pulsed whereas proton beams are quasi-continuous; this inherent difference in temporal beam structure dictates major differences in instantaneous dose rates that might impact early physico-chemical and biological outcomes. This prompted us to perform a systematic comparison between electron and proton beams at conventional and UHDR. While opera-

tional constraints and uncertainty on the dose prevented us from using the exact same beam parameters impacting dose rates across the experiments, our aim was to be as close as possible to assess dose rate-specific vs beam-specific physico-chemical (radiolytic) and biological (developmental) responses. The radiolytic yields of hydrogen peroxide produced in pure water equilibrated at 4% O₂ to mimic physioxia as well as the early development of zebrafish embryos was investigated upon irradiation with conventional (≤ 1 Gy/s) and UHDR (≥ 1260 Gy/s) electron and proton beams. In ZF, functional and molecular outcomes were investigated including survival, growth as well as cell death and proliferation. A conventional dose rate 225 kV photon beam was also included as a reference.

Material and methods

Full material and method can be found in the [supplementary material](#).

Irradiation devices

Irradiations and dosimetry were performed as already described using [8–13]:

Abbreviations: UHDR, ultra-high dose rate; ZF, zebrafish; DMF, dose modifying factor.

* Corresponding author.

E-mail address: marie-catherine.vozenin@chuv.ch (M.-C. Vozenin).

<https://doi.org/10.1016/j.radonc.2022.07.011>

0167-8140/© 2022 The Authors. Published by Elsevier B.V.

This is an open access article under the CC BY license (<http://creativecommons.org/licenses/by/4.0/>).

- 1) Xrad 225CX/225 keV (Pxi Precision X-ray), at 0.037 Gy/s.
- 2) eRT6/Oriatron 5.5 MeV electron beam (PMB-Alcen), at 0.1 Gy/s for conventional dose rate and 100 Gy/s, \geq 1400 Gy/s for UHDR.
- 3) PSI Comet Cyclotron 235 MeV (Gantry 1) in transmission mode, at 0.1, and 0.9 Gy/s for conventional dose-rate, 90 Gy/s and 1260 Gy/s for UHDR

Full beams parameters can be found in [Table sup 1](#).

Water radiolysis experiments

Milli-Q water was equilibrated at 4% O₂ and irradiated as indicated in [Table sup 1](#). Water samples were probed immediately after irradiation with Amplex Red assay kit (ThermoFisher). Fluorescence quantification was performed using Promega Glo-Max plate reader (Excitation: 520 nm Emission: 580–640 nm). G-value of hydrogen peroxide was calculated from the slope of plots of H₂O₂ concentrations as a function of the dose.

Zebrafish embryos experiments

AB Wild Type and transgenic Fl1a ZF embryos (to visualize the vascular tree) were irradiated 4 h to 4 h30 post-fertilization as indicated [Table sup 1](#). Survival and radiation-induced developmental alterations (n = 15 to 39 embryos) were investigated by measuring the body length 5 days post-fertilization as allowed by the Swiss ethics regulations. Temporal dynamics of radiation-induced cell death and proliferation were quantified on the whole body of ZF embryos (n = 5 embryos) using immunofluorescence and confocal microscopy analysis. Duplicate experiments were performed except for photon irradiation that was performed once.

Results

H₂O₂ yield is reduced at UHDR

We thought to use G-value of H₂O₂ in pure water as a surrogate for normal tissue sparing after UHDR irradiation. Therefore, the impact of dose and dose rate on H₂O₂ production and recombination when delivered with different type of beams was measured ([Fig. 1](#)). H₂O₂ yield increased linearly with the dose with all 3 beams. With 225 kV X-rays, the H₂O₂ yield was relatively higher and ranged between 3.8 to 4 molecules per 100 eV. For UHDR electron and proton beams H₂O₂ yield were globally lower, inversely proportional to the dose rate and did not vary linearly.

ZF embryos are sensitive to both the nature of the beam and dose rate

Dose and dose rate responses were investigated using a rapidly responding *in vivo* model with different beams. Dose responses were found for the 3 beams whereas dose rate responses were found for the electron but not for the proton beam. At isodose, two main patterns of response were found on ZF embryos: quasi-normal development/sparing effect and abnormal development/toxic effect. The FLASH sparing effect was found with electron at \geq 1400 Gy/s and proton at 0.1 and 1260 Gy/s with a minimal impact on embryo survival and growth 5 days post-fertilization ([Fig. 2a](#) and [b](#)). Toxicity was found with 225 kV photon and electron beam at conventional dose rate at respectively 0.037 Gy/s and 0.1 Gy/s. The photon beam was the most toxic with a 50% size reduction at 10 Gy and a high level of mortality (LD75 at 12 Gy) ([Fig. 2a](#)) whereas the lethal dose was never reached with the two other beams.

We speculated that developmental sparing effect induced by proton (conventional and UHDR) and electron UHDR could be

mediated by a decreased level of cell death and/or increased proliferation rate, to enable cellular mass recovery and preserve ZF development, whereas in photon and electron at 0.037 Gy/s and 0.1 Gy/s massive cell death could not be compensated. TUNEL and PhosphoH3 staining on full-body ZF embryos 24, 48 and 72 h post-irradiation were performed and analyzed by confocal microscopy and image reconstruction. Typical images of non-irradiated and ZF embryos 48 h post-irradiation at 10 Gy with the various beams (photon, electron and proton) are shown [Fig. 2c](#) and followed the two main patterns described above (normal vs abnormal). Non-irradiated embryos and embryos irradiated with proton beam (0.9 and 1260 Gy/s) and electron beam \geq 1400 Gy/s (1 pulse) showed quasi-normal developmental features. A dose dependent acute apoptotic peak was measured at 24 h in all irradiated groups, which is opposite to our hypothesis ([Figure sup 1 and 2](#)). However, with electron \geq 1400 Gy/s, it was compensated by a subsequent peak of proliferation 72 h post-irradiation. With proton (0.9 and 1260 Gy/s) and electron (\geq 1400 Gy/s), the apoptotic to proliferation ratio returned to the level of the control non-irradiated animals at 72 h post-irradiation, suggesting a full recovery ([Figure sup 1 and 2](#)). With photon and electron beam at conventional dose rate apoptosis rate occur early but was sustained over time, suggesting an ongoing radiation-induced cellular depletion process consistent with the severe morphological impact. Quantitative analysis was performed and is shown in [Figure sup 1 and 2](#), whereas [Figure sup 3](#) show the proportion of apoptosis vs proliferation in the different condition.

Discussion

Our results are the first systematic comparison of the radiolytic production of H₂O₂ and development of Zebrafish embryos after conventional and UHDR exposure with electron and proton beams. The temporal structure of the beam had no impact on H₂O₂ production but the mean dose rate did. A production of H₂O₂ \leq 2.33 molecule/100 eV also correlated with the preservation of ZF embryo development. Preserved developmental features also correlated with the onset of proliferation, presumably to compensate for apoptosis. Surprisingly, ZF embryos showed an exquisite sensitivity to the nature of the beam and dose rate. In our experiments, ZF embryos seemed resistant to proton irradiation, suggesting that this irradiation modality and/or beam configuration was intrinsically less toxic than low energy photon and electron beams in this specific model. These results point to the need for further systematic study; as such, an impact has not been reported *in vitro* or *in vivo*.

Understanding the physical parameters (*i. e.* mean dose rate vs instantaneous dose rate, time of exposure) able to trigger the FLASH effect is one important goal in the field of FLASH-RT research. Here, we took advantage of two beams (electron and proton) with intrinsic differences in temporal structure but able to operate at conventional and UHDR [10,12]. The maximal dose rate achievable with the proton beam was 1260 Gy/s delivered in a quasi-continuous manner whereas the electron beam was more flexible, able to deliver dose rates between 100 to 6.6.10⁶ Gy/s. For the latter, this flexibility was achieved by varying the number of pulses (see [Table sup 1](#)). In both cases dose uncertainty was around 4%. We compared the impact of conventional vs UHDR and electron vs proton beam on H₂O₂ production. H₂O₂ radiolytic yield was linear with the dose and inversely proportional to the dose rate. G° value of H₂O₂ after proton, electron and γ -rays at conventional dose rates are available and found to be similar [14–18], whereas direct measurement of H₂O₂ yields comparing conventional and UHDR irradiation has not been well investigated so far. Only one of our previous studies suggested that a decreased

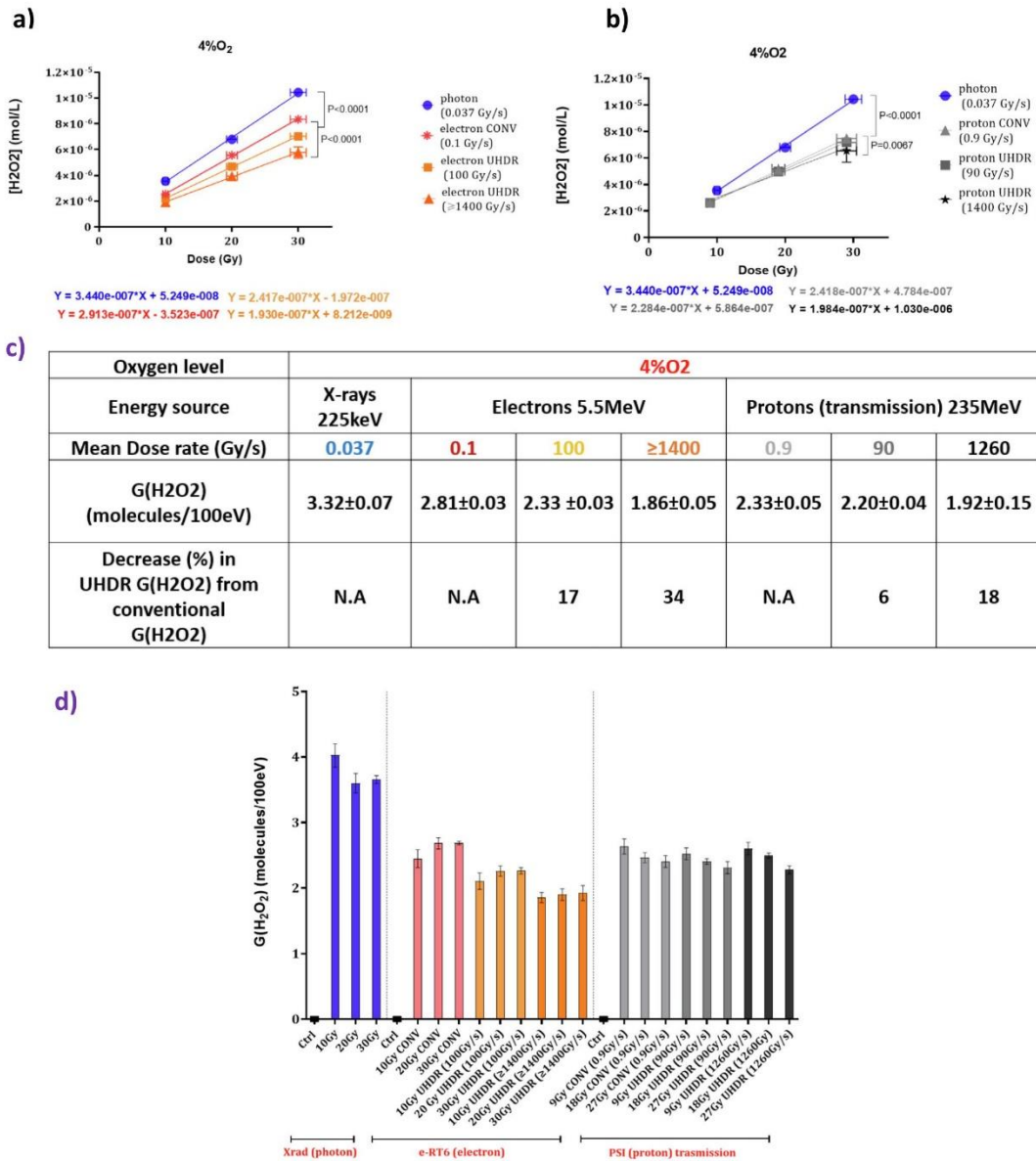


Fig. 1. Dose and dose rate impact on water radiolysis in physiological O₂ conditions (4% O₂) after exposure to photon, electron and proton beam a) [H₂O₂] concentrations vs the irradiated dose obtained after water exposure to X-rays, electrons (CONV and UHDR) b) Similar plot obtained with proton beam (conventional and UHDR). Slopes were assessed by t-test and were significantly different as follow: photons vs electrons (CONV&UHDR): P < 0.0001; CONV electrons vs UHDR electrons: P < 0.001 and CONV protons vs UHDR protons: P = 0.0067 c) Summary table d) Radiolytic yield of H₂O₂ obtained from the previous figure by dividing [H₂O₂] over the dose. Uncertainties on the dose for electron and proton irradiations were 4% and 10% respectively from the prescribed dose. Results are from duplicate experiments for X-rays and protons irradiation and triplicate experiments for electrons irradiations.

production of H₂O₂ after exposure to UHDR electron (>100 Gy/s) could trigger normal tissue sparing in ZF embryos' and mouse [1,19]. Here, we calculated G values of H₂O₂ produced by photon, electron and proton beams and could ranked them from the highest production to the lowest: CONVphoton > CONVelectron > CON

Vproton > UHDRproton > UHDRelectron. We also found that 2.33 molecules of H₂O₂/100 eV or less correlated with the preservation of ZF embryo development. Whether this value can be considered as a threshold and/or a surrogate marker of normal tissue protection remains to be established.

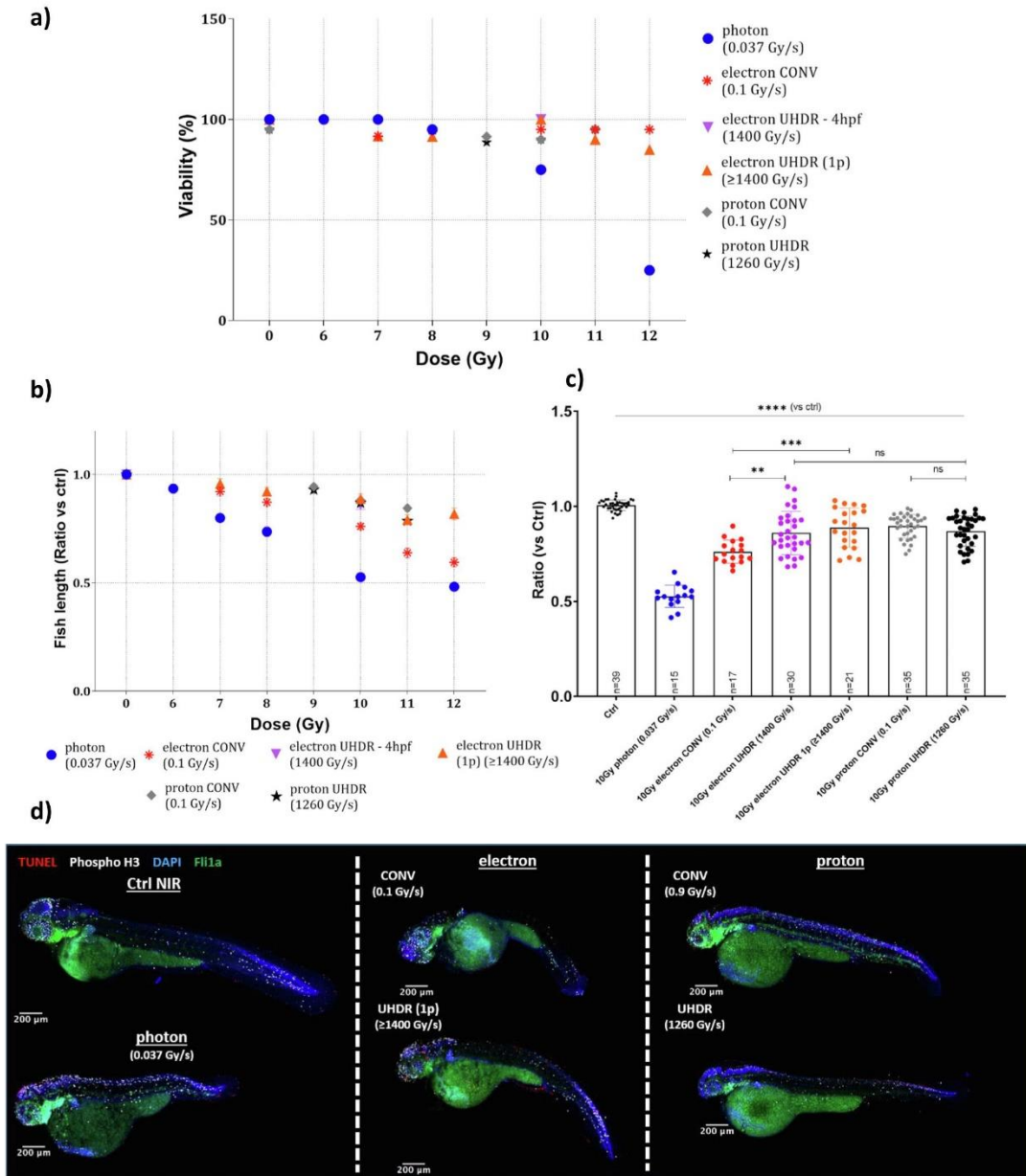


Fig. 2. Dose and dose rate impact on zebrafish embryos exposed to photon, electron and proton beams 4–4.30 h post-fertilization. a) Embryonic survival b) Fish length assess developmental retardation induced by irradiation at 5 days post-fertilization. (Embryos $n = 20$ per each dose, results are the average of two experiments) c) Fish length in bargraph at 10 Gy d) Comparison of radiation induced cell death and apoptosis response in ZF embryos (Fli1a) triggered by TUNEL assay and Phospho H3 staining after irradiation with 10 Gy (48 h post RT) using photon, electron and proton beam at different dose rates. Images were acquired over the embryo total body with confocal microscopy (10x); Red: TUNEL, White: Phospho H3, Blue: DAPI and Green: Fli1a. (Embryos $n = 5$ per each dose).

The ZF embryo is relatively new model in the field of radiation biology. It has several distinct advantages including the fact that it is a fully integrated in vivo model and it's a short-term model with a fast biological response (5 days). These embryos also have other

interesting characteristics such as a very rapid shift in their radiation resistance profile according to developmental status (DL100 ranging from 15 to 50 Gy within the first 24 h of their development) [20]. To investigate the impact of clinically relevant doses

(in the range of 10 Gy), we chose to work at 4–4.30 hpf. At this early stage of their development, ZF embryos can be considered to be stem cell-like, behaving like acute responding tissues. A lower magnitude of the FLASH sparing effect (about 10%) found here is similar to what has been reported in other early responding tissues such as the gut of mice [21,22]. Interestingly in this study, ZF embryos appear to be more sensitive to the nature of the beam and/or dose rate variation than mice for reasons that remain to be determined. Other nuances of the ZF model exist, where a past report showed no FLASH sparing effect with proton beams at 100 Gy/s [23]. Conversely, normal tissue sparing by proton FLASH beams (>70 Gy/s) has been consistently reported by many groups working with various murine models (gut, skin, brain) [3,5–7]. Our present results are consistent and extend Beyreuther's previous results showing no FLASH effect between 0.1 Gy/s and 1260 Gy/s with proton beams. Interestingly, the apparent lack of the FLASH effect was not related to enhanced damage, but rather to a preservation of ZF development after proton irradiation at either dose rate. When compared with photon and electron beams at conventional dose rates, a DMF of 1.6 and 1.1 was found respectively, whereas at UHDR ZF embryo development was similar with proton and electron beam. Recently, Beyreuther's group suggested that hypoxia was required in ZF embryos to trigger the FLASH sparing effect in response to UHDR with VHEE [24], a factor that was not found to be required in our previous experiments with 5.5 MeV. [19,25] The current investigation did not evaluate this, since we chose to work at physiologically relevant normoxic conditions. Here, the molecular pattern associated with the preservation of ZF embryo development was investigated and found to be beam and dose rate independent for protons but not for electrons. In fact, full recovery of the ZF embryo observed after UHDR electron and proton irradiation was associated with an early apoptotic peak followed by high levels of compensatory proliferation. This was not found however, after conventional dose rate photon and electron exposures, where sustained apoptosis was not compensated by proliferation.

Conclusions

In summary, our observations point to an unexpected but significant protective advantage of proton irradiation on ZF embryos that is coincident with a lower production of H₂O₂. The translation of these findings to higher mammals is unclear but suggests that investigations to systematically characterize the impact of dose rate modulation using protons, photons and electrons response is clearly needed. Our findings also suggest that H₂O₂ ≤ 2.33 molecule/100 eV might serve as marker of the FLASH sparing effect and identifies transient vs sustained apoptosis has a possible switch leading to normal vs abnormal development of ZF embryos.

Declaration of Competing Interest

The authors declare the following financial interests/personal relationships which may be considered as potential competing interests: [The proton studies were funded by a research grant from Varian, a Healthineers company (Palo Alto, CA, USA) (to MCV, SP and TL).]

Acknowledgements

HK and electron studies were funded by MAGIC-FNS CRS I15_186369 (to MCV) and proton studies were funded by a research grant from Varian, a Healthineers company (Palo Alto, CA, USA) (to MCV, SP and TL), VG was funded by NIH program project grant P01CA244091 (to MCV). We would like to thank Drs P Froidevaux

and C Bailat for their critical contribution; Paula Barrera-Gomez and the PTZ from UNIL for ZF breeding and well as Dr A Benechet from IVIF/UNIL/CHUV and Dr F Morgenthaler from CIF for help in imaging procedures.

Appendix A. Supplementary material

Supplementary data to this article can be found online at <https://doi.org/10.1016/j.radonc.2022.07.011>.

References

- [1] Kacem H, Almeida A, Cherbuin N, Vozenin M-C. Understanding the FLASH effect to unravel the potential of ultra-high dose rate irradiation. *Int J Radiat Biol* 2022;98:506–16. <https://doi.org/10.1080/09553002.2021.2004328>.
- [2] Diffenderfer ES, Sørensen BS, Mazal A, Carlson DJ. The current status of preclinical proton FLASH radiation and future directions. *Med Phys* 2022;49:2039–54. <https://doi.org/10.1002/mp.15276>.
- [3] Diffenderfer ES, Verginadis II, Kim MM, Shoniyozov K, Velalopoulou A, Goia D, et al. Design, Implementation, and in Vivo Validation of a Novel Proton FLASH Radiation Therapy System. *Int J Radiat Oncol*Biophys* 2020;106:440–8. <https://doi.org/10.1016/j.ijrobp.2019.10.049>.
- [4] Evans T, Cooley J, Wagner M, Yu T, Zwart T. Demonstration of the FLASH Effect Within the Spread-out Bragg Peak After Abdominal Irradiation of Mice. *Int J Particle Therapy* 2022;8:68–75. <https://doi.org/10.14338/IJPT-20-00095>.
- [5] Singers Sørensen B, Krzysztof Sitarz M, Ankjærgaard C, Johansen J, Andersen CE, Kanouta E, et al. In vivo validation and tissue sparing factor for acute damage of pencil beam scanning proton FLASH. *Radiother Oncol* 2022;167:109–15. <https://doi.org/10.1016/j.radonc.2021.12.022>.
- [6] Cunningham S, McCauley S, Vairamani K, Speth J, Girdhani S, Abel E, et al. FLASH Proton Pencil Beam Scanning Irradiation Minimizes Radiation-Induced Leg Contracture and Skin Toxicity in Mice. *Cancers* 2021;13:1012. <https://doi.org/10.3390/cancers13051012>.
- [7] Kim MM, Irmen P, Shoniyozov K, Verginadis II, Cengel KA, Koumenis C, et al. Design and commissioning of an image-guided small animal radiation platform and quality assurance protocol for integrated proton and x-ray radiobiology research. *Phys Med Biol* 2019;64:135013. <https://doi.org/10.1088/1361-6560/ab20d9>.
- [8] Jaccard M, Durán MT, Petersson K, Germond J-F, Liger P, Vozenin M-C, et al. High dose-per-pulse electron beam dosimetry: Commissioning of the Oriatron eRT6 prototype linear accelerator for preclinical use. *Med Phys* 2018;45:863–74. <https://doi.org/10.1002/mp.12713>.
- [9] Gonçalves Jorge P, Grilj V, Bourhis J, Vozenin M-C, Germond J-F, Buchd F, et al. Technical note: Validation of an ultrahigh dose rate pulsed electron beam monitoring system using a current transformer for FLASH preclinical studies. *Med Phys* 2022;49:1831–8. <https://doi.org/10.1002/mp.15474>.
- [10] Jorge PG, Jaccard M, Petersson K, Gondré M, Durán MT, Desorgher L, et al. Dosimetric and preparation procedures for irradiating biological models with pulsed electron beam at ultra-high dose-rate. *Radiother Oncol* 2019;139:34–9. <https://doi.org/10.1016/j.radonc.2019.05.004>.
- [11] Christensen JB, Togno M, Nesteruk KP, Psoroulas S, Meer D, Weber DC, et al. Al₂O₃: C optically stimulated luminescence dosimeters (OSLDs) for ultra-high dose rate proton dosimetry. *Phys Med Biol* 2021;66:085003. <https://doi.org/10.1088/1361-6560/abe554>.
- [12] Nesteruk KP, Togno M, Grossmann M, Lomax AJ, Weber DC, Schippers JM, et al. Commissioning of a clinical pencil beam scanning proton therapy unit for ultrahigh dose rates (FLASH). *Med Phys* 2021;48:4017–26. <https://doi.org/10.1002/mp.14933>.
- [13] Togno M, Meer D, Nesteruk K, Schaefer R, Psoroulas S. Ultra-high dose rate dosimetry for pre-clinical experiments with mm-small proton fields. Submitted to *Phys Medica*. n.d.
- [14] Draganić D. Studies on the Formation of Primary Yields of Hydrogen Peroxide and Molecular Hydrogen (GH₂O₂ and GH₂) in the Radiolysis of Neutral Aqueous Solutions. n.d.:8.
- [15] Pastina B, LaVerne JA. Hydrogen peroxide production in the radiolysis of water with heavy ions. *J Phys Chem A* 1999;103:1592–7. <https://doi.org/10.1021/jp984433o>.
- [16] Hiroki A, Pimblott SM, LaVerne JA. Hydrogen peroxide production in the radiolysis of water with high radical scavenger concentrations. *J Phys Chem A* 2002;106:9352–8. <https://doi.org/10.1021/jp0207578>.
- [17] Wasselin-Trupin V, Baldacchino G, Bouffard S, Hicel B. Hydrogen peroxide yields in water radiolysis by high-energy ion beams at constant LET. *Radiat Phys Chem* 2002;65:53–61. [https://doi.org/10.1016/S0969-806X\(01\)00682-X](https://doi.org/10.1016/S0969-806X(01)00682-X).
- [18] Baldacchino G, Brun E, Denden I, Bouhadoun S, Roux R, Khodja H, et al. Importance of radiolytic reactions during high-LET irradiation modalities: LET effect, role of O₂ and radiosensitization by nanoparticles. *Cancer Nano* 2019;10. <https://doi.org/10.1186/s12645-019-0047-y>.
- [19] Montay-Gruel P, Acharya MM, Petersson K, Alikhani L, Yakkala C, Allen BD, et al. Long-term neurocognitive benefits of FLASH radiotherapy driven by reduced reactive oxygen species. *PNAS* 2019;116:10943–51. <https://doi.org/10.1073/pnas.1901777116>.

- [20] Traver D, Winzeler A, Stern HM, Mayhall EA, Langenau DM, Kutok JL, et al. Effects of lethal irradiation in zebrafish and rescue by hematopoietic cell transplantation. *Blood* 2004;104:1298–305. <https://doi.org/10.1182/blood-2004-01-0100>.
- [21] Ruan J-L, Lee C, Wouters S, Tullis IDC, Verslegers M, Mysara M, et al. Irradiation at ultra-high (FLASH) dose rates reduces acute normal tissue toxicity in the mouse gastrointestinal system. *Int J Radiat Oncol Biol Phys* 2021;111:1250–61. <https://doi.org/10.1016/j.ijrobp.2021.08.004>.
- [22] Velalopoulou A, Karagounis IV, Cramer GM, Kim MM, Skoufos G, Goia D, et al. FLASH proton radiotherapy spares normal epithelial and mesenchymal tissues while preserving sarcoma response. *Cancer Res* 2021;81:4808–21. <https://doi.org/10.1158/0008-5472.CAN-21-1500>.
- [23] Beyreuther E, Brand M, Hans S, Hideghéty K, Karsch L, Leßmann E, et al. Feasibility of proton FLASH effect tested by zebrafish embryo irradiation. *Radiother Oncol* 2019;139:46–50. <https://doi.org/10.1016/j.radonc.2019.06.024>.
- [24] Pawelke J, Brand M, Hans S, Hideghéty K, Karsch L, Lessmann E, et al. Electron dose rate and oxygen depletion protect zebrafish embryos from radiation damage. *Radiother Oncol* 2021;158:7–12. <https://doi.org/10.1016/j.radonc.2021.02.003>.
- [25] Vozenin M-C, Hendry JH, Limoli CL. Biological Benefits of Ultra-high Dose Rate FLASH Radiotherapy: Sleeping Beauty Awoken. *Clinical Oncol* 2019;31:407–15. <https://doi.org/10.1016/j.clon.2019.04.001>.

Supplementary data

Supplementary materials and methods

Water radiolysis experiments

Aqueous solutions

Milli-Q water was used with a conductivity of 18.2 $\mu\text{S}/\text{cm}$. Water was equilibrated in glass bottle at room temperature in hypoxia hood (Biospherix) to physiological oxygen levels (4% O_2) overnight. The day of the experiment, water was transferred to 2mL Eppendorf tubes as described in Jorge et al., 2019, which were fully filled and then irradiated with e-RT6/Oriatron (5.5MeV) to 10, 20 and 30Gy UHDR and Conventional dose rate and conventional X-ray source (Xrad225, Pxi). Transmission proton irradiation was performed in 200 μL PCR tubes fitted in Plexiglas cylinders adapted by the PSI team for chemistry and small biological samples irradiations. Details regarding beam parameters of the three-irradiation devices are summarized in Supplementary Table 1.

Measurement of the irradiated samples

Water samples were probed immediately after irradiation with Amplex Red assay kit purchased from Thermofisher. Amplex Red was added at a final concentration of 50 μM and incubated for 30min protected from light. Freshly H_2O_2 solutions from 0.3125 μM to 10 μM were prepared and used to establish the calibration curve. Fluorescence quantification was performed using Promega Glo-Max plate reader (Excitation: 520nm Emission: 580-640nm). G-value of hydrogen peroxide were calculated from the slope of plots of hydrogen peroxide concentrations as a function of the irradiated dose.

Zebrafish embryos experiments

AB Wild Type (#1175, F7 generation) and transgenic Fli1a: EGFP (#20466, F4 generation) zebrafish embryos (Danio rerio) were provided from the European Zebrafish Resource Center (EZRC) and produced at PTZ (CHUV/UNIL, Lausanne, Switzerland) and used according to the Swiss and European ethics' regulation.

For irradiation, embryos of 4h to 4h30 post fertilization were washed and sorted in Egg water (H_2O + 60 mg/L of ocean salt). For e-RT6 irradiation, (n>20) embryos were transferred into 2mL Eppendorf tubes containing Egg water without methylene blue (MB) and irradiated at 8-12Gy at UHDR and conventional dose rate. Zebrafish embryos were irradiated with 6-12Gy with X-rays (Xrad225, Pxi) in 60mm petri dish containing 2mL of Egg water without MB. For proton, embryos were placed in custom plexiglass cylindrical holders, using the same set up described in [11], to allow irradiation along the central beam axis'. After irradiation, embryos were transferred into 60mm petri dish and incubated at 28°C up to 5 days post-fertilization (dpf).

Morphological and survival assessments of Zebrafish embryos

Radiation-induced alteration of zebrafish morphology was investigated through body length measurement 5dpf. Then, they were euthanized and fixed in a formaldehyde solution of (FA 4%) and 1% sucrose prepared in Egg water. Microscopic acquisitions were performed using Evos XL Core Cell Imaging System; Thermofisher (4X). Fish length was measured using ImageJ Software.

Cell death and Proliferation quantification

We quantified temporal dynamics of radiation induced cell death and proliferation in zebrafish embryos. 24h, 48h and 72h post-irradiation, ZF embryos were euthanized, fixed in 4% PFA and prepared for IHC. Cell death was monitored by TUNEL assay (Apop Tag Red Kit with Rhodamine, S7165; Merck) and Phospho Histone3 (pH3) (Anti-Phospho Histone H3 (Ser10), #3377; Cell Signaling Technology) was used to evaluate proliferation after irradiation. ZF embryos were incubated with Apop Tag kit as recommended by the provider and Anti-Phospho Histone H3 (1/200; clone D2C8) as primary

antibodies. Alexa Fluor 647 Donkey anti-Rabbit (1/250) (ThermoFisher, A31573) secondary antibody was used. Finally, embryos were stained with DAPI (D35571, Life Tech). Then transferred in 96 glass bottom multi-well culture plates (ref: P96G-0-5-F, MatTek), mounted in 1% low melting agarose, and stored at 4°C until image acquisition. Images were acquired at (10x) over the whole body of ZF embryo using upright Zeiss AxioObserver confocal microscope. Then, images were stitched in order to adjust their alignment from Z-stacks. TUNEL (Threshold: 2.59/10µm) and @H3 (Threshold: 1.26/12µm) expression were analyzed with spot quantification tool using IMARIS software.

Statistics and analysis

Statistical analyses were carried out using GraphPad Prism (v9.1) for both water radiolysis and ZF embryos experiments software.

Slopes (G-values) were assessed by t-test and found significantly different as follows: photons vs electrons (CONV&UHDR): $P < 0.0001$; CONV electrons vs UHDR electrons: $P < 0.001$ and CONV protons vs UHDR protons: $P = 0.0067$

For cell death and proliferation quantification comparison of control ZF embryos and the different irradiated groups (photons/electrons (CONV&UHDR) and protons (CONV&UHDR)) were done and p-values were calculated using Kruskal-Wallis test: GP: 0.1234 (ns), 0.0332(*), 0.0021(**), 0.002(***), < 0.0001 (****).

Proton experiments irradiations

The doses and dose rates reported for the proton experiments are determined from measurements with a synthetic single-crystal microdiamond detector and corrected by the reading of a Faraday cup when necessary. As such, the reported dose values for protons can differ from the prescribed doses, as well as from the dose values quoted for electrons, due to a systematic overestimation of the prescribed proton dose and to possible delivery uncertainties. More details about the model to calculate the prescribed proton dose and its comparison with experimental data are presented in Togno et al [13]

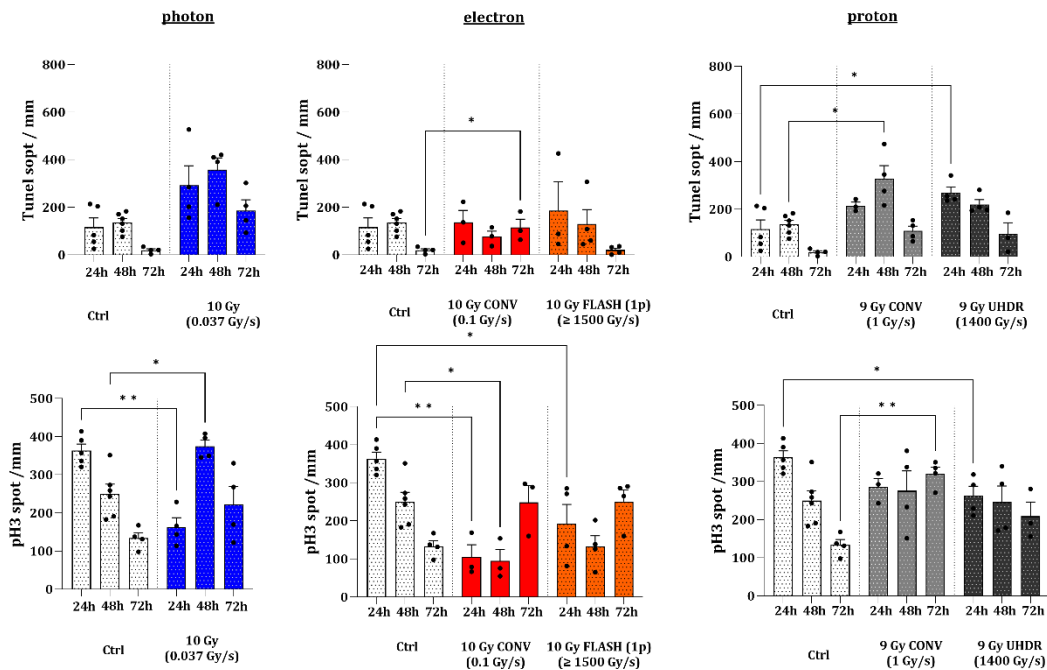
Uncertainties on the delivered dose using the PSI setup [[11–13]] are about 4%. For the lowest dose rate considered in the study, 0.1 Gy/s, it was challenging to achieve the desired accuracy on the delivered dose, mainly due to beam current fluctuations at the very low beam currents used. This dose rate level was thus used only for the survival and development experiments; since no significant effect was observed in these experiments, a higher dose rate (1 Gy/s) - but still within the 'conventional' regime - was used for the apoptosis and proliferation experiments, to maximize precision.

References

- [11] Christensen JB, Togno M, Nesteruk KP, Psoroulas S, Meer D, Weber DC, et al. Al₂O₃:C optically stimulated luminescence dosimeters (OSLDs) for ultra-high dose rate proton dosimetry. *Phys Med Biol* 2021;66:085003. <https://doi.org/10.1088/1361-6560/abe554>.
- [12] Togno M, Meer D, Nesteruk K, Schaefer R, Psoroulas S. Ultra-high dose rate dosimetry for pre-clinical experiments with mm-small proton fields. Submitted to *Physica Medica* n.d.
- [13] Nesteruk KP, Togno M, Grossmann M, Lomax AJ, Weber DC, Schippers JM, et al. Commissioning of a clinical pencil beam scanning proton therapy unit for ultrahigh dose rates (FLASH). *Medical Physics* 2021;48:4017–26. <https://doi.org/10.1002/mp.14933>.

Supplementary Figures

a)



b)

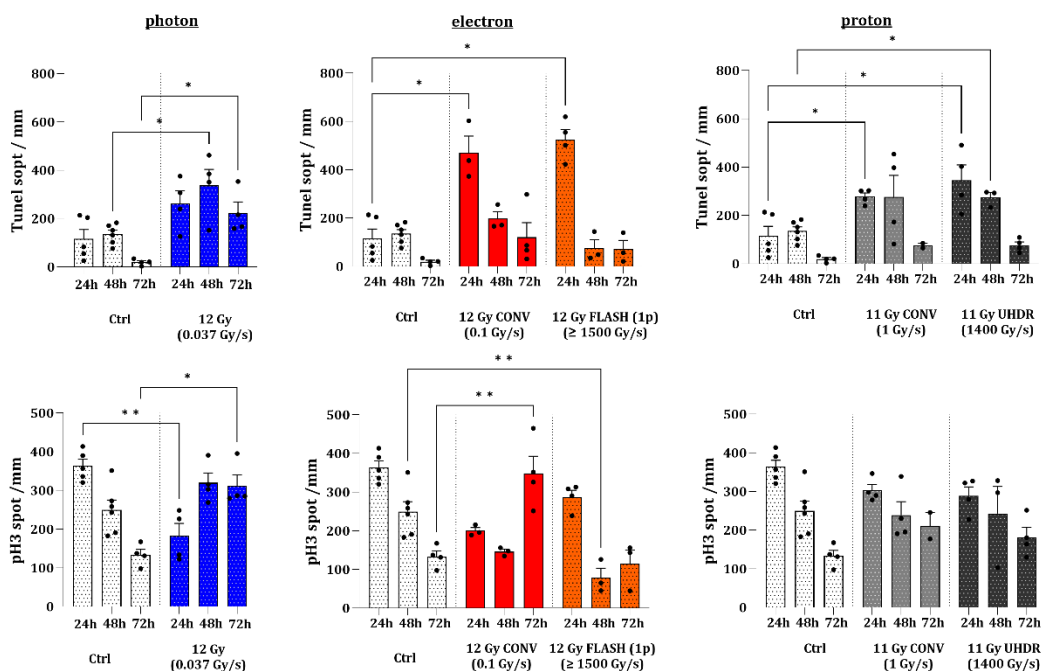
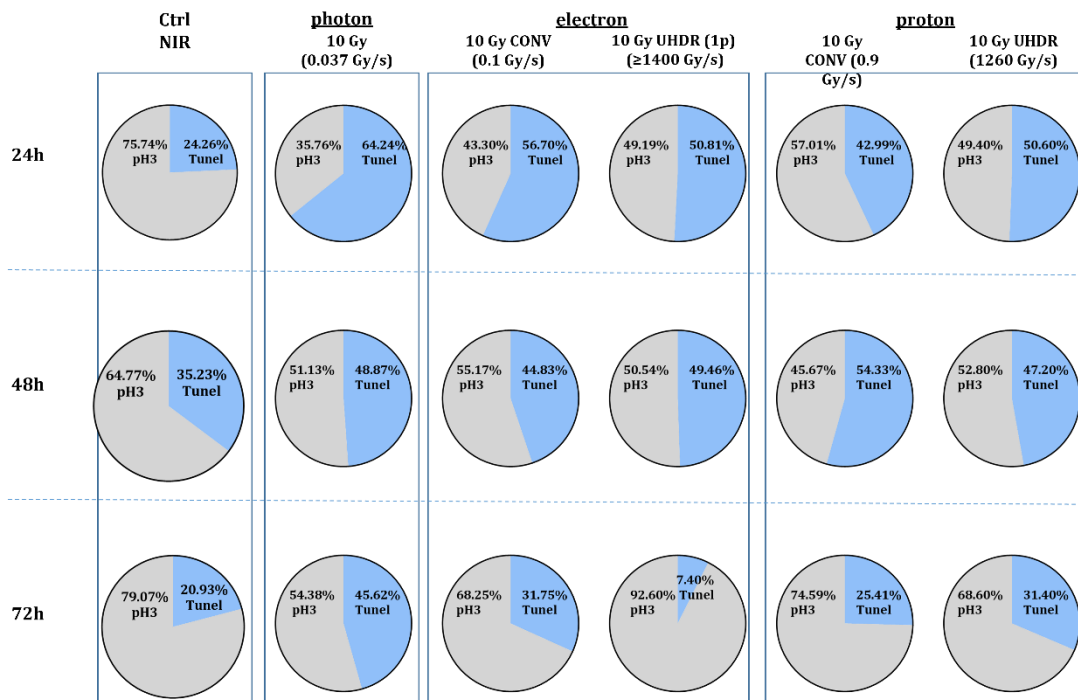


Figure sup 1: Cell death and proliferation kinetics after exposure photon, electron and proton beams
a) Quantification of apoptosis measured by TUNEL assay at 24, 48, 72h post RT and cellular proliferation measured by pH3 staining 24, 48, 72h post 9/10Gy. n=5 embryos. **b)** Similar quantification post 11/12Gy. Results are the average of duplicate experiments except for photon that were performed once. p Values derived from Kruskal-Wallis test: GP: 0.1234 (ns), 0.0332(*), 0.0021(**), 0.002(***), <0.0001(****).

a)



b)

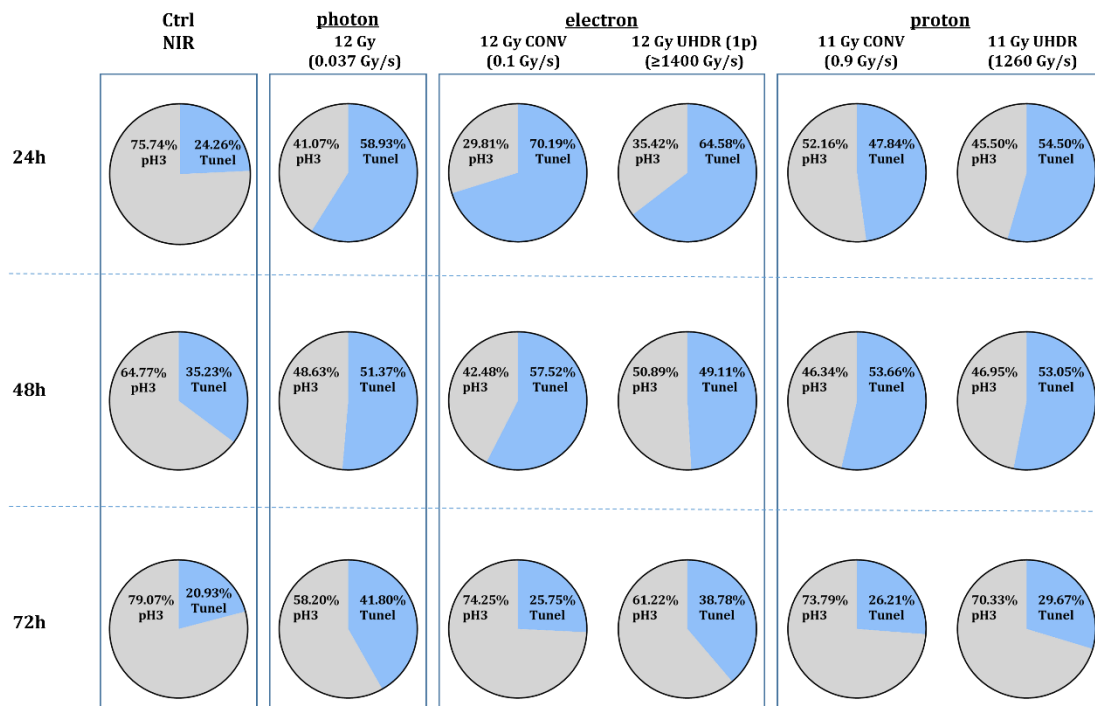
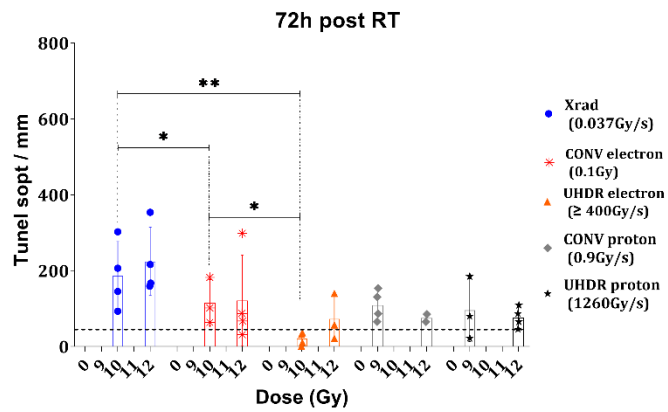
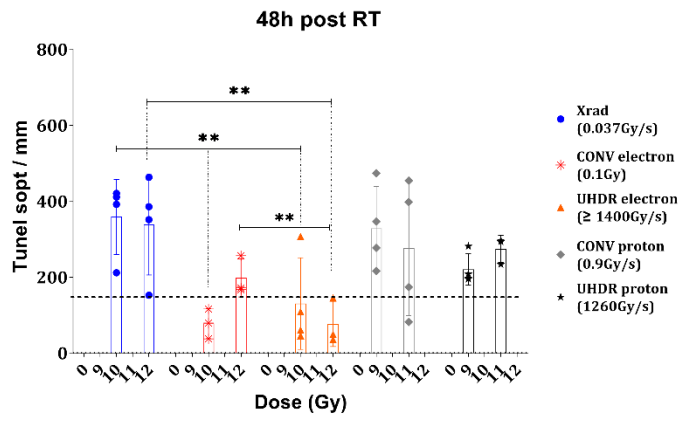
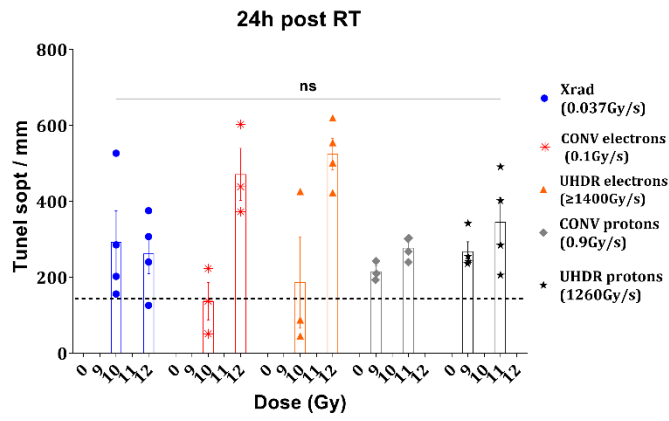


Figure sup 2: Cell death and proliferation kinetics after exposure to photon, electron and proton beams a) Pie chart illustrating the pattern of radiation induced apoptosis and proliferation spots in ZF embryos irradiated at 10 Gy, 24, 48 and 72h post-irradiation. **b)** Similar analysis at 11/12 Gy n=5 embryos. Results are the average of duplicate experiments except for photon that were performed once.

a)



b)

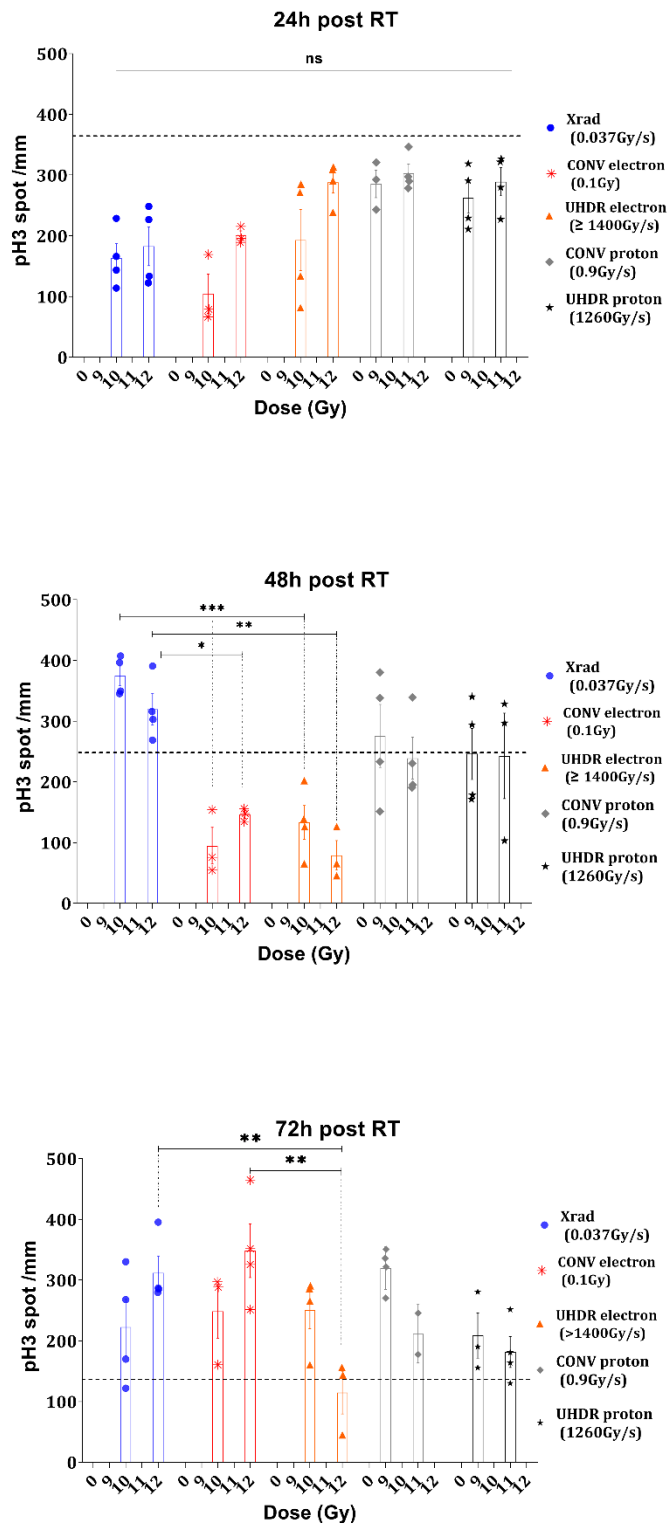


Figure sup 3: Cell death and proliferation kinetics after exposure to photon, electron and proton beams a) Bargraph illustrating the pattern of radiation induced apoptosis as a function of the dose and dose rate from different beams at 24h,48h & 72h post RT b) Bargraph illustrating the pattern of

radiation induced proliferation as a function of the dose and dose rate from different beams at 24h,48h & 72h post RT. The dashed line presented the pattern of the control cohort. n=5 embryos. Results are the average of duplicate experiments except for photon that were performed once. Patterns from photon irradiation were statistically significant from controls cohorts over the 3 irradiation time points. Electrons irradiation showed also significant dose rate dependent pattern from the controls cohort at 48h, and 72h post RT. Proton patterns were also significant from controls but dose rate independent.

Supplementary Tables

Supplementary table 1: Beam parameters employed for water radiolysis and ZF embryos irradiations at conventional and ultra-high dose rates **a)** e-RT6 (5.5MeV) electrons **b)** X-rad (225keV) photons **c)** PSI (235MeV) protons.

a)

Mode	Experiment	Delivered dose [Gy]	SSD [mm]	Grid tension [V]	Number of pulses	Pulse width [μ s]	Frequency [Hz]	Dose per pulse [Gy]	Treatment time [s]	Mean dose-rate [Gy/s]	Instantaneous dose-rate [Gy/s]
UHDR (≥ 1400 Gy/s)	ZF RT	7	400	300	1	1.8	100	7	1.8×10^{-6}	3.89×10^6	3.89×10^6
		8	390		1			8	1.8×10^{-6}	4.44×10^6	4.44×10^6
		10	345		1			10	1.8×10^{-6}	5.62×10^6	5.56×10^6
		11	325		1			11	1.8×10^{-6}	6.11×10^6	6.11×10^6
		12	310		1			12	1.8×10^{-6}	6.66×10^6	6.66×10^6
	Water radiolysis	10	345		1			10	1.8×10^{-6}	5.62×10^6	5.56×10^6
		20	345		2			10	0.01	2000	5.56×10^6
		30	345		3			10	0.02	1500	5.56×10^6
UHDR (1400Gy/s)	ZF RT	10	470	300	2	1.95	140	5	0.007	1.40×10^3	2.60×10^6
UHDR (100Gy/s)	Water radiolysis	10	980	300	10	1.8	100	1	0.09	110	5.56×10^5
		20			20				0.19	105	
		30			30				0.29	103	
CONV-RT (0.1Gy/s)	ZF RT	7	600	100	490	1	10	0.01	48.9	0.1	1.00×10^4
		8			560				55.9		
		10			700				69.9		
		11			770				76.9		
		12			840				83.9		
		Water radiolysis			10				700		
	20				1400				139.9		
	30				2100				209.9		

b)

Mode	Experiment	Prescribed dose [Gy]	Treatment time [s]	[kV]	[mA]	Filter
X-rays (0.037Gy/s)	ZF RT	6	162	225	13	Cu 3mm
		7	189			
		8	216			
		10	264			
		12	318			
	Water radiolysis	10	264			
		20	529			
		30	793			

c)

Mode	Experiment	Delivered dose [Gy]	Delivered dose rate [Gy/s]	Uncertainty on delivered dose/dose rate [%] (k=1)	Cyclotron Beam Current [nA]	Treatment time [s]	Cyclotron frequency [Hz]	Pulse width [μ s]
UHDR (1260Gy/s)	ZF RT	9	1260	4	609	7.14×10^{-3}	7.285×10^7	8.00×10^{-4}
		9.9	1260			7.86×10^{-3}		
		10.8	1260			8.57×10^{-3}		
	Water radiolysis	9	1260	4	609	7.1×10^{-3}		
		18	1260			1.43×10^{-2}		
		27	1260			2.14×10^{-2}		
UHDR (90Gy/s)	Water radiolysis	9	90	4	43.5	1.00×10^{-1}		
		18	90			2.00×10^{-1}		
		27	90			3.00×10^{-1}		
CONV-RT (0.9Gy/s)	ZF RT	9	0.9	4	0.44	10		
		9.9	0.9			11		
		10.8	0.9			12		
	Water radiolysis	9	0.9	4	0.44	10		
		18	0.9			20		
		27	0.9			30		
CONV-RT (0.1Gy/s)	ZF RT	9.5	0.1	4	0.044	95		
		10.5	0.1			105		
		11.4	0.1			114		

3- Publication 3: Instantaneous dose rate is a critical parameter linking the FLASH sparing effect across different high dose rate modalities.

Submitted

In this paper, we extended our investigations with the aim of defining the essential parameter(s) required to trigger the FLASH effect. This study is a collaboration between the groups of MC Vozenin and R Corsini's team at CERN. I have been responsible for conducting water radiolysis experiments, analyzing all experimental data, and drafting the article.

We examined the impact of a broad range of dose rate from different beam structures operating at picoseconds to minutes on primary physico-chemical events to zebrafish embryos (ZFE). Three beams were utilized: the very high energy electron (VHEE) source CLEAR (190-210 MeV), the FLASH-validated intermediate energy electron (IEE) beam the eRT6 (5.5 MeV), and a reference X-ray source (160 – 225 kVp).

Early physico-chemical events were investigated in water at two-time scales:

- 1) Events occurring in the microsecond range were studied using scavenging experiments lead to computation of primary yields of hydrogen peroxide: $G^{\circ}(\text{H}_2\text{O}_2)$.
- 2) Long-term scale investigations were conducted in neat water without scavengers and long-term yields of hydrogen peroxide were calculated: $G(\text{H}_2\text{O}_2)$. The long-term G-value was also evaluated in different chemical environments such as oxygen, temperature, and the presence of scavengers.

Chemical investigations were then conducted with a biomolecule, plasmid DNA, and radiation-induced DNA damage was quantified. Various oxygen tension and iron levels were also studied.

Biological studies were performed using ZFE, a high-throughput model, used as a surrogate for normal tissue damages. The model allowed us to explore a wide range of beam parameters such as average and instantaneous dose rate, pulse width, and frequency. This was performed to define the necessary parameters needed to induce the sparing effect.

Our results indicated that chemical systems are poor surrogate for the complex biological response occurring after FLASH and may not be useful for validating FLASH beams or investigating the FLASH effect. However, using ZFE, we identified instantaneous dose rate as a key parameter to trigger the FLASH effect, at least with electron beams. This result suggests that a differential biological response can be initiated between the picosecond and nanosecond scale and be expressed days after irradiation. We believe these conclusions will have significant implications for the design of new FLASH devices and guide future research dedicated at understanding the mechanistic basis of FLASH.

Instantaneous dose rate is a critical parameter linking the FLASH sparing effect across different high dose rate modalities.

Houda Kacem¹, Louis Kunz¹, Pierre Korysko², Jonathan Ollivier¹, Adrien Martinotti¹, Vilde Rieker², Joseph Bateman⁴, Wilfrid Farabolini², Charles Limoli³, Manjit Dosanjh^{2,4}, Roberto Corsini² and Marie-Catherine Vozenin^{1,5}

¹ Department of Oncology, Laboratory of Radiation Oncology, Radiation Oncology Service, CHUV, Lausanne University Hospital and University of Lausanne, Lausanne, Switzerland.

²CERN, Geneva, Switzerland.

³ Department of Radiation Oncology, University of California, Irvine, CA 92697-2695

⁴JAI, University of Oxford, Oxford, UK.

⁵ Radiotherapy and Radiobiology Sector, Radiation Therapy Service, University Hospital of Geneva, Geneva, Switzerland (current address).

Abstract

FLASH has recently emerged as a significant breakthrough for the future of radiation oncology. To investigate the beam parameters able to trigger the FLASH sparing effect, we harnessed the potential of very high energy electrons (VHEE), and intermediate energy electrons (IIE). These are capable of delivering dose rates spanning from 10^{11} Gy/s to 1 Gy/min. To develop a high-throughput assay for detecting the FLASH effect, chemical investigations were conducted in water under various conditions of oxygen tension, scavengers, iron, and temperature and supplemented or not with plasmid DNA. These results were then extended to morphological outcomes in irradiated zebrafish embryos, serving as a direct biological indicator of the FLASH sparing effect. Our findings show that early physico-chemical assessments, based on hydrogen peroxide and DNA damage, are inadequate surrogates for *in vivo* the biological response. A crucial discovery from our study in the identification of the instantaneous dose rate as a critical factor in observing the FLASH sparing effect. These results carry a substantial implication. From a physics perspective, our data suggests that scanning with high-intensity beamlets will be the modality of choice for clinical developments of FLASH. Mechanistically, they imply that the FLASH effect is a biological phenomenon that defies simple modelling using controlled chemical environments.

Introduction

Radiotherapy at ultra-high dose rate (UHDR), also known as FLASH radiotherapy, is currently seen as one of the most promising innovations in radiation oncology¹. Experimental evidence from various preclinical models indicated that shortening radiation exposure time below 100-200 milliseconds can protect normal tissues while remains efficient against tumors, a phenomenon referred to as the FLASH effect. Recent studies have investigated the biological basis of normal tissue protection. Data reveal that classical pathological patterns typically activated by standard dose rate irradiations are not triggered by FLASH. Biological responses associated with FLASH exposures consistently demonstrate low levels of inflammation and protect normal cells, including vascular and stem cells, but not tumors². Interestingly, more recent studies suggest that FLASH remains efficient under conditions classically known to induce tumor radiation resistance such as hypoxia³ and immuno-depletion⁴. These findings are promising and could expand the therapeutic window of radiotherapy, offering new opportunities for cancer cure. However, several critical questions need to be answered for safe and meaningful clinical transfer. First, the mechanisms responsible for the differential effect on normal *versus* tumor tissues must be elucidated. Second, optimizing beam characteristics and temporal structures remains a priority⁵. Addressing these questions is essential to unlock the full potential of FLASH radiotherapy for the improvement of cancer treatment.

To date, the FLASH effect has been observed to be particle and beam-type agnostic. It has been reported with various beams, including intermediate energy pulsed electron (4-10 MeV)⁶⁻⁸, photon^{9,10} superconducting devices^{11,12}, and modified clinical proton beams¹³⁻¹⁵. Nevertheless, the precise parameters able to trigger the FLASH effect are still somewhat uncertain. The average dose rate of 40 Gy/s is often cited as the reference FLASH dose rate, despite negative reports published using this dose rate¹⁶⁻¹⁸.

Similarly, the mechanism/s underlying the FLASH effect, which are the subject of intense scrutiny. One hypothesis our group is exploring is that the biological impact of FLASH vs CONV could stem from radiation interactions with matter starting at “t0”. This involves the transfer of radiation energy to the substrate during the physical stage, at femtosecond time scales, potentially altering the free radical cascades that begin at sub-picosecond scales and last over milliseconds in FLASH vs CONV.

This study was designed to investigate the early physico-chemical events and the temporal parameters required to trigger the FLASH effect. We conducted a systematic study examining early physico-chemical and biological endpoints across various beam-types, including the 190-210 MeV very high energy electron beam (VHEE) at CLEAR/CERN, the 5.5MeV beam eRT6/Oriatron/CHUV, and a conventional dose rate with 160 keV and 225 keV X-ray beams as references. Our research delved into the effects of these three distinct beams, each characterized by unique temporal structures and covering spanning a broad dose rate spectrum from 10¹¹ Gy/s to 1 Gy/min. The study spanned across four distinct time scales: 1)

Primary radiolytic yields of hydrogen peroxide gave access to the events occurring at the microsecond scale; 2) Secondary radiolytic yields of hydrogen peroxide were measured, shedding light on events unfolding beyond the microsecond scale; 3) DNA damage was assessed in pBR322 plasmids, providing information within minutes post-irradiation, and 4) Early changes in the developmental stage of zebrafish embryos (ZFE) were analyzed to gather information on events occurring within hours to days post-irradiation. We correlated the acute physico-chemical events with ZFE development as a function of the beam-types and dose rates and found distinctive features specific to each beam-type and temporal structure.

Materials and Methods

Irradiation beam lines

In this study we took advantages of various beam lines able to deliver a range of dose rates:

- 1) CLEAR (CERN): 190-210MeV MeV electrons were delivered at conventional (0.125 Gy/s and 0.2 Gy/s), FLASH (10^8 to 10^{11} Gy/s). Chemical samples, cells and ZFE were placed in individual PCR tubes (0.2mL) positioned in a 3D-printed holder within a water tank. The samples were then placed in the beam using c-robot as shown in **Figure 1a**.
- 2) eRT6 (Oriatron, PMB/Alcen): 5.5MeV electrons were delivered at conventional (0.1Gy/s) and FLASH (60Gy/s up to 10^7 Gy/s). Chemical samples, cells and ZFE were placed in individual Eppendorf tubes (2mL) and positioned vertically in a water tank as illustrated in **Figure 1a**.
- 3) The Xrad 225CX/225keV (Pxi Precision X-ray) and RS2000 160keV (Rad Source Technologies)
X-ray tubes were used as a reference for photon irradiation at conventional dose rates (0.037 and 0.07 Gy/s).

Irradiation parameters are detailed in **Supp Table 1, 2 & 3**. Dosimetry was performed according to previously cross-validated protocols^{19,20}.

Water radiolysis

G°(H₂O₂): Primary yields of hydrogen peroxide

To determine the primary yield of hydrogen peroxide produced during water radiolysis, we followed the production of H₂O₂ as a function of HO• scavenger concentration (NaNO₂/NaNO₃), as described in Wasselin et al.²¹. Milli-Q water was used with a conductivity of 18.2 μS/cm was equilibrated to 1% O₂ using a hypoxia hood (Biospherix, Xvivo-system X3) and irradiated as indicated in **Supp Table 1, 2 & 3**. Water samples were immediately probed post-irradiation with Amplex Red assay kit (Thermo Fisher). Fluorescence quantification was performed using Promega Glo-Max plate reader (Excitation: 520 nm; Emission: 580-640 nm).

G(H₂O₂): Long-term yields of hydrogen peroxide.

To get closer from biological conditions, water samples were subject to various conditions known to influence radiation response in biological systems. Oxygen levels, temperature, and scavengers were varied according to **Supp Material Table 1**, and water samples were irradiated as previously described (**Supp Table 1,2 &3**). H₂O₂ measurement was conducted similarly to the earlier method.

DNA damage in pBR322 plasmid

To investigate DNA damage, pBR322 plasmid (Thermo Fisher Inc.) was purified and diluted to 40 ng/ μ l in deionized, RNAase and DNAase-free water (UltraPure). Plasmids were irradiated as described earlier in **Supp Table 1, 2 & 3**). Damages were resolved using Agarose Gel Electrophoresis (AGE) with 0.8% agarose in Tris-acetate-EDTA (TAE) buffer. The compact supercoiled form and the two relaxed forms, open circular, and linear, were quantified using densitometric analysis (UVITEC Cambridge) and ImageJ software “gels” add-on. DNA damage was also investigated in various environmental conditions such as different oxygen levels, scavengers, and the presence of labile iron (Fe^{2+}) concentrations, as shown in **Supp Material Table 3**.

The MacMahon model was applied to the data to describe the kinetics of plasmid damage post-irradiation²². The model helped in quantifying the rates of single strand breaks (SSB) and double strand breaks (DSB), denoted as β_s and β_d , respectively. This allowed for a quantitative comparison of the number of damaged plasmids by different irradiation types and in different environments.

Zebrafish embryo irradiations

AB Wild Type ZF (*Danio rerio*, #1175, F7 generation, EZRC) were bred to produce zebrafish embryos at the PTZ (CHUV/UNIL, Lausanne, Switzerland). According to Swiss and European ethics regulation, no ethical approval is required to use ZFE before 5 days of development. 4 hours post fertilization (hpf) ZFE were irradiated at 28°C using the various beam lines as described in **Supp Table 1,2 &3**.

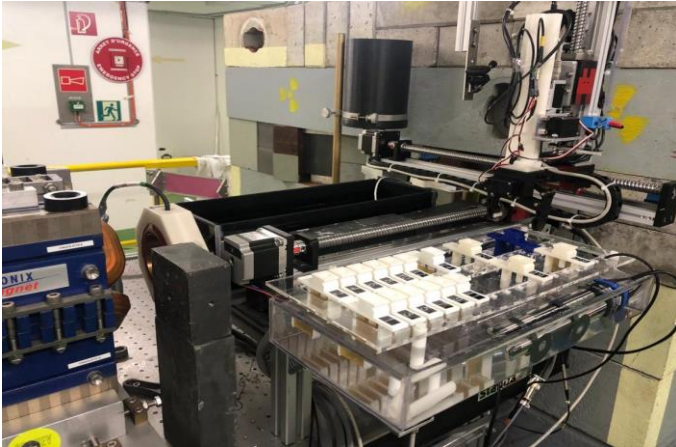
Radiation-induced alterations in ZFE morphology were measured at 5 days post-fertilization (dpf) following embryo fixation (4% PFA) and microscopic imaging (Evos XL Core Cell Imaging System, Thermo Fisher). Analysis was conducted using ImageJ software. Length deficit analysis was realized as in Horst et al ²³.

Results

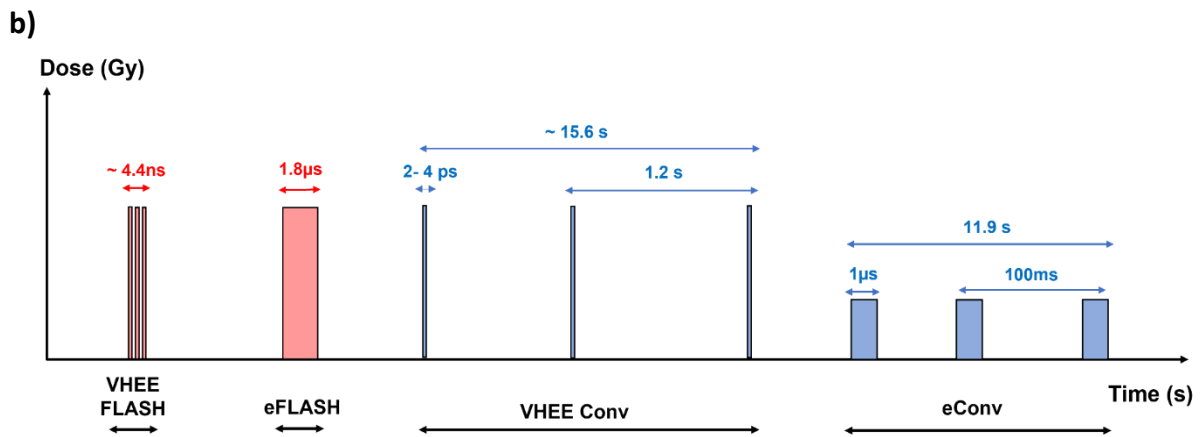
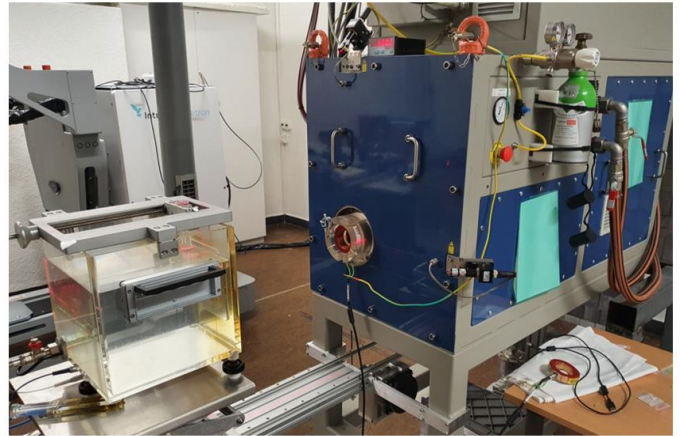
Temporal structure and characteristics of the beams

We experimentally characterized the various steps of the radiolytic cascade following water exposure to irradiation using CONV and FLASH electron beams, which possess distinct micro and macro-structures (**Figure 1**). The 190-210 MeV very high energy electron beam (VHEE) at CLEAR/CERN features a temporal structure comprising trains of bunches, that can be modified over a large spectrum of dose rate ranging from 10^{11} to 0.1 Gy/s. The 5.5MeV beam eRT6/Oriatron at CHUV, recognized as the reference for the FLASH mechanisms studies, delivers pulsed electron beam with dose rates ranging from 10^7 Gy/s to 0.1 Gy/s. Additionally, conventional dose rates using 225 keV and 160 keV photon beams, with dose rates exceeding 1 Gy/min, were included for comparison.

VHEE CLEAR CERN



IEE eRT6 CHUV



c)

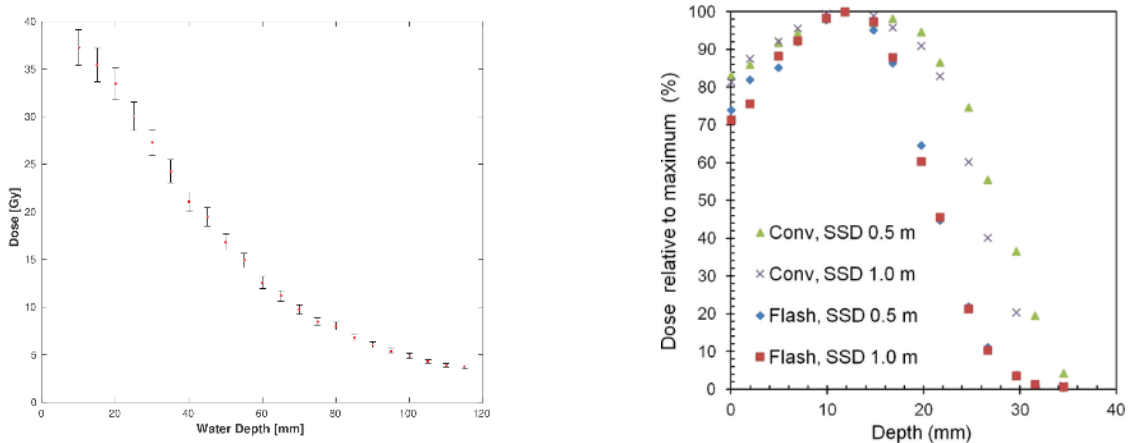


Figure 1: Overview of the beams description CLEAR (VHEE) and eRT6 (IEE) a) Experimental set up; b) Illustration of beam structure, red representation is for FLASH modality and blue is for the conventional modality; c) Dose depth profile of the two beams. VHEE: very high energy electrons; IEE: intermediate energy electrons. eFLASH stands for electrons FLASH, VHEE FLASH stands for very high energy electron FLA

G°-values of H₂O₂ are beam type and dose rate independent.

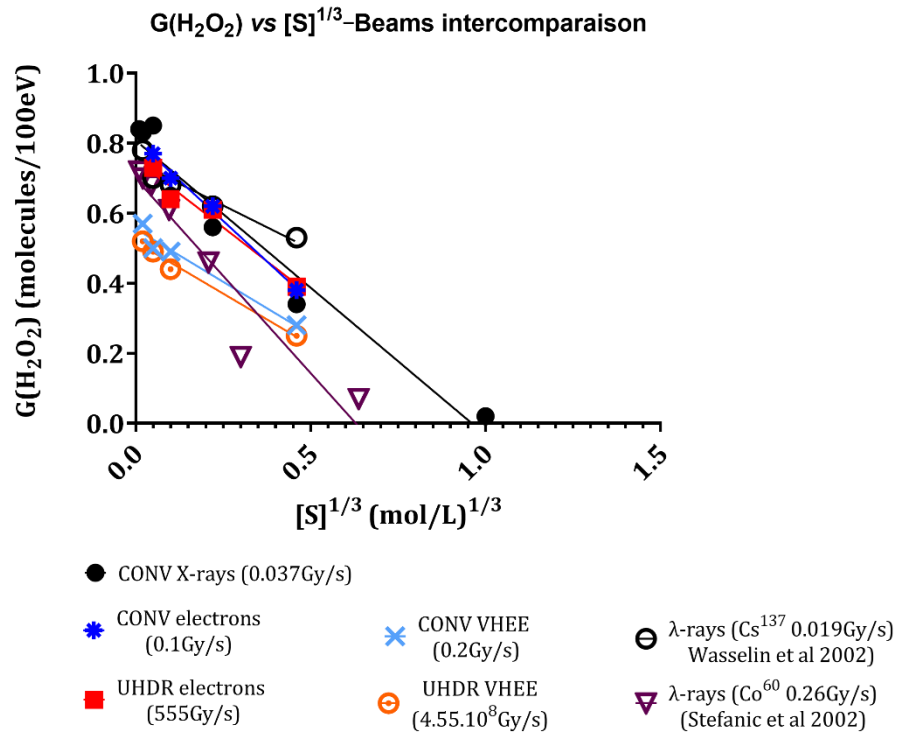
Measurement of primary yield of H₂O₂ in hypoxia was used as a surrogate of the initial radiation-induced free radical production. For each concentration of HO• scavenger used, we plotted the G-value against the cubic root of the HO• scavenger following the Swroski's method²⁴ (**Figure 2a**), and also considered the scavenging capacity²⁵ (**Supp Figure 1a&b**). These values, detailed in **Table 1**, were similar for both FLASH and CONV exposures, aligning with previous literature findings (0.6-0.8 molecules/100eV)^{21,25-28}.

Protracted yields of H₂O₂ are lower after FLASH exposure.

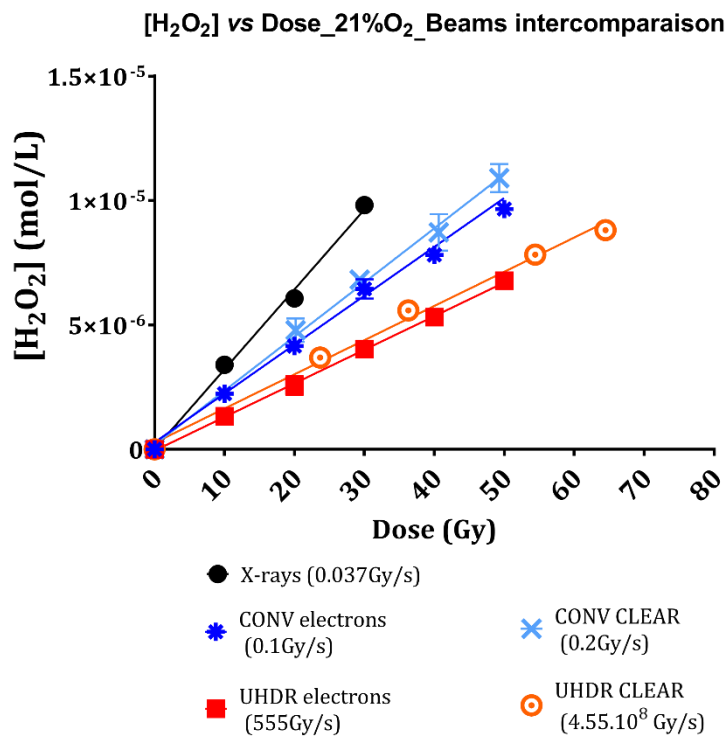
The protracted yield of H₂O₂, referred to as G(H₂O₂), was assessed minutes after water irradiation under atmospheric oxygen conditions (21% O₂), with or without scavengers. Interestingly, a 30% reduction in H₂O₂ production was observed after FLASH compared to CONV exposures, regardless of beam type (as shown **Figure 2b** and **Table 2**). This suggests that FLASH diminishes radical production under atmospheric conditions.

The complexity of the irradiated solution was modified to move closer to cellular biochemical conditions. Oxygen escalation experiments showed a bell-shaped curve for G(H₂O₂) relative to oxygen levels. Lowest yields were in hypoxic conditions, peaking at physioxic levels (4% O₂), then decreasing under atmospheric conditions, independent of dose rate. FLASH irradiation consistently reduced H₂O₂ yields by about 30%, with a maximum reduction of 34% under physioxic conditions (**Figure 1c**). When nitrate ions 25 mM were added to scavenge the hydrated electrons, the long-term yield of H₂O₂ after CONV and FLASH dose rates were reduced by 51% and 14% respectively and became similar between both modalities (**Figure 1d**). Temperature variation from room temperature (22°C) to physiological temperature (37-38°C) showed increased H₂O₂ yields at higher temperature. Additionally, the difference between CONV and FLASH was more pronounced at 37°C (**Supp Figure 2 and Supp Table 5c**). These results indicate a reduced production of free radicals following FLASH exposure, which is further enhanced under biological-like conditions.

a)



b)



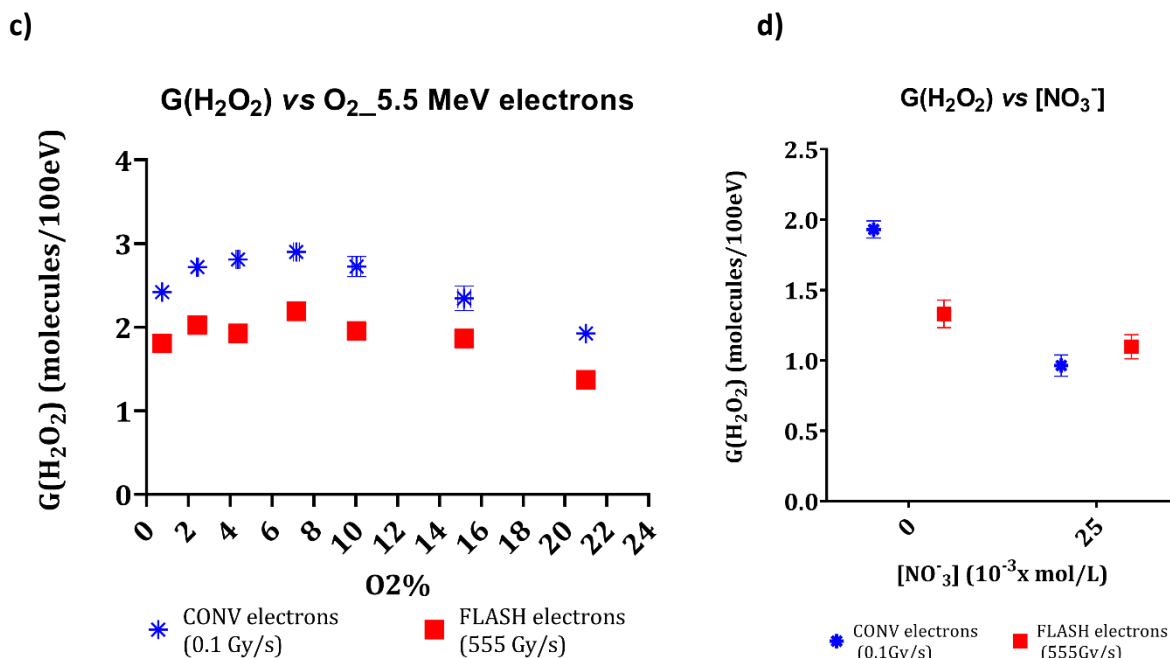


Figure 2: Primary and long-term yields of hydrogen peroxide after CONV and FLASH irradiation **a)** G-values measured in anoxic conditions (1% O₂) versus cubic root of a scavenger denoted by [S] (NO₂⁻ ions for our experiments) obtained after irradiation with CONV and FLASH (190-220MeV) VHEE, (5.5 MeV) IEE and CONV (225 kVp) X-rays compared to reported experiments performed with CONV (0.6 MeV) ¹³⁷Cs γ -rays; [S] = [NO₂⁻]²¹ and CONV (1.2 MeV) ⁶⁰Co γ -rays; [S] = [Br⁻]²⁷. **b)** Production of H₂O₂ vs dose at 21% O₂ in pure water after irradiations with CONV and FLASH VHEE, IEE and CONV X-rays **c)** Long-term G(H₂O₂) vs different O₂ levels after irradiation with CONV and FLASH IEE. **d)** Long-term G(H₂O₂) in presence or not of [NO₃⁻] = 25 mM (scavenger of aqueous electrons) after irradiation with CONV and FLASH IEE. Long-term G-values were calculated from the slopes of H₂O₂ concentrations vs the delivered dose. Scavenging experiments are results of 6 experiments for IEE and duplicate experiments for CONV X-rays and VHEE (CONV and FLASH). Long-term G-values at 21% O₂ are results of triplicate experiments with all beams. [NO₃⁻] experiments were done with CONV and FLASH IEE. Each experiment had 8 points of measurements per dose.

Table 1 Primary yields of hydrogen peroxide, $G^\circ(\text{H}_2\text{O}_2)$, in hypoxia calculated from the Swroski model²⁴ for the different beam sources.

Source	Energy	LET [keV/ μm]	Dose rate [Gy/s]	[O ₂] [M]	Chemical system	$G^\circ(\text{H}_2\text{O}_2)$ [molecules/100eV]
CONV VHEE	190-210 MeV	0.2	0.2	1.19×10^{-5}	[NO ₂ ⁻]/[NO ₃ ⁻]	0.6 ± 0.02
FLASH VHEE			4.55×10^8			0.59 ± 0.02
CONV electrons	5.5 MeV	0.2	0.1			0.8 ± 0.02
FLASH electrons			≥ 555			0.75 ± 0.03
CONV X-rays	225 kVp	3	0.037			0.78 ± 0.04

Table 2: Long-term radiolytic yields of hydrogen peroxide, $G(\text{H}_2\text{O}_2)$, calculated after irradiation with FLASH and CONV VHEE, IEE and CONV X-rays. $\Delta\text{FLASH}/\text{CONV}$ represents the reduction percentage in G-value from CONV dose rate to FLASH dose rate.

Source	Energy	LET [keV/ μm]	Dose rate [Gy/s]	[O ₂] ([M])	$G(\text{H}_2\text{O}_2)$ [molecules/100eV]	$\Delta\text{FLASH}/\text{CONV}$
CONV VHEE	190-210 MeV	0.2	0.2	2.50×10^{-4}	1.9 ± 0.06	32%
FLASH VHEE			4.55×10^8		1.3 ± 0.04	
CONV electrons	5.5 MeV	0.2	0.1		1.9 ± 0.04	31%
FLASH electrons			≥ 555		1.3 ± 0.04	
CONV X-rays	225 kVp	3	0.037		3.1 ± 0.05	N.A

DNA damage to plasmid is dose rate insensitive

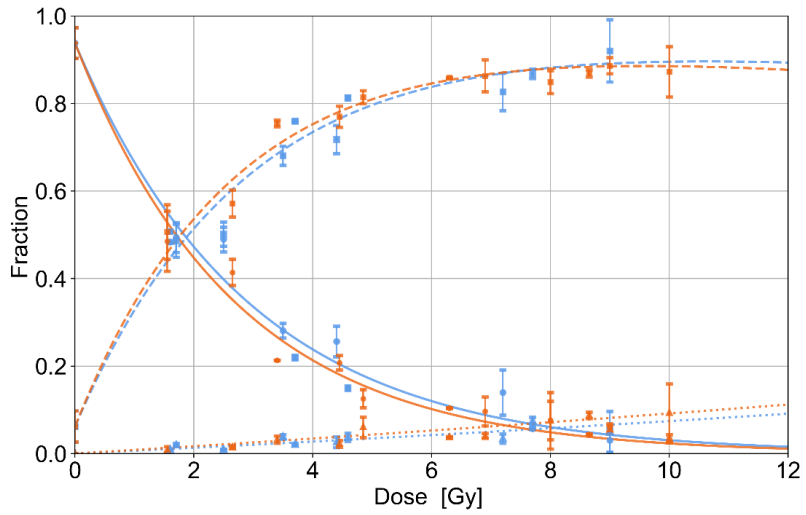
To move a step closer to biological systems, a plasmid was irradiated, and DNA damage was investigated under various conditions. In atmospheric conditions, when the plasmid was in pure water, a dose-dependent induction of SSB and DSB was found but was dose rate independent (**Figure 3a**). The summary of the results produced by these systematic investigations are found in **Table 3**.

Adding 14 mM DMSO, a concentration 10 times lower than cellular antioxidant levels, significantly protected the plasmid from radiolytic damage, with a dose modifying factor (DMF) of about 10-fold, independent of dose rate (**Figure 3b**). Under hypoxic conditions and increased Fe^{2+} concentrations, mimicking tumor environment, FLASH irradiation reduced damage levels for doses above 20 Gy (**Figure 3c**), whereas increased Fe^{2+} levels did not significantly affect FLASH-induced damages (**Supp Figure 4b**). These findings suggest that FLASH irradiation may induce less DNA damage than CONV in pseudo-tumoral conditions.

a)

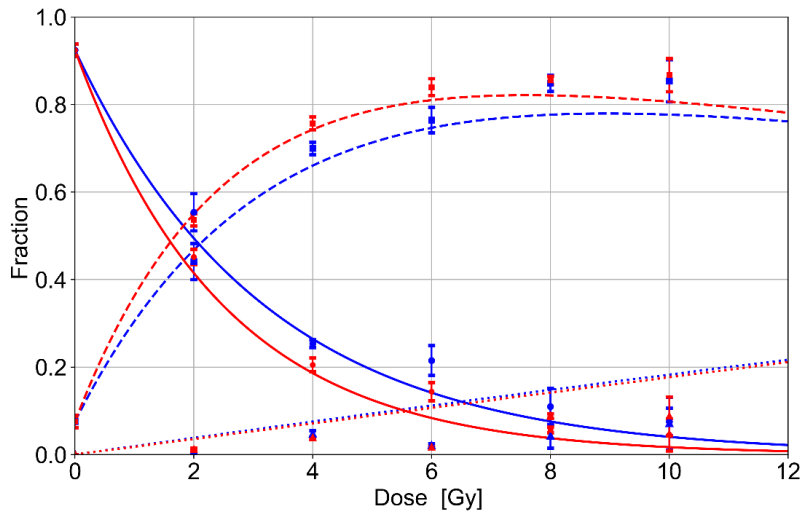
21% O₂ – VHEE (CLEAR)

CONV ● (0.125 Gy/s) - FLASH ● (4.55x10⁸ Gy/s)



21% O₂ – IEE (eRT6)

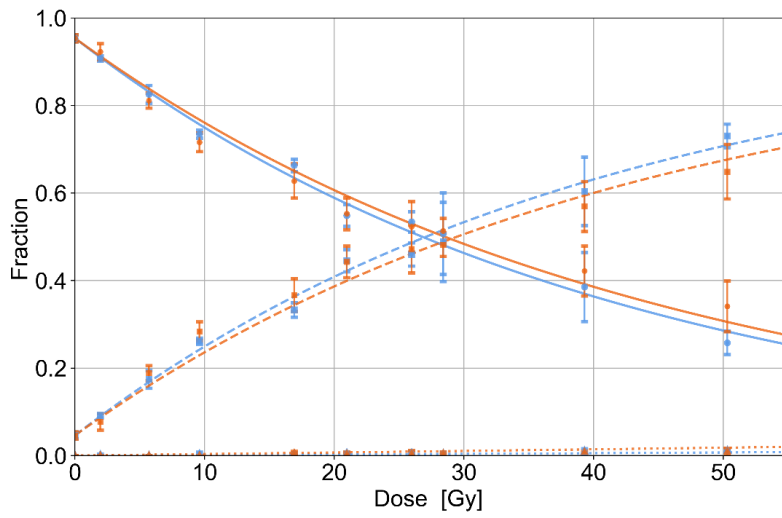
CONV ● (0.1 Gy/s) - FLASH ● (≥ 555 Gy/s)



b)

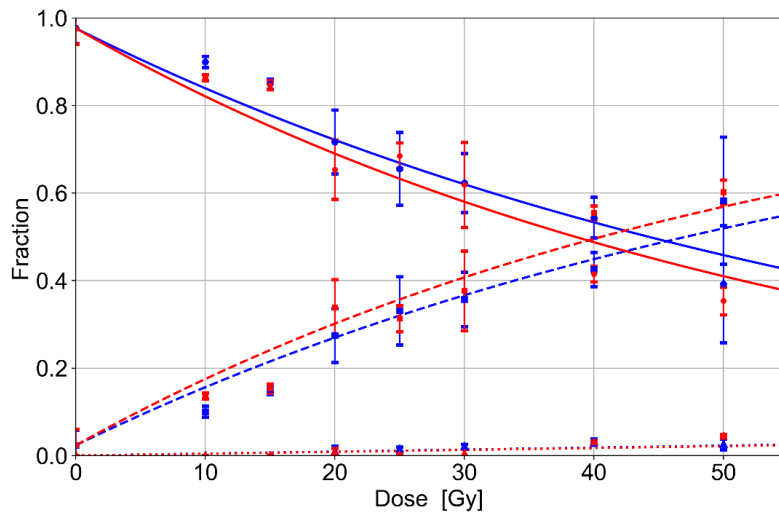
21% O₂ 14 mM DMSO – VHEE (CLEAR)

CONV ● (0.125 Gy/s) - FLASH ● (4.55x10⁸ Gy/s)



21% O₂ 14 mM DMSO – IEE (eRT6)

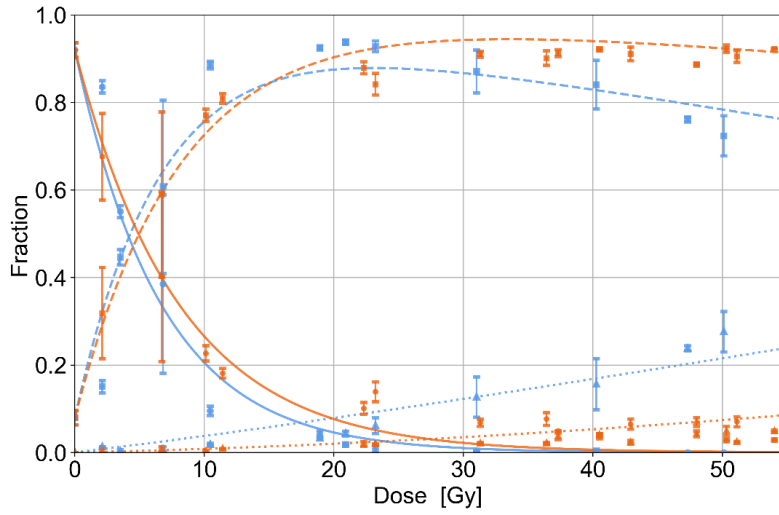
CONV ● (0.1 Gy/s) - FLASH ● (≥ 555 Gy/s)



c)

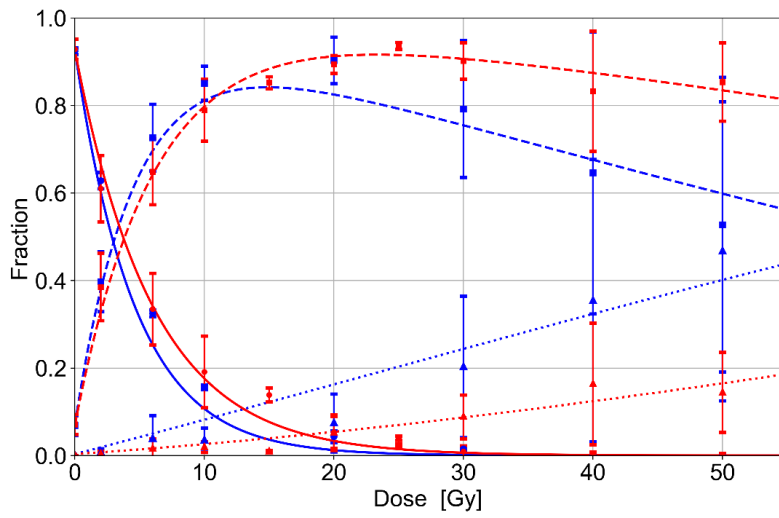
1% O₂ – VHEE (CLEAR)

CONV ● (0.125 Gy/s) - FLASH ● (4.55x10⁸ Gy/s)



1% O₂ – IEE (eRT6)

CONV ● (0.1 Gy/s) - FLASH ● (≥555 Gy/s)



d)

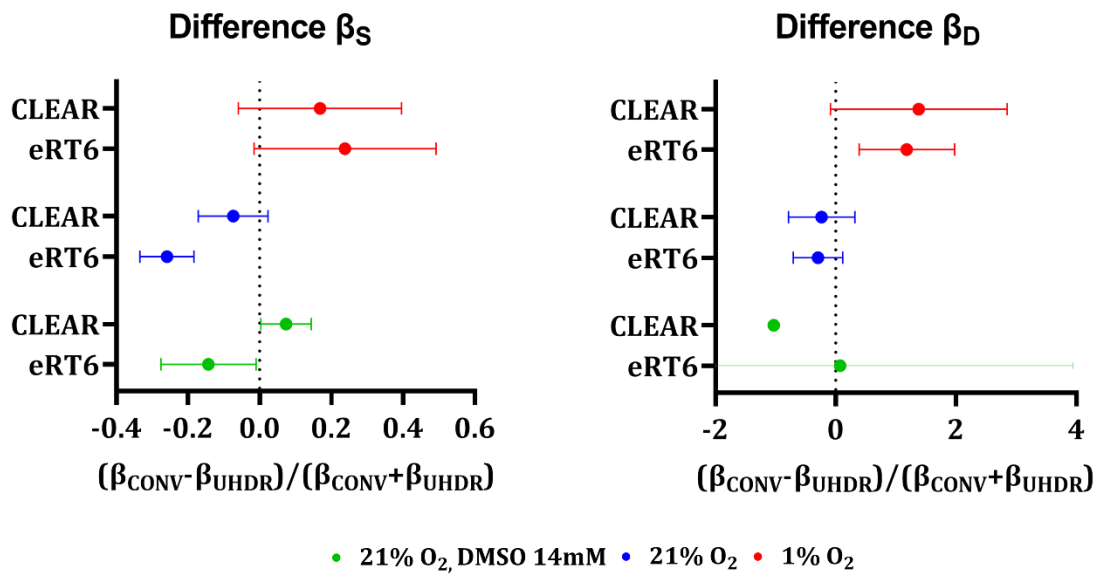


Figure 3: Fraction of DNA damage development forms in plasmids at a) 21% O₂ b) in presence of 14 mM DMSO and c) 1% O₂ with CONV and FLASH VHEE and IEE beams. d) Relative difference of damage yields, β_S for single strand break (SSB) yields and β_D for double strand break (DSB) yields between CONV and FLASH for the three conditions (21% O₂; 21% O₂ + 14 mM DMSO and 1% O₂). The two beams are pulled together on the top figure and separated at the bottom. Results are a pull of three independent experiments for both beams.

Table 3: Summary table of DSB (β_D) and SSB yields (β_S) calculated at atmospheric oxygen conditions from different beam structures. Similarly, as in Table 2, the Δ FLASH/CONV represents the reduction percentage in G-value from CONV dose rate to FLASH dose rate.

Source	Energy	LET [keV/ μ m]	Dose rate [Gy/s]	β_D [10^{-2} /Gy]	β_S [10^{-2} /Gy]
CONV VHEE	190-210 MeV	0.2	0.2	0.6 ± 0.3	34 ± 2
FLASH VHEE			4.55×10^8	0.8 ± 0.2	36 ± 2
CONV electrons	5.5 MeV	0.2	0.1	0.6 ± 0.2	27 ± 2
FLASH electrons			≥ 555	0.8 ± 0.2	35 ± 2
CONV X-rays	160 kVp	3	0.07	0.5 ± 0.1	22 ± 1

Instantaneous dose rate is a critical parameter to trigger the FLASH sparing effect in ZFE.

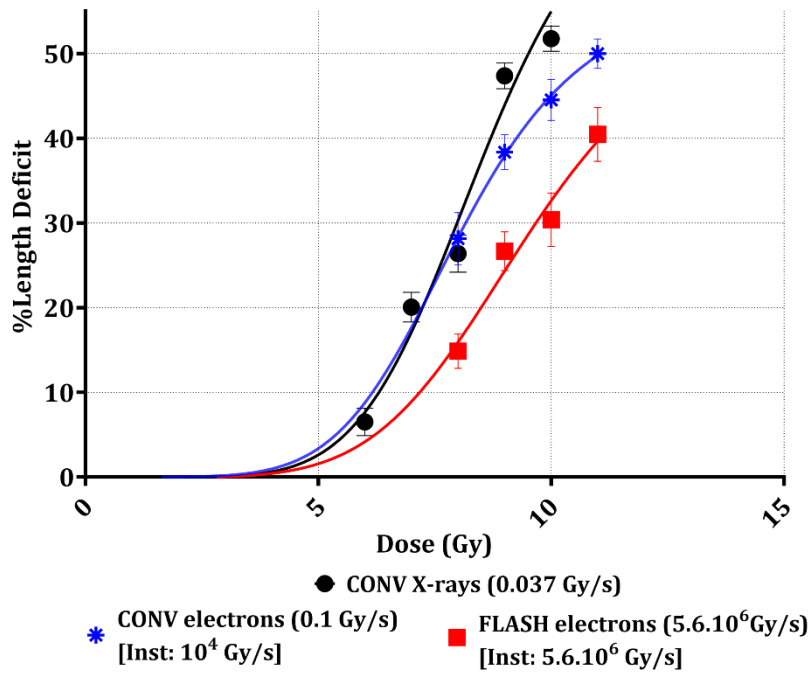
To correlate the results obtained with these reductionist approaches with biological outcomes, we used ZFE irradiated with various beams and parameters were tested to determine the required parameters to trigger normal tissue sparing (see **Figure 1b**).

We compared biological outcomes obtained after ZFE irradiation performed using X-rays, eRT6 and CLEAR. At conventional conditions, X-rays at 0.037 Gy/s and eRT6 at 0.1 Gy/s produce similar dose-dependent defects in the morphogenesis of ZFE (**Figure 4a**) and the length deficit at 10 Gy (LD10) was 50% with X-rays and 45% with eRT6-CONV. With eRT6-FLASH, when the dose was delivered in 1 pulse meaning that both average and instantaneous dose rate were equal and set at 0.5×10^6 Gy/s, the LD10 was 30%, contrasting with 45% for eRT6-CONV. The DMF was ~ 1.2 . CLEAR irradiation with a conventional dose rate of 0.125 Gy/s and a FLASH dose rate of 4.55×10^8 Gy/s, similar dose in the bunch of 0.15 Gy, and similar instantaneous dose rate of 5×10^{10} Gy/s, showed no differential effect and indicating a LD10 of 40% reached in both cases (**Figure 4b**). Then, we varied the dose in the bunch/instantaneous dose rate. The VHEE-CONV parameters were: Average Dose Rate = 0.2 Gy/s, dose in the bunch = 0.019 Gy and Instantaneous Dose Rate = 6.4×10^9 Gy/s and the VHEE-FLASH parameters were: Average Dose Rate = 10^9 Gy/s, dose in the bunch = 0.3 Gy and Instantaneous Dose Rate = 10^{11} Gy/s. With these parameters, the LD10 for VHEE-CONV was 45% and 30% for VHEE-FLASH as illustrated in **Figure 4c**. The DMF was ~ 1.3 . These results are the first to suggest that the instantaneous dose rate is indeed driving the FLASH effect.

Then to confirm our findings we used the eRT6, a versatile device, allowed varying average dose rate, pulse/instantaneous dose rate, dose in the pulse, pulse width, and frequency keeping while maintaining a constant delivered dose at 10 Gy and ZFE developmental stage at 4hpf. A dose rate escalation study ranging from 0.1 to 5.6×10^6 Gy/s identified an average dose rate of 100 Gy/s, 100 Hz and 10 pulses of 1 Gy with a pulse width of 1.8 μ s i.e., instantaneous dose rate of 0.5×10^6 Gy/s as threshold parameters for protecting ZFE morphogenesis (**Figure 4d**). Modification to pulse width from 1.8 μ s to 4 μ s when a dose of 10 Gy was delivered in one, two and 5 pulses, did not modify the sparing outcome (**Figure 4e**). Surprisingly, modification of the pulse frequencies from 100 Hz = 10 milliseconds up to a 10 min interval did not modify the sparing outcome as well (**Figure 4f**). These unexpected results revealed that neither overall time nor pulse multiplicity are crucial for the FLASH sparing effect. Importantly, these findings highlight that an instantaneous dose rate above 10^6 Gy/s and a dose of 1 Gy in the pulse are the relevant parameters.

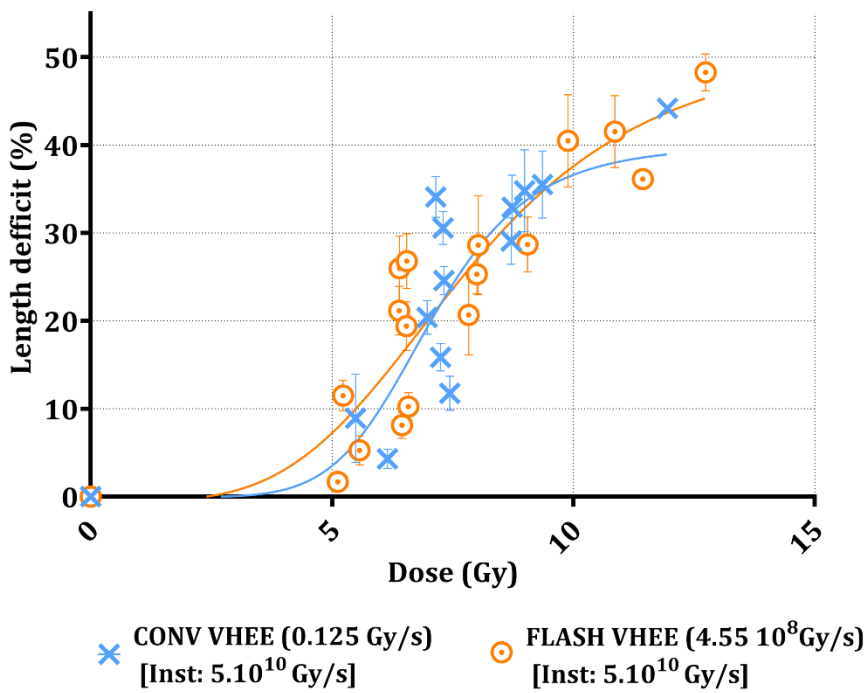
a)

% of length deficit in ZFE_225 kVp X-rays and 5.5 MeV IEE_5-11Gy_4hpf

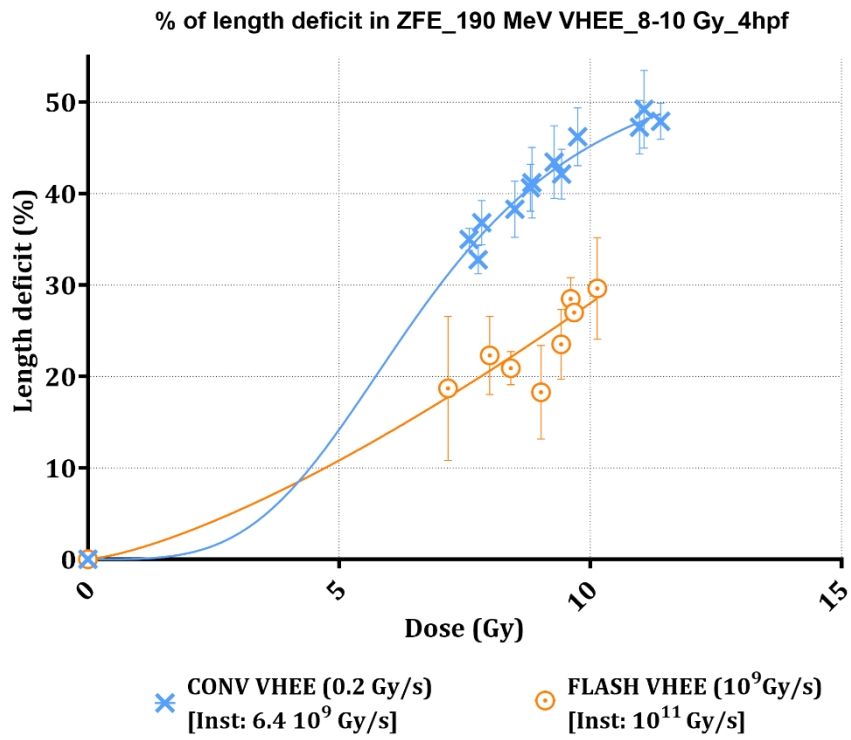


b)

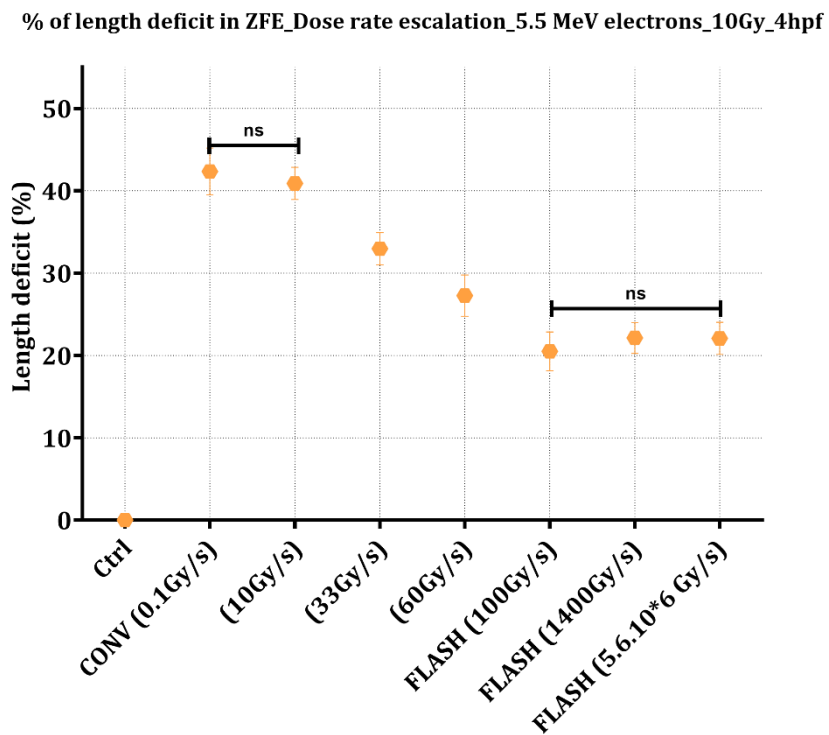
% of length deficit in ZFE_190 MeV VHEE_8-10Gy_4hpf



c)

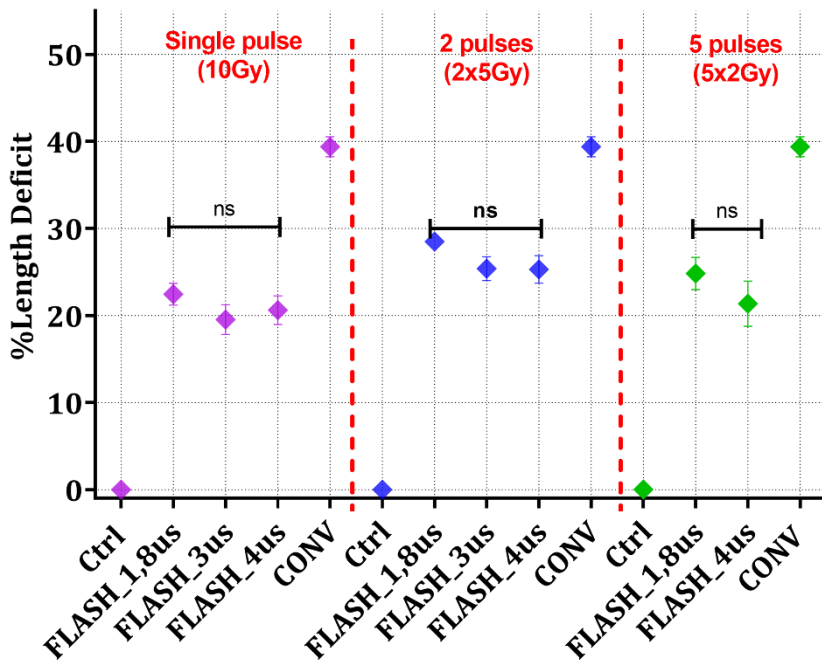


d)



e)

% of Length deficit_Pulse width variation_5.5 MeV electrons_10Gy_4hpf



f)

% of Length deficit_Frequency variation_5.5MeV electrons_10Gy_4hpf

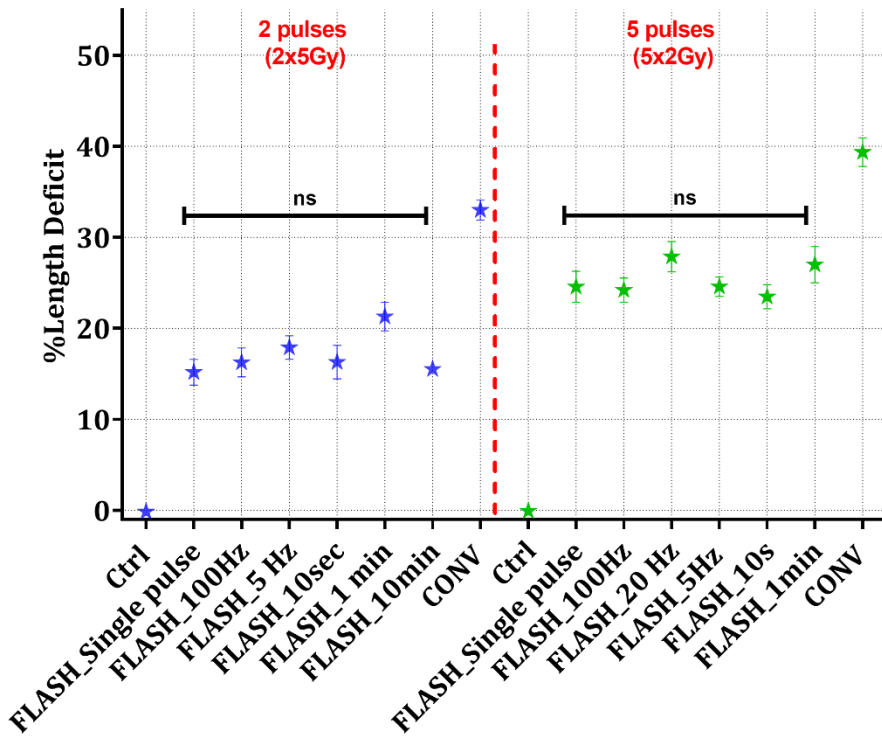


Figure 4: Parametrization experiment's on 4hpf ZFE Length deficiency. Dose response of 4hpf ZFE after exposure to **a)** CONV X-rays (0.037 Gy/s), CONV (0.1 Gy/s) and FLASH (5.6x10⁶ Gy/s) IEE. **b)** CONV (0.125 Gy/s) and FLASH (4.55x10⁸ Gy/s) VHEE with similar instantaneous dose rate (5x10¹⁰ Gy/s). **c)** CONV (0.2 Gy/s) and FLASH (10⁹ Gy/s) VHEE with different instantaneous dose rates (6.4x10⁹ Gy/s) and (10¹¹ Gy/s) respectively. **d)** increasing dose rates **e)** different pulse widths and **f)** different frequencies. For IEE, embryos n = 20 per each dose and for VHEE irradiations, embryos n = 8 per dose. Results are the average of 3 experiments for IEE (CONV and FLASH) and 2 experiments for CONV X-rays and VHEE (CONV and FLASH).

Radiolytic H₂O₂ production in water is a poor surrogate of the *in vivo* FLASH effect

When applying the FLASH sparing parameters identified with CLEAR in chemistry experiments, increased H₂O₂ yields and a lower Δ FLASH/CONV ratio were observed (**Supp Figure 2b&c and Table 4**). This suggests that the radiolytic production of H₂O₂ does not correlate with the *in vivo* sparing effect and is not an effective indicator for assessing the biological impact of FLASH irradiation.

Table 4: Long-time radiolytic yields of hydrogen peroxide produced at physioxic O₂ conditions after irradiation with FLASH and CONV VHEE, IEE and CONV X-rays.

Source	Energy	LET [keV/μm]	Dose rate [Gy/s]	[O ₂] [M]	G(H ₂ O ₂) [molecules/ 100eV]	ΔFLASH/CONV
CONV VHEE	190-210 MeV	0.2	0.125 [Inst: 5x10 ¹⁰]	4.76x10 ⁻⁵	2.79 ± 0.08	N.A
			0.2 [Inst: 4.6x10 ⁹]		3.71 ± 0.04	N.A
4.55x10 ⁸ [Inst: 5x10 ¹⁰]			1.72 ± 0.08		38%	
1x10 ⁹ [Inst: 1x10 ¹¹]			2.67 ± 0.05		28%	
CONV electrons	5.5 MeV	0.2	0.1 [Inst: 1x10 ⁴]		2.81 ± 0.03	N.A
FLASH electrons			100 [Inst: 5.56x10 ⁵]		2.33 ± 0.03	17%
			≥555 [Inst: ≥1500]		1.86 ± 0.05	34%
CONV X-rays	225 kVp	3	0.037			3.32 ± 0.07

Discussion

This study is the first comprehensive exploration performed into the impact of a large range of dose rates, extending from early physico-chemical events to more complex biological systems. Our results show that reductionist radiochemical approaches using water and plasmids are poor surrogates of the *in vivo* responses that define the FLASH effect. Consequently, such approaches may not be reliable for high-throughput validation of FLASH beams or for investigating the FLASH effect. Our findings show that a different biological response can be expressed days after irradiation with a dose delivered at the picosecond time scale. More importantly, we identified the instantaneous dose rate as a critical parameter to trigger the FLASH sparing effect, particularly with electron beams. These conclusions have significant implications for designing future FLASH devices and guiding research into the mechanisms of FLASH radiotherapy.

In the present study, aligning with historical data in water radiolysis literature, we observed that primary radiolytic yields of hydrogen peroxide remain unaffected to changes in dose rate. These findings are in agreement with previous measurements made using pulsed electrons²⁹ or conventional γ -ray sources^{21,25,27,30,31}. Additional insights can be taken from our study, namely that despite those primary yields of H₂O₂ obtained with IEE, and VHEE irradiations were not modified by the dose rate. There was a decrease in the primary yields of VHEE beam compared with IEE beam. This phenomenon can be attributed to a hypothetical spur overlapping at high dose rates such as the ones used by CLEAR (Inst CONV-VHEE dose rate = Inst FLASH-VHEE dose rate = 5×10^{10} Gy/s). However, we noted a reduced secondary production of H₂O₂ following FLASH irradiation, suggesting a possible alteration in the subsequent chemical reactions after the homogeneous phase. These results align with our previous findings and other recent reports³²⁻³⁴, yet they contradict the findings of Anderson et al.²⁹ and Sehested et al.³⁵ These researchers reported an increased long-term yield of hydrogen peroxide yield with pulsed electrons ($> 5 \times 10^6$ Gy/s) compared to conventional γ -rays. These discrepancies may stem from the oxygen conditions in the studies by Anderson et al. and Sehested et al., who used an oxygen concentration equal to 1×10^{-3} M, which is four times higher than the atmospheric oxygen pressure (2.50×10^{-4} M) used in our experiments. In a previous work, we proposed that the reduced radiolytic production of H₂O₂ achieved upon FLASH irradiation could be used as a proxy to probe FLASH beam capability. We even proposed the existence of a threshold where H₂O₂ yield ≤ 2.33 molecule/100 eV could be correlated with the preservation of ZFE morphogenesis³³. However, our current results invalidate this hypothesis, as the chemical measurements did not correlate (**Figure 5**) with biological outcomes *in vivo* using the ZFE model, even under biochemically relevant conditions.

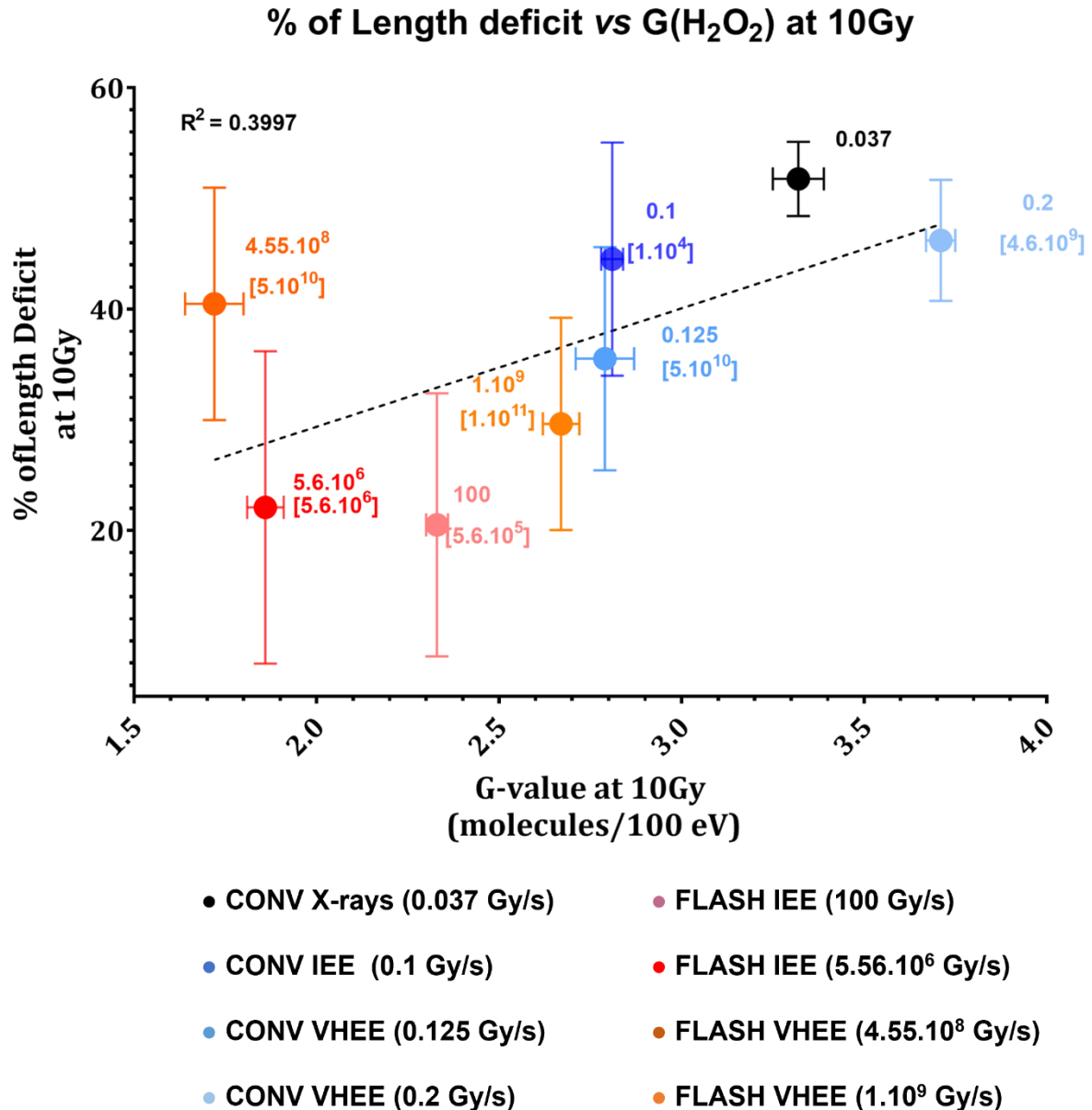


Figure 5: Correlation of ZFE Length deficiency as a function physioxic G-value after 10 Gy exposure to VHEE and IEE (CONV et FLASH): The dashed line represents the linear fitting. The R squared = 0.3997 suggesting a poor correlation between the two models. The filled circles indicate the different modalities of beams with their average dose rates and in instantaneous dose rates in brackets.

In efforts to investigate more complex macromolecules, pBR322 plasmids were irradiated. Results show that DNA damage in cell-free systems were dose rate insensitive and were not modified when beam characteristics such as the mean dose rate, instantaneous dose rate, beam structure, particle type, particle energy were modulated. More importantly, when the plasmid was placed in biochemical conditions mimicking tumors microenvironment (hypoxia, high Fe²⁺ level), plasmid DNA was protected by FLASH. Our results are consistent with older results by Milligan et al.³⁶⁻³⁸ performed with dose rates ranging between 0.1 Gy/s and 1 Gy/s

that included scavengers, as well as with published results produced at CLEAR³⁹ with dose rate above 10^9 Gy/s. However, these findings are in contradiction with a recent report claiming a reduced DNA damage in plasmids at UHDR electrons (46.6 Gy/s)⁴⁰. In this study, experimental conditions were improperly controlled as the plasmid was not properly purified which likely confounded their conclusions. In addition, data was fitted based on a very low number of experimental data points which rendered their interpretations suspect. Considering our results more robust, they still contrast the majority of *in vivo* data published to date^{2,41}, suggesting that this model is not adequate to identify the biological determinant(s) responsible for the FLASH effect in tumor-like environment. The relevance of DNA damage after FLASH vs CONV has been explored *in vivo* in mice and lead to contradictory conclusions. Fouillade et al.⁴² reported less γ H2AX foci after FLASH electrons (2×10^2 to 4×10^7 Gy/s) in the normal lung, Levy et al.⁴³ showed similar levels of γ H2AX foci in ID8 tumors after FLASH electrons (216 Gy/s) and CONV electrons (0.079 Gy/s), and a slight decrease in repair foci after FLASH in the normal gut at early time-points, that normalized by 24h post-irradiation. *In ex-vivo* study of whole-blood peripheral blood lymphocytes (WB-PBL) and using a comet assay, Cooper et al.⁴⁴ also reported reduced DNA damage burden after FLASH electrons (2000 Gy/s) at doses higher than 20Gy and in reduced oxygen conditions (0.25-0.5% O₂), whereas Barghouth et al.⁴⁵ used a functional and quantitative DNA damage repair (DDR) assay *in vitro* and showed that FLASH electrons (1×10^2 to 5×10^6 Gy/s) does not affect chromosome translocations and junction structures in HEK293T cells more than CONV electrons (0.08 Gy/s to 0.13 Gy/s). In summary, combined with ours, these experiments suggest that DNA damage is unlikely to explain the FLASH effect.

Our most important finding is related to the identification of the instantaneous dose rate as the key parameter to trigger the FLASH sparing effect with electron beams. This was demonstrated using early-stage ZFE and modulating two pulsed beams electron temporal structures. We showed that the sparing effect was occurring when the dose is delivered with pulses of 1 Gy or more delivered at the microsecond scale and when the dose is delivered with bunches of 0.3 Gy or more delivered at the picosecond scale. This suggest that higher the instantaneous dose rate is, lower is the dose in the bunch required to trigger the FLASH sparing affect i.e., 0.3 Gy at 10^{11} Gy/s and 1 Gy at 10^6 Gy/s. Interestingly, other groups found a FLASH sparing effect using ZFE using doses above 30 Gy and average/instantaneous dose rates ranging from 300 to 7500 Gy/s^{46,47}. As well, Ruan et al. showed the highest number of intestinal crypt cells was spared with a dose of 11.2 Gy delivered in a single pulse FLASH of 3.4 μ s after electron irradiation⁴⁸. Together these results support the idea that if the instantaneous dose rate is low the dose to trigger the FLASH sparing effect must be high and inversely.

In conclusion, our findings support the idea that the FLASH effect is a biological response to ultra-high dose rate beam in complex but highly organized biological systems. This also show that the parameters able to trigger the FLASH effect are dependent upon the temporal structures of the beams. However, identification of the instantaneous dose rate as a key

parameter to trigger the FLASH sparing effect is transformational to traditional radiobiology and challenging for the field. Yet, it gives a framework for the future design of new clinical accelerators as they suggest that narrow pencil/spot operating with high instantaneous dose rate such as what is feasible with VHEE and proton beams and scanned over the target would be possible. The idea is that if the instantaneous dose rate is high and the dose able to trigger the FLASH sparing effect can be low, suggests that VHEE beams are the best candidates for clinical developments of FLASH.

Supplementary Materials and Methods

Water radiolysis experiments

Aqueous solutions

Milli-Q water was used with a conductivity of 18.2 $\mu\text{S}/\text{cm}$. For scavenging experiments, aqueous solutions were prepared of different concentrations of NaNO_2 from 10 μM to 100 mM and one constant concentration of $[\text{NaNO}_3] = 25 \text{ mM}$. Water samples were equilibrated in glass bottles at room temperature in hypoxia hood (Biospherix) to achieve hypoxic oxygen conditions (1% O_2) for 48h. The day of the experiment, water was transferred to required tubes and irradiated to 10-50 Gy with the different beams. Details regarding beam parameters of the three-irradiation devices are summarized in **Supplementary Table 1**. Long time yields experiment at 21% O_2 were performed in Milli- Q water without any scavenger and irradiated to similar doses as for the scavenging experiments. In **Table 1** are shown the biochemical parameters investigated to mimic biological conditions.

Table 1: Summary of bio-chemical parameters that can influence the yield of hydrogen peroxide.

Chemical parameter	Conditions
Oxygen	1 to 21 % O_2
Temperature	22°C to 37-38°C
Scavenging aqueous electron	25 mM NaNO_3

Measurement of the irradiated samples

Water samples were probed immediately after irradiation with Amplex Red assay kit purchased from Thermo Fisher. Amplex Red was added at a final concentration of 50 μM and incubated for 30min protected from light. Freshly H_2O_2 solutions from 0.3125 μM to 10 μM were prepared and used to establish the calibration curve. Fluorescence quantification was performed using Promega Glo-Max plate reader (Excitation: 520 nm Emission: 580-640 nm). G-value of hydrogen peroxide were calculated from the slope of plots of hydrogen peroxide concentrations as a function of the irradiated dose.

DNA damage experiments

Table 2: Summary of biochemical parameters that can influence the fractions of damages plasmids.

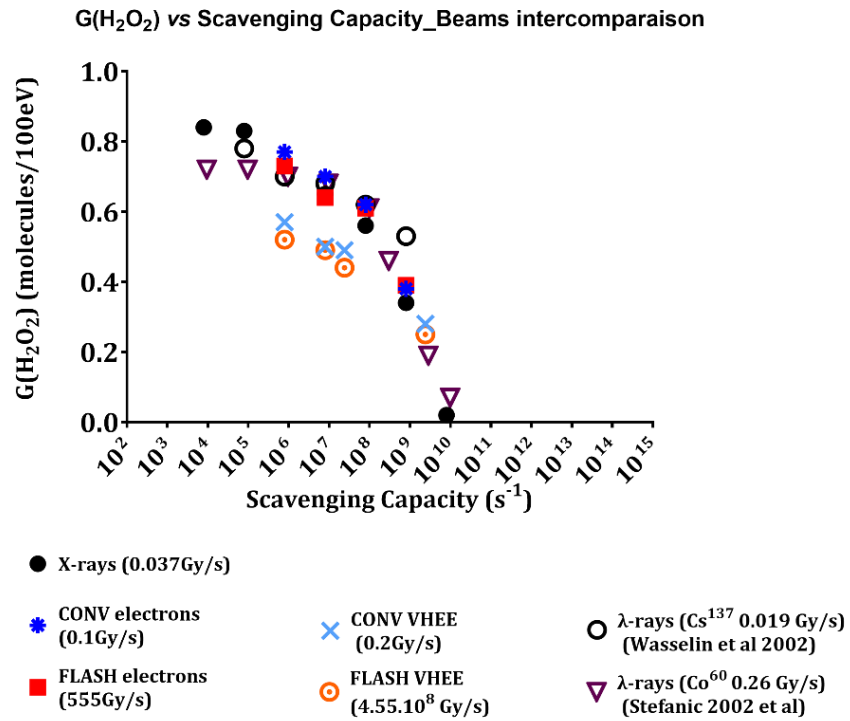
Chemical parameter	Conditions
Oxygen	1% and 21% O_2
Scavengers	14 mM DMSO
$[\text{Fe}^{2+}]$	1.5 μM , 5 μM and 10 μM

Statistical analysis

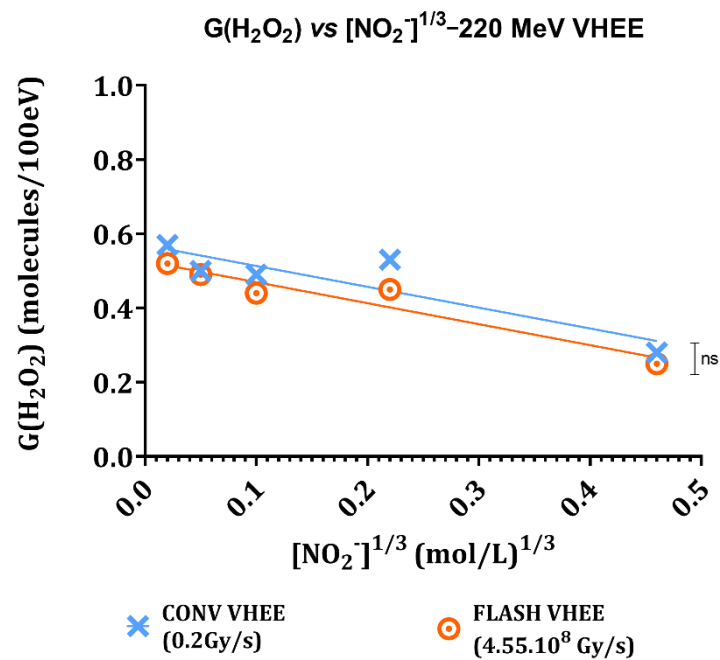
Statistical analyses were carried out using GraphPad Prism (v9.1) for water radiolysis, plasmids and ZF embryos experiments. Slopes (G-values) were assessed by t-test. For plasmids, the error bars correspond to standard deviation. For ZFE, data are presented as mean +/- SEM and analysis was done using Kruskal-Wallis test.

Supplementary Figures

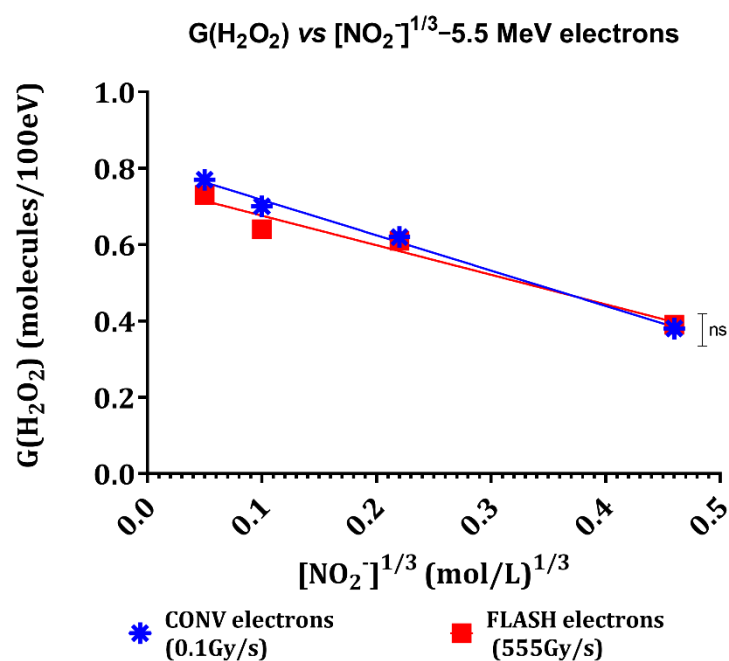
a)



b)

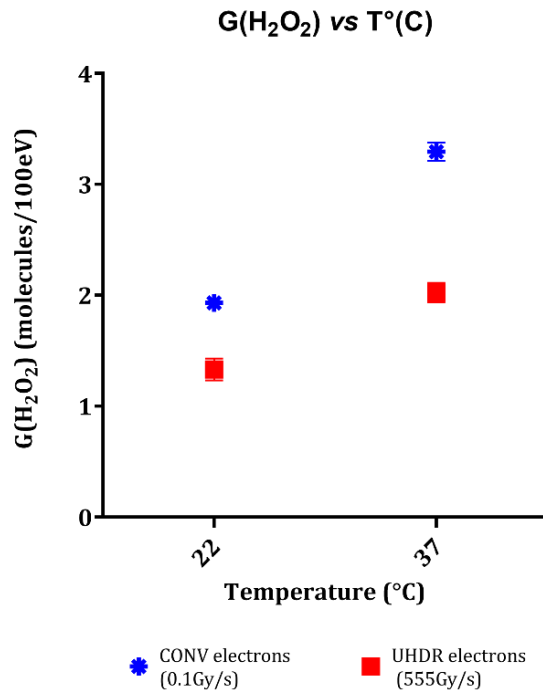


c)

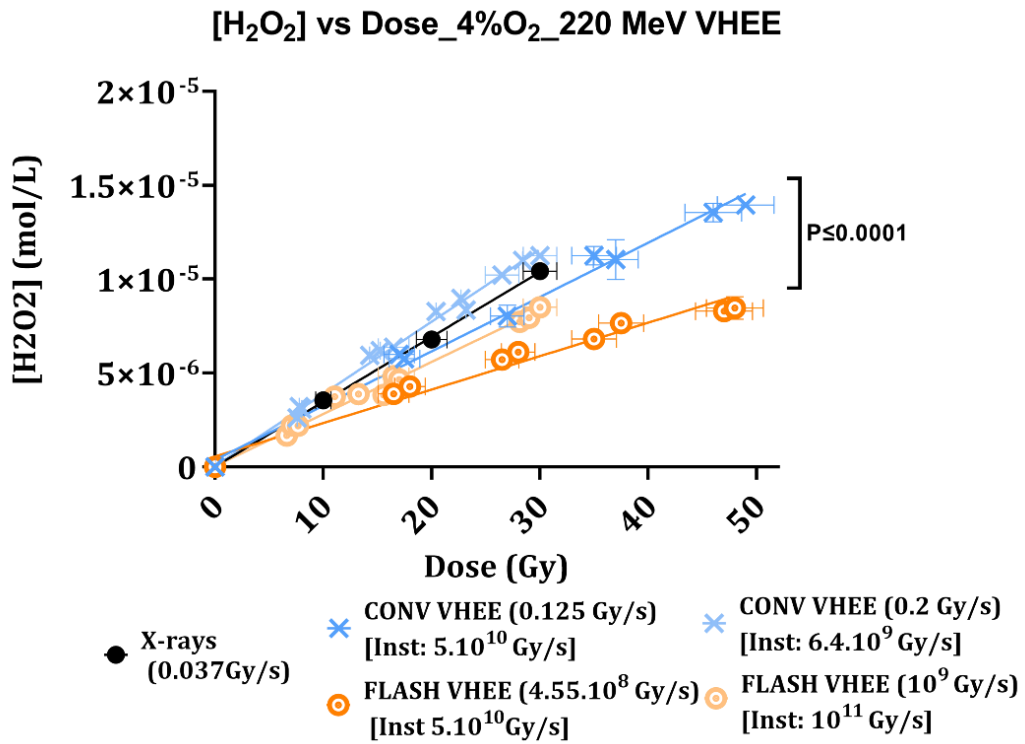


Supplementary Figure 1 a) G-value of hydrogen peroxide yields as a function of the scavenging capacity of a scavenger (NO₂⁻ ions for our experiments) obtained after irradiation with CONV and FLASH VHEE, IEE and CONV X-rays and compared to reported irradiations with CONV ¹³⁷Cs γ-rays; [S] = [NO₂⁻] (G°(H₂O₂) = 0.75 molecules/100eV) and CONV ⁶⁰Co γ-rays; [S] = [CH₃OH] (G°(H₂O₂) = 0.73 molecules/100eV). **b)** G(H₂O₂) production from solutions of various NO₂⁻ concentrations and constant concentrations of NO₃⁻ (25 mM) after exposure to VHEE at CONV and FLASH. **c)** G(H₂O₂) production from solutions of various NO₂⁻ concentrations and constant concentrations of NO₃⁻ (25 mM) after exposure IEE at CONV and FLASH.

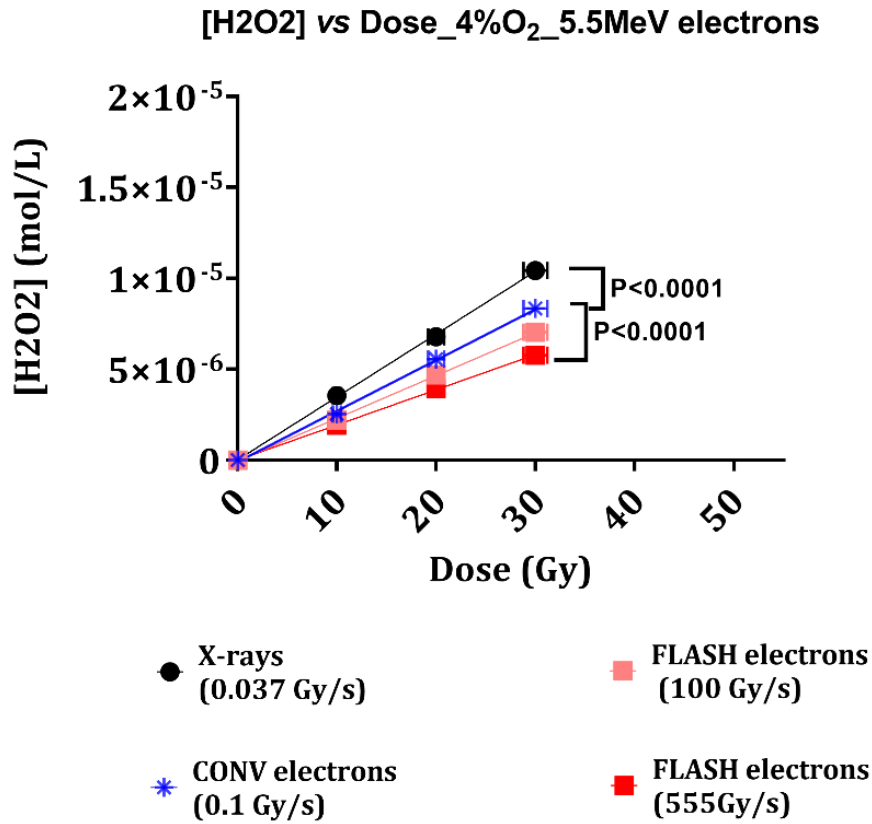
a)



b)



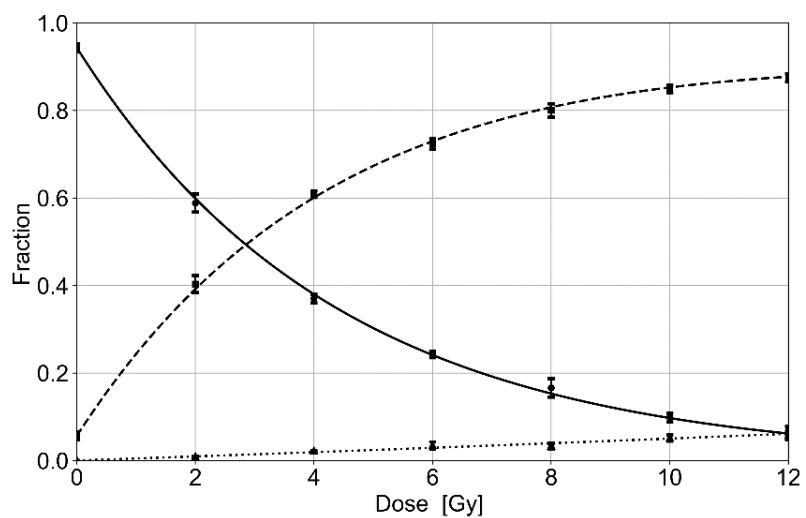
c)



Supplementary Figure 2: a) Comparison of long-term yield of H₂O₂ at room temperature (22°C) and physiological temperature (37-38°C). Dose and dose rate impact on production of H₂O₂ in physiological O₂ conditions (4% O₂) after exposure to b) CONV and FLASH VHEE, c) CONV and FLASH IEE. CONV X-rays plot was added to both figures for comparison. Long-term G-value was calculated from the slopes of H₂O₂ concentration vs the delivered dose and were assessed by t-test. Significance was accorded as follow: CONV VHEE vs UHDR VHEE: P < 0.0001; CONV X-rays vs IEE (CONV & FLASH): P < 0.0001; CONV IEE vs FLASH IEE: P < 0.001. Uncertainties on the delivered dose for IEE and VHEE irradiations were 2% and 5% respectively from the prescribed dose. Results are from duplicate experiments for X-rays irradiations and triplicate experiments for electrons (IEE and VHEE) irradiations at both dose rates.

a)

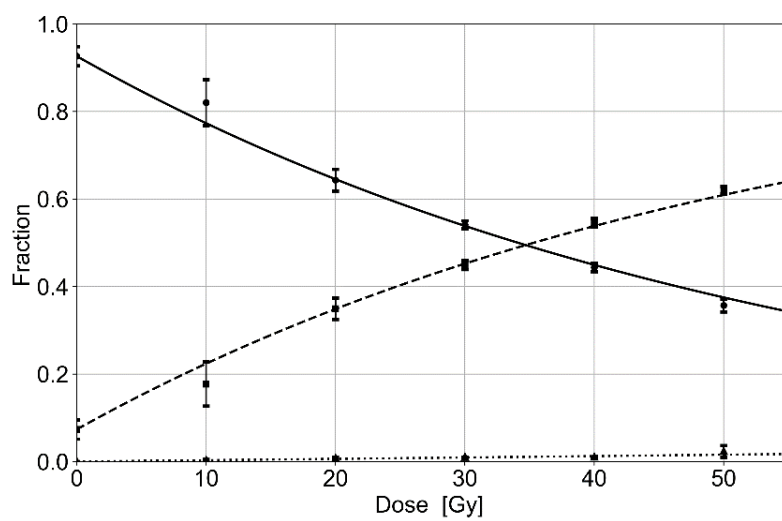
21% O₂ – X-rays
CONV • (0.07 Gy/s)



21% O₂, DMSO 14 mM – X-rays

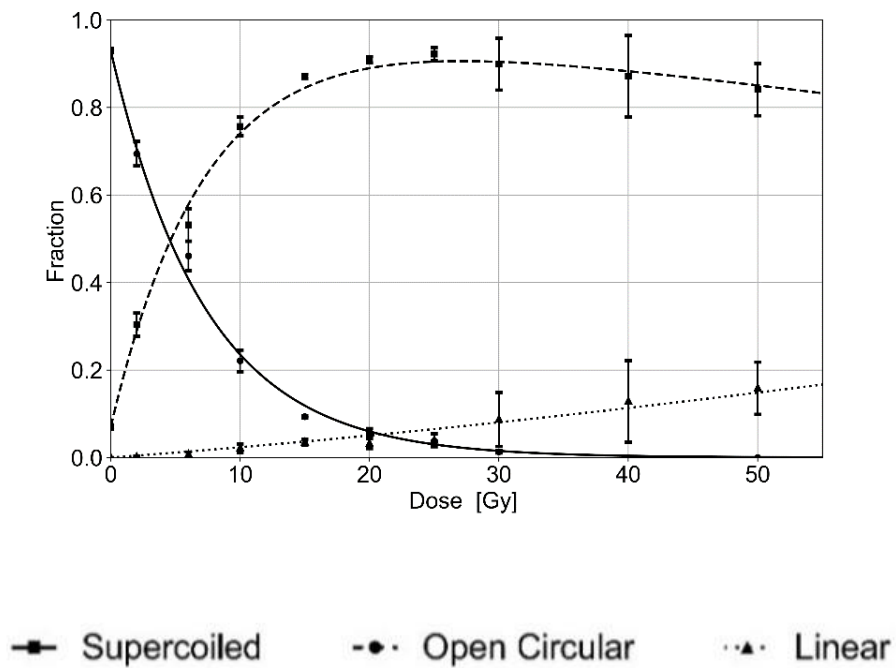
CONV • (0.07 Gy/s)

b)



c)

1% O₂ – X-rays
CONV • (0.07 Gy/s)

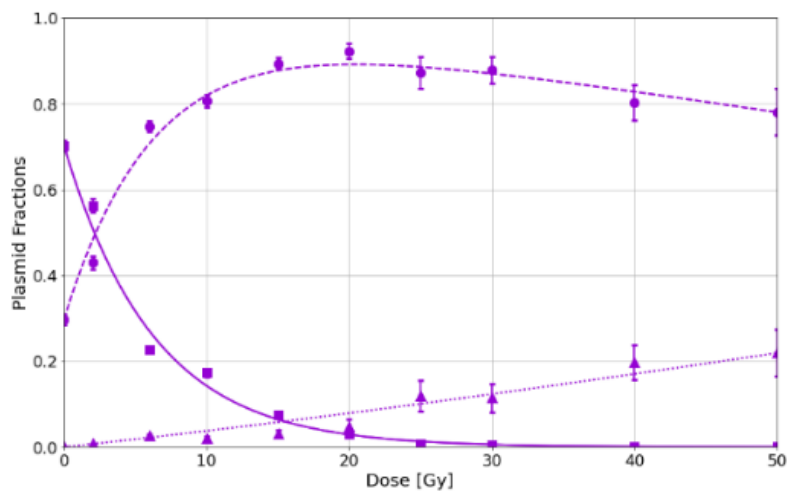


Supplementary Figure 3: Fraction of DNA damage development forms in plasmids after doses delivered with 0 Gy to 10 Gy with conventional 160 keV X-rays (0.07 Gy/s) **a)** at atmospheric oxygen conditions 21% O₂ **b)** in presence of 14 mM DMSO **c)** at hypoxic oxygen conditions 1% O₂.

a)

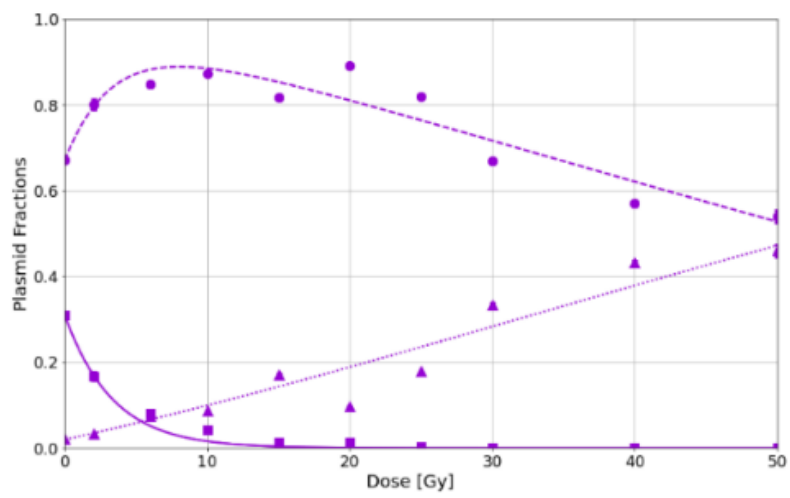
1% O₂ – 1.5 μM Fe(II) – X-rays

CONV ● (0.07 Gy/s)



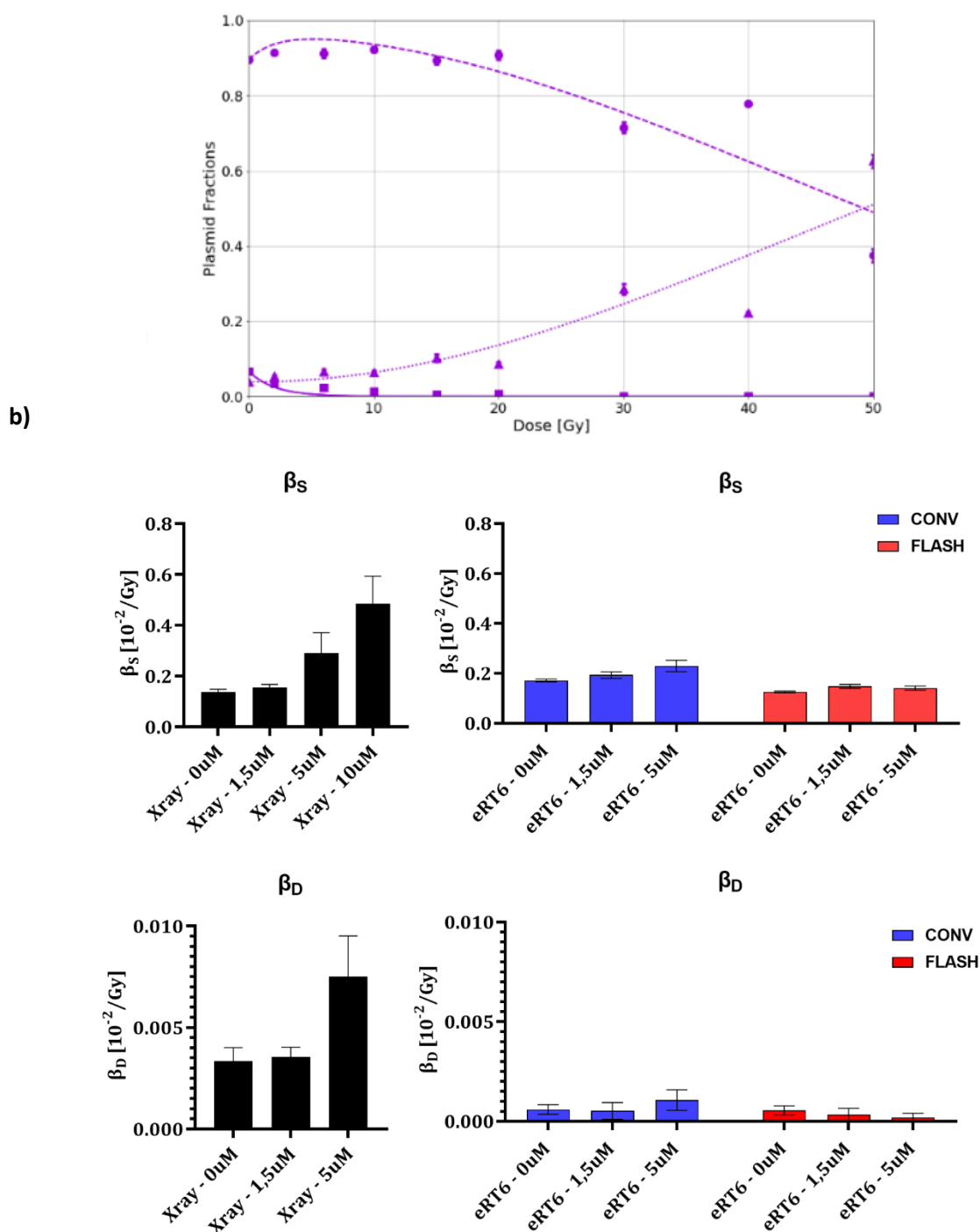
1% O₂ – 5 μM Fe(II) – X-rays

CONV ● (0.07 Gy/s)



1% O₂ – 10 μM Fe(II) – X-rays

CONV • (0.07 Gy/s)



Supplementary Figure 4: a) Fraction of DNA damage development forms in plasmids in hypoxic conditions (1% O₂) and incubated for different Fe²⁺ concentrations (1.5 μM, 5 μM and 10 μM) obtained after exposure to 160 kVp CONV X-rays (0.07 Gy/s) from 0 Gy to 50 Gy b) β_s and β_D (SSB and DSB yields) from 160 kVp CONV X-rays (0.07 Gy/s) and 5.5 MeV IIE (CONV 0.1 Gy/s and FLASH dose rates 555 Gy/s) with various concentrations of Fe²⁺.

Supp Table 1: Beam parameters employed for irradiations at FLASH and CONV irradiation with VHEE

a) Water radiolysis and plasmid irradiations: Similar instantaneous dose rates per bunch.

Modality	CONV VHEE					FLASH VHEE				
Aimed Dose [Gy]	10	20	30	40	50	10	20	30	40	50
Aimed Current [pC]	10000	20000	30000	40000	50000	10000	20000	30000	40000	50000
Nominal energy [MeV]	190-210									
Frequency [Hz]	0.833	0.833	0.833	0.833	0.833	0.833	0.833	0.833	0.833	0.833
Charge per train [C]	150	150	150	150	150	10000	20000	30000	40000	50000
Charge per bunch [pC]	150	150	150	150	150	160	160	160	160	160
Bunch width [ps]	3	3	3	3	3	3	3	3	3	3
Number of trains	67	133	200	267	333	1	1	1	1	1
Repetition periods of Trains [s]	1.2	1.2	1.2	1.2	1.2	-	-	-	-	-
Bunch per Trains	1	1	1	1	1	63	125	188	250	313
Repetition period of bunches [ns]	-	-	-	-	-	0.333	0.333	0.333	0.333	0.333
Train duration [ns]	0.003	0.003	0.003	0.003	0.003	20.646	41.625	62.604	83.25	104.22
Total duration of irradiation [s]	79.2	158.4	238.8	319.2	398.4	2.06×10^{-8}	4.16×10^{-8}	6.26×10^{-8}	8.33×10^{-8}	1.04×10^{-8}
Mean dose-rate [Gy/s]	0.125	0.125	0.125	0.125	0.125	4.84×10^8	4.80×10^8	4.79×10^8	4.80×10^8	4.80×10^8
Instantaneous dose-rate (per train) [Gy/s]	5×10^{10}	5×10^{10}	5×10^{10}	5×10^{10}	5×10^{10}	5.33×10^8	5.33×10^8	5.33×10^8	5.33×10^8	5.33×10^8
Instantaneous dose rate (per bunch) [Gy/s]	5×10^{10}	5×10^{10}	5×10^{10}	5×10^{10}	5×10^{10}	5.33×10^{10}	5.33×10^{10}	5.33×10^{10}	5.33×10^{10}	5.33×10^{10}
Dose per Train [Gy]	0.15	0.15	0.15	0.15	0.15	10	20	30	40	50
Dose per Bunch [Gy]	0.15	0.15	0.15	0.15	0.15	0.16	0.16	0.16	0.16	0.16

b) Water radiolysis: Different instantaneous dose rates per bunch.

Modality	CONV VHEE					FLASH VHEE				
Aimed Dose [Gy]	10	20	30	40	50	10	20	30	40	50
Aimed Current [pC]	10000	20000	30000	40000	50000	10000	20000	30000	40000	50000
Nominal energy [MeV]	190-210									
Frequency [Hz]	10	10	10	10	10	0.833	0.833	0.833	0.833	0.833
Charge per train [C]	20	20	20	20	20	10000	20000	30000	40000	50000
Charge per bunch [pC]	20	20	20	20	20	370	370	370	370	370
Bunch width [ps]	3	3	3	3	3	3	3	3	3	3
Number of trains	500	1000	1500	2000	2500	1	1	1	1	1
Repetition periods of Trains [s]	0.1	0.1	0.1	0.1	0.1	-	-	-	-	-
Bunch per Trains	1	1	1	1	1	27	54	81	108	135
Repetition period of bunches [ns]	-	-	-	-	-	0.333	0.333	0.333	0.333	0.333
Train duration [ns]	0.333	0.333	0.333	0.333	0.333	9	18	27	36	45
Total duration of irradiation [s]	60.02	120.04	180.07	240.09	300.12	9×10^{-9}	1.80×10^{-8}	2.70×10^{-8}	3.60×10^{-8}	4.5×10^{-8}
Mean dose-rate [Gy/s]	0.17	0.17	0.17	0.17	0.17	1.11×10^9	1.11×10^9	1.11×10^9	1.11×10^9	1.11×10^9
Instantaneous dose-rate (per train) [Gy/s]	6.67×10^9	6.67×10^9	6.67×10^9	6.67×10^9	6.67×10^9	1.11×10^9	1.11×10^9	1.11×10^9	1.11×10^9	1.11×10^9
Instantaneous dose rate (per bunch) [Gy/s]	6.67×10^9	6.67×10^9	6.67×10^9	6.67×10^9	6.67×10^9	1.23×10^{11}	1.23×10^{11}	1.23×10^{11}	1.23×10^{11}	1.23×10^{11}
Dose per Train [Gy]	0.02	0.02	0.02	0.02	0.02	10	20	30	40	50
Dose per Bunch [Gy]	0.02	0.02	0.02	0.02	0.02	0.37	0.37	0.37	0.37	0.37

c) ZFE irradiations: Similar instantaneous dose rates per bunch

Modality	CONV		FLASH	
Aimed Dose [Gy]	8	10	8	10
Aimed Current [pC]	8000	10000	8000	10000
Nominal energy [MeV]	190-210			
Frequency [Hz]	0.833	0.833	0.833	0.833
Charge per train [C]	150	150	8000	10000
Charge per bunch [pC]	150	150	150	150
Bunch width [ps]	3	3	3	3
Number of trains	53	67	1	1
Repetition periods of Trains [s]	1.2	1.2	-	-
Bunch per Trains	1	1	53	67
Repetition period of bunches [ns]	0.333	0.333	0.333	0.333
Train duration [ns]	0.003	0.003	17.32	21.98
Total duration of irradiation [s]	62.4	79.2	1.73×10^{-8}	2.20×10^{-8}
Mean dose-rate [Gy/s]	0.128	0.126	4.62×10^8	4.55×10^8
Instantaneous dose-rate (per train) [Gy/s]	5.00×10^{10}	5.00×10^{10}	4.62×10^8	4.55×10^8
Instantaneous dose rate (per bunch) [Gy/s]	5.00×10^{10}	5.00×10^{10}	5.00×10^{10}	5.00×10^{10}
Dose per Train [Gy]	0.15	0.15	8	10
Dose per Bunch [Gy]	0.15	0.15	0.15	0.15

d) ZFE irradiations: Different instantaneous dose rates per bunch

Modality	CONV		FLASH	
Aimed Dose [Gy]	8	10	8	10
Aimed Current [pC]	8000	10000	8000	10000
Nominal energy [MeV]	190-210			
Frequency [Hz]	10	10	0.833	0.833
Charge per train [C]	20	20	8000	10000
Charge per bunch [pC]	20	20	327	336
Bunch width [ps]	3	3	3	3
Number of trains	400	500	1	1
Repetition periods of Trains [s]	0.1	0.1	-	-
Bunch per Trains	1	1	24	30
Repetition period of bunches [ns]	0.333	0.333	0.333	0.333
Train duration [ns]	0.003	0.003	7.66	9.66
Total duration of irradiation [s]	40.00	50.00	7.66×10^{-9}	9.66×10^{-9}
Mean dose-rate [Gy/s]	0.200	0.200	1.04×10^9	1.04×10^9
Instantaneous dose-rate (per train) [Gy/s]	6.67×10^9	6.67×10^9	1.04×10^8	1.04×10^9
Instantaneous dose rate (per bunch) [Gy/s]	6.67×10^9	6.67×10^9	1.09×10^{11}	1.12×10^{11}
Dose per Train [Gy]	0.02	0.02	8	10
Dose per bunch [Gy]	0.02	0.02	0.33	0.34

Supplementary Table 2: Beam parameters employed for irradiations at FLASH and CONV irradiation with IEE: a) Water radiolysis, plasmid irradiations and zebrafish embryos irradiations.

Modality	CONV IEE									
Aimed Dose [Gy]	2	4	6	8	10	20	25	30	40	50
Nominal energy [MeV]	5.5									
Grid tension [V]	100									
Number of pulses	120	235	350	465	585	1170	1460	1755	2340	2925
Pulse width [μ s]	1									
Frequency [Hz]	10									
Dose per pulse [Gy]	0.02									
Treatment time [s]	11.9	23.4	34.9	46.4	58.4	116.9	145.9	175.4	233.9	292.4
Mean dose-rate [Gy/s]	0.17									
Instantaneous dose-rate [Gy/s]	1.00×10^4									

Modality	FLASH IEE									
Aimed Dose [Gy]	2	4	6	8	10	20	25	30	40	50
Nominal energy [MeV]	5.5									
Grid tension [V]	300									
Number of pulses	1	1	1	1	1	4	5	6	8	10
Pulse width [μ s]	1.8									
Frequency [Hz]	100									
Dose per pulse [Gy]	2	4	6	8	10	5	5	5	5	5
Treatment time [s]	1.80×10^{-6}	1.80×10^{-6}	1.80×10^{-6}	1.80×10^{-6}	1.80×10^{-6}	0.03	0.04	0.05	0.07	0.09
Mean dose-rate [Gy/s]	1.11×10^6	2.22×10^6	3.33×10^6	4.44×10^6	5.56×10^6	667	625	600	571	556
Instantaneous dose-rate [Gy/s]	1.11×10^6	2.22×10^6	3.33×10^6	4.44×10^6	5.56×10^6	2.78×10^6				

b) Dose rate escalation in zebrafish embryos

Average dose rate (Gy/s)	0.1	10	33	60	100	1400	5.6x10⁶
Delivered dose [Gy]	10						
Nominal energy [MeV]	5.5						
Grid tension [V]	100	147	300				
Number of pulses	700	100	30	17	10	2	1
Pulse width [μs]	1	1.8	1.8	1.8	1.8	1.8	1.8
Frequency [Hz]	10	100	100	100	100	140	100
Dose per pulse [Gy]	0.014	0.100	0.333	0.588	1.000	5.000	10.000
Treatment time [s]	6.99x10 ¹	9.90x10 ⁻¹	2.90x10 ⁻¹	1.60x10 ⁻¹	9.00x10 ⁻²	7.14x10 ⁻³	1.80x10 ⁻⁶
Instantaneous dose-rate [Gy/s]	1.43x10 ⁴	5.56 x10 ⁴	1.85 x10 ⁵	3.27 x10 ⁵	5.56 x10 ⁵	2.78 x10 ⁶	5.56 x10 ⁶

c) Pulse width variation

	FLASH (Single pulse)			FLASH (2x5 Gy)			FLASH (5x2 Gy)		CONV
Pulse width [μs]	1.8	3	4	1.8	3	4	1.8	4	1
Delivered dose [Gy]	10								
Nominal energy [MeV]	5.5								
Grid tension [V]	300								100
Number of pulses	1	1	1	2	2	2	5	5	700
Frequency [Hz]	100								
Dose per pulse [Gy]	10	10	10	5	5	5	2	2	0.01
Treatment time [s]	1.80x10 ⁻⁶	3.00x10 ⁻⁶	4.00x10 ⁻⁶	0.01	0.01	0.01	0.04	0.04	70
Average dose rate (Gy/s)	5.56x10 ⁶	3.33x10 ⁶	2.50x10 ⁶	1000	1000	1000	250	250	0.143
Instantaneous dose-rate [Gy/s]	5.56x10 ⁶	3.33x10 ⁶	2.50x10 ⁶	2.78x10 ⁶	1.67x10 ⁶	1.25x10 ⁶	1.11x10 ⁶	5.00x10 ⁵	1.00x10 ⁴

d) Frequency variation

	FLASH (Single pulse)	FLASH (2x5 Gy)					FLASH (5x2 Gy)				CONV
Frequency [Hz]	100	100	5	0.1	0.016667	0.001667	100	20	5	0.016667	10
Delivered dose [Gy]	10										
Nominal energy [MeV]	5.5										
Grid tension [V]	300										100
Number of pulses	1	2	2	2	2	2	5	5	5	5	700
Pulse width [μs]	1.8	1.8	1.8	1.8	1.8	1.8	1.8	1.8	1.8	1.8	1
Dose per pulse [Gy]	10	5	5	5	5	5	2	2	2	2	0.01
Treatment time [s]	1.80×10^{-6}	0.01	0.2	1.00	6.00	60	0.04	0.2	0.8	240	70
Average dose rate [Gy/s]	5.56×10^6	1000	50	1.00	0.167	0.0167	250	50	12.5	0.04	0.143
Instantaneous dose-rate [Gy/s]	5.56×10^6	2.78×10^6					1.11×10^6				1.00×10^4

Supplementary Table 3: Beam parameters employed for conventional X-rays irradiations a) Water radiolysis using 225 kVp XRAD (0.037 Gy/s) b) Plasmid irradiations using 160 kVp RS2000 (0.07 Gy/s) and c) ZFE irradiations with 225 kVp XRAD (0.037 Gy/s).

a)

Mode	CONV X-rays		
Dose rate [Gy/s]	0.037		
Prescribed dose [Gy]	10	20	30
Treatment time [s]	264	529	793
[kV]	225		
[mA]	13		
Filter	Cu 0.3mm		

b)

Mode	CONV X-rays								
Dose rate [Gy/s]	0.07								
Prescribed dose [Gy]	2	4	6	8	10	20	30	40	50
Treatment time [s]	28	56	84	112	140	279	419	558	698
[kV]	160								

c)

Mode	CONV X-rays				
Dose rate [Gy/s]	0.037				
Prescribed dose [Gy]	6	7	8	10	12
Treatment time [s]	162	189	216	264	318
[kV]	225				
[mA]	13				
Filter	Cu 0.3mm				

Supplementary Table 4: a) Summary table of primary G°-values from reported experiments.

Reference	Source	Energy [MeV]	LET [keV/μm]	Dose rate [Gy/s]	[O ₂] [M]	Measurement method	G(H ₂ O ₂) [molecules/100eV]
Blain et al. 2022	CONV protons	68	N-A	0.2	2.50x10 ⁻⁴	Ghormley method	0.95
	UHDR protons			40-6000			0.58
Roth et al. 2011	⁶⁰ Co γ-rays	1.25	0.36	0.96	2.50x10 ⁻⁴		1
	Protons	5	20.7	N.A			1.2
Sehested et al. 1968	pulsed electrons	10	N.A	5x10 ⁻⁶	1.20x10 ⁻³		1.98
Anderson et al. 1962	pulsed electrons	15	N.A	3.2 x10 ⁻⁷	1.00x10 ⁻³		1.98 ± 0.06
	⁶⁰ Co γ-rays	1.25	0.36	1		1.24 ± 0.06	

b) Summary table of long-term G-values from reported experiments.

Reference	Source	Energy [MeV]	LET [keV/μm]	Dose rate [Gy/s]	Chemical system	[O ₂] [M]	G(H ₂ O ₂) [molecules/100eV]
Wasselin et al. 2002	¹³⁷ Cs γ-rays	0.6	0.53	0.019	[NO ₂]/[NO ₃ ⁻]	Anoxia (Argon bubbling)	0.75
	Protons	30	2.5	N.A	[NO ₂]/[NO ₃ ⁻]		0.65
		30	2.5	N.A	[CH ₃ OH]/[NO ₃ ⁻]		0.73
Stefanic et al. 2002	⁶⁰ Co γ-rays	1.2	0.2	0.18-0.63 & 3.17	[CH ₃ OH]/[NO ₃ ⁻]		0.73
		1.2	0.2	0.18 & 3.17	[Br ⁻]/[NO ₃ ⁻]		0.7
Pastina et al. 1999	⁶⁰ Co γ-rays	1.25	0.36	0.26	[CH ₃ OH]/[NO ₃ ⁻]		0.7
Anderson et al. 1962	Pulsed electrons	15	N.A	3.2 x10 ⁻⁷	N.A	0.76	

Supplementary Table 5: Long term G-values obtained with 5.5 MeV electrons irradiations at eRT6 after exposure to CONV (0.1 Gy/s) and FLASH (≥ 555 Gy/s) dose rates a) at different oxygen levels (1% to 21% O₂) b) in presence or not of 25 mM [NO₃⁻] c) at room temperature (22°C) and physiological temperature (37-38°C). The long-term yields calculated from the slope of [H₂O₂] vs the delivered dose. Standard errors on the slopes are given in the tables. Δ FLASH/CONV represents the reduction percentage in G-value from CONV dose rate to FLASH dose rate. Experiments are done in triplicate. For each experiment there were eight measurements points per dose.

a)

O ₂ %		G(H ₂ O ₂) [molecules/100eV]		Δ FLASH/CONV
Theoretical	Measured	CONV electrons (0.1 Gy/s)	FLASH electrons (≥ 555 Gy/s)	
1	0.75	2.42 ± 0.03	1.81 ± 0.02	25
2	2.4	2.72 ± 0.04	2.03 ± 0.03	26
4	4.4	2.81 ± 0.03	1.86 ± 0.05	34
7	7.2	2.90 ± 0.03	2.19 ± 0.03	24
10	10.04	2.73 ± 0.05	1.96 ± 0.05	28
15	15.2	2.35 ± 0.04	1.87 ± 0.05	21
21	21	1.9 ± 0.04	1.3 ± 0.04	31

b)

Experimental condition	G(H ₂ O ₂) [molecules/100eV]	Δ FLASH/CONV
CONV electrons_21% O ₂	1.9 ± 0.04	31%
FLASH electrons_21% O ₂	1.3 ± 0.04	
CONV electrons_21% O ₂ _25 mM [NO ₃ ⁻]	0.92 ± 0.01	-21%
FLASH electrons_21% O ₂ _25 mM [NO ₃ ⁻]	1.11 ± 0.02	

c)

Experimental condition	G(H ₂ O ₂) (molecules/100eV)	ΔFLASH/CONV
CONV electrons_21% O ₂ _22°C	1.9 ± 0.04	31%
FLASH electrons_21% O ₂ _22°C	1.3 ± 0.04	
CONV electrons_21% O ₂ _37°C	3.33 ± 0.04	36%
FLASH electrons_21% O ₂ _37°C	2.12 ± 0.02	

Acknowledgments

The authors thank Prs J. Bourhis, F. Bochud for their support and Drs C. Bailat and V Grilj for the optimization of the dosimetry and support in irradiation procedure at CHUV. We also thank the PTZ (CHUV/UNIL) for zebrafish work.

References

1. physics-world-reveals-its-top-10-breakthroughs-of-the-year-for-2022.
2. Limoli, C. L. & Vozenin, M.-C. Reinventing Radiobiology in the Light of FLASH Radiotherapy. *Annu. Rev. Cancer Biol.* **7**, 1–21 (2023).
3. Leavitt, R. J. *et al.* Hypoxic Tumors Are Sensitive to FLASH Radiotherapy. <http://biorxiv.org/lookup/doi/10.1101/2022.11.27.518083> (2022) doi:10.1101/2022.11.27.518083.
4. Almeida, A. *et al.* Antitumor Effect by Either FLASH or Conventional Dose Rate Irradiation Involves Equivalent Immune Responses. *International Journal of Radiation Oncology*Biological*Physics* S0360301623080355 (2023) doi: 10.1016/j.ijrobp.2023.10.031.
5. FLASH new intersection of physics, chemistry, biology, and 1 cancer medicine.pdf.
6. Favaudon, V. *et al.* Ultrahigh dose-rate FLASH irradiation increases the differential response between normal and tumor tissue in mice. *Sci. Transl. Med.* **6**, (2014).
7. Montay-Gruel, P. *et al.* Irradiation in a flash: Unique sparing of memory in mice after whole brain irradiation with dose rates above 100 Gy/s. *Radiotherapy and Oncology* **124**, 365–369 (2017).
8. Schüller, A. *et al.* The European Joint Research Project UHDpulse – Metrology for advanced radiotherapy using particle beams with ultra-high pulse dose rates. *Physica Medica* **80**, 134–150 (2020).
9. Montay-Gruel, P. *et al.* X-rays can trigger the FLASH effect: Ultra-high dose-rate synchrotron light source prevents normal brain injury after whole brain irradiation in mice. *Radiotherapy and Oncology* **129**, 582–588 (2018).
10. Gao, F. *et al.* First demonstration of the FLASH effect with ultrahigh dose rate high-energy X-rays. *Radiotherapy and Oncology* **166**, 44–50 (2022).
11. Shi, X. *et al.* FLASH X-ray spares intestinal crypts from pyroptosis initiated by cGAS-STING activation upon radioimmunotherapy. *Proc. Natl. Acad. Sci. U.S.A.* **119**, e2208506119 (2022).
12. Kim, M. M. *et al.* Design and commissioning of an image-guided small animal radiation platform and quality assurance protocol for integrated proton and x-ray radiobiology research. *Phys. Med. Biol.* **64**, 135013 (2019).
13. Diffenderfer, E. S. *et al.* Design, Implementation, and in Vivo Validation of a Novel Proton FLASH Radiation Therapy System. *International Journal of Radiation Oncology*Biological*Physics* **106**, 440–448 (2020).
14. Cunningham, S. *et al.* FLASH Proton Pencil Beam Scanning Irradiation Minimizes Radiation-Induced Leg Contracture and Skin Toxicity in Mice. *Cancers* **13**, 1012 (2021).
15. Singers Sørensen, B. *et al.* In vivo validation and tissue sparing factor for acute damage of pencil beam scanning proton FLASH. *Radiotherapy and Oncology* **167**, 109–115 (2022).

16. Smyth, L. M. L. *et al.* Comparative toxicity of synchrotron and conventional radiation therapy based on total and partial body irradiation in a murine model. *Sci Rep* **8**, 12044 (2018).
17. Beyreuther, E. *et al.* Feasibility of proton FLASH effect tested by zebrafish embryo irradiation. *Radiotherapy and Oncology* **139**, 46–50 (2019).
18. Venkatesulu, B. P. *et al.* Ultra-high dose rate (35 Gy/sec) radiation does not spare the normal tissue in cardiac and splenic models of lymphopenia and gastrointestinal syndrome. *Sci Rep* **9**, 17180 (2019).
19. Jorge, P. G. *et al.* Design and validation of a dosimetric comparison scheme tailored for ultra-high dose-rate electron beams to support multicenter FLASH preclinical studies. *Radiotherapy and Oncology* **175**, 203–209 (2022).
20. Almeida, A. *et al.* *Dosimetric and Biologic Intercomparison between Electron and Proton FLASH Beams*. <http://biorxiv.org/lookup/doi/10.1101/2023.04.20.537497> (2023) doi:10.1101/2023.04.20.537497.
21. Wasselin-Trupin, V., Baldacchino, G., Bouffard, S. & Hickel, B. Hydrogen peroxide yields in water radiolysis by high-energy ion beams at constant LET. *Radiation Physics and Chemistry* **65**, 53–61 (2002).
22. McMahon, S. J. & Currell, F. J. A Robust Curve-Fitting Procedure for the Analysis of Plasmid DNA Strand Break Data from Gel Electrophoresis. *Radiation Research* **175**, 797–805 (2011).
23. Horst, F. *et al.* In Regard to Böhlen *et al.* *International Journal of Radiation Oncology*Biolog*Physics* **115**, 1006–1007 (2023).
24. Sworski, T. J. Yields of Hydrogen Peroxide in the Decomposition of Water by Cobalt γ -Radiation. I. Effect of Bromide Ion. *J. Am. Chem. Soc.* **76**, 4687–4692 (1954).
25. Pastina, B. & LaVerne, J. A. Hydrogen Peroxide Production in the Radiolysis of Water with Heavy Ions. *J. Phys. Chem. A* **103**, 1592–1597 (1999).
26. Draganić, D. Studies on the Formation of Primary Yields of Hydrogen Peroxide and Molecular Hydrogen (GH₂O₂ and GH₂) in the Radiolysis of Neutral Aqueous Solutions.
27. Štefanić, I. & LaVerne, J. A. Temperature Dependence of the Hydrogen Peroxide Production in the γ -Radiolysis of Water. *J. Phys. Chem. A* **106**, 447–452 (2002).
28. Hiroki, A., Pimblott, S. M. & LaVerne, J. A. Hydrogen Peroxide Production in the Radiolysis of Water with High Radical Scavenger Concentrations. *J. Phys. Chem. A* **106**, 9352–9358 (2002).
29. Anderson, A. R. & Hart, E. J. RADIATION CHEMISTRY OF WATER WITH PULSED HIGH INTENSITY ELECTRON BEAMS ¹. *J. Phys. Chem.* **66**, 70–75 (1962).
30. Draganic, Z. D. & Draganic, I. G. Formation of primary yields of hydrogen peroxide and molecular hydrogen (GH₂O₂ and GH₂) in the. gamma. radiolysis of neutral aqueous solutions. *J. Phys. Chem.* **75**, 3950–3957 (1971).

31. Roth, O. & LaVerne, J. A. Effect of pH on H₂O₂ Production in the Radiolysis of Water. *J. Phys. Chem. A* **115**, 700–708 (2011).
32. Montay-Gruel, P. *et al.* Long-term neurocognitive benefits of FLASH radiotherapy driven by reduced reactive oxygen species. *Proc. Natl. Acad. Sci. U.S.A.* **116**, 10943–10951 (2019).
33. Kacem, H. *et al.* Comparing radiolytic production of H₂O₂ and development of Zebrafish embryos after ultra high dose rate exposure with electron and transmission proton beams. *Radiotherapy and Oncology* **175**, 197–202 (2022).
34. Blain, G. *et al.* Proton Irradiations at Ultra-High Dose Rate vs. Conventional Dose Rate: Strong Impact on Hydrogen Peroxide Yield. *Radiation Research* **198**, (2022).
35. Sehested, K., Rasmussen, O. L. & Fricke, H. Rate constants of OH with HO₂, O₂⁻, and H₂O₂⁺ from hydrogen peroxide formation in pulse-irradiated oxygenated water. *J. Phys. Chem.* **72**, 626–631 (1968).
36. Milligan, J. R., Arnold, A. D. & Ward, J. F. The Effect of Superhelical Density on the Yield of Single-Strand Breaks in γ -Irradiated Plasmid DNA. *Radiation Research* **132**, 69 (1992).
37. Milligan, J. R., Aguilera, J. A. & Ward, J. F. Variation of Single-Strand Break Yield with Scavenger Concentration for Plasmid DNA Irradiated in Aqueous Solution. *Radiation Research* **133**, 151 (1993).
38. Milligan, J. R. & Ward, J. F. Yield of Single-Strand Breaks Due to Attack on DNA by Scavenger-Derived Radicals. *Radiation Research* **137**, 295 (1994).
39. Small, K. L. *et al.* Evaluating very high energy electron RBE from nanodosimetric pBR322 plasmid DNA damage. *Sci Rep* **11**, 3341 (2021).
40. Perstin, A., Poirier, Y., Sawant, A. & Tambasco, M. Quantifying the DNA-damaging Effects of FLASH Irradiation With Plasmid DNA. *International Journal of Radiation Oncology*Biological*Physics* **113**, 437–447 (2022).
41. Vozenin, M.-C., Bourhis, J. & Durante, M. Towards clinical translation of FLASH radiotherapy. *Nat Rev Clin Oncol* **19**, 791–803 (2022).
42. Fouillade, C. *et al.* FLASH Irradiation Spares Lung Progenitor Cells and Limits the Incidence of Radio-induced Senescence. *Clinical Cancer Research* **26**, 1497–1506 (2020).
43. Levy, K. *et al.* Abdominal FLASH irradiation reduces radiation-induced gastrointestinal toxicity for the treatment of ovarian cancer in mice. *Sci Rep* **10**, 21600 (2020).
44. Cooper, C. R., Jones, D., Jones, G. D. & Petersson, K. FLASH irradiation induces lower levels of DNA damage ex vivo, an effect modulated by oxygen tension, dose, and dose rate. *BJR* **95**, 20211150 (2022).
45. Barghouth, P. G. *et al.* FLASH-RT does not affect chromosome translocations and junction structures beyond that of CONV-RT dose-rates. *Radiotherapy and Oncology* **188**, 109906 (2023).

46. Saade, G. *et al.* Ultrahigh-Dose-Rate Proton Irradiation Elicits Reduced Toxicity in Zebrafish Embryos. *Advances in Radiation Oncology* **8**, 101124 (2023).
47. Karsch, L. *et al.* Beam pulse structure and dose rate as determinants for the flash effect observed in zebrafish embryo. *Radiotherapy and Oncology* **173**, 49–54 (2022).
48. Ruan, J.-L. *et al.* Irradiation at Ultra-High (FLASH) Dose Rates Reduces Acute Normal Tissue Toxicity in the Mouse Gastrointestinal System. *International Journal of Radiation Oncology*Biography*Physics* **111**, 1250–1261 (2021).

Chapter III: Supplementary results

1- Impact of transmission proton irradiations on physico-chemical events, DNA damage and development of zebrafish embryos

We have investigated impact of temporal structure of transmission proton beams at conventional and FLASH dose rates.

Material and Methods

Irradiation:

Gantry 1 (PSI): transmission 235MeV protons were delivered at conventional (0.1 and 1 Gy/s) and UHDR (100Gy/s, 1260 Gy/s and 1400 Gy/s). Chemical samples and ZFE were put in individual PCR tubes (0.2mL) placed in Plexiglas cylindrical holders confined in a horizontal Plexiglas block as shown **Figure 1**.

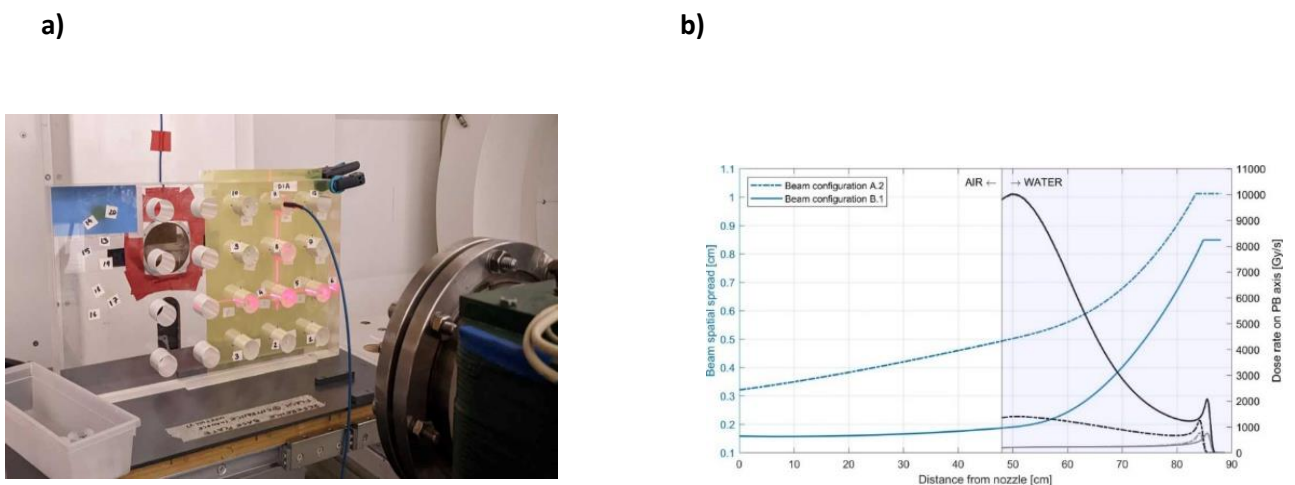


Figure 1: Overview of the proton PSI Gantry 1 proton beam a) Experimental set up b) Dose depth profile of the proton beam.

Water radiolysis

G°(H₂O₂): Primary yields of hydrogen peroxide

To Primary yields of H₂O₂ were determined as a function of HO• scavenger concentration (NaNO₂/NaNO₃) as described in Wasselin et al. (272). Milli-Q water was used with a conductivity of 18.2 μS/cm was equilibrated in hypoxia using a hypoxia hood (Biospherix Xvivo-system X3) and irradiated as indicated in **Table1**. Water samples were probed immediately after irradiation with Amplex Red assay kit (Thermo Fisher). Fluorescence quantification was performed using Promega Glo-Max plate reader (Excitation: 520nm Emission: 580-640nm).

G(H₂O₂): Long term yields of hydrogen peroxide

To get closer from biological samples, water solutions were equilibrated to physiological oxygen conditions using hypoxia hood overnight. Water samples were irradiated as previously and H₂O₂ was measured as previously described.

Plasmid irradiations

DNA damage was investigated using pBR322 plasmid (ThermoFisher inc) was purified and diluted at 400 ng/μl in deionized, RNAase and DNAase free water (UltraPure). Plasmids were irradiated as described earlier. Damages were resolved using AGE (0.8% Agarose in TAE) and the compact supercoiled form as in the two relaxed forms, open circular and linear were quantified using densitometric analysis (UVITEC Cambridge) and ImageJ software “gels” add-on. DNA damage was also investigated in various environments conditions like Oxygen, impact of scavenger as well as impact of acidity (pH).

The MacMahon model was used to describe the plasmid damage kinetics after irradiation (273) and the rates of SSB and DSB were determined to compare the number of damaged plasmids by different irradiation type and in different environments in a more quantitative way.

Zebrafish embryo irradiations

AB Wild Type ZF (Danio rerio, #1175, F7 generation, EZRC) were crossed to produce zebrafish embryos at the PTZ (CHUV/UNIL, Lausanne, Switzerland). According to Swiss and European ethics' regulation no ethical approval is required to use ZFE before 5 days of development. 4h40 post fertilization ZFE were irradiated at 28°C using proton beam line.

Radiation-induced alteration of ZFE morphology and survival were measured at 5 days post-fertilization (dpf) after embryo fixation in a formaldehyde solution (FA 4%) and microscopic imaging (Evos XL Core Cell Imaging System, Thermo Fisher) and analysis using ImageJ Software.

Statistical analysis

Statistical analyses were carried out using GraphPad Prism (v9.1) for water radiolysis, plasmids and ZF embryos experiments. Slopes (G-values) were assessed by t-test. For plasmids, the error bars correspond to standard deviation. For ZFE, data are presented as mean +/- SEM and analysis was done using Kruskal-Wallis test.

Results

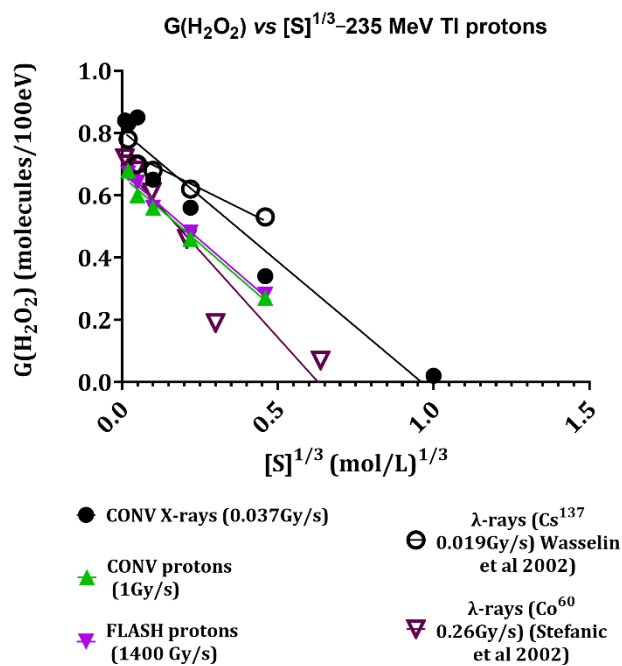
Primary yields of hydrogen peroxide are similar after proton irradiations.

Primary H₂O₂ yields in anoxia were measured as a surrogate of the initial radiation-induced free radical production. For each concentration of HO• scavenger, the G-value found was plotted as a function of the cubic root of HO• scavenger according to the method of Swroski et al. (289) and as a function of scavenging capacity (276). Plots given in **Figure 2a, b and c**. Values are given in **Table 2** and showed to be similar after FLASH and CONV and in the range of previous measurements (0.6-0.8 molecules/100 eV) found in the literature (276,272).

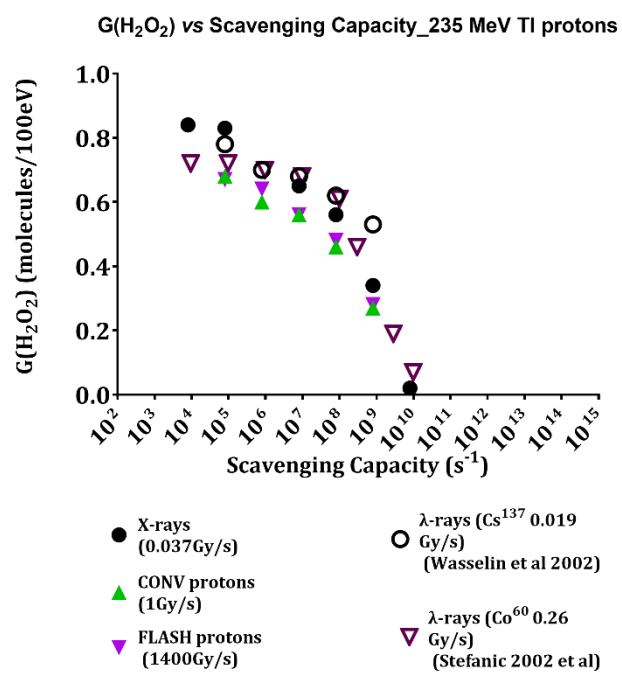
Long-term radiolytic yields are reduced after exposure to FLASH protons.

The long-term yield of H₂O₂ called G(H₂O₂) was calculated several minutes after irradiation under atmospheric oxygen conditions (21% O₂) and physioxic conditions (4% O₂). Slopes were calculated and the yields converted from mol/J to molecules/100eV. Interestingly, more than a 30% decrease in the production of hydrogen peroxide yields was observed after FLASH vs CONV in atmospheric conditions. Whereas production of hydrogen peroxide in physioxic conditions was found to be inserted and was also dose rate dependent as shown **Figure 3a&b** and **Table 3a&b**, suggesting that FLASH reduces the radiolytic production of radicals in atmospheric conditions.

a)



b)



c)

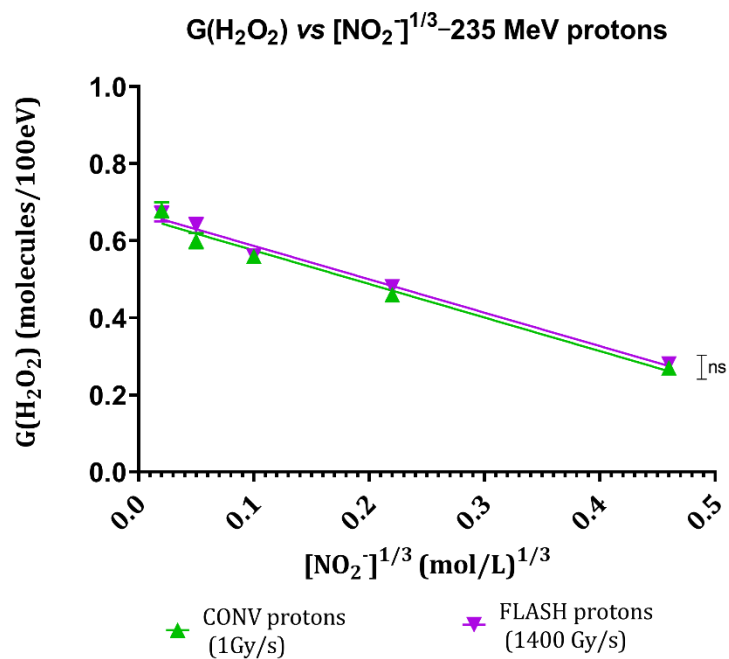
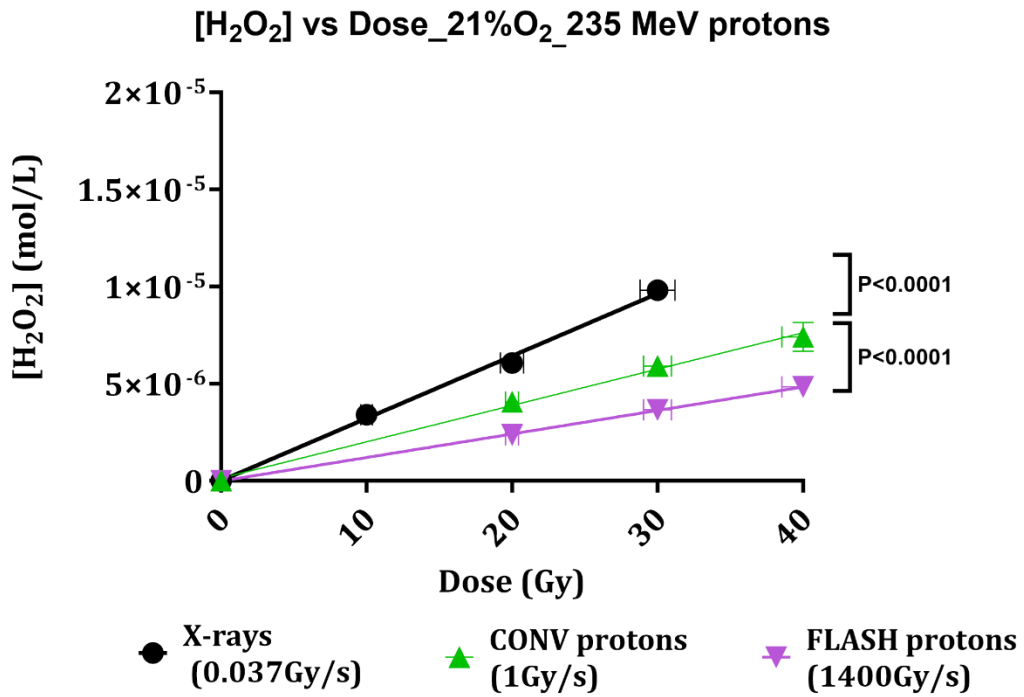


Figure 2 Primary yields production of hydrogen peroxide after exposure to conventional (1 Gy/s) and FLASH protons (1400 Gy/s). a) G-value as a function of cubic root HO scavenger (NO_2^-) b) G-value as a function of scavenging capacity of a scavenger. c) Comparison of CONV and FLASH proton plots of G-values vs cubic root of nitrite ions. Plots of from Conventional X-rays results and from reported data Wasselin et al. and Stefanic et al. were added for comparison (272,278).

a)



b)

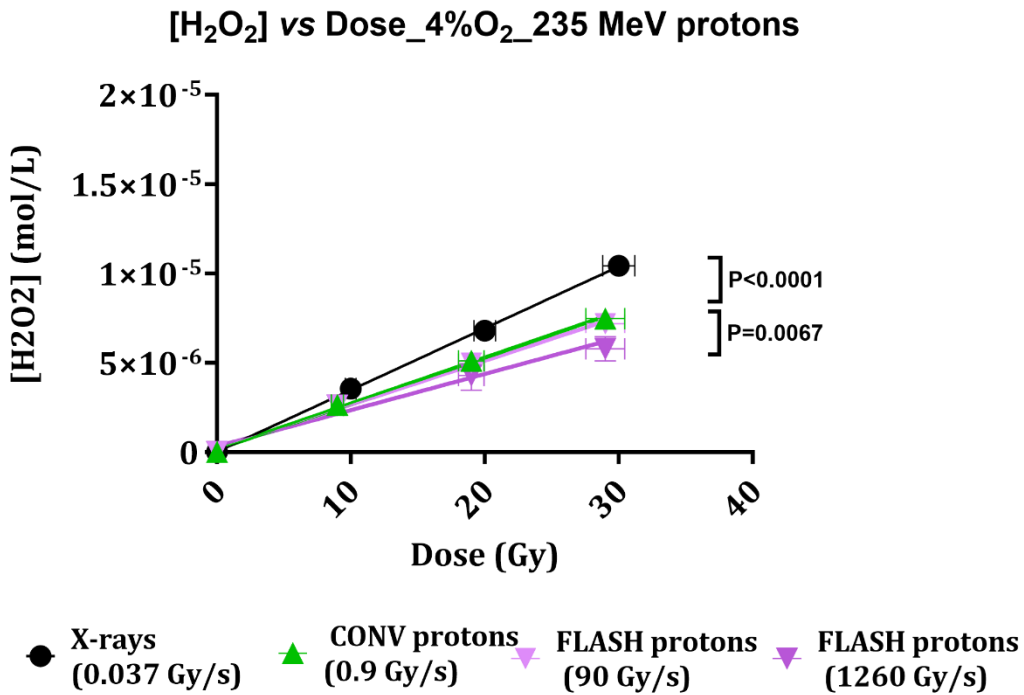


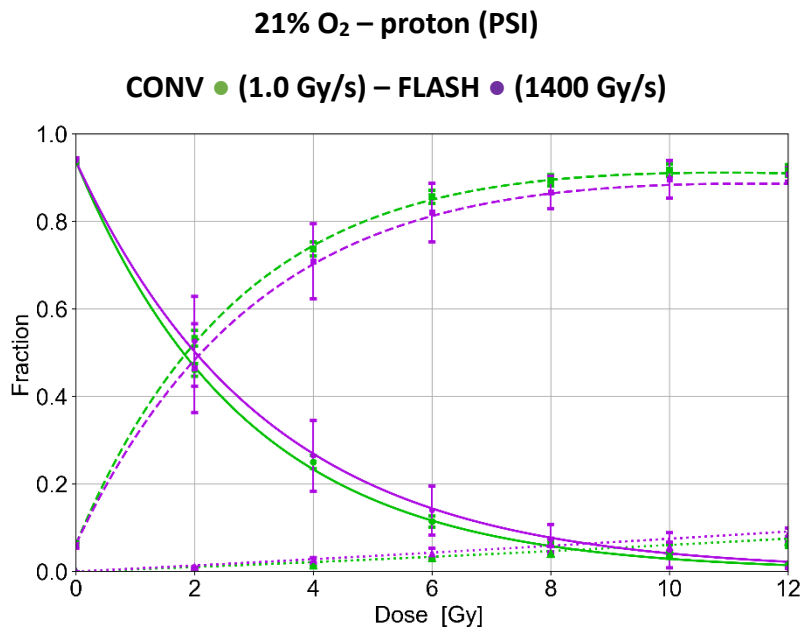
Figure 3: Secondary yields production of hydrogen peroxide after exposure to conventional (1 Gy/s) and FLASH protons (1260-1400 Gy/s). a) G-value as a function of the dose at 21% O₂ b) G-value as a function the dose at 4% O₂.

DNA damage patterns are independent of dose rate.

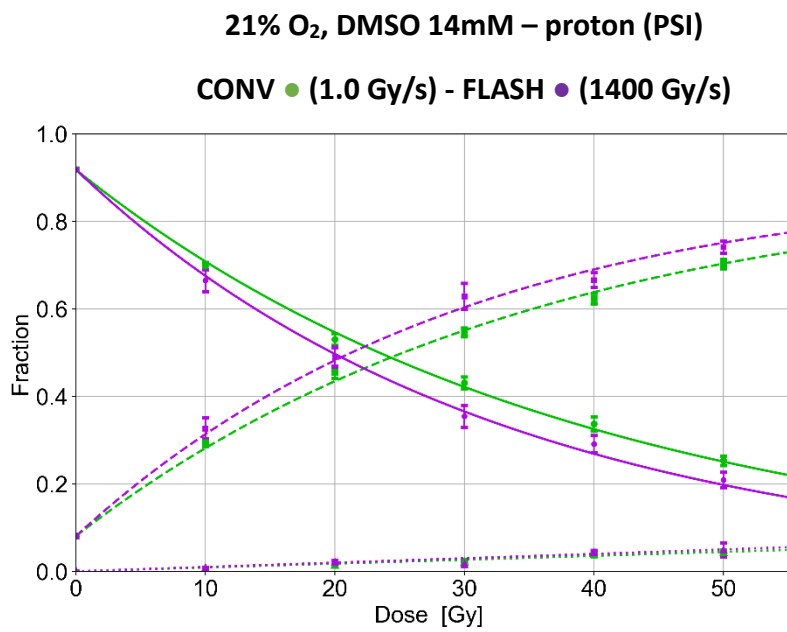
DNA damage was investigated in various conditions. In atmospheric conditions, when the plasmid is in pure water, a dose-dependent induction of single strand breaks (SSB) and double strand breaks (DSB) was found but was dose rate independent (**Figure 4a**).

When 14 mM DMSO was added which is 10 times lower than the antioxidant level found usually in cells, this DMSO concentration was sufficient to protect the plasmid from radiation damages this also occurs in a dose rate independent manner (**Figure 4b**). DNA damage yields can be found in **Table 4**. Next, to mimic the tumor microenvironment, hypoxic and acidic conditions were used (**Figure 5**). SSB were found to be lower above 20 Gy with FLASH vs CONV in hypoxic conditions, whereas acidic conditions seemed to enhance the level of damages in both modalities. In any case, DNA damages were reduced after FLASH irradiation as compared with irradiation at conventional dose rate, suggesting that FLASH should protect both normal tissues and tumors. Therefore, these results are difficult to reconcile with biological results where FLASH has not been shown to protect tumor *in vivo* (34,35).

a)



b)



c)

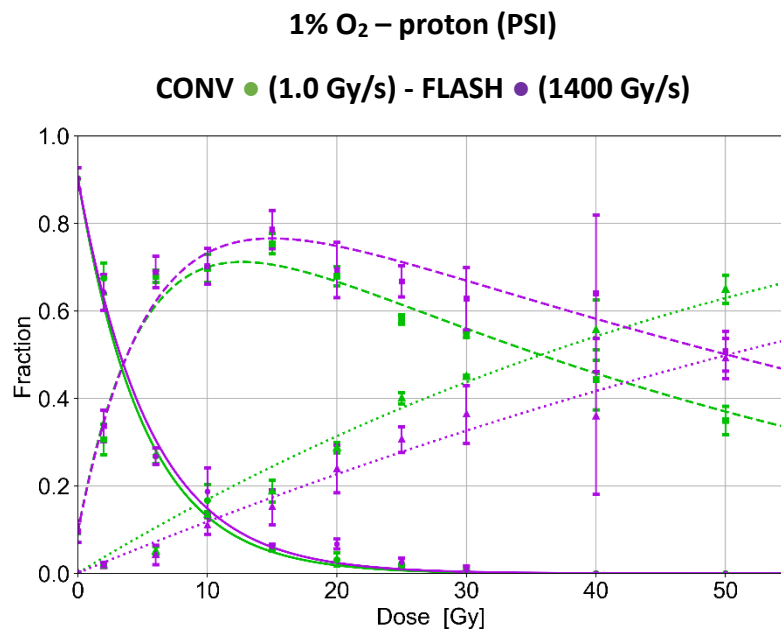
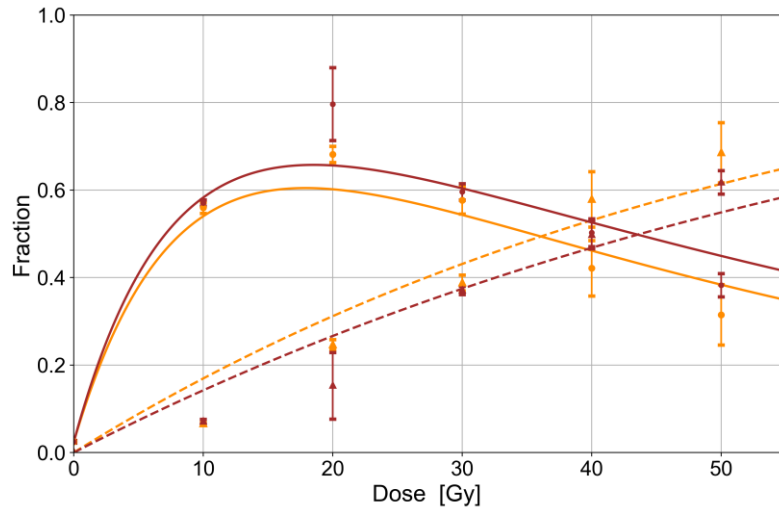


Figure 4: DNA damage pattern after exposure to conventional (1Gy/s) and FLASH protons (1400 Gy/s) in a) atmospheric conditions (21% O₂) b) presence of 14 mM DMSO c) in hypoxic conditions (1% O₂)

a)

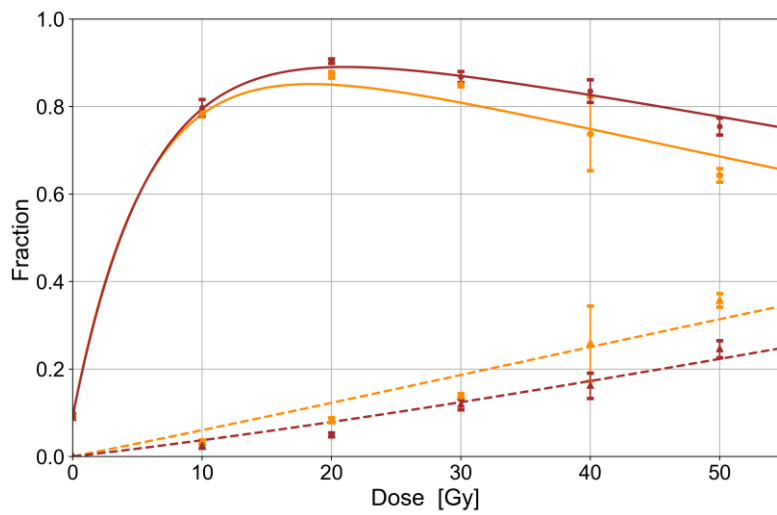
1% O₂ – pH = 4 - proton (PSI)

CONV ● (1.0 Gy/s) - FLASH ● (1400 Gy/s)



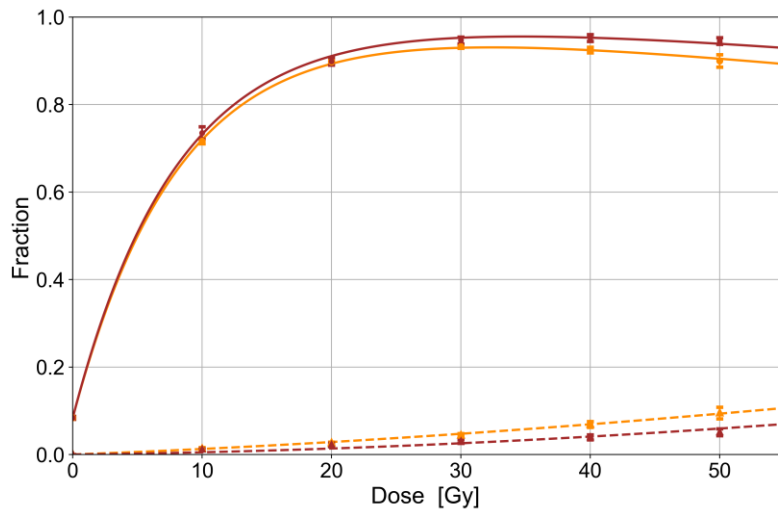
1% O₂ – pH = 5 - proton (PSI)

CONV ● (1.0 Gy/s) - FLASH ● (1400 Gy/s)



1% O₂ – pH = 7.2 - proton (PSI)

CONV ● (1.0 Gy/s) - FLASH ● (1400 Gy/s)



b)

pH-yields after 235 MeV TI protons

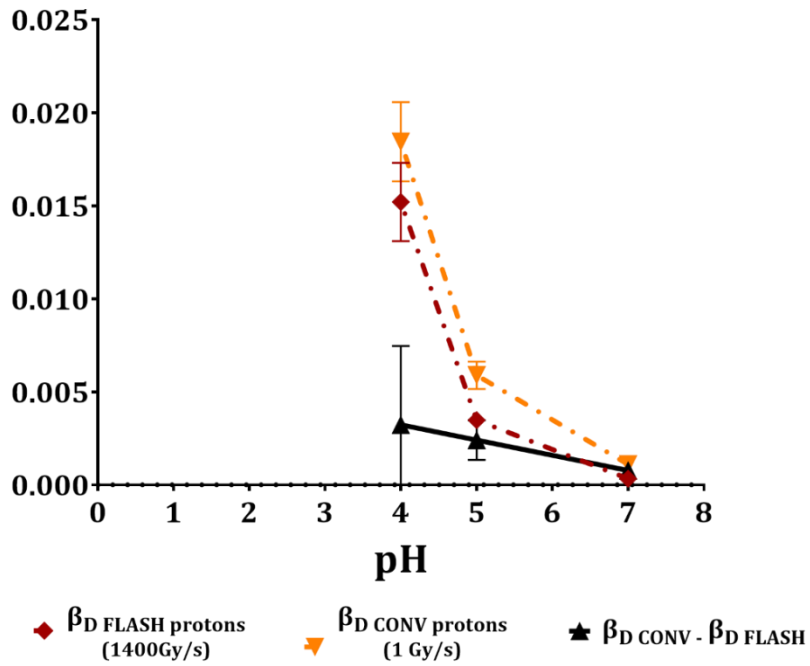


Figure 5: DNA damage in acidic conditions after exposure to conventional (1 Gy/s) and FLASH protons (1400 Gy/s) in a) DNA damage forms in different pH conditions (7.2, 5, and 4) b) Comparison of DNA damage yields in different pH conditions.

ZFE are non-sensitive to proton irradiation.

These results obtained previously PSI have been already published (252) and are included here for a comprehensive analysis related to the impact of the temporal structure on a biological model. Proton beam which is a quasi-continuous beam, average and instantaneous dose rate are also equal. Surprisingly, in that case dose rate between 1 Gy/s to 10^3 Gy/s barely cause any defect in ZFE morphogenesis at the doses investigated (**Figure 6**).

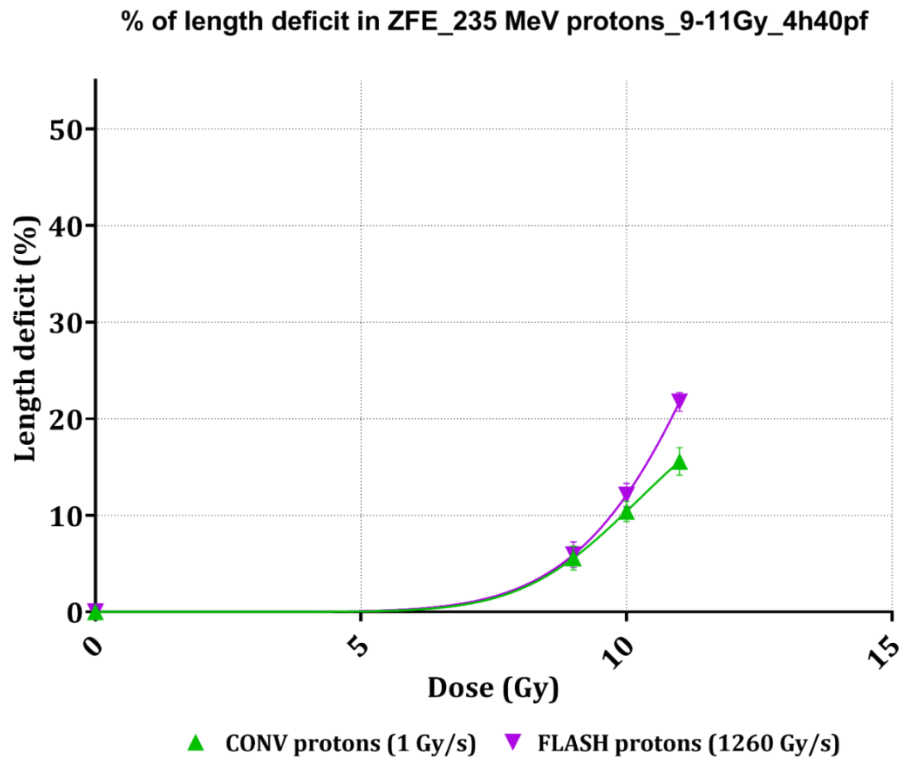


Figure 6: Percentage of length deficit in 4h40 ZFE after exposure to CONV (1 Gy/s) and FLASH proton (1400 Gy/s) conditions.

Table 1: Proton beams parameters for the different set of irradiations a) Water radiolysis at 21% O₂ b) water radiolysis at 4% O₂ c) Plasmid irradiations and d) ZFE irradiations.

a)

Mode	CONV (1 Gy/s)					FLASH (1400 Gy/s)				
Delivered dose [Gy]	10	20	30	40	50	10	20	30	40	50
Delivered dose rate [Gy/s]	1					1400				
Uncertainty on delivered dose/dose rate [%] (k=1)	2					2				
Cyclotron Beam Current [nA]	0.5					725				
Treatment time [s]	10	20	30	40	50	7.14×10^{-3}	1.43×10^{-2}	2.14×10^{-2}	2.86×10^{-2}	3.57×10^{-2}
Cyclotron frequency [Hz]	7.285×10^7									
Pulse width [μ s]	8.00×10^{-4}									

b)

Mode	CONV (0.9 Gy/s)			FLASH (90 Gy/s)			FLASH (1260 Gy/s)		
Delivered dose [Gy]	9	18	27	9	18	27	9	18	27
Delivered dose rate [Gy/s]	0.9	0.9	0.9	90	90	90	1260	1260	1260
Uncertainty on delivered dose/dose rate [%] (k=1)	4			4			4		
Cyclotron Beam Current [nA]	0.44			43.5			609		
Treatment time [s]	10	20	30	1.00×10^{-1}	2.00×10^{-1}	3.00×10^{-1}	7.14×10^{-3}	1.43×10^{-2}	2.14×10^{-2}
Cyclotron frequency [Hz]	7.285×10^7								
Pulse width [μ s]	8.00×10^{-4}								

c)

Mode	CONV (1 Gy/s)										FLASH (1300 Gy/s)							
Delivered dose [Gy]	2	4	6	8	10	20	30	40	50	2	4	6	8	10	20	30	40	50
Delivered dose rate [Gy/s]	1										1300							
Uncertainty on delivered dose/dose rate [%] (k=1)	4					2					4				2			
Cyclotron Beam Current [nA]	0.5										725							
Treatment time [s]	2	4	6	8	10	20	30	40	50	1.54 $\times 10^{-3}$	3.08 $\times 10^{-3}$	4.62 $\times 10^{-3}$	6.15 $\times 10^{-3}$	7.96 $\times 10^{-3}$	1.54 $\times 10^{-2}$	2.31 $\times 10^{-2}$	3.08 $\times 10^{-2}$	3.85 $\times 10^{-2}$
Cyclotron frequency (Hz)	7.285 $\times 10^7$																	
Pulse width (μ s)	8.00 $\times 10^{-4}$																	

d)

Mode	CONV (0.9 Gy/s)			FLASH (1260 Gy/s)		
Delivered dose [Gy]	9	9.9	10.8	9	9.9	10.8
Delivered dose rate [Gy/s]	0.9			1260		
Uncertainty on delivered dose/dose rate [%] (k=1)	4			4		
Cyclotron Beam Current [nA]	0.44			609		
Treatment time [s]	10	11	12	7.14 $\times 10^{-3}$	7.86 $\times 10^{-3}$	8.57 $\times 10^{-3}$
Cyclotron frequency (Hz)	7.285 $\times 10^7$					
Pulse width (μ s)	8.00 $\times 10^{-4}$					

Table 2: Primary yields of hydrogen peroxide after exposure to CONV (1 Gy/s) and FLASH (1400 Gy/s) 235 MeV transmission protons.

Source	Energy	LET (keV/μm)	Dose rate(Gy/s)	Chemical system	G°(H2O2) (molecules/100eV)
CONV protons	235 MeV	0.2	1	[NO ₂ -]/[NO ₃ -]	0.66±0.02
FLASH protons			1400		0.67±0.01
CONV X-rays	225 kVp	3	0.037		0.78 ± 0.04

Table 3: Long-term yields of hydrogen peroxide calculated after irradiation with FLASH and CONV VHEE TI protons and compared to CONV X-rays. **a)** G-value in atmospheric conditions **b)** G-value in physioxic conditions.

a)

Source	Energy	LET (keV/μm)	Dose rate(Gy/s)	[O ₂] (M)	G(H2O2) (molecules/100eV)	ΔFLASH/CONV
CONV protons	235 MeV	0.2	1	2.50E-04	1.81±0.05	35.36
FLASH protons			1400		1.17±0.02	
CONV X-rays	225 kVp	3	0.037		3.1±0.05	N.A

b)

Source	Energy	Dose rate(Gy/s)	[O ₂] (M)	G(H2O2) (molecules/100eV)	ΔFLASH/CONV
CONV protons	235 MeV	0.9	4.76E-05	2.33 ± 0.05	N.A
FLASH protons		90		2.2 ± 0.04	6
		1260		1.92 ± 0.15	18%
CONV X-rays	225 kVp	0.037		3.32 ± 0.07	N.A

Table 4: DNA damage yields after proton exposure at CONV (1 Gy/s) and FLASH (1300 Gy/s) and CONV X-rays (0.07 Gy/s).

Source	Energy	Dose rate [Gy/s]	β _D [10 ⁻² /Gy]	β _S [10 ⁻² /Gy]
CONV protons	235 MeV	1	0.5 ± 0.1	34 ± 1
FLASH protons		1300	0.6 ± 0.3	34 ± 2
CONV X-rays	160 kVp	0.07	0.5 ± 0.1	22 ± 1

2- Investigations of cellular ROS levels after FLASH exposure using 2D cell culture

Kinetics of ROS production were measured in one normal cell line (Jurkat) and one tumor cell line (U87) under hypoxic and physioxic conditions. ROS-Glo™ H₂O₂ luminescent assay was used to detect intracellular H₂O₂ levels after FLASH vs CONV.

Material and Methods

ROS assay and irradiations

Immortalized human T lymphocyte cells (Jurkat) (ATTC) were cultured in RPMI medium supplemented with 10% FBS (Thermo Fisher) and human Glioblastoma cells U87 (ATTC) were cultured in DMEM + 10% FBS (ThermoFisher) at 37°C. Mediums were changed 24h before irradiations and cells were incubated under 4% O₂. The day of irradiation, cells were harvested with trypsin + EDTA 0.25% (Thermo Fisher), counted and placed (500'000 cells per tube) in 2 mL Eppendorf tubes for cell suspension irradiations. Cells were irradiated with e-RT6/Oriatron, 5.5 MeV electrons at single pulse FLASH ($\geq 7.78 \times 10^6$ Gy/s) or conventional dose-rate (0.1 Gy/s) in a water-tank heated at 37°C and maintained along the irradiation to 0, 2, 4, 6 and 8 Gy for Jurkat cells and to 0, 8, 10, 12 and 14 Gy for U87. Then, cells were plated in 96 well white microplates at a concentration of 20'000/well and incubated at 37°C; 5% CO₂, 21% O₂. H₂O₂ substrate was added 18h post-irradiation and 24h post RT, ROS Glo reagents were added at 100µl/well and incubated for 20 min at room temperature. Luminescence measurements were recorded using microplate reader from Promega as shown in **Figure 1**.

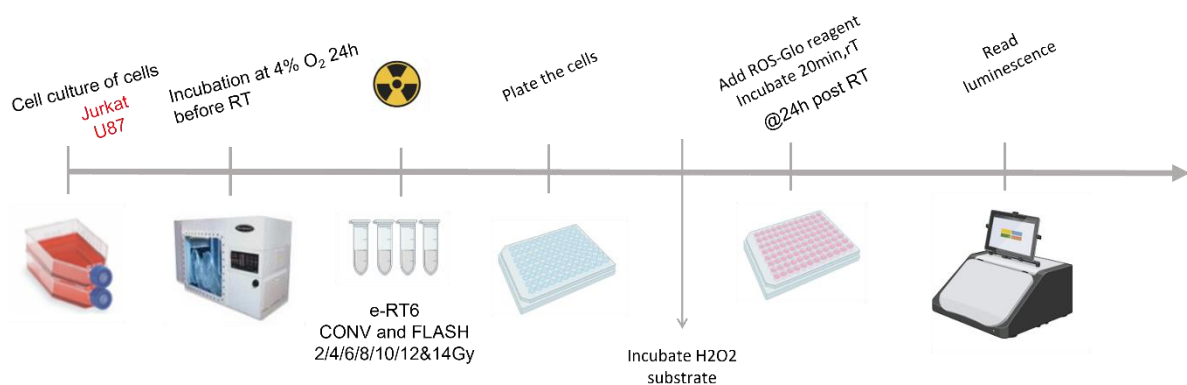
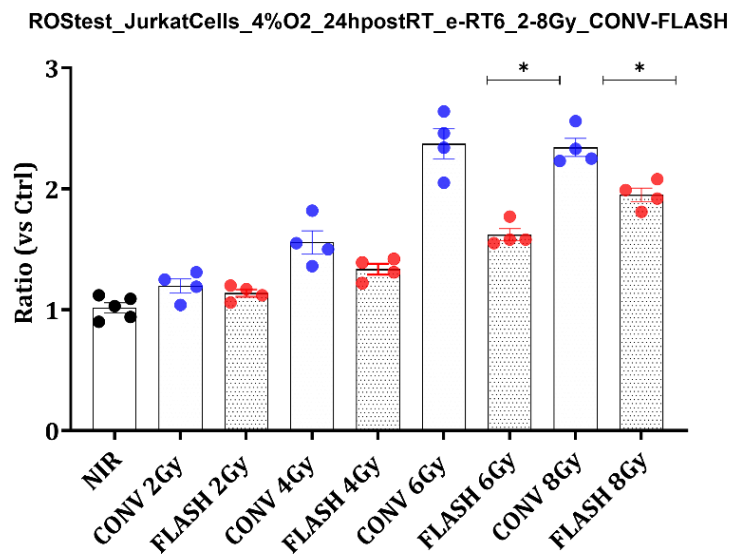


Figure 1: Methodology of ROS measurement in cell lines.

Results

Preliminary results revealed lower ROS induction in normal cells (Jurkat) after exposure to FLASH vs CONV at relatively high doses (6 Gy and 8 Gy) (**Figure 2a**), whereas in the glioblastoma U87 cell, both CONV and FLASH failed to induce ROS, levels were similar to non-irradiated cells (NIR), except at very high dose 14 Gy where FLASH seemed more potent than CONV in inducing ROS. These results suggest intrinsic differences between normal and tumor cells in response to FLASH.

a)



b)

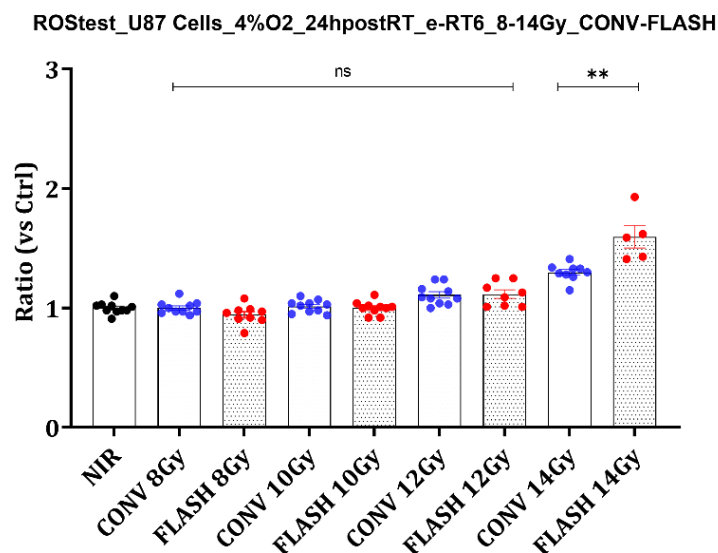


Figure 2: Ratio of ROS levels after FLASH (7.78×10^6 Gy/s) and CONV (0.1 Gy/s) electrons irradiations as a function of the irradiated dose in **a)** Jurkat cell line and **b)** U87 cell line. NIR refers to non-irradiated cells.

3- Investigation of ROS involvement after FLASH vs CONV exposure using a transgenic zebrafish model deficient in Nrf2

Oxidative stress induces the nuclear translocation of the nuclear factor (erythroid-derived2)-like 2 (Nrf2) that transactivates the expression of the major antioxidant genes, therefore the deficiency in Nrf2 is known to alter global antioxidant signaling cascades and sensitize tissue to oxidative stress including irradiation at conventional dose rate. Here, an Nrf2 deficient ZFE model was used to probe the role of ROS after exposure to FLASH vs CONV.

Material and methods

ZFE experiments

AB Wild-Type (AB WT) and NF-E2-related factor 2 (Nrf2) (*nfe2l2a*, ZFin) ZFE (Danio Rio) were used. Heterozygote ZFE (Nrf2 +/-) were produced first whereas the production of homozygote (Nrf2 -/-) is ongoing. Deficiency was confirmed by genotyping using RT-PCR. In a first set of experiments (n=25 ZFE; 6hpf) were placed in 2mL Eppendorf tubes and irradiated at 10-18Gy with e-RT6/Oriatron, 5.5MeV electrons at 0.1 Gy/s (conventional) and ≥ 1400 Gy/s (FLASH, 2 pulses) under controlled dosimetry (290). Survival and morphogenesis were monitored 5 days post fertilization (dpf) as shown in **Figure 1**.

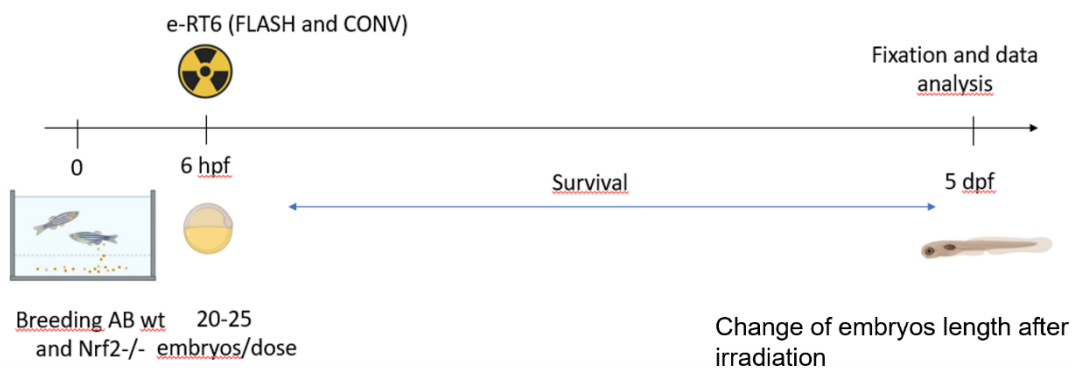
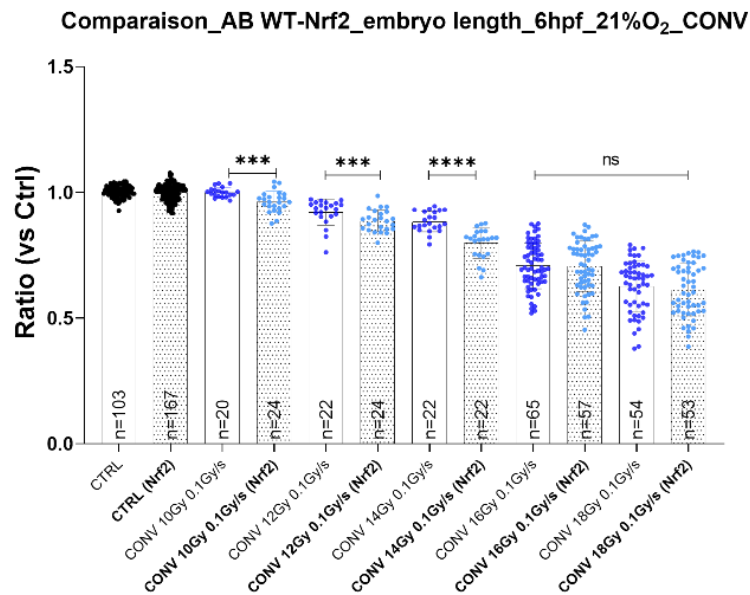


Figure 1: Methodology of morphogenesis assessment in ABWT and Nrf2+/- zebrafish embryos.

Results

The development of AB Wt and Nrf2 +/- embryos was similar after 10 to 18Gy delivered with FLASH electron (**Figure 2**), whereas doses from 10 to 14Gy delivered at conventional dose rate irradiation (0.1Gy/s), decreased the size of Nrf2 +/- ZFE by 13 to 20% as compared to WT embryos. Similar growth defects after exposure to 16 and 18Gy on WT and Nrf2 +/- ZFE.

a)



b)

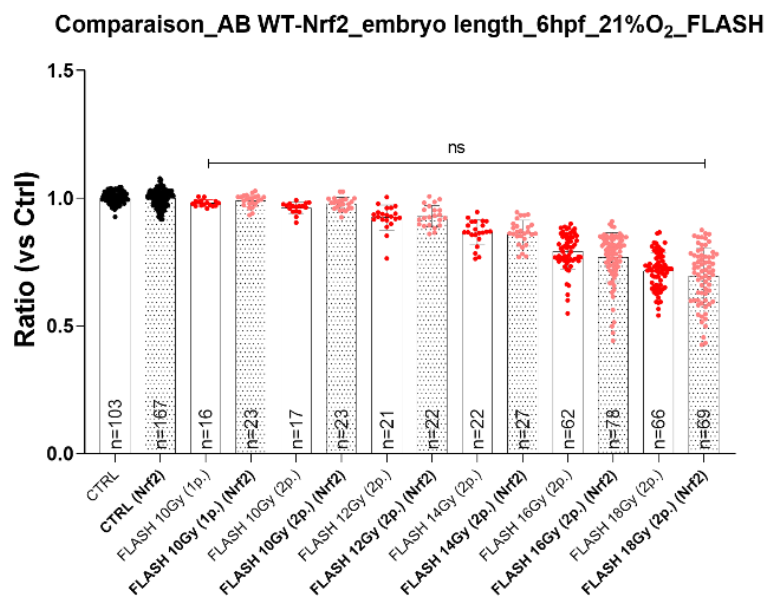


Figure 2: Comparison of fish length ratio between AB WT and Nrf2 +/- embryos after exposure to a) CONV-RT (0.1 Gy/s) and b) FLASH-RT (≥ 1400 Gy/s).

These results suggest that Nrf2 initiates a protective antioxidant response after exposure to conventional radiation at doses up to 14 Gy, but this response is insufficient at higher doses

(>14 Gy). Interestingly, the oxidative stress threshold (> n14 Gy) needed for Nfr2 pathway activation was not reached with FLASH, even at 18 Gy. Experiments are currently performed with homozygous KO.

Chapter IV: General Discussion

1- Discussion

My work aimed to decipher the existence of a potential continuum between the physico-chemical and radiobiological mechanisms that trigger the FLASH effect. This investigation involved cell-free systems, *in vitro* models including tumoral and normal cell lines, and *in vivo* studies on normal tissue using zebrafish embryos. Various beams capable of delivering doses at conventional and ultra-high dose rates were employed, including Very High-Energy Electron beams (VHEE) at CLEAR-CERN, intermediate electron energy (IEE) beams eRT6/Oriatron at CHUV, transmission proton beams at Gantry1-PSI, and conventional photon beams.

Although the FLASH effect is today well-documented in experimental rodent models, translating these findings directly to human patients is not straightforward. To address this gap, our laboratory has developed a program involving veterinary clinical trials in domestic animals and mini pigs. While my thesis work does not relate to this translational aspect, I have focused on another crucial question associated with the development of high-throughput assays. My goal was to integrate chemical and/or biological models to validate FLASH beams and investigate the conditions and physics parameters required to systematically trigger the FLASH effect. This systematic analysis revealed:

1. The FLASH effect requires specific critical beam parameters.
2. Water radiolysis products in simple solutions cannot serve as a surrogate of the biological FLASH effect.
3. ROS-mediated damage on plasmid DNA is a poor proxy for the FLASH effect.

1- The FLASH sparing effect is obtained using specific beam parameters.

Over the past decade, the FLASH sparing capability and anti-tumor impact has been reported in several animal models including mice, rat, zebrafish, pig, cats across various organs such as lung, brain, skin, and gut. Preclinical studies by several groups showed that the FLASH effect can occur with single and fractionated dose regimens. The FLASH effect is currently thought to occur when the irradiation time is extremely short (a few 100 of milliseconds or less) and when the dose rate is high enough (mean dose rate $\geq 40\text{Gy/s}$). However, this definition is not entirely satisfactory and cannot be generalized, as some negative studies have been published and showed no FLASH effect. For instance, exposure of 24-hour post-fertilization (hpf) zebrafish embryos with a proton beam at 100 Gy/s and 0.08 Gy/s showed no difference in survival and morphology (268). Similarly, with synchrotron X-rays at 37–41 Gy/s and 0.06 Gy/s, no difference was reported after total body, thoracic, and abdominal irradiation (267). Likewise, cardiac and splenic irradiation of mice with an electron FLASH beam delivered at 35 Gy/s and 0.1 Gy/s showed no sparing effect and caused lymphopenia (269).

When I started my PhD thesis, the physics parameters required to produce the FLASH effect were still unclear. In this context, I took advantage of various beams able to deliver UHDR such as VHEE, IEE, Proton beams as illustrated in **Figure 1**.

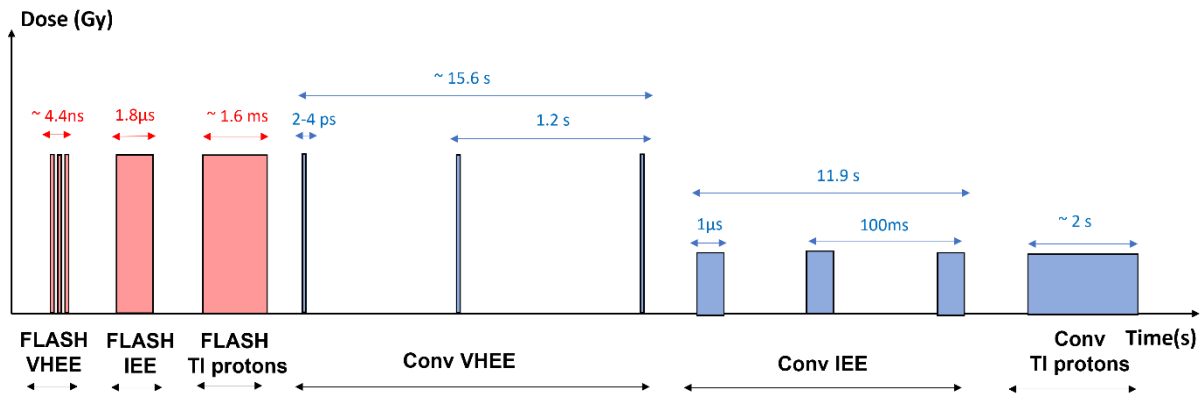


Figure 1: Temporal structure of CLEAR Very High Energy Electron (VHEE), eRT6 intermediate energy electron (IEE) beam and Gantry1 transmission (TI) proton beam at CONV and FLASH dose rate. eFLASH and eCONV stand for electron FLASH and electron CONV dose rate. pFLASH and pCONV stand for proton FLASH and proton CONV dose rate.

My work showed that the FLASH effect was a biological effect independent from the beam nature. It identified the instantaneous dose rate as the critical beam parameter to trigger the FLASH sparing effect and suggests that higher is the instantaneous dose rates and lower doses in the bunch/pulse are required to trigger the FLASH sparing effect.

Most of the studies done in our group in mice have been performed using a single pulse of electrons (1.8 μs) where average and instantaneous dose rate are equal and reach 5.6×10^6 Gy/s. However, other studies using electrons, reported a sparing effect with lower parameters such as irradiation ranging between 33 to 2500 Gy/s (34,229,230,291–294). In the first dose rate escalation study done in the brain of mice (253), our group showed that neurocognition was spared above 100 Gy/s, when a 10 Gy dose was delivered in 10 pulses (1.8 μs width) at a frequency of 100 Hz. I reproduced this result in ZFE in Kacem et al.(295) and Ruan et al. also showed the highest number of intestinal crypt cells was spared with a single pulse FLASH of 3.4 μs after electron irradiation (294).

While these dose rate escalation studies are of utmost importance to characterize the FLASH effect *in vivo*, such studies are ethically burdensome, costly and time consuming, especially for late responding tissue (lung, brain, bone) that are largely devoid of rich stem cell population and necessitate a focus on functional outcomes that can take months to appear (e.g., cognitive dysfunction, lung fibrosis, osteoradionecrosis). As such, other easily manipulated *in vivo* or *in vitro* assays, able to provide more rapid, cheaper, and convenient assessments to trigger the FLASH effect from multiple beam paths and modalities of irradiation would be very useful.

In this context, my thesis work aimed at using chemistry assays as surrogate for biological response. We also used ZFE that is a relatively new model in the field of radiation biology. It

has several distinct advantages including the fact that it is a fully integrated *in vivo* model, ethics' approval is not required at early stages and it's a short-term model with a fast biological response (5 days). ZFE also have other interesting characteristics such as a very rapid shift in their radiation resistance profile according to developmental status with the lethal dose 100% (LD100) ranging from 15 to 50 Gy within the first 24 h of their development (296). To investigate the impact of clinically relevant doses (in the range of 10 Gy), we chose to work at 4-4.30 hours post fertilization (hpf). At this early stage of their development, ZFE are stem cell-like, behaving like acute responding tissues.

We report a lower magnitude of the FLASH sparing effect with a dose modifying factor (DMF) = 1.2 which is similar to what has been reported in other early responding tissues such as the gut of mice [19,72]. In a dose rate escalation study ranging from 0.1 to 5.6×10^6 Gy/s, we identified an average dose rate of 100 Gy/s, 100 Hz and 10 pulses of 1 Gy with a pulse width of 1.8 μ s with an instantaneous dose rate of 0.5×10^6 Gy/s as threshold to protect ZFE morphogenesis. Interestingly, ZFE findings were of a remarkable consistency (**correlation coefficient > 0.94**) (295) with the mice study. We also modified the pulse width from 1.8 μ s to 4 μ s. Under these conditions, when a dose of 10 Gy was delivered in one, two or 5 pulses, it did not modify the sparing outcome. More surprisingly, the modification of the frequencies from 100 Hz = 10 milliseconds up to a 10 min interval between pulses did not modify the sparing efficacy. This unexpected result revealed that **neither the overall time nor pulse multiplicity of irradiation are critical parameters to trigger the FLASH sparing effect** but suggest that **an instantaneous dose rate in the range of 10^6 Gy/s and using a minimum of 1 Gy per pulse matters the most in ZFE.**

Next, we used various beams with various time structures such as VHEE (nanosecond operating beam) and transmission protons (milliseconds operating beam) in addition to eRT6 (microsecond operating beam) and conventional X-rays. At conventional dose rate, X-rays (0.037 Gy/s) and electrons (0.1 Gy/s) induced a similar dose-dependent deficit in the morphogenesis of ZFE. A length deficit of 50% was found with 10 Gy X-rays, which was 45% with eCONV, but only 30% with eFLASH when average and instantaneous dose rate are equal and set above 10^6 Gy/s. This sparing effect occurred when 10 Gy was delivered with pulses of **1 Gy or more delivered at the microsecond scale (eRT6) and when it was delivered with bunches of 0.33 Gy or more delivered at the picosecond scale (CLEAR).**

These results suggest that higher is the instantaneous dose rate, lower the dose in the bunch/pulse can be: 1 Gy at 10^6 Gy/s but only 0.33 Gy at 10^{11} Gy/s. In contrast, others groups working with proton beams found a FLASH sparing effect using ZFE using doses above 30 Gy and average/instantaneous dose rates ranging from 300 to 7500 Gy/s (286,287).

2- Can water radiolysis products measured in simple chemical solutions be used as a surrogate of the biological FLASH effect?

Our initial idea was to use radiolysis in chemical solutions as surrogate for the FLASH effect. Therefore, primary (G°) and long-term (G) yields were computed. On one hand, primary G° -values has been extensively evaluated in the past literature (272,280,281,297–299) mainly in anoxic conditions. These studies focused on the computation of primary yields to compare impact of high LET radiations owing a special track structure, able to induce dense ionizations following their interaction with water molecules. These previous reports showed that primary G° -values increased for very high LET particles (above 200 keV/ μm) (36). Our hypothesis was that G° values could be different after CONV vs FLASH. Our findings refute this hypothesis. The primary radiolytic yield of hydrogen peroxide $G^\circ(\text{H}_2\text{O}_2)$, calculated at the microsecond time scale, is not impacted by dose rate modifications and

$G^\circ(\text{VHEE FLASH}) = G^\circ(\text{VHEE CONV})$; $G^\circ(\text{eFLASH}) = G^\circ(\text{eCONV})$ and $G^\circ(\text{pFLASH}) = G^\circ(\text{pCONV})$.

These results are consistent with previous experimental reports obtained by Anderson et al. (280) who used pulsed electrons operating at high dose rates ranged between $2.6\text{-}3.7 \times 10^7$ Gy/s and found primary yields of hydrogen peroxide equal to 0.76 molecules/100eV. Moreover, when comparing with previous reports that used the same scavenging chemical system (Nitrite/Nitrate ions) or different chemical scavenging systems (bromide ions/nitrate ions) / (methanol/nitrate ions), primary yields from conventional Cesium or Cobalt sources were also consistent with our results. Recent simulations of primary yields of H_2O_2 performed by the Institute of Radiation Physics (IRA) group at the CHUV (300) are also compatible with our results. These data suggest that initial physico-chemical events are not different between CONV and FLASH and cannot explain the biological findings.

Additional insights can be taken from our study, namely that despite those primary yields of H_2O_2 obtained with electrons, TI protons and VHEE irradiations were not modified by the dose rate. There was a slight decrease in the primary yields was observed with TI protons but this was found also in the previous literature (272,299) and VHEE compared with electron beam. This phenomenon can be attributed to the intrinsic temporal beam structure (pulsed for electrons/semi-continuous for protons). In the case of VHEE, the reduction in primary G-values might be related to a certain dose rate threshold at which, G° of molecular products like hydrogen peroxide will decrease due to the interference with heterogeneous phase of chemistry caused by the high dose rate. In our case, VHEE irradiations at both dose rates, had similar high instantaneous dose rates (5×10^{10} Gy/s). In summary, **yields of molecular radicals “escaping” track recombination after ionization is dose rate independent and not affected by beams operating at nanosecond, microsecond, and millisecond time scale.**

Only few studies investigated long-term G-values (280,284,299). We found a reduction of hydrogen peroxide yield after FLASH vs CONV. This finding is confirmed by Blain et al. (283) but not by Anderson et al. (280) and Sehested et al. (284) who have found an increase in the

hydrogen peroxide yield with pulsed electrons vs conventional γ rays from ^{60}Co source. While the basis of this discrepancy is unclear, it is important to consider the fact that previous reports have measured the production of hydrogen peroxide with oxygen concentration equal to 1×10^{-3} M (4 times higher than the atmospheric O_2) whereas we have been working under standard atmospheric conditions (2.50×10^{-4} M). In addition, H_2O_2 was quantified using the Ghormley method unlike in our experiments, where we used the Amplex Red, an enzymatic assay, for H_2O_2 quantification. More recently, Roth et al. 2011. (299) estimated the long-term yield of hydrogen peroxide in aerated water samples ($[\text{O}_2] = 2.50 \times 10^{-4}$ M) from conventional ^{60}Co source and conventional proton irradiations and found similar yields.

Next, when experiments were done under more relevant biochemical environments that included variation of oxygen levels from hypoxia (1% O_2) to atmospheric conditions (21% O_2) and changes in temperature as well as addition of scavengers, we found that long-term yield of H_2O_2 followed a bell-shaped curve as a function of the oxygen level. Low radiolytic yields were found in hypoxic conditions, whereas these yields increased at intermediate levels reaching a maximum at physioxic conditions then decreasing again under atmospheric conditions. FLASH reduced the yield of H_2O_2 in every oxygen condition by about 30% with a maximal reduction factor of 34% under physioxic conditions (4% O_2). Also, we showed that FLASH dose rate resulted in less H_2O_2 production under hypoxia (tumor-like condition) compared to CONV dose rate. When nitrate ions were added (efficient scavengers of aqueous electrons), the long-time G-values of H_2O_2 at CONV and FLASH dose rates were reduced by 51% and 14%, respectively, and became similar between the two modalities. These findings are consistent with Roth et al. (299), whose measurements who found long-term H_2O_2 yields ($G(\text{H}_2\text{O}_2) = 1$ molecules/100eV) with conventional γ rays. The experiments varying temperature from 22 to 37-38°C showed that long term H_2O_2 yields were increased at 37°C by 43% and 39% using CONV and FLASH, respectively. The difference between the results obtained with FLASH and CONV was only 31% at 22°C while it reached 36% at 37-38°C. This temperature-related increase in G-values yields after CONV and FLASH dose rates might be related to the increase in molecular dynamics of free radicals. Therefore, an increase in the diffusion kinetics of oxidizing species during water radiolysis could be enhancing radical-radical recombination. So far, no such experiments have been reported and we think that measurements should be done in biological models to retrieve significant results.

In fact, when we wanted to correlate $G(\text{H}_2\text{O}_2)$ measured in physioxic conditions with biological outcomes in ZFE, we initially thought (249) that a threshold $G(\text{H}_2\text{O}_2)$ value ≤ 2.33 molecule/100 eV could correlate with the biological outcome in ZFE. Unfortunately, later using VHEE, we could not validate this threshold value.

Globally, our chemical results could fit with the normal tissue sparing impact of FLASH but are difficult to reconcile with the antitumor impact (31,32). Putting together all our results, from primary molecular yields found at the microsecond time scale to long term yields measured after the microsecond in various chemical conditions, it seems that simple water radiolysis products are not a satisfactory approach to approximate the biological FLASH effect.

3- Is it possible to use the impact of ROS on plasmid DNA as a surrogate of the biological effect?

The next step was to use plasmid DNA for a quick and qualitative evaluation of the DNA damage upon dose rate modulation. We found that DNA damages in this simple in cell-free systems was dose rate insensitive and was not modified by beam characteristics such as the mean dose rate, instantaneous dose rate, beam structure, particle type and particle energy were modulated. Moreover, when the plasmid was placed in biochemical conditions mimicking tumors (hypoxia, acidic milieu, high Fe²⁺ level), FLASH induced less DNA damages suggesting that “tumor DNA” would be protected and contrasting with *in vivo* data published to date (RV in Vozenin et al. and Limoli et al.) (31,32). Our results suggest that plasmid is not a relevant model to identify the biological determinant(s) responsible for the FLASH effect. They are however consistent with older results produced by Milligan et al. (224,226,227) with dose rates ranging between 0.1 Gy/s and 1 Gy/s that included scavengers, as well as with results produced at CLEAR in Small et al. (222) with dose rate above 10⁹ Gy/s. However, these findings are in contradiction with a recent report that claimed to observe a dose rate impact on DNA damage in plasmids (221). In this study, experimental conditions were improperly controlled (scavenging contaminants), which likely confounded their conclusions. In addition, data was fitted based on a very low number of experimental data points which rendered their interpretations suspect. *In an ex-vivo* study of whole-blood peripheral blood lymphocytes (WB-PBL) and using a comet assay, Cooper et al.(228) also reported reduced DNA damage burden after FLASH electrons (2000 Gy/s) at doses higher than 20 Gy and in reduced oxygen conditions (0.25-0.5% O₂). Additionally, in biological systems, the relevance of DNA damage after FLASH vs CONV has also been explored *in vivo* mice by Fouillade et al.(229). They reported less γ H2AX foci after FLASH electrons (2 x10² to 4 x10⁷ Gy/s) in the normal lung. Likewise, Levy et al.(230) showed similar levels of γ H2AX foci in ID8 tumors after FLASH electrons (216 Gy/s) and CONV electrons (0.079 Gy/s), and a slight decrease in repair foci after FLASH in the normal gut at early time-points, that normalized by 24h post-irradiation. However, in a recent study, Barghough et al. (285) used a functional and quantitative DNA damage repair (DDR) assay *in vitro* and showed that FLASH electrons (1 x10² to 5 x10⁶ Gy/s) does not affect chromosome translocations and junction structures in HEK293T cells more than CONV electrons (0.08 Gy/s to 0.13 Gy/s). In summary, combined with ours, these experiments suggest that DNA damage is unlikely to explain the FLASH effect.

2- Conclusion

Our results show that reductionist radiochemical approaches using water and plasmids are poor surrogates of the *in vivo* responses that define the FLASH effect. Subsequently, we think that such approaches cannot be used as high throughput assays to validate FLASH beams or investigate the FLASH effect.

The most important finding of this work is related to the identification of the instantaneous dose rate as a critical parameter to trigger the FLASH effect with electron beams. This finding is transformational to traditional radiobiology and challenging for the field. However, it is critical for the future design of new clinical accelerators as it suggests that narrow pencil/spot operating with high instantaneous dose rate such as what is feasible with VHEE and proton beams and scanned over the target would be possible. The idea that that higher instantaneous dose rate will enable the use of lower doses also suggest that VHEE beams are the best candidates for clinical developments of FLASH.

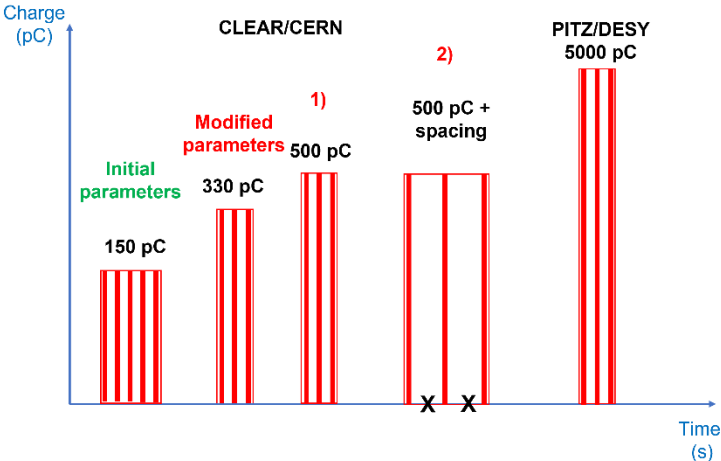
3- Perspectives

Confirmatory studies: the next strategy to validate our findings.

Our next short-term investigations will aim at validating our findings suggesting that the higher the dose rate is, the lower can be to still trigger the FLASH sparing effect in ZFE. Several pulsed beam lines can be used including the Linear Electron Accelerator for Research at the European Organization for Nuclear Research (CLEAR/CERN), the Photoinjector test facility in Zeuthen at the German electron synchrotron (PITZ/DESY) and the Arronax cyclotron in Nantes.

At CLEAR two strategies will be used: 1) The charge will be enhanced up to 500 pC providing a dose rate in the bunch up to 3×10^{11} Gy/s, for enhancing the sparing capability. 2) we will space very high dose rates bunches by manual interruption of the beam, with the expectation of losing the sparing capability (**Figure 1a**).

a)



b)

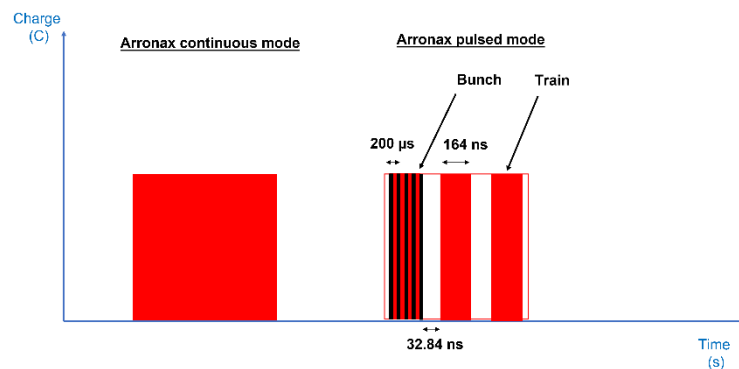


Figure 1 a) Example of variable time structure with VHEE and proton beam a) the FLASH VHEE-CLEAR is represented with its initial, modified and the future structure in addition to VHEE PITZ able to deliver x10 higher charged bunches **b)** Arronax cyclotron with the new pulsing chopper, proton beam structure can be varied from continuous mode to pulsed mode with 3 trains containing each (301).

Similar approach can be used at PITZ/DESY, which is a platform for 25 MeV (eventually up to 250 MeV) very high energy electrons as well. Picoseconds scale electron bunches can be provided up to 5nC bunch charge where individual bunches can provide peak dose rates up to 10^{14} Gy/s (302). Whereas at Arronax/Nantes, a high intensity cyclotron is available accelerating pulsed protons and Helium ions up to 70 MeV. With this facility, 7000 Gy/s dose rates can be reached with protons and 9000 Gy/s are achieved with He ions. Thanks to the technology of pulsing chopper, Arronax cyclotron proton beam can be delivered from continuous mode to pulses mode with 3 trains containing each 5 bunches separated by 200 μ s as shown in **Figure 1b** (301).

Oxidative stress and the FLASH effect

We will continue our investigations related to the redox metabolism. Our preliminary results pointed out decreased ROS levels in normal cells after FLASH vs CONV exposure but a dose dependent increase in ROS level. Whereas, in tumor cells, ROS levels seemed to be the same between both modalities and an unexpected increase in ROS levels was found after high dose FLASH (14Gy FLASH). We will confirm these results by using other normal and tumor cell lines like HaCat (Transformed keratinocytes) and H454 (GBM) and perform irradiation in physioxic (4% O_2) and hypoxic conditions (1% O_2) with CLEAR VHEE beam as well. Liperflu assay will also be used to detect lipid peroxidation in cells. Our hypothesis is that the antioxidant response following FLASH might not be activated, and normal cells will compensate faster for the low ROS levels (free radicals and organic radicals) by enzymatic reactions. However, in tumor cells, due to a permanent imbalance in their redox system, an increase in ROS levels and high level of labile iron will sustain oxidative stress after FLASH as well.

In ZFE, experiments will be performed with homozygotes Nrf2 KO ZFE, these initial results suggest that Nrf2 pathway is not needed upon FLASH exposure.

Early transcription events and the FLASH effect

Another angle to understanding the FLASH effect is by investigating the molecular basis of this irradiation in ZFE. Interestingly, ZFE undergo maternal-to-zygotic transition (MZT) at 2.5 to 3 hours post-fertilization (hpf), when zygotic transcription is initiated (**Figure 2a**). Therefore, ZFE provide a unique high throughput model to study the role of transcription in response to FLASH vs CONV. In short, before 2.5 hpf embryonic transcription is disabled and the development of the ZFE relies exclusively on pre-existing maternal factors. After 3 hpf, transcription is activated by the “pioneer” transcription factors (TFs) Sox (named Sox19b in ZFE), Oct4 (named Pou5F1 in ZFE) and Nanog also known as Yamanaka factors. They can bind closed chromatin and start transcriptional activity required for proper development of the embryo. The developmental program then continues, involving a handful of additional early TFs (Tfam, Setdb1a, Eomesa, Mta2, Hmgb2b and Sall4) as well as miRNAs, such as miR-430, necessary for the clearance of maternal factors. Recent work showed that the activity of the various TFs is further regulated by the maturation of nuclear pore complex. Simultaneously, three important maternally provided morphogens - BMP, Nodal, and Wnt - are required for the asymmetrical development of embryos. The gradients of these morphogens (as shown in **Figure 2b**) determine axis specification and proper development of embryos during MTZ. In summary, MTZ provides a well characterized framework and a dozen of selected transcriptional and morphogenic targets that may help to identify the elusive molecular determinant that differentially respond to dose rate modulation during FLASH vs CONV-RT.

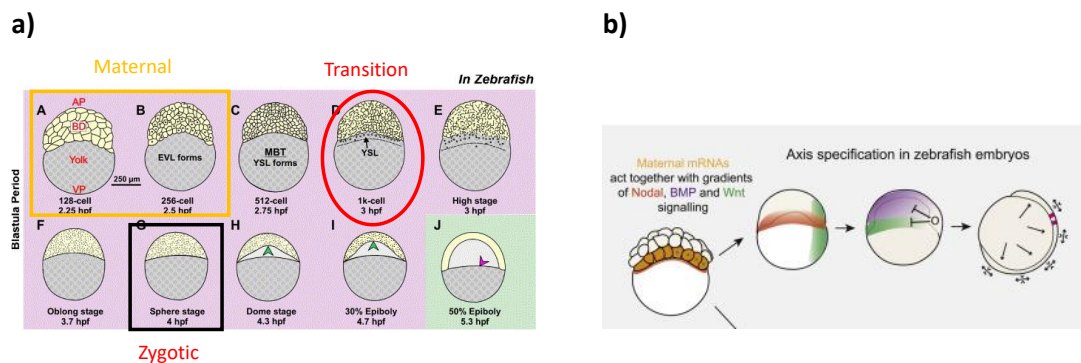


Figure 2: **a)** Schematic view of zebrafish development during the Blastula period (303). **b)** Anterior-posterior and dorso-ventral axis specification in ZFE and expression of the morphogens Nodal, BMP and Wnt (304).

The off/on nature of the MTZ system will enable us to probe the transcriptional dependency of FLASH vs CONV and whether FLASH sparing requires a certain level of transcription activity. Could it be that CONV irradiation interferes with early transcriptional programs whereas FLASH does not? Whether this is at the level of the transcription factors themselves, specific chromatin structure/targets or morphogen gradients is the focus of this future work.

Curriculum Vitae

Houda Kacem

Biopole III Bureau AA11 9A rue de la
corniche,
1066 Epalinges, Switzerland.
+41 76 578 22 45
Houda.Kacem@chuv.ch
Houda.kacem@unil.ch

**PhD Student**

SERP+ Alumni Class of 2019
Biochemistry assistant
Tunisian citizen, Swiss Residency
29yo, 10.09.1994
Single

SCIENTIFIC EXPERIENCE

JAN 2020 – NOWADAYS

PhD Studies - Radiation Oncology Department, CHUV, Lausanne, Switzerland. "Oxygen contribution, production and impact of Reactive Oxygen Species after FLASH irradiation" Supervised by Pr. Marie-Catherine Vozenin, PhD and funded by SNF Synergia to MCV.

FEB 2019 – AUG 2019

M.Sc. Internship - Institute of Matter and Radiation, CEA SACLAY, Gif-Sur-Yvette, France. "Using Fluorescent Probes in New Modalities of Irradiation: Femtosecond Electrons accelerated from High Intensity Laser: "FLASH Radiotherapy", Beta Particles generated from Strontium Sealed Source, Cold Atmospheric Plasma Jets, and the use of nanoparticles" Supervised by Dr. Gérard Baldacchino, PhD and funded by NanoTheRad to GB.

EDUCATION

2021 – NOWADAYS

PhD studies in life science - University of Lausanne Biology and Medicine faculty, Switzerland.

2019

M.Sc. Thesis - In Radiation Chemistry - University Paris Saclay, CEA Saclay, France.

2019

Graduated from University Paris Saclay and University of Porto - Department of Chemistry, Joint international diploma in Physical Chemistry from the international ERASMUS SERP+ (Surface, Electro, Radiation, and Photochemistry) program.

2018-2019

2nd Year of M.Sc. - University Paris Saclay, France. – Specialization in **Nanoparticles, Nano dosimetry and Advanced Radiation techniques in Cancer Therapy.**

2017-2018**1st Year of M.Sc.**

- **1st semester at University Paris Saclay, France,**

Analytical chemistry, Biophysics, Biochemistry and Microscopy techniques for Life Sciences.

- **2nd semester at University of Porto, Portugal,**

Interfacial electrochemistry, Molecular Energetics and Physical Chemistry of Solid State.

UNIVERSITY SERVICE

- **2021 – Nowadays** – Biochemistry practical work for medical students (BM2), University of Lausanne.
- **2021 – Nowadays** – Biochemistry practical work and exams supervision for biology students (BSc2&3), University of Lausanne.

GENERAL SKILLS

- **Arabic** – Native
- **French** – Bilingual
- **English** – Fluent (level C1 IELTS 7.0)
- **Spanish** – A2
- **Lab technical skills** – Physical-chemist: Initial training.
Acquired skills: Cell culture, Animal experimentation (Zebrafish embryos), Irradiation procedures.
- **Software** – Word, Excel, PowerPoint, ImageJ, Prism GraphPad, EndNote/Zotero, Adobe Illustrator.

GRANT SUPPORT

- **JUL 2018** – Summer School Scholarship in Science Management for Scientists and Engineers, funded by the University of Genova, Italy.
- **JAN 2018 - JUN 2018** – Erasmus Mobility Scholarship for Master studies, funded by the University of Paris Sud (XI) /Paris- Saclay (France) and the University of Porto (Portugal).

SCIENTIFIC PUBLICATIONS

- **Kacem Houda**, Serena Psoroulas , Gael Boivin, Michael Folkerts, Veljko Grilj, Tony Lomax, Adrien Martinotti, David Meer, Jonathan Ollivier, Benoit Petit, Sairos Safai, Ricky A. Sharma, Michele Togno, Marta Vilalta, Damien C. Weber, Marie-Catherine Vozenin.
Comparing radiolytic production of H₂O₂ and development of Zebrafish embryos after ultra-high dose rate exposure with electron and Transmission proton beams.
Radiother Oncol. 2022 Oct; 175:197-202. doi: 10.1016/j.radonc.2022.07.011. Epub 2022 Jul 19.PMID: 35868604
- **Kacem Houda**, Almeida Aymeric, Cherbuin Nicolas, Vozenin Marie-Catherine.
Understanding the FLASH effect to unravel the potential of ultra-high dose rate irradiation.
Int J Radiat Biol. 2022; 98(3):506-516. doi: 10.1080/09553002.2021.2004328. Epub 2021 Dec2. PMID: 34788193

ORAL COMMUNICATIONS AND AWARDS.

- **JUL 11-13, 2023** – **Houda Kacem**, Pierre Korysko, Wilfrid Frabolini, Jonathan Ollivier, Adrien Martinotti, Joseph Bateman, Vilde Rieker, Manjit Dosanjh, Serena Psoroulas, Roberto Corsini & Marie-Catherine Vozenin. –“ *Impact of VHEE beam parameters on G(H₂O₂) and zebrafish embryos morphogenesis after UHDR and conventional irradiation.*” **VHEE conference in DESY, Hamburg, Germany.**
- **JUN 3-8, 2023** – **Houda Kacem**, Louis Kunz, Michele Togno, Pierre Korysko, Nicolas Cherbuin, Wilfrid Frabolini, Robert Schaeffer, Veljko Grilj, Claude Bailat, Joseph Bateman, Tony Lomax,

Jonathan Ollivier, Adrien Martinotti, Sairos Safai, David Meer, Damien Weber, Manjit Dosanjh, Serena Psoroulas, Roberto Corsini & Marie-Catherine Vozenin – “*Impact of temporal structure of UHDR beams on water radiolysis and DNA damage.*” **32nd Miller conference on Radiation Chemistry in Corsica, France.**

- **NOV 30-2 DEC, 2022** – **Houda Kacem**, Michele Togno, Pierre Korysko, Nicolas Cherbuin, Wilfrid Frabolini, Robert Schaeffer, Veljko Grilj, **Claude Bailat**, **Joseph Bateman**, **Tony Lomax**, **Jonathan Ollivier**, Sairos Safai, David Meer, Damien Weber, Manjit Dosanjh, Serena Psoroulas, Roberto Corsini & Marie-Catherine Vozenin – “*Impact of temporal structure of electron, proton and VHEE beams on $G^{\circ}(H_2O_2)$, $G(H_2O_2)$ and DNA damage.*” **FRPT conference in Barcelona, Spain.**
- **NOV 11th, 2022** – **Houda Kacem**–“*FLASH Mechanisms: Impact of temporal structure of electron, proton and VHEE beams on $G^{\circ}(H_2O_2)$, $G(H_2O_2)$, DNA damage and Zebrafish embryos.*” Oral presentation. **Ludwig Trainee Meetings, Centre Laboratories Epalinges, Lausanne, Switzerland.**
- **NOV 4th, 2022** – **Houda Kacem**–“*Oxygen and impact of reactive oxygen species production following FLASH Radiotherapy.*” Oral presentation. **2nd Lausanne Fish User Meeting SV building, EPFL, Lausanne, Switzerland.**
- **AUG 31st-02nd SEP, 2022** – **Houda Kacem**, Michele Togno, Pierre Korysko, Nicolas Cherbuin, Wilfrid Frabolini, Robert Schaeffer, Veljko Grilj, **Claude Bailat**, **Joseph Bateman**, **Tony Lomax**, **Jonathan Ollivier**, Sairos Safai, David Meer, Damien Weber, Manjit Dosanjh, Serena Psoroulas, Roberto Corsini & Marie-Catherine Vozenin – “*Impact of temporal structure of electron, proton and VHEE beams on $G^{\circ}(H_2O_2)$, $G(H_2O_2)$, DNA damage and zebrafish embryos.*” **R3C conference, Nice, France.**
- **July 18th-20th, 2022** – **Houda Kacem**, Michele Togno, Nicolas Cherbuin, Robert Schaeffer, Veljko Grilj, **Claude Bailat**, **Tony Lomax**, **Jonathan Ollivier**, Sairos Safai, David Meer, Damien Weber, Serena Psoroulas, & Marie-Catherine Vozenin – “*Impact of temporal structure of electron and proton on $G^{\circ}(H_2O_2)$, $G(H_2O_2)$, DNA damage and Zebrafish embryos.*” **The 8th Annual Loma Linda Workshop, Loma Linda, CA.**
- **DEC 1-3rd, 2021** – **Houda Kacem**, Veljko Grilj, Patrik Jorge Gonçalves, Jean Bourhis, Marie-Catherine Vozenin and Pascal Froidevaux – “*Comparison of H_2O_2 and $HO\cdot$ primary yields and O_2 depletion after irradiation at UHDR and Conventional-dose rate with 6MeV eRT6/Oriatron.*” **Best Abstract award at FRPT conference in Vienna, Austria.**
- **NOV 19th, 2021** – **Houda Kacem**– “*Characterization of physico-chemical events after FLASH radiotherapy.*” Oral presentation. **Ludwig Trainee Meetings (virtual).**
- **JUNE 26th, 2020** – **Houda Kacem**, Veljko Grilj– “*Chemical Principles behind the FLASH Effect: From Hypothesis to Measurements.*” **Radiation Oncology Research Meeting, CHUV, Lausanne, Switzerland.**
- **APRIL 09th, 2019** – **Houda Kacem**, Jean Daniel Ahui, Gerard Baldacchino, Tiberio Ceccotti, Jozo Declic, Sandrine Dobosz Dufrénoy and Pierre Forestier-Colleoni “*Dosimetry by an ultra-short electron source of the deposited dose on human cells cultured in vitro.*” **Second workshop Nanotherad, Institute of Molecular Science of Orsay, France.**

SCIENTIFIC POSTERS

- **Houda Kacem**, Jonathan Ollivier, Adrien Martinotti Kevin Sprengers, Ryan Paisley and Marie-Catherine Vozenin—*Importance of Nrf2 pathway after FLASH irradiation.* Accepted for **FRPT23 conference in Toronto, Canada (5-7 Dec 2023)**.
- **Houda Kacem**, Pierre Korysko, Wilfrid Frabolini, Jonathan Ollivier, Adrien Martinotti, Joseph Bateman, Vilde Rieker, Manjit Dosanjh, Roberto Corsini & Marie-Catherine Vozenin. —*Impact of VHEE beam parameters on G(H₂O₂) and zebrafish embryos morphogenesis after UHDR and conventional irradiation.* **VHEE conference in DESY, Hamburg, Germany (11-13 Jul 2023)**.
- **Houda Kacem**, Michele Togno, Veljko Grilj, Claude Bailat, Jonathan Ollivier, Benoit Petit, Adrien Martinotti, Tony Lomax, Sairos Safai, David Meer, Damien Weber, Serena Psoroulas, & Marie-Catherine Vozenin —*Impact of dose rate delivered with electron, proton and photon beams on Zebrafish embryos.* **15th Annual Swiss Zebrafish meeting in Geneva, Switzerland (30th Jun 2023)**.
- **Houda Kacem**, Serena Psoroulas, David Meer, Sairos Safai, Michele Togno, Tony Lomax, Damien C. Weber M Folkerts, S X Pfister, R A Sharma, Marie-Catherine Vozenin. *Hydrogen peroxide production after irradiation with protons beam at various dose rates.* **FRPT conference in Vienna, Austria (1-3rd Dec 2021)**.
- **Houda Kacem**, Jean Daniel Ahui, Gerard Baldacchino, Tiberio Ceccotti, Jozo Declic , Sandrine Dobosz Dufrenoy and Pierre Forestier-Colleoni *Effect of the high dose rates associated with the new Particle Source for Radiotherapy.* **Fundamental Research Direction (DRF Impulsion) July 16th, 2019 at CEA-Saclay, France.**

Bibliography

1. Siegel R, Naishadham D, Jemal A. Cancer statistics, 2012. CA: A Cancer Journal for Clinicians. janv 2012;62(1):10-29.
2. Roentgen WC. [On a new kind of ray (first report)]. Munch Med Wochenschr. 24 juill 1959;101:1237-9.
3. Discovery of radioactivity.pdf.
4. Grubbé EH. Priority in the Therapeutic Use of X-rays. Radiology. août 1933;21(2):156-62.
5. Kogelnik HD. Inauguration of radiotherapy as a new scientific speciality by Leopold Freund 100 years ago. Radiotherapy and Oncology. mars 1997;42(3):203-11.
6. Bernier J, Hall EJ, Giaccia A. Radiation oncology: a century of achievements. Nat Rev Cancer. sept 2004;4(9):737-47.
7. The Treatment of Malignant Disease by Radium and X-Rays, Being a Practice of Radiotherapy. Arch Intern Med. 1 sept 1949;84(3):521.
8. A Study of the Ionization Method for Measuring the Intensity and Absorption of Roentgen Rays and of the Efficiency of Different Filters Used in Therapy. JAMA. 28 juill 1934;103(4):284.
9. Kramer R. Radiation therapy in early laryngeal cancer. J Mt Sinai Hosp N Y. 1947;14(1):24-8.
10. Bergonie J, Tribondeau L. Interpretation of some results of radiotherapy and an attempt at determining a logical technique of treatment. Radiat Res. oct 1959;11:587-8.
11. Champetier C, Gross E, Pointreau Y, Zaccariotto A, Dubergé T, Guerder C, et al. Dose de tolérance à l'irradiation des tissus sains : les testicules. Cancer/Radiothérapie. juill 2010;14(4-5):376-8.
12. Coutard, H. Principles of X-ray therapy of malignant disease. Lancet 224, 1-8 (1934)..pdf.
13. Joliot JF. I Our History and Heritage.
14. Laugier A. [The first century of radiotherapy in France]. Bull Acad Natl Med. janv 1996;180(1):143-60.
15. Physics-of-Radiology-Harold-Elford-Johns-John-Robert-Cunningham-Fourth-Edition-Charles-C-Thomas-Pub-Ltd-1983.pdf.
16. Tiemann J. [Practical irradiation planning using a « dedicated system »]. Strahlentherapie. nov 1974;148(5):463-7.
17. Purdy JA. Current ICRU definitions of volumes: limitations and future directions. Semin Radiat Oncol. janv 2004;14(1):27-40.
18. Hounsfield GN. Nobel Award address. Computed medical imaging. Med Phys. 1980;7(4):283-90.
19. Dutreix A. [The computer in radiotherapy]. Rev Prat. 11 mars 1972;22(8):1359-1360 passim.
20. Mohan R. Field Shaping for Three-Dimensional Conformal Radiation Therapy and Multileaf Collimation. Semin Radiat Oncol. avr 1995;5(2):86-99.

21. Oldham M, Neal A, Webb S. A comparison of conventional « forward planning » with inverse planning for 3D conformal radiotherapy of the prostate. *Radiother Oncol.* juin 1995;35(3):248-62.
22. Leksell L. The stereotaxic method and radiosurgery of the brain. *Acta Chir Scand.* 13 déc 1951;102(4):316-9.
23. Gérard JP, Aubert B, Buchheit I, Derreumaux S, Lartigau É, Latorzeff I, et al. Avis du groupe de travail missionné par l’Autorité de sûreté nucléaire concernant la radiothérapie stéréotaxique. *Cancer/Radiothérapie.* juin 2012;16:S5-9.
24. Salama JK, Kirkpatrick JP, Yin FF. Stereotactic body radiotherapy treatment of extracranial metastases. *Nat Rev Clin Oncol.* nov 2012;9(11):654-65.
25. Bucci MK, Bevan A, Roach M. Advances in radiation therapy: conventional to 3D, to IMRT, to 4D, and beyond. *CA Cancer J Clin.* 2005;55(2):117-34.
26. Ling CC, Yorke E, Fuks Z. From IMRT to IGRT: frontierland or neverland? *Radiother Oncol.* févr 2006;78(2):119-22.
27. Tsujii H, Mizoe J, Kamada T, Baba M, Tsuji H, Kato H, et al. Clinical Results of Carbon Ion Radiotherapy at NIRS. *J Radiat Res.* 2007;48 Suppl A:A1-13.
28. Suit HD, Goitein M, Munzenrider J, Verhey L, Urie M, Gragoudas E, et al. Increased efficacy of radiation therapy by use of proton beam. *Strahlenther Onkol.* janv 1990;166(1):40-4.
29. Rossi S. Hadron Therapy Achievements and Challenges: The CNAO Experience. *Physics.* 22 févr 2022;4(1):229-57.
30. Mohan R, Grosshans D. Proton therapy – Present and future. *Advanced Drug Delivery Reviews.* janv 2017;109:26-44.
31. Vozenin MC, Bourhis J, Durante M. Towards clinical translation of FLASH radiotherapy. *Nat Rev Clin Oncol.* déc 2022;19(12):791-803.
32. Limoli CL, Vozenin MC. Reinventing Radiobiology in the Light of FLASH Radiotherapy. *Annu Rev Cancer Biol.* 11 avr 2023;7(1):1-21.
33. Favaudon V, Caplier L, Monceau V, Pouzoulet F, Sayarath M, Fouillade C, et al. Ultrahigh dose-rate FLASH irradiation increases the differential response between normal and tumor tissue in mice. *Sci Transl Med.* 16 juill 2014;6(245).
34. Vozenin MC, De Fornel P, Petersson K, Favaudon V, Jaccard M, Germond JF, et al. The Advantage of FLASH Radiotherapy Confirmed in Mini-pig and Cat-cancer Patients. *Clinical Cancer Research.* 1 janv 2019;25(1):35-42.
35. Vozenin MC, Hendry JH, Limoli CL. Biological Benefits of Ultra-high Dose Rate FLASH Radiotherapy: Sleeping Beauty Awoken. *Clinical Oncology.* juill 2019;31(7):407-15.
36. Baldacchino G, Brun E, Denden I, Bouhadoun S, Roux R, Khodja H, et al. Importance of radiolytic reactions during high-LET irradiation modalities: LET effect, role of O₂ and radiosensitization by nanoparticles. *Cancer Nano.* déc 2019;10(1):3.

37. Baatout S, éditeur. Radiobiology Textbook [Internet]. Cham: Springer International Publishing; 2023 [cité 23 oct 2023]. Disponible sur: <https://link.springer.com/10.1007/978-3-031-18810-7>
38. Coldwell DM, éditeur. Manual of Interventional Oncology [Internet]. Stuttgart: Georg Thieme Verlag; 2018 [cité 23 oct 2023]. Disponible sur: <http://www.thieme-connect.de/products/ebooks/book/10.1055/b-006-149765>
39. Hatano Y, Katsumura Y, Mozumder A, éditeurs. Charged Particle and Photon Interactions with Matter [Internet]. 0 éd. CRC Press; 2010 [cité 29 déc 2023]. Disponible sur: <https://www.taylorfrancis.com/books/9781439811801>
40. How particles can be therapeutic – Physics World [Internet]. [cité 19 janv 2024]. Disponible sur: <https://physicsworld.com/a/how-particles-can-be-therapeutic/>
41. Samuel AH, Magee JL. Theory of Radiation Chemistry. II. Track Effects in Radiolysis of Water. *The Journal of Chemical Physics*. 1 juin 1953;21(6):1080-7.
42. Giesel F. Ueber Radium und radioactive Stoffe. *Ber Dtsch Chem Ges*. juill 1902;35(3):3608-11.
43. Debierne MA. Recherches sur les gaz produits par les substances radioactives. Décomposition de l'eau. *Ann Phys*. 1914;9(2):97-127.
44. News of Science. *Science*. 4 janv 1957;125(3236):18-22.
45. Zimbrick JD. Radiation Chemistry and the Radiation Research Society: A History from the Beginning. *Radiation Research*. août 2002;158(2):127-40.
46. Bazan JG, Le QT, Zips D. Radiobiology of Lung Cancer. In: IASLC Thoracic Oncology [Internet]. Elsevier; 2018 [cité 23 oct 2023]. p. 330-336.e2. Disponible sur: <https://linkinghub.elsevier.com/retrieve/pii/B9780323523578000354>
47. Vítor AC, Huertas P, Legube G, De Almeida SF. Studying DNA Double-Strand Break Repair: An Ever-Growing Toolbox. *Front Mol Biosci*. 21 févr 2020;7:24.
48. Hirayama R, Ito A, Tomita M, Tsukada T, Yatagai F, Noguchi M, et al. Contributions of Direct and Indirect Actions in Cell Killing by High-LET Radiations. *Radiation Research*. févr 2009;171(2):212-8.
49. Le Caër S. Water Radiolysis: Influence of Oxide Surfaces on H₂ Production under Ionizing Radiation. *Water*. 28 févr 2011;3(1):235-53.
50. Dertinger H, Jung H. Molecular Radiation Biology [Internet]. New York, NY: Springer US; 1970 [cité 23 oct 2023]. (Heidelberg Science Library). Disponible sur: <http://link.springer.com/10.1007/978-1-4684-6247-0>
51. Belloni JV, Mostafavi M, Douki T. Radiation Chemistry: From basics to applications in material and life sciences [Internet]. EDP Sciences; 2020 [cité 23 oct 2023]. Disponible sur: <https://www.degruyter.com/document/doi/10.1051/978-2-7598-0317-0/html>
52. Henglein A. J. W. T. Spinks. R. J. Woods: An Introduction to Radiation Chemistry, Third Edition, John-Wiley and Sons, Inc., New York, Toronto 1990. ISBN 0-471-61403-3. 574 Seiten, Preis: DM 91,45. *Ber Bunsenges Phys Chem*. mars 1991;95(3):451-451.

53. Appleby A, Schwarz HA. Radical and molecular yields in water irradiated by .gamma.-rays and heavy ions. *J Phys Chem.* juin 1969;73(6):1937-41.
54. Hayes JD, Dinkova-Kostova AT, Tew KD. Oxidative Stress in Cancer. *Cancer Cell.* août 2020;38(2):167-97.
55. Nakai K, Tsuruta D. What Are Reactive Oxygen Species, Free Radicals, and Oxidative Stress in Skin Diseases? *IJMS.* 6 oct 2021;22(19):10799.
56. Huang M, Li J. Physiological regulation of reactive oxygen species in organisms based on their physicochemical properties. *Acta Physiologica.* janv 2020;228(1):e13351.
57. Marusawa H, Ichikawa K, Narita N, Murakami H, Ito K, Tezuka T. Hydroxyl radical as a strong electrophilic species. *Bioorganic & Medicinal Chemistry.* juill 2002;10(7):2283-90.
58. Cheng Q, Gu J, Compaan KR, Schaefer HF. Hydroxyl Radical Reactions with Adenine: Reactant Complexes, Transition States, and Product Complexes. *Chemistry A European J.* 18 oct 2010;16(39):11848-58.
59. Aust AE, Eveleigh JF. Mechanisms of DNA Oxidation. *Proc Soc Exp Biol Med.* déc 1999;222(3):246-52.
60. Mitroka S, Zimmeck S, Troya D, Tanko JM. How Solvent Modulates Hydroxyl Radical Reactivity in Hydrogen Atom Abstractions. *J Am Chem Soc.* 10 mars 2010;132(9):2907-13.
61. Rodebush WH, Keizer CR, McKee FS, Quagliano JV. The Reactions of the Hydroxyl Radical ¹. *J Am Chem Soc.* mars 1947;69(3):538-40.
62. Samuni A, Goldstein S, Russo A, Mitchell JB, Krishna MC, Neta P. Kinetics and Mechanism of Hydroxyl Radical and OH-Adduct Radical Reactions with Nitroxides and with Their Hydroxylamines. *J Am Chem Soc.* 1 juill 2002;124(29):8719-24.
63. Chen SC, Chen WC. Vascular leakage induced by exposure to arsenic via increased production of NO, hydroxyl radical and peroxynitrite. *Microvascular Research.* avr 2008;75(3):373-80.
64. Cheng FC, Jen JF, Tsai TH. Hydroxyl radical in living systems and its separation methods. *Journal of Chromatography B.* déc 2002;781(1-2):481-96.
65. Yang F, Zhang R ping, He J ming, Abliz Z. [The generation, trapping and detection methods of hydroxyl radical]. *Yao Xue Xue Bao.* juill 2007;42(7):692-7.
66. Lipinski B. Hydroxyl Radical and Its Scavengers in Health and Disease. *Oxidative Medicine and Cellular Longevity.* 2011;2011:1-9.
67. Du J, Gebicki JM. Proteins are major initial cell targets of hydroxyl free radicals. *The International Journal of Biochemistry & Cell Biology.* nov 2004;36(11):2334-43.
68. Xu B, Wang W, Guo H, Sun Z, Wei Z, Zhang X, et al. Oxidative stress preferentially induces a subtype of micronuclei and mediates the genomic instability caused by p53 dysfunction. *Mutat Res.* déc 2014;770:1-8.

69. Su LJ, Zhang JH, Gomez H, Murugan R, Hong X, Xu D, et al. Reactive Oxygen Species-Induced Lipid Peroxidation in Apoptosis, Autophagy, and Ferroptosis. *Oxid Med Cell Longev*. 2019;2019:5080843.
70. Halliwell B, Gutteridge JMC. Free radicals in biology and medicine. Fifth edition. Oxford: Oxford University Press; 2015.
71. Scaiano JC. Kinetic Studies of Alkoxy Radicals. In: Simic MG, Taylor KA, Ward JF, Von Sonntag C, éditeurs. *Oxygen Radicals in Biology and Medicine* [Internet]. Boston, MA: Springer US; 1988 [cité 23 oct 2023]. p. 59-66. Disponible sur: http://link.springer.com/10.1007/978-1-4684-5568-7_9
72. Bietti M, DiLabio GA, Lanzalunga O, Salamone M. Electron Transfer Properties of Alkoxy Radicals. A Time-Resolved Kinetic Study of the Reactions of the *tert*-Butoxy, Cumyloxy, and Benzyloxy Radicals with Alkyl Ferrocenes. *J Org Chem*. 3 sept 2010;75(17):5875-81.
73. Quintiliani M. The Oxygen Effect in Radiation Inactivation of DNA and Enzymes. *International Journal of Radiation Biology and Related Studies in Physics, Chemistry and Medicine*. janv 1986;50(4):573-94.
74. Sonntag C von. The chemical basis of radiation biology. London: Taylor & Francis; 1987. 515 p.
75. Marnett LJ, Wilcox AL. The chemistry of lipid alkoxy radicals and their role in metal-amplified lipid peroxidation. Rice-Evans C, Halliwell B, Lunt GG, éditeurs. *Biochemical Society Symposia*. 1 nov 1995;61:65-72.
76. Antosiewicz J, Spodnik JH, Teranishi M, Herman-Antosiewicz A, Kurono C, Soji T, et al. NADH-generating substrates reduce peroxy radical toxicity in RL-34 cells. *Folia Morphol (Warsz)*. nov 2009;68(4):247-55.
77. Greene LE, Lincoln R, Cosa G. Rate of Lipid Peroxy Radical Production during Cellular Homeostasis Unraveled via Fluorescence Imaging. *J Am Chem Soc*. 8 nov 2017;139(44):15801-11.
78. Garrec J, Monari A, Assfeld X, Mir LM, Tarek M. Lipid Peroxidation in Membranes: The Peroxy Radical Does Not “Float”. *J Phys Chem Lett*. 15 mai 2014;5(10):1653-8.
79. Roschek B, Tallman KA, Rector CL, Gillmore JG, Pratt DA, Punta C, et al. Peroxy Radical Clocks. *J Org Chem*. 1 avr 2006;71(9):3527-32.
80. Folkes LK, Bartesaghi S, Trujillo M, Radi R, Wardman P. Kinetics of oxidation of tyrosine by a model alkoxy radical. *Free Radical Research*. sept 2012;46(9):1150-6.
81. Tortolani AJ, Powell SR, Mišik V, Weglicki WB, Pogo GJ, Kramer JH. Detection of alkoxy and carbon-centered free radicals in coronary sinus blood from patients undergoing elective cardioplegia. *Free Radical Biology and Medicine*. avr 1993;14(4):421-6.
82. Andrés CMC, Pérez De La Lastra JM, Andrés Juan C, Plou FJ, Pérez-Lebeña E. Superoxide Anion Chemistry—Its Role at the Core of the Innate Immunity. *IJMS*. 17 janv 2023;24(3):1841.
83. Sawyer DT, Gibian MJ. The chemistry of superoxide ion. *Tetrahedron*. janv 1979;35(12):1471-81.

84. Radi R, Denicola A, Alvarez B, Ferrer-Sueta G, Rubbo H. The Biological Chemistry of Peroxynitrite. In: Nitric Oxide [Internet]. Elsevier; 2000 [cité 23 oct 2023]. p. 57-82. Disponible sur: <https://linkinghub.elsevier.com/retrieve/pii/B9780123704207500058>
85. Alegría AE, Ferrer A, Santiago G, Sepúlveda E, Flores W. Photochemistry of water-soluble quinones. Production of the hydroxyl radical, singlet oxygen and the superoxide ion. *Journal of Photochemistry and Photobiology A: Chemistry*. oct 1999;127(1-3):57-65.
86. Fukuto JM, Carrington SJ, Tantillo DJ, Harrison JG, Ignarro LJ, Freeman BA, et al. Small Molecule Signaling Agents: The Integrated Chemistry and Biochemistry of Nitrogen Oxides, Oxides of Carbon, Dioxygen, Hydrogen Sulfide, and Their Derived Species. *Chem Res Toxicol*. 16 avr 2012;25(4):769-93.
87. Villamena FA. Reactive species detection in biology: from fluorescence to electron paramagnetic resonance spectroscopy. Amsterdam: Elsevier; 2017.
88. Ponnalagu D, Singh H. Anion Channels of Mitochondria. In: Singh H, Sheu SS, éditeurs. *Pharmacology of Mitochondria* [Internet]. Cham: Springer International Publishing; 2016 [cité 19 janv 2024]. p. 71-101. (Handbook of Experimental Pharmacology; vol. 240). Disponible sur: http://link.springer.com/10.1007/164_2016_39
89. Mumbengegwi DR, Li Q, Li C, Bear CE, Engelhardt JF. Evidence for a Superoxide Permeability Pathway in Endosomal Membranes. *Molecular and Cellular Biology*. 1 juin 2008;28(11):3700-12.
90. Oakley FD, Abbott D, Li Q, Engelhardt JF. Signaling Components of Redox Active Endosomes: The Redoxosomes. *Antioxidants & Redox Signaling*. juin 2009;11(6):1313-33.
91. Chance B, Sies H, Boveris A. Hydroperoxide metabolism in mammalian organs. *Physiological Reviews*. juill 1979;59(3):527-605.
92. Sies H. Role of Metabolic H₂O₂ Generation. *Journal of Biological Chemistry*. mars 2014;289(13):8735-41.
93. Kamsler A, Segal M. Hydrogen Peroxide As a Diffusible Signal Molecule in Synaptic Plasticity. *MN*. 2004;29(2):167-78.
94. Sikes HD. Scaffolding H₂O₂ signaling. *Nat Chem Biol*. août 2017;13(8):818-9.
95. Giorgio M, Trinei M, Migliaccio E, Pelicci PG. Hydrogen peroxide: a metabolic by-product or a common mediator of ageing signals? *Nat Rev Mol Cell Biol*. sept 2007;8(9):722-8.
96. Knaus UG, Hertzberger R, Pircalabioru GG, Yousefi SPM, Branco Dos Santos F. Pathogen control at the intestinal mucosa - H₂O₂ to the rescue. *Gut Microbes*. 2 janv 2017;8(1):67-74.
97. Veal E, Day A. Hydrogen Peroxide as a Signaling Molecule. *Antioxidants & Redox Signaling*. juill 2011;15(1):147-51.
98. Bienert GP, Møller ALB, Kristiansen KA, Schulz A, Møller IM, Schjoerring JK, et al. Specific Aquaporins Facilitate the Diffusion of Hydrogen Peroxide across Membranes. *Journal of Biological Chemistry*. janv 2007;282(2):1183-92.
99. Imlay JA. Pathways of Oxidative Damage. *Annu Rev Microbiol*. oct 2003;57(1):395-418.

100. Srinivas US, Tan BWQ, Vellayappan BA, Jeyasekharan AD. ROS and the DNA damage response in cancer. *Redox Biology*. juill 2019;25:101084.
101. Zhao R, Jiang S, Zhang L, Yu Z. Mitochondrial electron transport chain, ROS generation and uncoupling (Review). *Int J Mol Med*. 8 mai 2019;
102. Forrester SJ, Kikuchi DS, Hernandez MS, Xu Q, Griendling KK. Reactive Oxygen Species in Metabolic and Inflammatory Signaling. *Circ Res*. 16 mars 2018;122(6):877-902.
103. Turrens JF. Mitochondrial formation of reactive oxygen species. *The Journal of Physiology*. 15 oct 2003;552(2):335-44.
104. Cadenas E, Davies KJA. Mitochondrial free radical generation, oxidative stress, and aging. *Free Radical Biology and Medicine*. août 2000;29(3-4):222-30.
105. Brand MD. Mitochondrial generation of superoxide and hydrogen peroxide as the source of mitochondrial redox signaling. *Free Radical Biology and Medicine*. nov 2016;100:14-31.
106. Brand MD. The sites and topology of mitochondrial superoxide production. *Experimental Gerontology*. août 2010;45(7-8):466-72.
107. Turrens JF, Alexandre A, Lehninger AL. Ubisemiquinone is the electron donor for superoxide formation by complex III of heart mitochondria. *Archives of Biochemistry and Biophysics*. mars 1985;237(2):408-14.
108. Richter C, Gogvadze V, Laffranchi R, Schlapbach R, Schweizer M, Suter M, et al. Oxidants in mitochondria: from physiology to diseases. *Biochimica et Biophysica Acta (BBA) - Molecular Basis of Disease*. mai 1995;1271(1):67-74.
109. Bedard K, Krause KH. The NOX Family of ROS-Generating NADPH Oxidases: Physiology and Pathophysiology. *Physiological Reviews*. janv 2007;87(1):245-313.
110. D'Autréaux B, Toledano MB. ROS as signalling molecules: mechanisms that generate specificity in ROS homeostasis. *Nat Rev Mol Cell Biol*. oct 2007;8(10):813-24.
111. Muramoto K, Ohta K, Shinzawa-Itoh K, Kanda K, Taniguchi M, Nabekura H, et al. Bovine cytochrome c oxidase structures enable O₂ reduction with minimization of reactive oxygens and provide a proton-pumping gate. *Proc Natl Acad Sci USA*. 27 avr 2010;107(17):7740-5.
112. Marí M, Morales A, Colell A, García-Ruiz C, Fernández-Checa JC. Mitochondrial Glutathione, a Key Survival Antioxidant. *Antioxidants & Redox Signaling*. nov 2009;11(11):2685-700.
113. Fukai T, Ushio-Fukai M. Superoxide Dismutases: Role in Redox Signaling, Vascular Function, and Diseases. *Antioxidants & Redox Signaling*. 15 sept 2011;15(6):1583-606.
114. Ribas V, García-Ruiz C, Fernández-Checa JC. Glutathione and mitochondria. *Front Pharmacol* [Internet]. 1 juill 2014 [cité 1 déc 2023];5. Disponible sur: <http://journal.frontiersin.org/article/10.3389/fphar.2014.00151/abstract>
115. Sedeek M, Nasrallah R, Touyz RM, Hébert RL. NADPH oxidases, reactive oxygen species, and the kidney: friend and foe. *J Am Soc Nephrol*. oct 2013;24(10):1512-8.

116. Vermot A, Petit-Härtlein I, Smith SME, Fieschi F. NADPH Oxidases (NOX): An Overview from Discovery, Molecular Mechanisms to Physiology and Pathology. *Antioxidants*. 1 juin 2021;10(6):890.
117. Begum R, Thota S, Abdulkadir A, Kaur G, Bagam P, Batra S. NADPH oxidase family proteins: signaling dynamics to disease management. *Cell Mol Immunol*. juin 2022;19(6):660-86.
118. Moghadam ZM, Henneke P, Kolter J. From Flies to Men: ROS and the NADPH Oxidase in Phagocytes. *Front Cell Dev Biol*. 26 mars 2021;9:628991.
119. Lassègue B, San Martín A, Griendling KK. Biochemistry, physiology, and pathophysiology of NADPH oxidases in the cardiovascular system. *Circ Res*. 11 mai 2012;110(10):1364-90.
120. Panday A, Sahoo MK, Osorio D, Batra S. NADPH oxidases: an overview from structure to innate immunity-associated pathologies. *Cell Mol Immunol*. janv 2015;12(1):5-23.
121. Prieto-Bermejo R, Hernández-Hernández A. The Importance of NADPH Oxidases and Redox Signaling in Angiogenesis. *Antioxidants*. 13 mai 2017;6(2):32.
122. Pagano PJ, Chanock SJ, Siwik DA, Colucci WS, Clark JK. Angiotensin II Induces p67^{phox} mRNA Expression and NADPH Oxidase Superoxide Generation in Rabbit Aortic Adventitial Fibroblasts. *Hypertension*. août 1998;32(2):331-7.
123. Konior A, Schramm A, Czesnikiewicz-Guzik M, Guzik TJ. NADPH oxidases in vascular pathology. *Antioxid Redox Signal*. 10 juin 2014;20(17):2794-814.
124. Harris IS, DeNicola GM. The Complex Interplay between Antioxidants and ROS in Cancer. *Trends in Cell Biology*. juin 2020;30(6):440-51.
125. Jin S, Zhou F, Katirai F, Li PL. Lipid Raft Redox Signaling: Molecular Mechanisms in Health and Disease. *Antioxidants & Redox Signaling*. 15 août 2011;15(4):1043-83.
126. Xie Y, Zhu S, Song X, Sun X, Fan Y, Liu J, et al. The Tumor Suppressor p53 Limits Ferroptosis by Blocking DPP4 Activity. *Cell Reports*. août 2017;20(7):1692-704.
127. Yang M, Chen P, Liu J, Zhu S, Kroemer G, Klionsky DJ, et al. Clockophagy is a novel selective autophagy process favoring ferroptosis. *Sci Adv*. 5 juill 2019;5(7):eaaw2238.
128. Yagoda N, Von Rechenberg M, Zaganjor E, Bauer AJ, Yang WS, Fridman DJ, et al. RAS–RAF–MEK-dependent oxidative cell death involving voltage-dependent anion channels. *Nature*. juin 2007;447(7146):865-9.
129. Adachi Y, Shibai Y, Mitsushita J, Shang WH, Hirose K, Kamata T. Oncogenic Ras upregulates NADPH oxidase 1 gene expression through MEK-ERK-dependent phosphorylation of GATA-6. *Oncogene*. 21 août 2008;27(36):4921-32.
130. Wanders RJA, Waterham HR. Biochemistry of Mammalian Peroxisomes Revisited. *Annu Rev Biochem*. 1 juin 2006;75(1):295-332.
131. Bonekamp NA, Völkl A, Fahimi HD, Schrader M. Reactive oxygen species and peroxisomes: Struggling for balance. *BioFactors*. juill 2009;35(4):346-55.

132. Fransen M, Nordgren M, Wang B, Apanasets O. Role of peroxisomes in ROS/RNS-metabolism: Implications for human disease. *Biochimica et Biophysica Acta (BBA) - Molecular Basis of Disease*. sept 2012;1822(9):1363-73.
133. Loughran PA, Stolz DB, Vodovotz Y, Watkins SC, Simmons RL, Billiar TR. Monomeric inducible nitric oxide synthase localizes to peroxisomes in hepatocytes. *Proc Natl Acad Sci USA*. 27 sept 2005;102(39):13837-42.
134. Schrader M, Fahimi HD. Peroxisomes and oxidative stress. *Biochimica et Biophysica Acta (BBA) - Molecular Cell Research*. déc 2006;1763(12):1755-66.
135. Cao SS, Kaufman RJ. Endoplasmic Reticulum Stress and Oxidative Stress in Cell Fate Decision and Human Disease. *Antioxidants & Redox Signaling*. 20 juill 2014;21(3):396-413.
136. Tavender TJ, Springate JJ, Bulleid NJ. Recycling of peroxiredoxin IV provides a novel pathway for disulphide formation in the endoplasmic reticulum. *EMBO J*. 15 déc 2010;29(24):4185-97.
137. Espinosa-Diez C, Miguel V, Mennerich D, Kietzmann T, Sánchez-Pérez P, Cadenas S, et al. Antioxidant responses and cellular adjustments to oxidative stress. *Redox Biology*. déc 2015;6:183-97.
138. Hansen HG, Schmidt JD, Søltoft CL, Ramming T, Geertz-Hansen HM, Christensen B, et al. Hyperactivity of the Ero1 α Oxidase Elicits Endoplasmic Reticulum Stress but No Broad Antioxidant Response. *Journal of Biological Chemistry*. nov 2012;287(47):39513-23.
139. Malhotra JD, Miao H, Zhang K, Wolfson A, Pennathur S, Pipe SW, et al. Antioxidants reduce endoplasmic reticulum stress and improve protein secretion. *Proc Natl Acad Sci USA*. 25 nov 2008;105(47):18525-30.
140. Zangar R. Mechanisms that regulate production of reactive oxygen species by cytochrome P450. *Toxicology and Applied Pharmacology*. sept 2004;199(3):316-31.
141. Samhan-Arias AK, Gutierrez-Merino C. Purified NADH-cytochrome b5 reductase is a novel superoxide anion source inhibited by apocynin: sensitivity to nitric oxide and peroxynitrite. *Free Radical Biology and Medicine*. août 2014;73:174-89.
142. Wu RF, Ma Z, Liu Z, Terada LS. Nox4-Derived H₂O₂ Mediates Endoplasmic Reticulum Signaling through Local Ras Activation. *Molecular and Cellular Biology*. 1 juill 2010;30(14):3553-68.
143. Nandi A, Yan LJ, Jana CK, Das N. Role of Catalase in Oxidative Stress- and Age-Associated Degenerative Diseases. *Oxidative Medicine and Cellular Longevity*. 11 nov 2019;2019:1-19.
144. Kuehne A, Emmert H, Soehle J, Winnefeld M, Fischer F, Wenck H, et al. Acute Activation of Oxidative Pentose Phosphate Pathway as First-Line Response to Oxidative Stress in Human Skin Cells. *Molecular Cell*. août 2015;59(3):359-71.
145. Dick TP, Ralser M. Metabolic Remodeling in Times of Stress: Who Shoots Faster than His Shadow? *Molecular Cell*. août 2015;59(4):519-21.
146. Van Der Reest J, Lilla S, Zheng L, Zanivan S, Gottlieb E. Proteome-wide analysis of cysteine oxidation reveals metabolic sensitivity to redox stress. *Nat Commun*. 20 avr 2018;9(1):1581.

147. Sakamoto K, Iwasaki K, Sugiyama H, Tsuji Y. Role of the Tumor Suppressor PTEN in Antioxidant Responsive Element-mediated Transcription and Associated Histone Modifications. *Omary MB, éditeur. MBoC.* 15 mars 2009;20(6):1606-17.
148. Lee G, Won HS, Lee YM, Choi JW, Oh TI, Jang JH, et al. Oxidative Dimerization of PHD2 is Responsible for its Inactivation and Contributes to Metabolic Reprogramming via HIF-1 α Activation. *Sci Rep.* 7 janv 2016;6(1):18928.
149. Patterson AD, Carlson BA, Li F, Bonzo JA, Yoo MH, Krausz KW, et al. Disruption of Thioredoxin Reductase 1 Protects Mice from Acute Acetaminophen-Induced Hepatotoxicity through Enhanced NRF2 Activity. *Chem Res Toxicol.* 15 juill 2013;26(7):1088-96.
150. McDonald JT, Kim K, Norris AJ, Vlashi E, Phillips TM, Lagadec C, et al. Ionizing radiation activates the Nrf2 antioxidant response. *Cancer Res.* 1 nov 2010;70(21):8886-95.
151. Ahmed KM, Li JJ. NF-kappa B-mediated adaptive resistance to ionizing radiation. *Free Radic Biol Med.* 1 janv 2008;44(1):1-13.
152. Suman S, Johnson MD, Fornace AJ, Datta K. Exposure to Ionizing Radiation Causes Long-Term Increase in Serum Estradiol and Activation of PI3K-Akt Signaling Pathway in Mouse Mammary Gland. *International Journal of Radiation Oncology*Biography*Physics.* oct 2012;84(2):500-7.
153. Tonelli C, Chio IIC, Tuveson DA. Transcriptional Regulation by Nrf2. *Antioxidants & Redox Signaling.* 10 déc 2018;29(17):1727-45.
154. Kim S, Lee HG, Park SA, Kundu JK, Keum YS, Cha YN, et al. Keap1 Cysteine 288 as a Potential Target for Diallyl Trisulfide-Induced Nrf2 Activation. *Tsuji Y, éditeur. PLoS ONE.* 28 janv 2014;9(1):e85984.
155. Schae D, Micewicz ED, Ratikan JA, Iwamoto KS, Vlashi E, McDonald JT, et al. NRF2 Mediates Cellular Resistance to Transformation, Radiation, and Inflammation in Mice. *Antioxidants.* 25 août 2022;11(9):1649.
156. Kobayashi A, Kang MI, Okawa H, Ohtsuji M, Zenke Y, Chiba T, et al. Oxidative Stress Sensor Keap1 Functions as an Adaptor for Cul3-Based E3 Ligase To Regulate Proteasomal Degradation of Nrf2. *Molecular and Cellular Biology.* 1 août 2004;24(16):7130-9.
157. Hayes JD, Dinkova-Kostova AT. Epigenetic Control of NRF2-Directed Cellular Antioxidant Status in Dictating Life-Death Decisions. *Molecular Cell.* oct 2017;68(1):5-7.
158. Hirotsu Y, Katsuoka F, Funayama R, Nagashima T, Nishida Y, Nakayama K, et al. Nrf2–MafG heterodimers contribute globally to antioxidant and metabolic networks. *Nucleic Acids Research.* nov 2012;40(20):10228-39.
159. Reichard JF, Motz GT, Puga A. Heme oxygenase-1 induction by NRF2 requires inactivation of the transcriptional repressor BACH1. *Nucleic Acids Research.* déc 2007;35(21):7074-86.
160. Suzuki T, Yamamoto M. Stress-sensing mechanisms and the physiological roles of the Keap1–Nrf2 system during cellular stress. *Journal of Biological Chemistry.* oct 2017;292(41):16817-24.
161. Gao M, Yi J, Zhu J, Minikes AM, Monian P, Thompson CB, et al. Role of Mitochondria in Ferroptosis. *Molecular Cell.* janv 2019;73(2):354-363.e3.

162. LaVaute T, Smith S, Cooperman S, Iwai K, Land W, Meyron-Holtz E, et al. Targeted deletion of the gene encoding iron regulatory protein-2 causes misregulation of iron metabolism and neurodegenerative disease in mice. *Nat Genet.* févr 2001;27(2):209-14.
163. Arosio P, Elia L, Poli M. Ferritin, cellular iron storage and regulation. *IUBMB Life.* juin 2017;69(6):414-22.
164. Gao M, Monian P, Pan Q, Zhang W, Xiang J, Jiang X. Ferroptosis is an autophagic cell death process. *Cell Res.* sept 2016;26(9):1021-32.
165. Torii S, Shintoku R, Kubota C, Yaegashi M, Torii R, Sasaki M, et al. An essential role for functional lysosomes in ferroptosis of cancer cells. *Biochemical Journal.* 15 mars 2016;473(6):769-77.
166. Dodson M, Castro-Portuguez R, Zhang DD. NRF2 plays a critical role in mitigating lipid peroxidation and ferroptosis. *Redox Biology.* mai 2019;23:101107.
167. Schieber M, Chandel NS. ROS Function in Redox Signaling and Oxidative Stress. *Current Biology.* mai 2014;24(10):R453-62.
168. Lucero M, Suarez AE, Chambers JW. Phosphoregulation on mitochondria: Integration of cell and organelle responses. *CNS Neurosci Ther.* juill 2019;25(7):837-58.
169. Sauer H, Wartenberg M, Hescheler J. Reactive Oxygen Species as Intracellular Messengers During Cell Growth and Differentiation. *Cell Physiol Biochem.* 2001;11(4):173-86.
170. Kaminsky VO, Zhivotovsky B. Free Radicals in Cross Talk Between Autophagy and Apoptosis. *Antioxidants & Redox Signaling.* juill 2014;21(1):86-102.
171. Emerling BM, Weinberg F, Snyder C, Burgess Z, Mutlu GM, Viollet B, et al. Hypoxic activation of AMPK is dependent on mitochondrial ROS but independent of an increase in AMP/ATP ratio. *Free Radical Biology and Medicine.* mai 2009;46(10):1386-91.
172. Massaad CA, Klann E. Reactive Oxygen Species in the Regulation of Synaptic Plasticity and Memory. *Antioxidants & Redox Signaling.* 15 mai 2011;14(10):2013-54.
173. Betzen C, White R, Zehendner CM, Pietrowski E, Bender B, Luhmann HJ, et al. Oxidative stress upregulates the NMDA receptor on cerebrovascular endothelium. *Free Radical Biology and Medicine.* oct 2009;47(8):1212-20.
174. Shetty PK, Huang FL, Huang KP. Ischemia-elicited Oxidative Modulation of Ca²⁺/Calmodulin-dependent Protein Kinase II. *Journal of Biological Chemistry.* févr 2008;283(9):5389-401.
175. Hidalgo C, Arias-Cavieres A. Calcium, Reactive Oxygen Species, and Synaptic Plasticity. *Physiology.* mai 2016;31(3):201-15.
176. Beckhauser TF, Francis-Oliveira J, De Pasquale R. Reactive Oxygen Species: Physiological and Physiopathological Effects on Synaptic Plasticity: Supplementary Issue: Brain Plasticity and Repair. *J Exp Neurosci.* janv 2016;10s1:JEN.S39887.
177. Limoli CL, Kramár EA, Almeida A, Petit B, Grilj V, Baulch JE, et al. The sparing effect of FLASH-RT on synaptic plasticity is maintained in mice with standard fractionation. *Radiotherapy and Oncology.* sept 2023;186:109767.

178. Allen BD, Alaghband Y, Kramár EA, Ru N, Petit B, Grilj V, et al. Elucidating the neurological mechanism of the FLASH effect in juvenile mice exposed to hypofractionated radiotherapy. *Neuro-Oncology*. 4 mai 2023;25(5):927-39.
179. Gasperini RJ, Pavez M, Thompson AC, Mitchell CB, Hardy H, Young KM, et al. How does calcium interact with the cytoskeleton to regulate growth cone motility during axon pathfinding? *Molecular and Cellular Neuroscience*. oct 2017;84:29-35.
180. Hongpaisan J, Winters CA, Brian Andrews S. Calcium-dependent mitochondrial superoxide modulates nuclear CREB phosphorylation in hippocampal neurons. *Molecular and Cellular Neuroscience*. déc 2003;24(4):1103-15.
181. Kumari S, Badana AK, G MM, G S, Malla R. Reactive Oxygen Species: A Key Constituent in Cancer Survival. *Biomark Insights*. 1 janv 2018;13:117727191875539.
182. Sullivan LB, Chandel NS. Mitochondrial reactive oxygen species and cancer. *Cancer Metab*. déc 2014;2(1):17.
183. Ishikawa K, Takenaga K, Akimoto M, Koshikawa N, Yamaguchi A, Imanishi H, et al. ROS-Generating Mitochondrial DNA Mutations Can Regulate Tumor Cell Metastasis. *Science*. 2 mai 2008;320(5876):661-4.
184. Cairns RA, Harris IS, Mak TW. Regulation of cancer cell metabolism. *Nat Rev Cancer*. févr 2011;11(2):85-95.
185. Park MT, Kim MJ, Suh Y, Kim RK, Kim H, Lim EJ, et al. Novel signaling axis for ROS generation during K-Ras-induced cellular transformation. *Cell Death Differ*. août 2014;21(8):1185-97.
186. Bae I, Fan S, Meng Q, Rih JK, Kim HJ, Kang HJ, et al. BRCA1 Induces Antioxidant Gene Expression and Resistance to Oxidative Stress. *Cancer Research*. 1 nov 2004;64(21):7893-909.
187. Sablina AA, Budanov AV, Ilyinskaya GV, Agapova LS, Kravchenko JE, Chumakov PM. The antioxidant function of the p53 tumor suppressor. *Nat Med*. déc 2005;11(12):1306-13.
188. Chandel NS, Maltepe E, Goldwasser E, Mathieu CE, Simon MC, Schumacker PT. Mitochondrial reactive oxygen species trigger hypoxia-induced transcription. *Proc Natl Acad Sci USA*. 29 sept 1998;95(20):11715-20.
189. Liao Z, Chua D, Tan NS. Reactive oxygen species: a volatile driver of field cancerization and metastasis. *Mol Cancer*. déc 2019;18(1):65.
190. Chan JSK, Tan MJ, Sng MK, Teo Z, Phua T, Choo CC, et al. Cancer-associated fibroblasts enact field cancerization by promoting extratumoral oxidative stress. *Cell Death Dis*. 19 janv 2017;8(1):e2562-e2562.
191. Awadallah NS, Dehn D, Shah RJ, Russell Nash S, Chen YK, Ross D, et al. NQO1 Expression in Pancreatic Cancer and Its Potential Use as a Biomarker. *Applied Immunohistochemistry & Molecular Morphology*. janv 2008;16(1):24-31.
192. Shibata T, Kokubu A, Gotoh M, Ojima H, Ohta T, Yamamoto M, et al. Genetic alteration of Keap1 confers constitutive Nrf2 activation and resistance to chemotherapy in gallbladder cancer. *Gastroenterology*. oct 2008;135(4):1358-68, 1368.e1-4.

193. Rodic S, Vincent MD. Reactive oxygen species (ROS) are a key determinant of cancer's metabolic phenotype. *Intl Journal of Cancer*. févr 2018;142(3):440-8.
194. Le A, Cooper CR, Gouw AM, Dinavahi R, Maitra A, Deck LM, et al. Inhibition of lactate dehydrogenase A induces oxidative stress and inhibits tumor progression. *Proc Natl Acad Sci USA*. 2 févr 2010;107(5):2037-42.
195. Reczek CR, Chandel NS. The Two Faces of Reactive Oxygen Species in Cancer. *Annu Rev Cancer Biol*. 6 mars 2017;1(1):79-98.
196. Li X, Xu Q, Wu Y, Li J, Tang D, Han L, et al. A CCL2/ROS autoregulation loop is critical for cancer-associated fibroblasts-enhanced tumor growth of oral squamous cell carcinoma. *Carcinogenesis*. juin 2014;35(6):1362-70.
197. Xia C, Meng Q, Liu LZ, Rojanasakul Y, Wang XR, Jiang BH. Reactive Oxygen Species Regulate Angiogenesis and Tumor Growth through Vascular Endothelial Growth Factor. *Cancer Research*. 15 nov 2007;67(22):10823-30.
198. Liu X, Zhang Y, Wu X, Xu F, Ma H, Wu M, et al. Targeting Ferroptosis Pathway to Combat Therapy Resistance and Metastasis of Cancer. *Front Pharmacol*. 30 juin 2022;13:909821.
199. Liu R, Bian Y, Liu L, Liu L, Liu X, Ma S. Molecular pathways associated with oxidative stress and their potential applications in radiotherapy (Review). *Int J Mol Med*. 15 mars 2022;49(5):65.
200. Kim, Lee, Seo, Kim, Kim, Kim, et al. Cellular Stress Responses in Radiotherapy. *Cells*. 18 sept 2019;8(9):1105.
201. The action of radium on cancer cells. II.—Some factors determining the susceptibility of cancer cells to radium. *Proc R Soc Lond B*. juill 1933;113(782):238-50.
202. Rockwell S, Dobrucki I, Kim E, Marrison S, Vu V. Hypoxia and Radiation Therapy: Past History, Ongoing Research, and Future Promise. *CMM*. 1 mai 2009;9(4):442-58.
203. Thomlinson RH, Gray LH. The Histological Structure of Some Human Lung Cancers and the Possible Implications for Radiotherapy. *Br J Cancer*. déc 1955;9(4):539-49.
204. Chapman JD, Sturrock J, Boag JW, Crookall JO. Factors Affecting the Oxygen Tension around Cells Growing in Plastic Petri Dishes. *International Journal of Radiation Biology and Related Studies in Physics, Chemistry and Medicine*. janv 1970;17(4):305-28.
205. McKeown SR. Defining normoxia, physoxia and hypoxia in tumours—implications for treatment response. *BJR*. mars 2014;87(1035):20130676.
206. Wilson JD, Hammond EM, Higgins GS, Petersson K. Ultra-High Dose Rate (FLASH) Radiotherapy: Silver Bullet or Fool's Gold? *Front Oncol*. 17 janv 2020;9:1563.
207. Carreau A, Hafny-Rahbi BE, Matejuk A, Grillon C, Kieda C. Why is the partial oxygen pressure of human tissues a crucial parameter? Small molecules and hypoxia. *J Cellular Molecular Medi*. juin 2011;15(6):1239-53.
208. Hendry JH, Moore JV, Hodgson BW, Keene JP. The Constant Low Oxygen Concentration in All the Target Cells for Mouse Tail Radionecrosis. *Radiation Research*. oct 1982;92(1):172.

209. Weiss H. An Equation for Predicting the Surviving Fraction of Cells Irradiated with Single Pulses Delivered at Ultra-High Dose Rates. *Radiation Research*. mai 1972;50(2):441.
210. Montay-Gruel P, Acharya MM, Petersson K, Alikhani L, Yakkala C, Allen BD, et al. Long-term neurocognitive benefits of FLASH radiotherapy driven by reduced reactive oxygen species. *Proc Natl Acad Sci USA*. 28 mai 2019;116(22):10943-51.
211. Prax G, Kapp DS. A computational model of radiolytic oxygen depletion during FLASH irradiation and its effect on the oxygen enhancement ratio. *Phys Med Biol*. 11 sept 2019;64(18):185005.
212. Labarbe R, Hotoiu L, Barbier J, Favaudon V. A physicochemical model of reaction kinetics supports peroxy radical recombination as the main determinant of the FLASH effect. *Radiotherapy and Oncology*. déc 2020;153:303-10.
213. Petersson K, Adrian G, Butterworth K, McMahon SJ. A Quantitative Analysis of the Role of Oxygen Tension in FLASH Radiation Therapy. *International Journal of Radiation Oncology*Biology*Physics*. juill 2020;107(3):539-47.
214. Jansen J, Knoll J, Beyreuther E, Pawelke J, Skuza R, Hanley R, et al. Does FLASH deplete oxygen? Experimental evaluation for photons, protons, and carbon ions. *Medical Physics*. juill 2021;48(7):3982-90.
215. Cao X, Zhang R, Esipova TV, Allu SR, Ashraf R, Rahman M, et al. Quantification of Oxygen Depletion During FLASH Irradiation In Vitro and In Vivo. *International Journal of Radiation Oncology*Biology*Physics*. sept 2021;111(1):240-8.
216. El Khatib M, Van Slyke AL, Velalopoulou A, Kim MM, Shoniyozov K, Allu SR, et al. Ultrafast Tracking of Oxygen Dynamics During Proton FLASH. *International Journal of Radiation Oncology*Biology*Physics*. juill 2022;113(3):624-34.
217. Shao L, Luo Y, Zhou D. Hematopoietic stem cell injury induced by ionizing radiation. *Antioxid Redox Signal*. 20 mars 2014;20(9):1447-62.
218. Hintermann G, Fischer HM, Cramer R, Hütter R. Simple procedure for distinguishing CCC, OC, and L forms of plasmid DNA by agarose gel electrophoresis. *Plasmid*. mai 1981;5(3):371-3.
219. Meyers JA, Sanchez D, Elwell LP, Falkow S. Simple agarose gel electrophoretic method for the identification and characterization of plasmid deoxyribonucleic acid. *J Bacteriol*. sept 1976;127(3):1529-37.
220. Pachnerová Brabcová K, Štěpán V, Karamitros M, Karabín M, Dostálek P, Incerti S, et al. Contribution of indirect effects to clustered damage in DNA irradiated with protons. *Radiat Prot Dosimetry*. sept 2015;166(1-4):44-8.
221. Perstin A, Poirier Y, Sawant A, Tambasco M. Quantifying the DNA-damaging Effects of FLASH Irradiation With Plasmid DNA. *International Journal of Radiation Oncology*Biology*Physics*. juin 2022;113(2):437-47.
222. Small KL, Henthorn NT, Angal-Kalinin D, Chadwick AL, Santana E, Aitkenhead A, et al. Evaluating very high energy electron RBE from nanodosimetric pBR322 plasmid DNA damage. *Sci Rep*. 8 févr 2021;11(1):3341.

223. Vyšín L, Pachnerová Brabcová K, Štěpán V, Moretto-Capelle P, Bugler B, Legube G, et al. Proton-induced direct and indirect damage of plasmid DNA. *Radiat Environ Biophys.* août 2015;54(3):343-52.
224. Milligan JR, Arnold AD, Ward JF. The Effect of Superhelical Density on the Yield of Single-Strand Breaks in γ -Irradiated Plasmid DNA. *Radiation Research.* oct 1992;132(1):69.
225. Ward JF. The Complexity of DNA Damage: Relevance to Biological Consequences. *International Journal of Radiation Biology.* janv 1994;66(5):427-32.
226. Milligan JR, Aguilera JA, Ward JF. Variation of Single-Strand Break Yield with Scavenger Concentration for Plasmid DNA Irradiated in Aqueous Solution. *Radiation Research.* févr 1993;133(2):151.
227. Milligan JR, Ward JF. Yield of Single-Strand Breaks Due to Attack on DNA by Scavenger-Derived Radicals. *Radiation Research.* mars 1994;137(3):295.
228. Cooper CR, Jones D, Jones GD, Petersson K. FLASH irradiation induces lower levels of DNA damage ex vivo, an effect modulated by oxygen tension, dose, and dose rate. *BJR.* 1 mai 2022;95(1133):20211150.
229. Fouillade C, Curras-Alonso S, Giuranno L, Queleñec E, Heinrich S, Bonnet-Boissinot S, et al. FLASH Irradiation Spares Lung Progenitor Cells and Limits the Incidence of Radio-induced Senescence. *Clinical Cancer Research.* 15 mars 2020;26(6):1497-506.
230. Levy K, Natarajan S, Wang J, Chow S, Eggold JT, Loo PE, et al. Abdominal FLASH irradiation reduces radiation-induced gastrointestinal toxicity for the treatment of ovarian cancer in mice. *Sci Rep.* 10 déc 2020;10(1):21600.
231. Barghouth PG, Melemenidis S, Montay-Gruel P, Ollivier J, Viswanathan V, Jorge PG, et al. FLASH-RT does not affect chromosome translocations and junction structures beyond that of CONV-RT dose-rates [Internet]. *Molecular Biology*; 2023 mars [cité 17 janv 2024]. Disponible sur: <http://biorxiv.org/lookup/doi/10.1101/2023.03.27.534408>
232. Kuhlman B, Bradley P. Advances in protein structure prediction and design. *Nat Rev Mol Cell Biol.* nov 2019;20(11):681-97.
233. Reisz JA, Bansal N, Qian J, Zhao W, Furdui CM. Effects of ionizing radiation on biological molecules--mechanisms of damage and emerging methods of detection. *Antioxid Redox Signal.* 10 juill 2014;21(2):260-92.
234. Gupta S, Inman JL, Chant JD, Obst-Huebl L, Nakamura K, Costello SM, et al. A Novel Platform for Evaluating Dose Rate Effects on Oxidative Damage to Peptides: Toward a High-Throughput Method to Characterize the Mechanisms Underlying the FLASH Effect. *Radiation Research* [Internet]. 28 nov 2023 [cité 10 déc 2023]; Disponible sur: <https://meridian.allenpress.com/radiation-research/article/doi/10.1667/RADE-23-00131.1/497255/A-Novel-Platform-for-Evaluating-Dose-Rate-Effects>
235. Arnone A. Dose rate and LET effects on the radiolysis of a small peptide in solution [Internet]. Oral presentation présenté à: 32nd Miller Conference on Radiation Chemistry; 2023 juin 3; Corsica, France. Disponible sur: <https://miller2023.sciencesconf.org>

236. Spitz DR, Buettner GR, Petronek MS, St-Aubin JJ, Flynn RT, Waldron TJ, et al. An integrated physico-chemical approach for explaining the differential impact of FLASH versus conventional dose rate irradiation on cancer and normal tissue responses. *Radiotherapy and Oncology*. oct 2019;139:23-7.
237. Froidevaux P, Grilj V, Bailat C, Geyer WR, Bochud F, Vozenin MC. FLASH irradiation does not induce lipid peroxidation in lipids micelles and liposomes. *Radiation Physics and Chemistry*. avr 2023;205:110733.
238. Dayal D, Martin SM, Limoli CL, Spitz DR. Hydrogen peroxide mediates the radiation-induced mutator phenotype in mammalian cells. *Biochemical Journal*. 1 juill 2008;413(1):185-91.
239. Dayal D, Martin SM, Owens KM, Aykin-Burns N, Zhu Y, Boominathan A, et al. Mitochondrial Complex II Dysfunction Can Contribute Significantly to Genomic Instability after Exposure to Ionizing Radiation. *Radiation Research*. déc 2009;172(6):737-45.
240. Leach JK, Van Tuyle G, Lin PS, Schmidt-Ullrich R, Mikkelsen RB. Ionizing radiation-induced, mitochondria-dependent generation of reactive oxygen/nitrogen. *Cancer Res*. 15 mai 2001;61(10):3894-901.
241. Spitz DR. METABOLIC OXIDATIVE STRESS AND LOW DOSE RADIATION RESPONSES: ARE MITOCHONDRIA INVOLVED? *Health Physics*. mars 2011;100(3):295.
242. Limoli CL, Giedzinski E. Induction of Chromosomal Instability by Chronic Oxidative Stress. *Neoplasia*. juill 2003;5(4):339-46.
243. Limoli CL, Hartmann A, Shephard L, Yang CR, Boothman DA, Bartholomew J, et al. Apoptosis, reproductive failure, and oxidative stress in Chinese hamster ovary cells with compromised genomic integrity. *Cancer Res*. 15 août 1998;58(16):3712-8.
244. Slane BG, Aykin-Burns N, Smith BJ, Kalen AL, Goswami PC, Domann FE, et al. Mutation of Succinate Dehydrogenase Subunit C Results in Increased O₂⁻, Oxidative Stress, and Genomic Instability. *Cancer Research*. 1 août 2006;66(15):7615-20.
245. Ameziane-El-Hassani R, Talbot M, De Souza Dos Santos MC, Al Ghuzlan A, Hartl D, Bidart JM, et al. NADPH oxidase DUOX1 promotes long-term persistence of oxidative stress after an exposure to irradiation. *Proc Natl Acad Sci USA*. 21 avr 2015;112(16):5051-6.
246. Collins-Underwood JR, Zhao W, Sharpe JG, Robbins ME. NADPH oxidase mediates radiation-induced oxidative stress in rat brain microvascular endothelial cells. *Free Radical Biology and Medicine*. sept 2008;45(6):929-38.
247. Coyle CH, Martinez LJ, Coleman MC, Spitz DR, Weintraub NL, Kader KN. Mechanisms of H₂O₂-induced oxidative stress in endothelial cells. *Free Radical Biology and Medicine*. juin 2006;40(12):2206-13.
248. Epperly MW, Sikora CA, DeFilippi SJ, Gretton JA, Zhan Q, Kufe DW, et al. Manganese Superoxide Dismutase (SOD2) Inhibits Radiation-Induced Apoptosis by Stabilization of the Mitochondrial Membrane. *Radiation Research*. mai 2002;157(5):568-77.
249. Fath MA, Diers AR, Aykin-Burns N, Simons AL, Hua L, Spitz DR. Mitochondrial electron transport chain blockers enhance 2-deoxy-D-glucose induced oxidative stress and cell killing in human colon carcinoma cells. *Cancer Biology & Therapy*. juill 2009;8(13):1228-36.

250. Zhu Y, Dean AE, Horikoshi N, Heer C, Spitz DR, Gius D. Emerging evidence for targeting mitochondrial metabolic dysfunction in cancer therapy. *Journal of Clinical Investigation*. 31 août 2018;128(9):3682-91.
251. Montay-Gruel P, Acharya MM, Petersson K, Alikhani L, Yakkala C, Allen BD, et al. Long-term neurocognitive benefits of FLASH radiotherapy driven by reduced reactive oxygen species. *Proc Natl Acad Sci USA*. 28 mai 2019;116(22):10943-51.
252. Kacem H, Psoroulas S, Boivin G, Folkerts M, Grilj V, Lomax T, et al. Comparing radiolytic production of H₂O₂ and development of Zebrafish embryos after ultra high dose rate exposure with electron and transmission proton beams. *Radiotherapy and Oncology*. oct 2022;175:197-202.
253. Montay-Gruel P, Petersson K, Jaccard M, Boivin G, Germond JF, Petit B, et al. Irradiation in a flash: Unique sparing of memory in mice after whole brain irradiation with dose rates above 100 Gy/s. *Radiotherapy and Oncology*. sept 2017;124(3):365-9.
254. physics-world-reveals-its-top-10-breakthroughs-of-the-year-for-2022 [Internet]. [cité 24 oct 2023]. Disponible sur: <https://physicsworld.com/a/physics-world-reveals-its-top-10-breakthroughs-of-the-year-for-2022/>
255. Leavitt RJ, Almeida A, Grilj V, Montay-Gruel P, Godfroid C, Petit B, et al. Hypoxic tumors are sensitive to FLASH radiotherapy [Internet]. *Cancer Biology*; 2022 nov [cité 26 sept 2023]. Disponible sur: <http://biorxiv.org/lookup/doi/10.1101/2022.11.27.518083>
256. Almeida A, Godfroid C, Leavitt RJ, Montay-Gruel P, Petit B, Romero J, et al. Antitumor Effect by Either FLASH or Conventional Dose Rate Irradiation Involves Equivalent Immune Responses. *International Journal of Radiation Oncology*Biophysics*Physics*. nov 2023;S0360301623080355.
257. FLASH new intersection of physics, chemistry, biology, and 1 cancer medicine.pdf.
258. Favaudon V, Caplier L, Monceau V, Pouzoulet F, Sayarath M, Fouillade C, et al. Ultrahigh dose-rate FLASH irradiation increases the differential response between normal and tumor tissue in mice. *Sci Transl Med* [Internet]. 16 juill 2014 [cité 26 sept 2023];6(245). Disponible sur: <https://www.science.org/doi/10.1126/scitranslmed.3008973>
259. Schüller A, Heinrich S, Fouillade C, Subiel A, De Marzi L, Romano F, et al. The European Joint Research Project UHDpulse – Metrology for advanced radiotherapy using particle beams with ultra-high pulse dose rates. *Physica Medica*. déc 2020;80:134-50.
260. Montay-Gruel P, Bouchet A, Jaccard M, Patin D, Serduc R, Aim W, et al. X-rays can trigger the FLASH effect: Ultra-high dose-rate synchrotron light source prevents normal brain injury after whole brain irradiation in mice. *Radiotherapy and Oncology*. déc 2018;129(3):582-8.
261. Gao F, Yang Y, Zhu H, Wang J, Xiao D, Zhou Z, et al. First demonstration of the FLASH effect with ultrahigh dose rate high-energy X-rays. *Radiotherapy and Oncology*. janv 2022;166:44-50.
262. Shi X, Yang Y, Zhang W, Wang J, Xiao D, Ren H, et al. FLASH X-ray spares intestinal crypts from pyroptosis initiated by cGAS-STING activation upon radioimmunotherapy. *Proc Natl Acad Sci USA*. 25 oct 2022;119(43):e2208506119.
263. Kim MM, Irmen P, Shoniyozov K, Verginadis II, Cengel KA, Koumenis C, et al. Design and commissioning of an image-guided small animal radiation platform and quality assurance protocol for integrated proton and x-ray radiobiology research. *Phys Med Biol*. 1 juill 2019;64(13):135013.

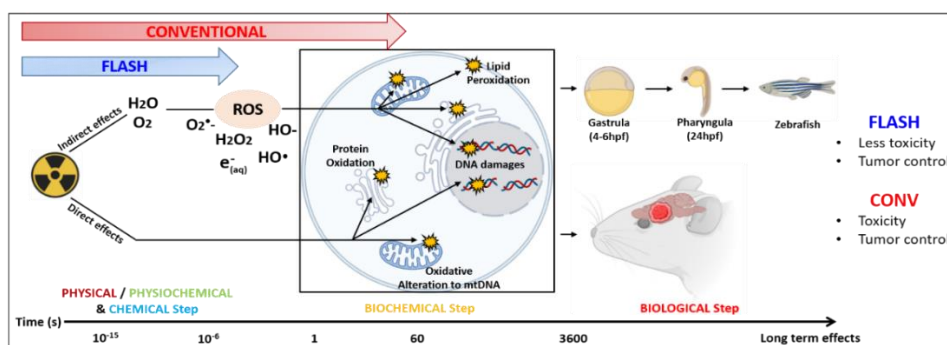
264. Diffenderfer ES, Verginadis II, Kim MM, Shoniyozov K, Velalopoulou A, Goia D, et al. Design, Implementation, and in Vivo Validation of a Novel Proton FLASH Radiation Therapy System. *International Journal of Radiation Oncology*Biology*Physics*. févr 2020;106(2):440-8.
265. Cunningham S, McCauley S, Vairamani K, Speth J, Girdhani S, Abel E, et al. FLASH Proton Pencil Beam Scanning Irradiation Minimizes Radiation-Induced Leg Contracture and Skin Toxicity in Mice. *Cancers*. 1 mars 2021;13(5):1012.
266. Singers Sørensen B, Krzysztof Sitarz M, Ankjærgaard C, Johansen J, Andersen CE, Kanouta E, et al. In vivo validation and tissue sparing factor for acute damage of pencil beam scanning proton FLASH. *Radiotherapy and Oncology*. févr 2022;167:109-15.
267. Smyth LML, Donoghue JF, Ventura JA, Livingstone J, Bailey T, Day LRJ, et al. Comparative toxicity of synchrotron and conventional radiation therapy based on total and partial body irradiation in a murine model. *Sci Rep*. 13 août 2018;8(1):12044.
268. Beyreuther E, Brand M, Hans S, Hideghéty K, Karsch L, Leßmann E, et al. Feasibility of proton FLASH effect tested by zebrafish embryo irradiation. *Radiotherapy and Oncology*. oct 2019;139:46-50.
269. Venkatesulu BP, Sharma A, Pollard-Larkin JM, Sadagopan R, Symons J, Neri S, et al. Ultra high dose rate (35 Gy/sec) radiation does not spare the normal tissue in cardiac and splenic models of lymphopenia and gastrointestinal syndrome. *Sci Rep*. 20 nov 2019;9(1):17180.
270. Jorge PG, Melemenidis S, Grilj V, Buchillier T, Manjappa R, Viswanathan V, et al. Design and validation of a dosimetric comparison scheme tailored for ultra-high dose-rate electron beams to support multicenter FLASH preclinical studies. *Radiotherapy and Oncology*. oct 2022;175:203-9.
271. Almeida A, Togno M, Ballesteros-Zebadua P, Franco-Perez J, Geyer R, Schaefer R, et al. Dosimetric and biologic intercomparison between electron and proton FLASH beams. *Cancer Biology*; 2023 avr.
272. Wasselin-Trupin V, Baldacchino G, Bouffard S, Hickel B. Hydrogen peroxide yields in water radiolysis by high-energy ion beams at constant LET. *Radiation Physics and Chemistry*. août 2002;65(1):53-61.
273. McMahon SJ, Currell FJ. A Robust Curve-Fitting Procedure for the Analysis of Plasmid DNA Strand Break Data from Gel Electrophoresis. *Radiation Research*. juin 2011;175(6):797-805.
274. Horst F, Brand M, Hans S, Karsch L, Lessmann E, Löck S, et al. In Regard to Böhlen et al. *International Journal of Radiation Oncology*Biology*Physics*. mars 2023;115(4):1006-7.
275. Sworski TJ. Yields of Hydrogen Peroxide in the Decomposition of Water by Cobalt γ -Radiation. I. Effect of Bromide Ion. *J Am Chem Soc*. sept 1954;76(18):4687-92.
276. Pastina B, LaVerne JA. Hydrogen Peroxide Production in the Radiolysis of Water with Heavy Ions. *J Phys Chem A*. 1 mars 1999;103(11):1592-7.
277. Draganić D. Studies on the Formation of Primary Yields of Hydrogen Peroxide and Molecular Hydrogen (GH₂O and GH₂) in the Radiolysis of Neutral Aqueous Solutions.
278. Štefanić I, LaVerne JA. Temperature Dependence of the Hydrogen Peroxide Production in the γ -Radiolysis of Water. *J Phys Chem A*. 1 janv 2002;106(2):447-52.

279. Hiroki A, Pimblott SM, LaVerne JA. Hydrogen Peroxide Production in the Radiolysis of Water with High Radical Scavenger Concentrations. *J Phys Chem A*. 1 oct 2002;106(40):9352-8.
280. Anderson AR, Hart EJ. RADIATION CHEMISTRY OF WATER WITH PULSED HIGH INTENSITY ELECTRON BEAMS ¹. *J Phys Chem*. janv 1962;66(1):70-5.
281. Draganic ZD, Draganic IG. Formation of primary yields of hydrogen peroxide and molecular hydrogen (GH₂O₂ and GH₂) in the .gamma. radiolysis of neutral aqueous solutions. *J Phys Chem*. déc 1971;75(26):3950-7.
282. Roth O, LaVerne JA. Effect of pH on H₂O₂ Production in the Radiolysis of Water. *J Phys Chem A*. 10 févr 2011;115(5):700-8.
283. Blain G, Vandenborre J, Villoing D, Fiegel V, Fois GR, Haddad F, et al. Proton Irradiations at Ultra-High Dose Rate vs. Conventional Dose Rate: Strong Impact on Hydrogen Peroxide Yield. *Radiation Research*. 8 juin 2022;198(3).
284. Sehested K, Rasmussen OL, Fricke H. Rate constants of OH with HO₂, O₂⁻, and H₂O₂⁺ from hydrogen peroxide formation in pulse-irradiated oxygenated water. *J Phys Chem*. févr 1968;72(2):626-31.
285. Barghouth PG, Melemenidis S, Montay-Gruel P, Ollivier J, Viswanathan V, Jorge PG, et al. FLASH-RT does not affect chromosome translocations and junction structures beyond that of CONV-RT dose-rates. *Radiotherapy and Oncology*. nov 2023;188:109906.
286. Saade G, Bogaerts E, Chiavassa S, Blain G, Delpon G, Evin M, et al. Ultrahigh-Dose-Rate Proton Irradiation Elicits Reduced Toxicity in Zebrafish Embryos. *Advances in Radiation Oncology*. mars 2023;8(2):101124.
287. Karsch L, Pawelke J, Brand M, Hans S, Hideghéty K, Jansen J, et al. Beam pulse structure and dose rate as determinants for the flash effect observed in zebrafish embryo. *Radiotherapy and Oncology*. août 2022;173:49-54.
288. Ruan JL, Lee C, Wouters S, Tullis IDC, Verslegers M, Mysara M, et al. Irradiation at Ultra-High (FLASH) Dose Rates Reduces Acute Normal Tissue Toxicity in the Mouse Gastrointestinal System. *International Journal of Radiation Oncology*Biological*Physics*. déc 2021;111(5):1250-61.
289. Yields of Hydrogen Peroxide in the Decomposition of Water by Cobalt γ -Radiation. I. Effect of Bromide Ion.pdf.
290. Jorge PG, Jaccard M, Petersson K, Gondré M, Durán MT, Desorgher L, et al. Dosimetric and preparation procedures for irradiating biological models with pulsed electron beam at ultra-high dose-rate. *Radiotherapy and Oncology*. oct 2019;139:34-9.
291. Simmons DA, Lartey FM, Schüler E, Rafat M, King G, Kim A, et al. Reduced cognitive deficits after FLASH irradiation of whole mouse brain are associated with less hippocampal dendritic spine loss and neuroinflammation. *Radiotherapy and Oncology*. oct 2019;139:4-10.
292. Favaudon V, Caplier L, Monceau V, Pouzoulet F, Sayarath M, Fouillade C, et al. Ultrahigh dose-rate FLASH irradiation increases the differential response between normal and tumor tissue in mice. *Sci Transl Med [Internet]*. 16 juill 2014 [cité 4 avr 2022];6(245). Disponible sur: <https://www.science.org/doi/10.1126/scitranslmed.3008973>

293. Kim MM, Verginadis II, Goia D, Haertter A, Shoniyozov K, Zou W, et al. Comparison of FLASH Proton Entrance and the Spread-Out Bragg Peak Dose Regions in the Sparing of Mouse Intestinal Crypts and in a Pancreatic Tumor Model. *Cancers*. 23 août 2021;13(16):4244.
294. Ruan JL, Lee C, Wouters S, Tullis IDC, Verslegers M, Mysara M, et al. Irradiation at Ultra-High (FLASH) Dose Rates Reduces Acute Normal Tissue Toxicity in the Mouse Gastrointestinal System. *International Journal of Radiation Oncology*Biography*Physics*. déc 2021;111(5):1250-61.
295. Kacem H, Almeida A, Cherbuin N, Vozenin MC. Understanding the FLASH effect to unravel the potential of ultra-high dose rate irradiation. *International Journal of Radiation Biology*. 4 mars 2022;98(3):506-16.
296. Traver D, Winzeler A, Stern HM, Mayhall EA, Langenau DM, Kutok JL, et al. Effects of lethal irradiation in zebrafish and rescue by hematopoietic cell transplantation. *Blood*. 1 sept 2004;104(5):1298-305.
297. Pastina B, LaVerne JA. Hydrogen Peroxide Production in the Radiolysis of Water with Heavy Ions. *J Phys Chem A*. 1 mars 1999;103(11):1592-7.
298. Štefanić I, LaVerne JA. Temperature Dependence of the Hydrogen Peroxide Production in the γ -Radiolysis of Water. *J Phys Chem A*. 1 janv 2002;106(2):447-52.
299. Roth O, LaVerne JA. Effect of pH on H₂O₂ Production in the Radiolysis of Water. *J Phys Chem A*. 10 févr 2011;115(5):700-8.
300. Chappuis F, Grilj V, Tran HN, Zein SA, Bochud F, Bailat C, et al. Modeling of scavenging systems in water radiolysis with Geant4-DNA. *Physica Medica*. avr 2023;108:102549.
301. Poirier F, Blain G, Bulteau-Harel F, Fattahi M, Goziou X, Haddad F, et al. The Pulsing Chopper-Based System of the Arronax C70XP Cyclotron. *Proceedings of the 10th Int Particle Accelerator Conf. 2019;IPAC2019:3 pages, 0.760 MB*.
302. Stephan F, Gross M, Grebinyk A, Aboulbanine Z, Amirkhanyan Z, Budach V, et al. FLASH I a b @PITZ : New R&D platform with unique capabilities for electron FLASH and VHEE radiation therapy and radiation biology under preparation at PITZ. *Physica Medica*. déc 2022;104:174-87.
303. Webb SE, Miller AL. Ca²⁺ signaling and early embryonic patterning during the Blastula and Gastrula Periods of Zebrafish and Xenopus development. *Biochimica et Biophysica Acta (BBA) - Molecular Cell Research*. nov 2006;1763(11):1192-208.
304. Fulton T, Trivedi V, Attardi A, Anlas K, Dingare C, Arias AM, et al. Axis Specification in Zebrafish Is Robust to Cell Mixing and Reveals a Regulation of Pattern Formation by Morphogenesis. *Current Biology*. août 2020;30(15):2984-2994.e3.

HOUDA KACEM

After completing an MSc in Physical Chemistry and Radiation Chemistry, this PhD thesis marks the conclusion of my studies and the end of an incredible journey. It is now time to advance my scientific career, with the hope that my PhD work will contribute to the clinical implementation of the FLASH radiotherapy and will improve the life of cancer patients.



Chronological cascade of physical, physicochemical, chemical (radiolysis of water), biochemical (different cellular compartments) and biological events (normal tissue and tumor response) occurring after irradiation from initial beam matter interact to the biological response. The difference in dose rate/exposure time between FLASH-RT and CONV-RT is shown respectively by blue and red arrow. Exposure to FLASH-RT is very short and ends up at the chemical step, it does not interfere with downstream biological steps while the duration of conventional radiation goes through the different steps. *Kacem et al., IJR 2021.*



UNIVERSITÉ DE LAUSANNE
Faculté de Biologie et de Médecine

CENTRE HOSPITALIER UNIVERSITAIRE VAUDOIS
Département d'Oncologie
Service de Radio-Oncologie

Lausanne, SUISSE